HEAT TRANSFER TO FIBER SUSPENSIONS - STUDIES OF PARTICLE CHARACTERIZATION AND FOULING AND CORROSION MITIGATION

GHULAMULLAH KHAN

FACULTY OF ENGINEERING
UNIVERSITY OF MALAYA
KUALA LUMPUR

2018

HEAT TRANSFER TO FIBER SUSPENSIONS - STUDIES OF PARTICLE CHARACTERIZATION AND FOULING AND CORROSION MITIGATION

GHULAMULLAH KHAN

THESIS SUBMITTED IN FULFILMENT OF THE REQUIREMENTS FOR THE DEGREE OF DOCTOR OF PHILOSOPHY

FACULTY OF ENGINEERING
UNIVERSITY OF MALAYA
KUALA LUMPUR

2018

UNIVERSITY OF MALAYA

ORIGINAL LITERARY WORK DECLARATION

Name of Candidate: Ghulamullah Khan

Registration/Matric No: KHA120069

Name of Degree: **DOCTOR OF PHILOSOPHY**

Title of Project Paper/Research Report/Dissertation/Thesis ("this Work"):

Heat transfer to fiber suspensions - studies of particle characterization and fouling and corrosion mitigation

Field of Study: **Heat transfer**

I do solemnly and sincerely declare that:

(1) I am the sole author/writer of this Work;
(2) This Work is original;
(3) Any use of any work in which copyright exists was done by way of fair dealing and for permitted purposes and any excerpt or extract from, or reference to or reproduction of any copyright work has been disclosed expressly and sufficiently and the title of the Work and its authorship have been acknowledged in this Work;
(4) I do not have any actual knowledge nor do I ought reasonably to know that the making of this work constitutes an infringement of any copyright work;
(5) I hereby assign all and every rights in the copyright to this Work to the University ofMalaya ("UM"), who henceforth shall be owner of the copyright in this Work and that any reproduction or use in any form or by any means whatsoever is prohibited without the written consent of UM having been first had and obtained;
(6) I am fully aware that if in the course of making this Work I have infringed any copyright whether intentionally or otherwise, I may be subject to legal action or any other action as may be determined by UM.

Candidate's Signature Date:

Subscribed and solemnly declared before,

Witness's Signature Date:

Name:

Designation:

āā

Heat transfer to fiber suspensions - studies of particle characterization and fouling and corrosion mitigation

ABSTRACT

Fibre suspension heat transfer and frictional pressure drop aspects were usually done in order to characterize fibres while flowing through a pipe lines. Fibre flow behaviour in pipe lines strongly depends on the fiber charateteristics like concentration, properties and suspension flow velocity. Moreover, fibre suspension flow is most significant scientific aspect paerticularly in the pulp and paper industry in such equipment as pipes, pumps, screens, washers etc. Many of them are well known, but still there is some lack of scientific research data regardign to the heat transfer and fricitonal losses to fibre suspensions and this is the major thrust of the current research reported in this thesis. A special conventional flow loop system with externally mounted heaters clamped on the outside of the pipe test section was constructed in order to measure the primarily heat transfer and frictional pressure drop to wood pulp. Fibre characterisation studies were examined employing various types of chemical and mechanical pulp fibre with the emphasis on three types of the one species of accasia mangium and accasia mangium hybrid. Heat trasfer coefficient *hc* values under the turbulent flow conditiosn, and all data were taken at different velocities and concentrations and at constant heat flux, similarly frictional pressure drops ΔP/L were aslo obtained simultaneously. The results show that most fibre dimensions and paper property data could be correlated with both hc and ΔP/L. The magnitude of hc and ΔP/L were found to depend on flow velocity, fibre concentration, flocculation, fibre population, fibre length, flexibility, coarseness, fibre surface topography, and the amount of fibrillar fines. Due to adhesive and hydrophilic nature of natural fibre, particularly at a lower flow rates, the accumulation of fibre at inner metallic wall surface cause stains and lead to metallic corrosion at particular fibre concnetration and may lead the fouling corosion as well. Alloys of iron

epically mild steel and carbon steel are reactive materials and susceptible to corrosion process. The appliation of organic or environmental friendly inhibitor is one of the most widely used and effective industrial technique for the protection of metals against corrosion and in different aggressive mediums due to the advantages of their environmentally friendly, biodegradable in nature and can be synthesized by simple procedure with low cost. This study investigated the effect of environmental friendly additives as Schiff Bases and Gelatin for the mitigation of both fouling and corrosion. These additives comprises electronegative heteroatoms as Nitrogen, Oxygen and Sulfur atoms, different functional groups like $-OCH_3$, -OH, $-NO_2$ and Glutamic acid are responsible to make these additivves as excellent corrosion and fouling inhibitors. The objective of the present research work was to investigate heat trasfer coefficent hc and fricitonal pressure losses for different fibre sepicies as well as corrosion and fouling mechanim to the aggressive and fouling solutions and their mitigation by the application of environmental friendly additives.

KEY WORDS

Fiber suspension; acacia mangium; heat transfer coefficient; Schiff Bases; corrosion inhibition; Gelatin; fouling mitigation.

ā

PEMINDAHAN HABA KE PENGGANTUNGAN SERAT - KAJIAN PENCIRIAN PARTIKEL DAN PENGURANGAN FOULING DAN KAKISAN

ABSTRAK

Pemindahan haba penggantungan serat dan aspek penurunan tekanan geseran biasanya dilakukan untuk mencirikan serat ketika mengalir melalui saluran paip. Tingkah aliran gentian dalam talian paip sangat bergantung pada serat charateteristics seperti kepekatan, sifat dan halaju aliran suspensi. Selain itu, aliran penggantungan gentian adalah aspek saintifik yang paling penting dalam industri pulpa dan kertas dalam peralatan seperti paip, pam, skrin, pencuci dan sebagainya. Ramai daripada mereka diketahui, tetapi masih ada kekurangan data penyelidikan saintifik pemindahan haba dan kerugian frisit kepada penggantungan gentian dan ini adalah teras utama penyelidikan semasa yang dilaporkan dalam tesis ini. Sistem gelung aliran konvensional khas dengan pemanas dipasang di luar di luar bahagian ujian paip telah dibina untuk mengukur pemindahan haba terutamanya dan penurunan tekanan geseran kepada pulpa kayu. Kajian-kajian pencirian serat telah diperiksa menggunakan pelbagai jenis serat pulp kimia dan mekanikal dengan penekanan pada tiga jenis spesies akasia mangium dan accasia mangium hybrid. Nilai pekali haba hc nilai di bawah conditiosn aliran turbulen, dan semua data diambil pada halaju dan kepekatan yang berlainan dan pada fluks haba tetap, tekanan geseran yang sama juga ΔP/L juga diperoleh pada masa yang sama. Keputusan menunjukkan bahawa kebanyakan dimensi serat dan data harta tanah boleh dikaitkan dengan kedua-dua hc dan ΔP/L. Besarnya hc dan ΔP/L didapati bergantung kepada halaju aliran, kepekatan serat, pemberbukuan, populasi serat, panjang serat, fleksibiliti, kasar, topografi permukaan serat, dan jumlah denda fibrillar. Disebabkan oleh sifat pelekat dan hidrofilik serat semulajadi, terutamanya pada kadar aliran yang lebih rendah, pengumpulan serat pada permukaan dinding logam dalaman menyebabkan

kesan dan mengakibatkan kakisan logam pada pengambilan serat tertentu dan boleh menyebabkan corak fouling juga. Paduan besi secara epal keluli lembut dan keluli karbon adalah bahan reaktif dan mudah terdedah kepada proses kakisan. Perantaraan perencat mesra organik atau alam sekitar adalah salah satu teknik perindustrian yang paling banyak digunakan dan berkesan untuk melindungi logam daripada kakisan dan dalam medium yang agresif yang berbeza kerana kelebihan alam mesra alam, biodegradable dan boleh disintesis dengan prosedur mudah dengan kos yang rendah. Kajian ini menyiasat kesan tambahan mesra alam sekitar seperti Schiff Bases dan Gelatin untuk mengurangkan kedua-dua fouling dan kakisan. Aditif ini terdiri daripada heteroatoms elektronegatif sebagai atom Nitrogen, Oksigen dan Sulfur, kumpulan fungsional yang berlainan seperti $-OCH_3$, -OH, $-NO_2$ dan asid glutamik bertanggungjawab untuk membuat penambahan ini sebagai kakisan yang sangat baik dan perencat fouling. Objektif kerja penyelidikan ini adalah untuk menyiasat hc coefficent hc dan kehilangan tekanan fricitonal untuk keperluan serat yang berlainan serta mekanisme pengikisan dan pengotoran kepada penyelesaian agresif dan fouling dan pengurangannya dengan penggunaan bahan tambahan mesra alam.

ACKNOWLEDGEMENTS

Firstand foremost, I wish to express my sincere appreciation to my project supervisors, Dr. Kazi MD. Salim Newaz and Prof. Wan Jeffery Basirun, for constantly guiding and encouraging me throughout this research work. Thanks a lot for giving me a professional training, advice and suggestions in order to bring this thesis to its final form. Without their kind and humble support and interest, this thesis would not have been the same as presented here. I am very gratefulfor her patience andconstructive comments that enriched this research project.

I would also like to acknowledge with much appreciation the crucial role of my family members especially my wife and my mother, for their unconditional love and continuous encouragements and confidence in my efforts.

And last, but not least thanks toall my sincere colleagues and others technical staff for their valuable comments, sharing their time and knowledge on this research project during the project was carried out and giving a permission to use all the necessary tools in the laboratory.

TABLE OF CONTENTS

LIST OF FIGURES

LIST OF TABLES

LIST OF SYMBOLS AND ABBREVIATIONS

A	:	Area, m^2
C_p	:	Specific heat, J/kg K
d	:	Inner diameter of tube, m
f	:	Friction factor
I	:	Current, Amp
h	:	Heat transfer coefficient, KW/m^2 K
k	:	Thermal conductivity, Wm/K
l	:	Length of the tube, m
Nu	:	Nusselt number
Pr	:	Prandtl number
P	:	Power, Watts
Q	:	Heat flow, Watts
q	:	Hat flux, W/m^2
Re	:	Reynolds Number
T	:	Temperature, ^oC
V	:	Velocity, m/s
η_{WL}	:	Inhibition efficiency by weightless method
ηp	:	Inhibition efficiency by polarization method

η_{EIS} : Inhibition efficiency by electrochemical impedance spectroscopy method

I^{o}_{CORR} : Corrosion current density in the absence of inhibitor

I_{CORR} : Corrosion current density in the presence of inhibitor

R^{o}_{P} : Polarization resistance in uninhibited solution

R_P : Polarization resistance in inhibited solution

W_1 : Average weights of specimens before exposure

W_2 : Average weights of specimens after exposure

A : Cross-sectional surface area

ɵ : Surface coverage

C^{0}_{R} : Corrosion rates in absence of the inhibitors

C_R : Corrosion rates in presence of the inhibitors

K_{ads} : Equilibrium adsorption constant

CCM : Calcium carbonate monohydrate

ACC : Amorphous calcium carbonate

CCH : Calcium carbonate hrxahydrate

q : Heat flux

k_L : Thermal onductivity of deposits

k_m : Thermal onductivity of metals

h_h : Heat transfer coefficient for hot fluid

h_c : Heat transfer coefficient for cold fluid

R_T : Total thermal resistance

U_C : Overall heat transfer coefficient for clean surfaces

ΔT_m : Log mean temperature difference

U_f : Overall heat transfer coefficient

R_{fi} : Inner surface resistances of the tubes

R_{fo} : Outer surface resistances of the tubes

ΔT_f : Temperature difference between the heated surface and the bulk temperature of the solution

d_C : Diameter of the clean tube

V : Volumetric flow rate

S : Degree of supersaturation

C_S : Equilibrium concentration for a given temperature

C : Solution concnetration

σ : Surface tension

r : Radius of nucleation

ΔGv : Free energy change of transformation per unit volume of the nucleation

LIST OF APPENDICES

CHAPTER 1: INTRODUCTION

1.1 Background

There are diverse applications of fibre suspensions in various prrocess industries like textile industries, food processing, and most significatly the major and most applicable use of the huge volume of fiber suspension in pulp and paper industry. Wood pulp fibres and other natural occurring cellulosic fibres are frequently handled as a suspension with water as the suspending medium. The raw materials for paper manufacturing are pulp which comprises of natural cellulose fibre mostly obtained from wood plants. Some common use of idustrial application particuarly in pulp and paper industry where handled in suspension form including washing, screening and refining. Moreover, mostly the hydraulic transportation of natural fibre suspensions is accomplished commonly in pipeline flow systems. To udnerstand the flow behaviour of pulp suspensions which has an important and cursial role in pulp and paper manufacture where an incredible amount of research has been carried out in this particualr field of research.

A significant research work has also been carried out on the heat transfer behaviour to polymeric drag reducing fluids but very small amout of research work has been reported previously on the heat transfer to drag reducing fibre suspensions, particularly in the case of natural fibre suspensions. At a specified conditions of temperature and flow during the transportation and processing of natural fibre suspensions, divesify the opportunity to characterise natural occuring fibres and fibre suspension systems. The major raw source of cellulose fibres for pulp and paper manufacturing process are trees. Two different kinds of wood like softwoods and hardwoods are used for different purposes. Soft woods (Pine, Fir, spruce etc.) are the primary source of fibres reinforcement for pulp and paper maufacturing, whereas hardwood fibre (eucalyptus,

ash, Aspen, etc.) havig a shorter fibre lenght as comapred to soft wood, but having a better foramtion properties, higher density as well as more smoothness paper production qualitites makes it more demanding for larger production.

Apart from the conventional slurries natural fibres suspension in water form a two-phase slurry system, commonly distinguished as visco-elastic suspensions. The flow behavior in pipe flow can be divided in three different regimes: Plug, mixed, and turbulent flow. Fibre suspensions behave in a different way from individual fibres by the interfering of neighbouring fibres interfere and causes entangle (twist ot knot) even at a very low fibre concentration. Whereas in most cases fibre interlock causing a three-dimentional network during water suspension ad thereby altering transport properties of suspension resulting a disticntive suspension behaviour. At the low velocities, atural fibre occup the entire pipe line forming flocs and coherent network resulting a greater pressure drop than individual water behaviour. Whereas, fibre-water anulus formation at higher velocities and due to fibre damp turbublence which resulting a reduced fricitional pressure drop relative to water, this phoemenon is termed as drag reduction. Hence, it would be expected that fibres and their consequent composite structures would also modify heat transfer in a heat exchanger and cause some unique phenomena. Correlation of heat transfer coefficient h_c to the acceptable paper product qualities, provides an indication or estimation for pulp quality parameter or indicator. Heat transfer coefficient depends on a number of variables including fibre concentration, fibre type, fibre lenght, luman diameter and specifications and velocity range too.

Fibers suspensions in water change the rheological tendency of the water system. The mutual interactions between the fibers and hydrodynamic disturbance to the flow field leading to a net increase in viscosity. Therefore, it is generally observed that the pulp suspension behaviour deviate those from the Newtonian characters. The suspension or the presence of fibers/filament in low concentration resembles as the individual particles

having the tendency to bend and absorb turbulent energy. Moreover, further increasing of fibre concentration results both the flocks formation and fiber network system as well.

The flow behaviour tendency of wood pulp suspension in a pipe line flow can be studied by means of heat transfer coefficient (h_C) and pressure drop (ΔP) and correlating these parameters in order to evaluate the paper quality. The corresponding values of heat transfer coefficient (h_C) have to be linked to the desired paper production qualities and therefore, can measure pulp quality parameters. It can be accomplished by the several factors including fiber concentration, type and specifications along with velocity flow.

The present work focus on a more deeply and significantly valueable information on heat transfer phenomenon and pressure losses durig the flow of natural fibre suspensions and co-relating them to paper properties as well. Thus by careful monitoring of these fudamental phomenons, the paper of desired quality could be properly examined and controlled. Moreover, the variations in heat transfer and pressure drop measurements of several natural fibres suspensions in pipe flow were correlate to fibre dimensions as well.

Corrosion is a surface phenomenon known as the attack of metals or alloy by their environment, such as air, water or soil in chemical or electrochemical reaction to form more stable compounds (Uhlig 1971 & Jones 1996). Corrosion may also be defined as an irreversible interfacial reaction between the material and its environment, emerging in the loss of material or the dissolution of one of the components into the environment. From the construction engineer point of view the term corrosion means “damaging”: which degrade or destroy the functional properties of the material, making it unsuitable for further use. This degradation of the materials occurs through the chemical reaction with the environment, which is often or sometimes hasten the damage. It is necessary to devote more attention to metallic corrosion due to:

(i) A more corrosive environment due to the increasing pollution of air and water.

(ii) An increased use of metals in most technological fields.

(iii) The use for special applications as in the atomic energy field of rare and expensive metals.

For corrosion to occur, three essential elements must be present: electrolyte, anode and cathode. An electrolyte is a solution which can conduct electrical current due to the presence of ions. Electrodes can be of different metals or the same metal with different sizes or areas. Corrosion occurs because there is a difference in electrical potential between the two electrodes/areas such that electricity flows in the electrolyte between them. This circuit must be completed by a metallic path between the two electrodes (Uhlig 1971 & Jones 1996).

Today, the corrosion impact and its associated degradation of engineering construction materials are far more complex due to the increased diversity of materials such as metals and non-metals as well likely ceramics, polymer, and composites. Whereas consequences of corrosion issues, technological improvement and requirement for the global sustainability, as well as emerging corrosion incidents whose adverse effects minimized by the proper selection of materials, development of the new materials and proper corrosion monitoring and mitigation, all must be addressed.

In most industrial application it is almost impossible to "prevent or stop" the metallic corrosion. Various strategies are carried out in order to mitigate or inhibit corrosion rate to an economically ecological level. Some important corrosion mitigation techniques including: the selection of material and design, shifting the interfacial potential, changing the environment, and most frequently used technique is the addition of corrosion inhibitors (Shreir et al., 1994). The additions of chemical compounds or additives to the aggressive solution enhance the corrosion reduction rate by the virtue of adsorption on the metal surface (Uling, 2000). The addition of corrosion inhibitor form

a protective layer due to the reaction with the available metal surface, resulting a reduction either the anodic or cathodic corrosion rate. Even a small quantity of the inhibitors required for the effective protection (~10^{-4} M). A variety of chemical compounds have been extensively used as effective corrosion inhibitorsnthat exhibits the inhibition properties. However, the final consideration absed on: the availability and cost, their toxic properties, ease of extraction methods and environmental friendly behavior factors are of prime importance. Mostly inorganic compounds like chromate, phosphate, arsenic, hydrazine etc. are employed as most effective industrial scale inhibitors, but due to their toxic nature, their applications have been limited by some environmental regulations organizations including OSHA, EPA and DoT. Therefore, the applications of organic/green corrosion inhibitors becoming more important due to their cost, ease of synthesis, environmentally friendly nature as well as ecological nature (Ostovari et al., 2009; Bockris & Swinkels, 1964; Oguzie et al., 2007; Khan et al., 2015).

In the pulp and paper industries, there occurs corrosion due to use of chemicals. Inaddition, the existence of corrosion products also observed at the fouling sites. So the explorations of noval metals, as well as corrosion and fouling mitigation techniques have taken under consideration in parallel. Fouling on heat transfer surfaces are mitigated by various means among them natural fibre additions as an eco-friendly additive is a promising one. Fouling mitigation is a persistent and expensive problem penalizing industries, billions of dollars annually (Muller-Stienhagen, 2000). Therefore, efforts have been given for assessment of the cost of fouling worldwide. The fouling cost was evaluated in United Kingdom was in the range of 300 – 500 M £ annually (Steinhagen et al., 1993). Similarly for United States, the fouling cost was estimation could be between 8,000 and 10,000 M$ per annum (Garrett-Price et al., 1984). Fouling cost is significant, having not only the financial impact but also leads an increase of the

pumping cost whose consequences are: additional pressure drop, a net decrease of fluid velocity in the processing units, unscheduled shut down and a higher pumping energy is required. Commonly scales are classified as alkaline, non-alkaline scale and silica base scale. Moreover the scale including calcium carbonates ($CaCO_3$), calcium sulfate ($CaSO_4.XH_2O$), barium sulfate ($BaSO_4$), Strontium sulfate ($SrSO_4$), and scilicet etc. (Darton, 1999 & Karime, 2008). Calcium carbonate and calcium sulfate are the most commonly non-alkaline scales. On the other hand the most dominant problems in water treatment plants is the cleaning of such deposited scales, which is relatively more difficult to the rest of alkaline scale. Corrosion fouling occurs due to the reaction between the heat transfer surface and materials in fluid. Moreover, corrosion fouling may also caused by a chemical reaction but it is different from chemical fouling reaction. As a consequence of corrosion fouling, the surface reacts with fouling fluids and exhibit corrosion on heat transfer surfaces (Bott, 1995). The presence of theses corrosion products further act as a catalyst affecting other fouling processes. The precipitation of calcium sulfate occurs in three different forms inluding: calcium sulfate anhydrite ($CaSO_4$), calcium sulfate hemihydrate ($CaSO_4.1/2H_2O$) commonly known as plaster of paris and calcium sulfate dihydrate ($CaSO_4.2H_2O$) may also known as gypsum, which is one of the most common forms at ambient temperatures (lee, 2000). Fouling mitigation studies have long been examined by different techniques including: chemical and mechanical methods. Fouling leads the deterioration of shell and tube type heat exchangers efficiency due to the foulant poor thermal design (Gilmour, 1965). However, several attempts have been proposed for the complete removal of deposits or minimizing degree of the fluid forming deposits (Kazi et al, 2009 and Muller-Steinhagen et al., 2007). Additives are one of the easiest, cheap and most effective approaches commonly used for fouling mitigation. Inaddition, additives are entirely divergent, and as well as more effective to impact crystallization consisting of

tremendous-valence metal ions, surfactants, anti-foulants and polymers (Puckorius & Zimmie, 1972). In chemical method, a variety of chemicals have been developed and investigated as competent additives widely used for fouling mitigation as well as to prevent scaling on industrial scale (Harris & Marshall, 1981; Krisher, 1978). Application and selection of scale inhibitors are one of the most frequently and effective way to impede undesirable inorganic or mineral salts deposition containing various effective functional groups like sulfonic acid, carboxylic acid, or phosphoric acid (Grohe et al., 2006). These inhibitors are designed in such a way that they possess the ability of producing a number of co-ordinate bonds with the surrounding cations of the available minerals surface, resulting to reduce surface energy sufficiently by the selective adsorption of the designed inhibitors or additives and suppress the growth rate.

1.2 Objectives of study

The overall and main important aspect of the present research work involves the following studies where multiple aspectswere taken under consideration

1. To develop a correlations between fibre properties (fibre length, slenderness ration and fibre flexcibility) and heat transfer coefficient *hc* as well as frictional pressure drop $\Delta P/m$ parameters of natural wood pulp fibre at different fibre suspension concentration (0.2 wt.%, 0.4 wt.% and 0.6 wt.%) and specified flow conditions.
2. To examine the influence of fibre processing (mechanical and chemical pulping, fibre beating) and paper formation properties (Tear, Tensile burst index) on heat transfer coefficient *hc* and frictional pressure drop $\Delta P/m$ data in order to characterize the investigated fibre and its paper quality as well.
3. To investigate the corrosion inhibition efficiency of the specific Quinazoline Schiff bases as effective corrosion inhibitors for mild steel which has got a multiple individual applications.
4. To evaluate the appliations of fouling mitigation mechanism on the heat transfer surfaces by the selection of the environmental friendly anti-fouling additives (Gelatin) as novel ecofriendly approach to support previous research on fouling mitigation by natural fibres in the same research lab.

1.3 Problem Statement

Wood pulp and other natural cellulosic fibres are frequently handled as suspension in water medium. In pulp and paper industries many operations including washing, screening and refining are carried out in suspension form. Moreover, the hydraulic transportation of natural fibre suspensions are commonly in pipeline systems. Transportation and processing of natural fibre suspensions at specified temperatures have opened new avenue of opportunity to characterise fibres and fibre suspension systems. The present work was thus undertaken to obtain more information on heat transfer characteristics of flowing natural fibre suspensions. Both softwoods and hardwoods are used in pulp and paper industry for different reasons. Soft woods are the main source of reinforcing fibres for pulp and paper production. Hardwood fibre structures are quite different from softwoods having a shorter length than softwood and they are often used for paper-making which provides good formation properties producing papers of better smoothness and higher density. In Malaysia, harwood source is available which acts as a source of paper production along with the reinforcing support pine fibres.

Natural fibres in water form a two-phase slurry system which is entirely different from conventional slurries and classified as viscoelastic suspensions. In fibre suspensions, neighbouring fibres interfere and entangle even at low populations and can form bundles or entities that behave differently from the individual fibres. In many cases fibres interlock to form three-dimensional structures or networks which in liquid suspension alter the transport properties of the suspension and cause distinctive flow from water flow characteristics. Natural fibres form flocs and coherent networks which produce a plug occupying the entire pipe line at low velocities where the suspension frictional pressure drop is greater than that of water flowing alone. At a specific range in higher velocities a fibre–water annulus forms and the fibres damp turbulence causing reduced

frictional pressure drops relative to water (drag reduction). Hence, it would be expected that fibres and their consequent composite structures would also modify heat transfer in a heat exchanger and cause some unique phenomena.

Variation of fibre properties produces reject paper reported that the variations in fibre properties can be monitored, so that changes can be made on the fibre processing before paper is made. The research work was taken as a scheme to correlate heat transfer and pressure drop characteristics of fibre suspensions to the paper properties. Thus by monitoring them paper quality could be controlled. Heat transfer and pressure drop measurements of pine natural fibre suspensions in pipe and annular flow were obtained to correlate fibre dimensions with variations in heat transfer coefficient and pressure drop characteristics. Malaysian hardwood fibres were not yet studied and sharacterized. So, the present work was taken in hand to develop corelations for the heat transfer and friction losses for local pulp fibre and paper properties.

Corrosion on the heat transfer surfaces as well as particle deposition and biological fouling is adversely affecting the performance in heat exchanger system. The heat transfer and pressure drop data from this study can be used to improve design of heat transfer equipment including pulp and paper industries. Thus fouling and corrosion play a vital role in process industries. Mitigation of corrosion and fouling is essential for prolonging the service and protection of heat exchanging equipements. Among different ways of corrosion mitigation, Schiff Bases of corrosion inhibition has considered and fouling mitigation being achieved by Gelatin additives.

In the ways of fouling mitigation strategy addition of natural fibre to the fouling liquid for mitigation is an effective eco-friendly means as noticed by other researchers.

1.4 Organization of present dissertation

Chapter 1 includes the mainhighlights of the problems existing in the field of heat transfer and pressure losses of fibre suspension. Similarly the study conducted for the corrosion inhibition of mild and carbon steel in different acidic mediums by the application of Schiff base compounds (organic compounds) and to mitigate fouling of calcium sulphate solution on heat transfer surfaces by means of environmentally friendly organic additives. Moreover it also covers the main objectives of the present research work as well.

Chapter 2 compriesliterature review for each section of the present work including the details of the fibers structures, various properties of fibers and papers, types of puling (mechanical and chemical), and possible effects of beating (refining) on paper making characteristics and paper and fibre properties. Furthermore, it also consists of the heat transfer and frictional pressure losses studies for fibre suspension as well.

In the case of corrosion inhibition of mild and carbon steel at a various concentration of different acidic solution in different acidic mediums, a variety of organic and environmental friendly additives in the form of corrosion inhibitors were studied. The details of the various techniques for corrosion inhibition measurements like weight loss method and electrochemical measurements including potentiodynamic and electrochemical impedance spectroscopy measurements were studied. In addition, the different adsorption method for the adsorption of inhibitors molecules on the solid surface was also considered in this section.

Chapter 3 covers the details of the investigated materials along with the experimental setup. The details of the test rigs for all additives and for fibre suspensions, test coupons of different metals, different concentration of fouling and acid solution data acquisition systems are deeply explained with all relevant accessories during the experiment of this performance stage.

In a similar fashion the methodology carried out for the electrodes and different concentration of acidic solutions preparation and the application of electrochemical techniques for measuring and analyzing corrosion rates of different metallic coupons. In addition to FeSEM surface morphology was carried out for adsorption and the surface characteristics of the adsorbed inhibitors layer on solution/metal interface.

Methodology for the fouling of inverse soluble salts like ($CaSO_4.2H_2O$) on heat transfer surfaces also include in this chapter. Moreover, the fouled surfaces of the coupons for both fouling solution with and without additives were characterized by SEM and XRD analysis.

Chapter 4 includes all the possible theoretical and experimental outcomes for whole experimental setup and for each individual section as well. In the case of fibre characterization it isthe water run data in the form of Nusselt number and pressure loss, and comparison between obtained data with existing correlations. Then the heat transfer and pressure loss studies e.g., effect of fiber concentration of pulp samples from different sources and beating process on h_C and pressure drop data are discussed in details. Relationship of h_C and pressure drop data with fiber and paper properties are studied.

Whereas in corrosion section, the details of the electrode preparation, inhibitors structure and IUPAC names, test solution preparation, weight loss and electrochemical measurements are carried out for the present work. Moreover, the effective inhibition efficiency of these Quinazoline Schiff base compounds as excellent corrosion inhibitors for carbon and mild steel were investigated in 1 molar different acid medium as HCl and H_2SO_4.

Similarly, for fouling mitigation sections, the application of environment friendly fouling mitigation additives (Gelatine gel), the solubility trends for $CaSO_4.2H_2O$, heat transfer coefficient, fouling resistance at the desired temperature and flow rate, as well

as the XRD and SEM analysis techniques were carried out for evaluating the additive performance.

Chapter 5 includes concise details of conclusion for each individual research work along with the important outcomes being investigated in the present work.

CHAPTER 2: LITERATURE REVIEW

2.1 Fibre structure and fibre and paper properties

Generally, in paper industry it is commenly required to modify the present quality of fiber and paper being used in order to improve the paper properties, these significant and scientific challenges still exixsts in the paper industries. Raw maretial for paper making process are pulps of various fibrs sources from both the wood and non-wood plants. Soft wood and hard wood (red wood, beech, acacia mangium, maple) as well as non wood (rice husk etc.) obtained from agriculture waste are the primary source for pulp (Gharehkhani et al., 2015).

Wood and non wood cell wall comprises cellulose, hemicellulose and lignin contents, whereas cellulose contaning polysaccharide having glucose (Pokhrel, 2010). Furthermore, cellulose primarly comprises several basic fibrils, very close to each others. Literature revealed that, these basic fibrils aggregated to form microfibrils with a diameter ranging from 10 to 35 nm (Chinga-Carrasco, 2011; Sixta, 2008; Abe & Yano, 2009; Donaldson, 2007). The term "microfibriller angles" abbriviated as MFA commenly used when microfibrils are distorted around the axis of their cell wall as illustrated in Fig. 2.2a (Barnett & Bonham, 2004; Wathen, 2006; Pulkkinen, 2010). Twisting of microfibrills producing a small fibril angle, which are important for tensile and folding strength of paper (Blomstedt, 2007; Courchene et al., 2006). Generally cellulose have a crystall structure and hemicellulose are non-crystalline or amorphous in structure having a strenght lower than cellulose, easily hydrolized and covered cellulose. A deatiled and comprehensive literature regarding the polysaccharides content in various fibre sources are available (Ebringerova et al., 2005; Sixta, 2008). After cellulose and hemicellulose, lignin is third cell wall component, having a glue contents and responsible for binding cell wal layers (Sutton et al., 2000). Lignin have a

hydrophobic behaviour in nature and easily detached during the chemical pulping and beleaching process. Fibre with a low lignin contents making it feaible and selective during paper making process. Cellulose, hemicellulose and lignin contents exists in various layers of fibre cell wall.

Cell wall further partitioned into different cell layers like, first layer is middle lamella, the sencond layer consists of primary cell wall, secondary wall is the third one layer and finally lumen (Sjöström 1993). The outer layer i.e. middle lamella is harder layer and acts as cementing agent to give protection due to higer lignin contents (Shafiei Sabet, 2013). Primary cell wall surrounded by middle lamella is characterized as a thin and flexible layer. Primary cell wall maily composed of hemicellulose and lignin and comprises a loosely bonded microfibrils with a random orientation. The third layer of the cell wall is secondary cell wall and positoned between primary cell wall and lumen and further classified in to three sperate and distint layers abbrivated as: S1, S2 and S3 respectively (Bergander & Salmen, 2002; Meier, 1962).

The study of literature review reported that S2 layer mostly consists of fibre mass ratio with MFA angle of 10-30^{o}, in contrast, the MFA angle for S2 and S3 are 50-70^{o} and 70-90^{o} with fairly horizental oriented micrfibrills (Blomstedt, 2007). The fourth and fianl inside layer of cell wall is lumen abrrivated as W, having a hollow core structure and capable of absorbing miosture in the form of water and vaopurs. Fibers having a larger lumen content having the ability to be flatten in a ribon shape during the pulping process leading fibre to a more strengthen properties.

Figure 2.1(a): Schematic fiber structure: consisting different layers of cell wall (middle lamella, primary and secondary cell walls (P, S1, S2, S3) and cell lumen (W)

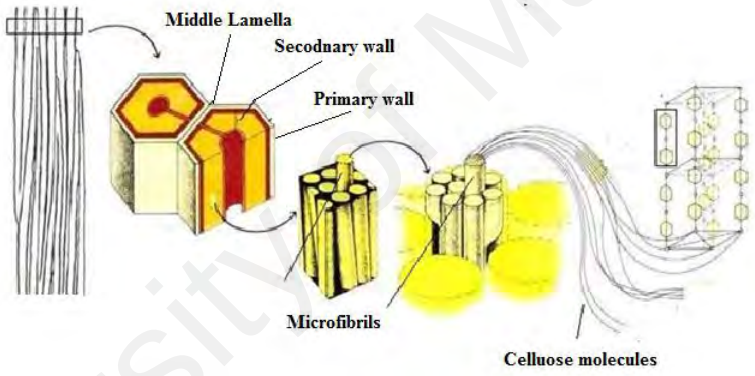

Figure 2.1(b): Febrile cell wall structure

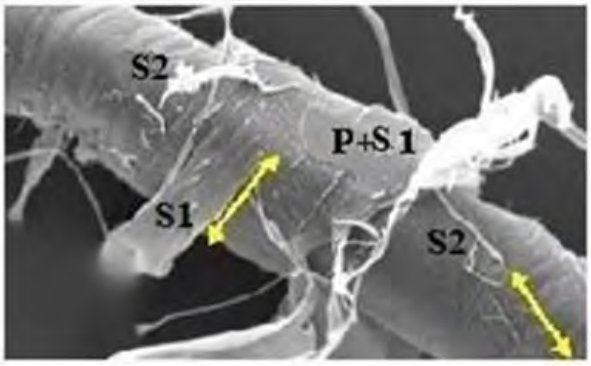

Figure 2.1(c): SEM morphological view of different wall layers

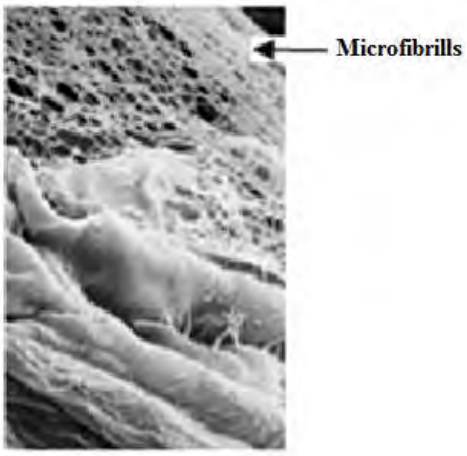

Figure 2.1(d): SEM photograph of microfibrils (Chinga-Carrasco, 2011; D. page, 1989a; Sixta, 2008)

Different pulping processes can be utilized for producing pulp from raw materials, depending upon the desired pulping processes including: mechanical pulping, chemical pulping (e.g., Kraft, Sulfite) and Chemi-thermo-mechanical pulping (CTMP). In mechanical pulping, mechanical energy was employed and mostly used for a good printing quality. In Thermo-mechanical pulping (TMP), pulps produced by a combined action of steam at higher temperature as well as mechanical process refining. Whereas, during chemical pulping almost pure celluloses produced by the application of combine heat and chemical treatments. Chemical pulping can further categorize into Kraft and Sulfite pulping, and produced by reacting fibre chips with a combination of salts of sodium hydroxide or sodiun sulfide. Sulfite pulp is obtained by treating various sulfurous acid salts and CTMPs are achieved by a combine action of both chemical as well mechanical pulping. The main advantages of CTMPs over other pulpinf processes is low requirement of mechanical energy, and the chemical pulping is achieved in a shorter time interval at relatively lower temperature resulting better strength. Among all types of pulping, the chemical pulping is the only pulping process yielding a higher pulp productions (80%). Whereas, literature data available for Kraft pulping in Europe revealed that only Kraft pulping yields a net amount of 65% of the total pulping yield (Abdul Khalil et al., 2012).

2.2 Suitability of wood Fibres

The main and primary source of cellulose fibres for pulp manufacturing process are the trees, and can be divided into two groups; softwood or coniferous, and hardwood or broadleaved. The wood and cell structures for these groups are very different and have a major effect on pulp properties. Nowadays softwoods are a main source of fibres for pulp and paper production and the common species are spruce, fir and various types of pine. Softwood mainly consists of two varieties of cell such as tracheids (fibres when liberated from the wood) and parenchyma (ray cells). Tracheids make up the majority of the wood (90 % or more by volume and about 98 - 99 % by mass) (Kokurek & Steven, 1983) and are the cells required for pulp and paper. Softwood consists of about 42 % cellulose, 27 % hemicellulose, 28 % lignin and 3 % extractives (Smook, 1992). They have an average length of about 3 mm depending on the species.

The wood grows quickly in spring which results a large diameter and thin walled tracheids and the opposite in the dry months which causes slow growth and yield, slightly smaller diameter, thicker walled tracheids. The relative proportions of early and late woods depend on the climate, species and age of the tree.

In order to get a high paper quality and other paper qualities blends of both softwood and hardwood (varying percentage of both hardwood and softwood) are necessary for fulfilling the demands for paper printing surface and the strength as well (Johansson, 2011).

One of the main important differences between hard and soft woods is their surrounding environment and the suitable climate in which the trees can grow up.Hardwood require less refining intensity and low refining for maintaining the fibre length as well as tensile stability as compared to soft wood. Furthermore, hardwood pulps have requirement of gentle refining and more energy in order to develop more strength as well (Johansson, 2011).

Hardwood structure is quite different from softwoods, with a variety of different cell types present. The fibres are generally shorter than those of softwoods (1mm average length) and are present in two different forms, libriform cells and fibre tracheids. Hardwoods exhibit seasonal growth patterns similar to softwoods, with early wood and latewood fibres present. Hardwood is made up of about 45 % cellulose, 30 % hemicellulose, 20 % lignin and 5 % extractives (Smook, 1992). Hardwoods are often used for papermaking because of their good formation properties, typical examples being ash, poplar and various eucalyptus species.

2.3 Physical properties of fibres and papers

Physical properties and dimensional constraints of fiber affect the sheet properties formed by them. The distributions of fiber dimensions, in particular the fiber length and fiber coarseness, are useful for pulp characterization and are often measured using optical techniques (Olson, Robertson, Finnigan, & Turner, 1995).

Fiber length is most commonly parameter which is used to describe the paper sheet properties (Jahan et al., 2010). An appropriate method for calculating the length of fibre is the application of average statistical lengths i.e. arithmetic or numerical length. The long fibers are more suitable for papermaking. Short fibers formed a denser sheet results a decrease in drainage on the paper machine and consequently an increase in energy requirements for drying.

In rare applications of paper making process, a reduced fiber length is more desirable effect in order to improve paper formation, leading an appropriate decrease in crowding number resulting of lowering flocculation behavior (Kerekes et al., 2001; Heinemann, & Fu, 2012; Kerekes et al., 2005). Furthermore, fibre shortening also resulting flocs formation smaller in size (Ramezani & Nazhad, 2005; Chen et al., 2012), therefore, producing a net desirable effect for making a smooth and uniform paper production. A comprehensive valuable detailed investigation were done regarding to a mutual

correlation between the length and the associated fibre paper properties (Seth & Page, 1988; Aittamaa, 2007; Richter et al., 1996).

The effect of fiber diameter, wall thickness and coarseness on sheet properties is rather complex and not clearly established. It has been reported that thick-walled fibers form the bulky sheets with low tensile and high tearing strength. Fibers with narrowest and most symmetrical wall thickness distributions yield the strongest sheets (Pulkkinen & Aittamaa, 2007).

Fibre-wall thickness plays a vital role during the paper properties, not only in the pulping process but paper making process as well. Thin cell-wall fibre has a tendency to collapse more easily than corresponding thick cell-wall fibre. Therefore, earlywood having thin walled fibres, will collapse easily during the process as compared to the latewood fibres, comprises thicker fibre-wall and also will remain the original shape in a larger extent. Figure 2.2, presenting a schematic layout of both earlywood and the latewood fibres and their capability of collapsing as well.

The extents of collapseness have large effects on the paper properties. Once fibre collapse it has a tendency to lead a network of much higher density and lower bulk, leading to a higher tensile, burst and compression strength as well as tensile stiffness and fibre elasticity. Furthermore, collapsed fibres tend to be more flexible in nature creating a higher surface area for bonding. Generally, fibre collapseness occurs in paper making and pulping process or during wet processing.

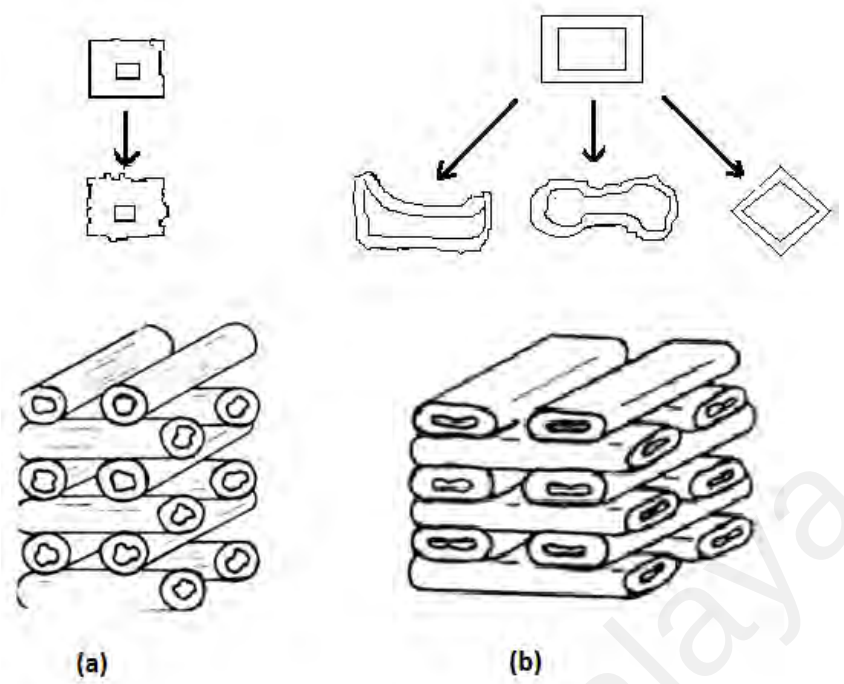

Figure 2.2: (a) Late wood with thick wall fibres maintain offer a less surface area (b) Early wood with thick wall with more surface area and build-up networks (Dutt & Tyagi, 2011)

Tensile strength measures the maximum force per unit width that a paper strip can resist before breaking when applying the load in a direction parallel to the length of the strip (Marin et al., 2009). Tensile properties of papers are affected by fiber length in a large extent. Moreover, tensile and tear index can be correlated with fiber wall thickness and coarseness (Pulkkinen, 2010). Decrease in fiber length often has negative effect on strength properties of papers (Tschirner et al., 2002). The tear strength decreases greatly with a reduction in fiber length. Coarseness also has significant effect on paper properties. Coarseness is defined as the mass per unit length of the fiber. The coarser fibers have thicker walls and lower specific surface area. Coarse and long fibers tend to produce higher tear and tensile resistance than fine fibers could do (Sridach, 2010).

The coarseness of filaments is generally expressed as denier. The coarseness of a wood fiber depends on its diameter, thickness, and density of its wall. Coarse fibers normally produce paper of higher permeability and have an enhanced capability of absorbing liquids (Duffy et al., 2000). Clarke and co-workers (1985) proposed a new definition of

coarseness based on the mass per unit projected area of fiber as measured by image analysis. The measured quantity is equivalent to the ratio of fiber coarseness and width and may therefore be considered as a measure of fiber grammage (I'Anson et al., 2006).

Another parameter that affects the quality of paper sheets is fiber bonding. Improving the bonding among inter connected fibres resulting an increase in indices values of burst and tensile (Main et al., 2015) as well as higher apparent density. Apparent density is related to Fiber bonding and flexibility. If the fibers are flexible the sheet will be compact with relatively little pore space. If the fibers are relatively rigid, the sheet will be porous, open and not well bonded.

Fibre flexibility factor plays a vital role in pulp optical and physical properties as well as paper properties such as: during the formation of paper and strengthening characteristics (forgaces, 1963; Fernando et al., 2011; Paavilainen, 1993; Peng & Johansson, 1996; Petit-Conil et al., 1994). Furthermore, fibre flexibility and collapse-ness factors leading to a closer contact among fires leading to a strong bond formation (Forsström et al., 2005; Lumiainen, 1990; Rusu et al., 2011).

The fiber bonding and total number of fibers involving in a sheet rupture having a desirable effect on paper tear index. Tear index is the energy required to propagate an initial tear through several sheets of paper for a fixed distance and expressed in g cm/sheet. Longer fibers can produce higher tear and tensile strength papers and decrease sheet density. In a weakly bonded fibre sheet, since more number of fibers withdrawn thus breaking in the tear zone, as tearing resistance strongly influenced by a more number of bonds that breakup lengthwise of fibers; thus fiber length has a strong influence on tearing resistance (Resalati, et al., 2010). It was found that flexible fibers form the sheets with more surface area. A very important effect of specific surface is its effect on drainage rate in the papermaking process. The higher the specific surface the slower the water will be drained from the sheet during its formation. It was reported

earlier that the fibre bending ability rises due to internal fibrillation, on the basis of fibre bendability, it was revealed that spruce fibres has a higher flexibility than that of pine fibres (Rusu, 2011).

Paper has often been referred to as a fibrous network. Micrographs of thin sheets and surfaces have provided some insight into the network structure of paper. The layered nature of paper structure has been observed for some time and more recent developments have enabled the assessment of the internal structure with respect to internal fiber orientation distribution. The quality of paper is limited by the properties of the pulp from which it is derived (Baptista et al., 2014; Gharehkhani et al., 2015).

The properties of the sheet mirror the properties of the pulp in many respects. The proportion of fiber types, their physical dimensions (length, diameter and coarseness), mechanical properties (strength and flexibility), optical properties (color and brightness), and chemical properties, are all important and influence the limit of similar properties in a sheet.

Literature review reveals that, wood fibres are one of the most common and earlier used raw materials for paper and pulp industries. In Malaysia, forestry remain a significant economic activity in order to fulfill the future demand of timber as well as pulp and paper industries and to increase pulp exporting demand as well. Sincere efforts have been done to establish the forest plantation in Malaysia. For this purpose, an area of one million ha land in Sarawak state has been reserved for the plantation forest by 2020 (Perkasa, 2009). Generally, Acacia mangiumis one of the main forest plantation species, whereas beside acacia mangium other species like Neolamarcki candamba, Eucalyptusspp and Paraserianthes falcate tree species planted in Sarawak, Malaysia as well. A survey established in 2006, regarding the Asian plantations exceeded more than 1.5 M ha in China, Malaysia, Indonesia, Thailand, Vietnam, Papua New Guinea, Philippines. Acacia mangium saplings can grow up to 5 m tall within a time period of 5

years and diameter increase of up to 5 cm per year (Ruskin, 1983). Because of its adaptability and fast growing rate, acacia mangium was selected for the plantation (Wahyudi et al., 1999; Yahya et al., 2010). In particular, the extreme vigorous growing rate, tolerance against highly acidic and soil having low nutrients as well as relatively free from disease are the advantages that make it more convenient to fulfill the present and future raw material demand of furniture, pulp and paper industries as well as conserve the natural forest (Fig. 2.2).

Figure 2.3: Acacia mangium pulp from Acacia mangium trees

The application of Acacia mangium is a relatively new from its short-fiber prospective in pulp market and observed close to eucalyptus particularly for applications in production of fine papers (Paavilainen, 2000; Hillman, 2003). Acacia mangium with small fiber dimensions make it more important particularly for printing papers.

Since the hard wood (A. mangium, Eucalyptus, Birch) fibers are short and thick in nature and having a low slenderness ratio which resulting the low tearing resistance. Therefore hardwoods fibres give better formation and are used in products require a smooth printing surface and high opacity. Unlike the hard wood, the soft wood (Pinus Radiata, Spruce, and Douglas Fir) fibers have longer length and high slenderness ratio, therefore, increase the strength properties of the papers. Moreover, the advantages of Hardwood pulps over soft wood are due to their ease of bleaching due to low lignin contents as compared to softwood.

Acacia hybrid is a clonal natural cross with Acacia mangium and Acacia auriculiformis. Hybrids have the potential to provide several benefits including fast growing plantation than their parent tress as well as environmental advantages are most dominant. It has the excellent capability to fix the ratio of atmospheric nitrogen and to improve infertile soil as well (Pinso & Nasi, 1992; Le, 2001).

Acacia hybrid has the advantage of more resistant to heart-rot disease, which grows dynamically and is one of the major industrial plantation species in Thailand, Malaysia and Indonesia. Moreover, hybrid tree has the growing rate of 8 - 10 m height and diameter of 7.5 - 9 cm with a time period of 2 years (Sein & Mitlöhner, 2011).

Converting the Acacia mangium hybrid trees into chips and finally into pulp is shown in figure 2.4.

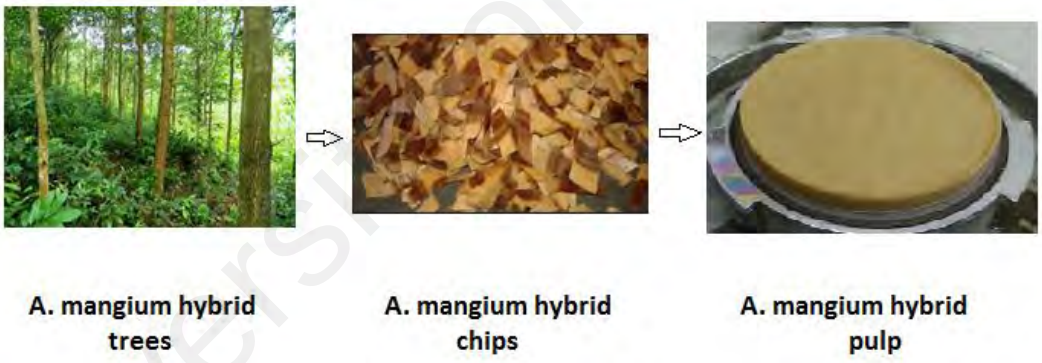

Figure 2.4: Acacia mangium hybrid pulp from Acacia mangium trees

2.4 Effects of the Pulp refining (beating)

A number of fundamental techniques for improving fibre quality have been employed to different types of pulps in order to meet future demand of better paper quality. One of the most important process have been carried out for stock preparation usually termed as "pulp refining" usually "beating “as well. During refining, the fibers are under the influence of forces like compression and shear yielding specific valuable changes in fibre characteristics. For a given pulp consistency (weight of pulp sample on the basis of

oven-dry fiber in 100 grams in a mixture of pulp-water) and specific refiner conditions, a varying fiber properties resulting fibre bonding at higher extent (Mohlin et al., 1995).

Nowadays, fiber modifications are desirable in order to get a special product. It can be done by the application of beating for obtaining the required properties. By a controlled beating process, the desired properties can be achieved successfully.Literature revealed that, fibre beating at different degree of beating producing a considerable change in fibre structure (Loijas, 2010; Oksanen et al., 1997; Page, 1989) including: fibrillation (External fibrillation and internal fibrillation), the fines production, fibre length shortening and fiber straightening as well.

Internal fibrillation due to beating effect of fibre layer is one of the most desirable effects and has been extensively studied by several investigators (Ingmanson & Thode, 1959; Kang, 2007). Delamination of both layers i.e. P and S1 layers due to cyclic compression force mechanism inside refiner (Haavisto et al., 2008). Due to the inward swelling tendency of wood pulps caused by fibre refining, leading the formation of a decreasing fibre lumen size (Mossello et al., 2010). During the beating process, it is speculated that delaminated layers during beating process are to be found a major obstacle against swelling, due to high fibril angle of S1 and the fibre hydrophobic nature. The elastic values of E-modulus decreases due to suppressing in fibre wall bending stiffness caused by decreasing effectiveness values of E-modulus. Internal fibrillation is the main cause responsible for altering the E-modulus.

Due to external fibrillation, a corresponding increases in the specific surface area of fibrils (Nugroho, 2012; Clark, 1969). Literature revealed that some specific kind of hydrophilic substance released by cell wall producing gelatinous layers functioning to enhance the inner fibre to fibre bonding observed to improve the fiber-fiber bonding and upon drying appeared as a thin film layer (Mou et al., 2013).

Another and most important effect of beating increases the amount of fines including some proportions of primary and secondary fibre cell walls having a smaller size around less than 0.3 mm (Heymer, 2009; Nugroho, 2012). Fine productions are characterized by higher surface area and therefore inner fibre bonding tendency can be improved, but having an adverse effect on drainage time. However, increase the degree of beating the fine production contents will be increased simultaneously (Zeng et al., 2012; Page, 1985).

Another undesirable impact during beating process is reduction of fiber length (Olson et al., 2003). Since, a mutual relation exists between the fiber cut and their corresponding fine production during refining process therefore, the problem faces during the perfect measuring of the fiber length (Batchelor et al., 1999). In order to avoid such a difficulty, it is necessary that fiber length reduction calculation on basis of length weighted average initially and finally after beating process. It is important that the change in length-weighted fiber may not entirely reflects the alterations of long fibers numbers per unit mass, since the average fiber length is influenced only by the formation of fine production in beating process (Batchelor et al., 1999).

Initially chemical pulped fibers are curly and after beating process it causes fiber straightening (Page, 1985; Mohlin & Alfredson, 1990). Literature review revealed that curl fibre has drainage resistance tendency mostly for all types of pulps and alternately a reduction in curl index values usually produced by the decreased in freeness values (Page, 1985). Fiber straightening is eminent factor and highly desirable for paper making properties. These advantages includes: increasing elastic modulus, paper tensile strength, enhancing load carrying capability and uniform stress distribution throughout the fibre network (Gärd, 2002; Hartler, 1995). The degrees of cellulose crystallinity are highly appreciated parameter for fibre crystalline structure. Increasing the degree of crystallinity causes the corresponding increase in paper tensile strength and paper

stiffness tendency and decreasing the chemical process (Chen et al., 2012; Tschirner et al., 2007; Yuan et al., 2013). Moreover, the swelling of fibre causes the degree of crystallinity during refining process. Increased degree of crystallinity decreases the adsorption of water on cell wall with increasing resistance to penetrate water through it. Research achievements confirm that increasing the degree of crystallinity resulting in a decrease in fibre swelling (Kongdee et al., 2004; Wan et al., 2011). Kočar and co-researchers (2004) investigated that crystallinity of pulp fibre commonly used in papermaking process in a range of 60-70%. Unbleached pulps containing some trace amount of lignin and hemicellulose resulting the increasing in degree of crystallinity (Leitner et al., 2013).

Research investigation concluded that during refining process, there is not significant change occur in the existing functional groups, however, a slight variation observed in the scattering of the surface chemical constituents (Penniman, 1992). Research investigated on the influence of beating on electrokinetic characteristics of fibers and concluded that as a result of beating, surface charge will be increased while, there is no significant influence on total charge (Bhardwajet al., 2004a; Bhardwajet et al., 2004b; Penniman, 1992; Herrington & Petzold, 1992).

Concluding the above studied literature outcomes cited throughout in present study, it is established that beating has a considerable effect on simultaneous changes on fiber structure and fibre properties. Since, the beating effects are desirable and may have either advantages or disadvantages for paper making, but it is accepted that beating have more beneficial effects on pulp improving quality as compared of the adverse effects. Figure 2.5 show typical PFI laboratory beating mill.

Figure 2.5: PFI laboratory beating mill

2.5 Freeness

The quantification of water contents in pulp suspension passing through a specified mesh screen mounted in a typical instrument called “Freeness” and one of the most important properties in order to monitor the occurred changes during the stock preparation as shown in figure 2.6.

Since the desired value of freeness is strongly dependent on fiber fibrillation tendency and fines formation, therefore, freeness testing is commonly carried out as an indicator of beating effects (Polan, 1993; Bhardwaj et al., 2007a).

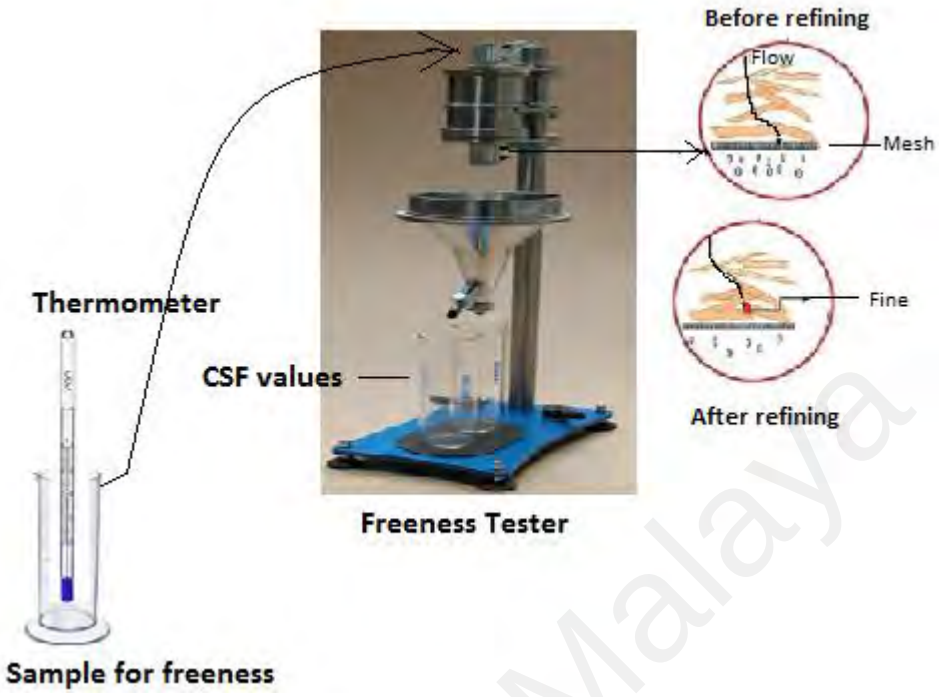

Figure 2.6: Schematic of measurement of CSF values

Beating results the swelling of fibre and therefore, fibers become flexible, leading to the fibers attached each other in knotted shape definitely making the formation of network during draining process. Moreover, during beating process the formation of fines created do not attached to the fibers being processed. Free movement of newly produced fines being trapped between fibers pores, leading to restriction of water flow way and reducing the water drainage as well (Hubbe & Heitmann, 2007; Paradis et al., 2002). Therefore, it is concluded that beating reduces the drain ability which is a major drawback during paper making process (Beg & Pickering, 2008; Gao et al., 2009).

One of the most widely and commonly used method for measuring pulp freeness in laboratory scale is Canadian Standard Freeness (CSF) [ml]. To measure the freeness of a given sample, the disintegrated pulp sample (3 g of pulp in 1 L of water) is decanted in the CSF chamber, passing to the attached (conduit) mesh. Water is allowed to be drained through vertical bottom and side orifice, where the volume collected through

side orifice is the desired freeness value. A higher CSF value corresponds to higher and quicker pulp drainage. Distilled water was used during the experiment for obtaining the purpose of higher accuracy. The obtained CSF values have to be correlated to the pulp consistency and pulp temperature accordingly to the standard tables (TAPPI, 1999).

Usually the pulps which are unrefined and unbleached softwood Kraft pulps, the standard CSF values are higher as 750 ml, whereas theses values drop down to 600-250 ml as a result of beating process (J. M. Genco, 1999; technology, 2001). The study of literature review reported the reduction in freeness values after beating process for wood and non-wood pulps (Bhardwaj et al., 2007a; Lumiainen, 2000; Nugroho, 2012). Moreover, it was also reported that at a fix degree of beating, pulps with a lesser Kappa number results in a lower degree of freeness (Gulsoy & Tufek, 2013; Rosli, et al., 2011).

2.6 Pulp suspension

Flow behavior of fiber suspensions remains one of the most complex and least understood in the industrial perspective. None of other Newtonian fluids is commercially pumped in huge volume except fibre suspension. Pulp concentration is one of the most significant parameter for pulp suspension. Flow range may be categorized like: low consistency (Cm = 0-5%), medium consistency (Cm = 5-20%) formed by mechanically pressing water from a medium consistency suspension and finally the consistency range above (Cm > 40%) fall in the range of ultra-high consistency (Kerekes et al., 1985). Research has been carried out regarding the existence of four different particles suspension phenomena of pulp (Duffy, 2006).

The Fibers/filament in the low concentration suspension is as the individual particles which can bend and absorb turbulent energy. Slightly increase in pulp concentration resulting to the limitation in fiber movements and existence of floccettes as the new particles. At the higher consistency these floccettes can entangle to each other to form entities called "floc". The last term is called network resulted from fibers in locked

status. Networks frequently take the shape of the vessel or conduit at the lower flow rates.

From the above mentioned pulp suspension behavior, the interface between fibers is the important parameter in suspension behavior. A number "N" proposed for the crowding number in order to explain the state of fiber interactions. It can be expressed as the number of fibers in a volume swept out by the length of a single fiber (Kerekes et al., 1985). The mass and volume forms of the N are presented in equation 2.1:

$$N = \frac{2}{3} C_v 2 \left(\frac{L}{d}\right)^2 \cong 5\, C_m \frac{L^2}{\omega} \qquad (2.1)$$

Where, *L* is the length-weighted average length of the pulp fibers; *Cm* is the mass concentration (%), and ω is the fiber coarseness (mass per unit length, kg/m). Whereas, the equation based on volume, the C, L and d, are the volumetric concentration, fiber length, and fiber diameter respectively.

Depending on the N number, if the values of N=1 is a critical concentration where below than this the suspension is considered as a dilute suspensions. At crowding number between 1 and 60, the suspension is semi-concentrated and at the value higher than 60, the suspension is concentrated (Fällman, 2009). Later on there was the introduction of another critical crowding number, N~16 named "gel crowding number" (Martinez et al., 2003). It is notable that in commercial papermaking, pulp suspensions are formed into paper by filtration in the range $16 < N < 60$ to minimize both water usage and flocculation (Derakhshandeh, 2011). It is stated that even a small amount of fibers can change the suspension properties significantly.

2.7 Rheology of pulp suspension

The rheological behavior of the water was changed when there was fibre in water. There is an increase in viscosity as a result of interactions between the fibers and hydrodynamic disturbance to the flow. It is notable that the behavior of the pulp suspension deviates from Newtonian behavior and the suspension can be shear thinning

or shear thickening. Furthermore, there might be time effects when the interaction forces between the particles are adjusted, causing thixotropy (Karppinen, 2014).

A typical rheogram for a pulp suspension is shown in Figure 2.7. Two stresses can be distinguished in the diagram. The yield stress, which is the minimum stress required to overcome the network stress of the suspension for generating the initial flow. Whereas, another stress labeled as "τ_D" is the magnitude of stress needed to fully disrupt the system to obtain turbulent flow (Bousfield, 2008). Between these two stress, the yield stress is arguably the most important rheological property of fiber suspensions (Derakhshandeh, 2011) as it has application in various fields particularly the flow of pulp through a circular pipe (Moller & Elmqvist, 1980) as well as pulp mixing operations (Sha et al., 2015).

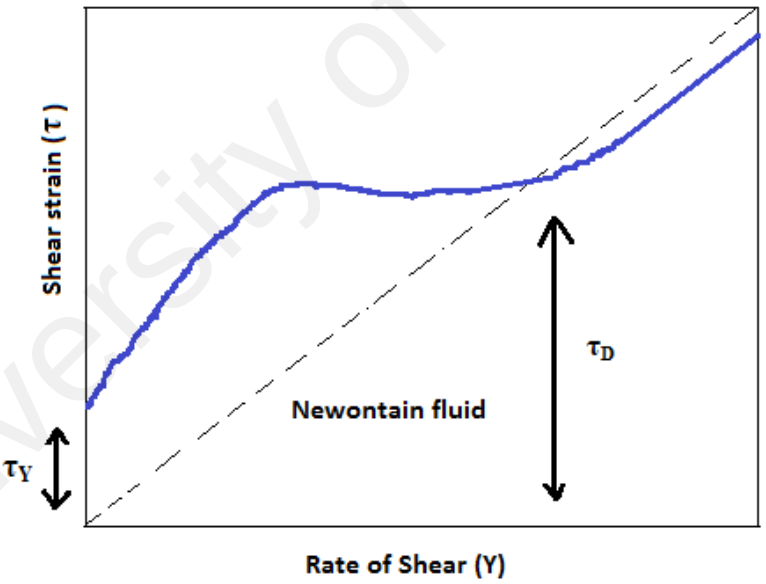

Figure 2.7: A typical rheogram for pulp suspension (Bousfield, 2008)

It is stated that the yield stress strongly depends on mass concentration by a relation presented in equation 2.2:

$$\tau_y = aC_m^b \qquad (2.2)$$

Where, τy presenting yield stress (Pa), both a and b are constants particular to the fiber type, and Cm denoting pulp suspension mass concentration in (%) (Kerekes et al., 1985). Moreover, research investigation reported that, the values of the constants *a* and *b* ranging from 1.18 to 24.5 as well as from 1.25 to 3.02 for commercial wood pulp fibers using a vane rotor (Bennington et al., 1990).

However, rheological characteristics are dependent mostly on pulp concentration, other factors such as fiber properties, fiber-fiber interaction, the co-existence of some other constituents in suspensions, temperature, shear forces, and shear history can change the rheology of pulp suspension as well (Derakhshandeh, 2011). Research has been reported that the effects of fiber properties on the pulp yield stress and evaluated it for a range of different species pulps, pulped in a differing approaches. They have reported that longer fibers resulting higher yield stress (Dalpke & Kerekes, 2005). Similar attempts have been done to associate the yielding stress values with a number of factors as; fiber length, concentration, and temperature. In another research is reported that increase in consistency resulting an increasing air fraction in the pulp fiber suspensions where the gas collects around the rotor, blocking the momentum transfer into the suspension (Ventura et al., 2007). According to the studies performed by Bennington et al. (1995), the yield stress depends on the fiber concentration and air content as correlated by equation 2.3:

$$\tau_y = aC_m^b(1 - \varphi)^c \qquad (2.3)$$

Where, φ is air volume fraction in the suspension (%) and the constants a, b and c are associated to the fiber properties (Sha et al., 2015). The pulp viscosity has been mentioned using capilliary rheometer (Bohlin RH 2000 Capillary Rheometer) Fig. 2.8.

Figure 2.8: Capillary Rheometer for measuring pulp viscosity (FIRM)

2.8 Flow of fibre suspension

2.8.1 Heat transfer and pressure drop of flow through tubes

The transfer of thermal energy to or from a solid interface and across thermal boundary layers has been the subject of numerous investigations. The published research literature related to these phenomena are examined in this chapter and critically reviewed. Particular emphasis is placed on the heat transfer to drag reducing fibre suspension and the frictional pressure losses using the flow of natural wood pulp fibres suspensions under the specified conditions.

A significant amount of work has been carried out in the study of heat transfer and pressure drop in order to generating data that have later been used as a basis for designing heat exchanger and cooling systems in industry. But the research requirement of that area is not over yet. The advancement of science and the rapid growth of problems emerging in industry have generated more avenues to continue research in this field.Empirical correlations are usually of greatest practical value for designing engineering purposes due to their simplicity.

The Darcy–Weisbach equation (Equation 2.4) can be used to calculate the energy loss due to friction in case of a Newtonian liquid flowing in a pipe:

$$H = f\frac{L}{D}\frac{u^2}{2g} \qquad (2.4)$$

Where, f is the Moody friction factor (Moody f_M), which is simply calculated by equation (2.5):

$$f_M = \frac{D}{L}\frac{g.H}{\left(\frac{1}{2}u\right)^2} = \frac{D}{L}\frac{\Delta P}{\left(\frac{1}{2}\rho u\right)^2} \qquad (2.5)$$

Apart from the Moody factor, the Fanning friction factor can also be used, which is defined by equation (2.6):

$$f = \frac{\tau_W}{\left(\frac{1}{2}\right)^2} = \frac{1}{4}\frac{D}{L}\frac{\Delta P}{\left(\frac{1}{2}\rho u\right)^2} \qquad (2.6)$$

It is well known that the friction factor depends on the Reynolds number (*Re*), and on the relative roughness of the pipe, ε/D. Based on these facts, a variety of equations have been developed for different regimes and pipe roughness ranges. For laminar and turbulent flows, the friction factors are calculated by the Hagen–Poiseuille and Colebrook and White equation equations (Colebrook & White, 1937) as presented by equations (2.7) and (2.8) respectively.

$$f = \frac{64}{Re} = \frac{64\,\mu}{uD\rho} \qquad (2.7)$$

$$\frac{1}{\sqrt{f}} = -2\log\left(\frac{\epsilon/D}{3.71} + \frac{2.52}{Re\sqrt{f}}\right) \qquad (2.8)$$

The Colebrook–White equation is valid for *Re* ranging from 4000 to 10^8 and values of relative roughness ranging from 0 to 0.05.

For convective heat transfer, Petukhov (1970) and Gnielinski (1976) developed correlations (Equations 2.9 & 2.10) based on the Nusselt number for fully developed turbulent flow in smooth and rough surfaced circular ducts.

{$0.5<Pr<10^6$}

$$N_u = \frac{\left(\frac{f}{8}\right)Re\ Pr}{1.07+12.7\left(\frac{f}{8}\right)^{0.5}\left(Pr^{\frac{2}{3}}-1\right)} \qquad (2.9)$$

Where, $4000 < Re < 5x10^6$}

{$f = (0.79 \ln Re - 1.64)^{-2}$}

$$N_u = \frac{\left(\frac{f}{8}\right)(Re-1000)\ Pr}{1+12.7\left(\frac{f}{8}\right)^{0.5}\left(Pr^{\frac{2}{3}}-1\right)} \qquad (2.10)$$

Where, {0.5 <Pr< 2000}

{$2300 < Re < 5x10^6$}

Martinelli (1947) proposed equation 2.11 as a correlation for full- developed turbulent flow in the fully-rough flow zone of a circular channel.

$$N_u = \frac{Re\ Pr\sqrt{\frac{f}{8}}}{5(Pr+ln(1+5Pr)+0.5\ ln\left(Re\sqrt{\frac{f}{8}}/60\right)} \quad (2.11)$$

2.9 Pressure study of fiber suspension flow

Pipe flow is a typical example of a fully developed flow used in papermaking processes. Due to the simple axi-symmetric geometry of a pipe flow, most experimental research has focused on this type of flow (Moayed, 1999). The earliest works on flow mechanisms of pulp suspension in pipes were presented by (Daily & Bugliarello, 1958; Forgacs, 1957) in which the flow behavior can divide in three different regimes: Plug, mixed, and turbulent. Further developments into this behaviour are given by (Duffy & Titchener, 1975; Duffy et al., 1976).

Duffy's outlines (Duffy, 1972) proposed for various regimes for chemically cooked pulps in terms of head loss-velocity curve for a consistency are shown in Figure 2.8. The letters used refer to points on the friction loss curve in Figure 2.9.

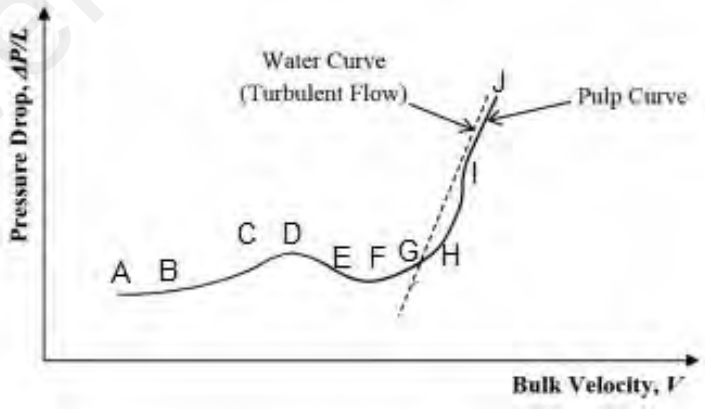

Figure 2.9: Typical friction loss curves for pulp suspension (Duffy, 1972)

Regime A to B

The weak shear stress due to low Reynolds number could not disrupts the fiber network, and therefore the suspension has pulg structure (Duffy, 1972). In this process, the turbulent energy of fibers is partly captured as the elastic energy of the network. This elastic energy manifests itself as an elastic force that pushes fibers towards the pipe wall. In this regime of low flow velocity, the elastic force is, however, large enough to keep the fiber plug in a contact with the wall.

Regime B to C

With increasing the velocity, a water layer would develop near the pipe wall (BC). In this region increase in velocity results in an increase in friction head loss. At point C, the laminar water annulus are formed.

Regime D to F

Region D to F corresponds to the plug flow with water annulus in laminar shear. This region characterized by the change in the head loss curve slop from positive to negative. Slightly before F, the point E is the onset of turbulence annulus.

Regime F to G

F to G region is attributed to the plug regime with water annulus in turbulent shear which is indicated as a change in the head loss curve slop from negative to positive. Point G is a unique point where the friction head loss of the suspension is same as water and corresponds to the onset of drag reduction.

Regime H to I

This region is known as mixed or transition regime. Point H shows the highest drag reduction which is the onset of plug flow disruption. The shear stress is bigger than yield stress and the fiber plug is only formed at the core and a turbulent annulus remains in proximity of the pipe wall. Research study showed that the thickness of plug in this

region is equal to the proportion of yield stress to shear stress times to pipe diameter (Moayed, 1999).

Regime I to J

Region I to J corresponds to the fully developed turbulence where the fibers are homogeneously dispersed in the suspension. In this region, the friction head loss curves are still below water curve. The transition from mixed flow regime into fully turbulent regime is gradual.

A schematic diagram of the flow behavior in the straight pipe according to the mechanisms described above and his new experiments were carried out to obtain more details of flow behavior of chemically released pine or birch pulps with consistency 0.52.0% by weight in a flow loop with pipe diameter of 40 mm as shown in figure 2.10 (Jasberg, 2007). Moreover, features of the plug flow by measuring the thickness of a lubrication layer based on the intensity of laser light reflected by fibers and showed that the thickness of the layer reduces with increasing the pulp concentration.

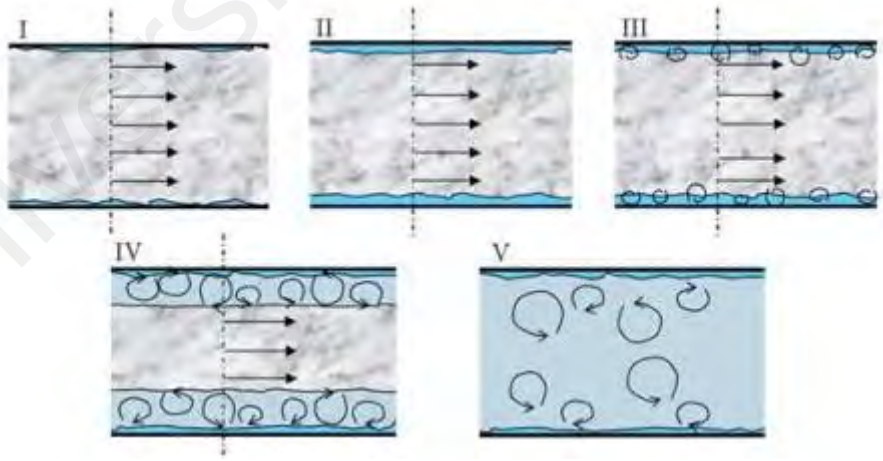

Figure 2.10: The main regimes of fully developed flow of fiber suspension. (I) Plug flow regime with direct fiber-wall contact, (II) Plug flow regime with lubrication layer, (III) Plug flow with a smearing annulus, (IV) Mixed flow and (V) fully turbulent flow (Jasberg, 2007)

Based on the results, it is proposed that the flow may be divided into five different regimes according to flow rate, namely plug flow with wall contact, plug flow with a

lubrication layer, plug flow with a smearing annulus, mixed flow, and fully turbulent flow.

2.9.1 Drag reduction

The drag reduction occurs when the pressure drop of a solvent–additive system is lower than the pressure drop of the pure solvent flowing at a similar flow rate (Duffy, 1972). Drag reduction phenomena can be described as any modification to a turbulent fluid flow system which results in a reduction in the normal rate of frictional energy loss and which leaves the resulting flow turbulent (a reduction in the wall friction where the shear in the boundary layer redistributed). This effect alters the nature and strength of the vortices formed, resulting in near-wall structural modification of the turbulent boundary layer (MacKenzie et al., 2014). A drag-reducing fluid has a value of D_R smaller than 1 (Duffy et al., 2000).

$$D_R = \left[\frac{\left(\frac{\Delta P}{L}\right)_{solvent-additive}}{\left(\frac{\Delta P}{L}\right)_{solvent}}\right] \qquad \text{at v = constant} \qquad (2.12)$$

2.9.2 Fiber- induced drag reduction

Kazi et al (1999) observed that the pulp slurries are one of the most consistent solid–liquid suspensions in which the drag reduction phenomena has been observed. Fundamentally, it is important to investigate the drag reduction in the fiber slurry to gain insight into pulp suspension turbulence. Studies of the drag reduction behavior of pulp slurries have been revealed that the existence of fibers and flocs results in turbulence damping (Amin et al., 2014; Luettgen et al., 1991). Addition of fiber to the suspension increases the pseudo-viscosity of slurry, providing more transport of the momentum without Reynolds stresses and consequently more drag. In fact, during transition from

plug flow to fully developed turbulent flow, the momentum transfer is enhanced by interlocking fibers in the network core, which behaves like a solid continuum, on the other hand, momentum transfer is reduced by fibers and flocs that have a damping effect on turbulence, thereby decreasing transfer rate. Momentum transfer enhancement will thus be dominating at low flow rates, while fiber damping will dominate at higher flow rates (Fällman, 2009). The competition between these two mechanisms result in maximum level of drag reduction at intermediate flow rates as was found by Duffy & Lee (1978). It has been stated that the changes in turbulence mechanisms induced by fibers occur in the turbulent core, not at or near the wall as fibers tend to migrate away from the wall and are not generally present there (Lee & Duffy, 1976; Vaseleski & Metzner, 1974).

To obtain a net reduction of drag, fibers must reduce turbulent momentum transfer without increasing other forms of momentum transfer (MacKenzie et al., 2014).

Moller and Duffy (1978) have proposed an empirical correlation (Equation 2.13) for the fractional drag reduction where it is applicable in a region between the commencement of drag decline and the maximum level of drag reduction.

$$\tau_W^* = \frac{\tau_W^3}{(1-\Lambda)\tau_W^2+\Lambda\tau_D^2} \qquad (2.13)$$

Where, τ_W, τ_W^* and τ_D are the wall shear stresses for the pulp suspension and for water for a given flow rate and the wall shear stress at the onset of drag reduction respectively. Λ is the maximum fractional drag reduction (Jäsberg, 2007).

It has been reported that the drag reduction can be obtained by adding enough amount of fibers with aspect ratio (fiber length / fiber diameter) > 30. Several researchers (Lee & Duffy, 1976; Vaezi et al., 2014) have observed the drag reduction increases with a

decrease in fiber diameter for the fibers with same aspect ratio (Bobkowicz & Gauvin, 1965).

Kazi and his research group members experimentally studied the drag reduction of fiber suspension over a range of velocities, concentration, fiber properties (flexibility) and some processes involving the pulping and paper making (e.g., bleaching and beating) (Duffy, 2006 and Kazi et al., 2014b). They conducted the experiments based on the various concentrations of bleached kraft pulp for pipe flow (0.05, 0.1, 0.3 and 0.4 %) and at varying velocity ranging from 0.26 to 1.3 m/s. Results showed the drag ratio of 0.92 for 0.4 % pulp consistency at the velocities higher than 1 m/s. Results stated that more drag reduction is achievable with fibers having more Coarseness. Moreover, they postulated that fiber flexibility and population are delicate fibre properties which affect turbulent eddy interactions and hence influencing the frictional losses in pressure drop characteristics of fibre suspensions.

2.10 Heat transfer study

Pressure loss behavior of fiber suspensions have been studied extensively by many researchers. However a few works have focused on the heat transfer characteristics of the pulp slurries. Middis and co-researchers who studied heat transfer properties of fiber suspensions containing the wood fibers and nylon filaments with different degrees of stiffness and aspect ratios flowing in the 25.3 mm ID horizontal brass pipe with constant ΔT (Middis et al., 1994).

They had given their main attention to fiber concentrations of more than 2% where fibers entangle and form network structures. The heat transfer ratio (heat transfer coefficient of fiber/heat transfer coefficient of water) for short fibers increased with velocity up to 3.5 m/s and then remained constant at higher velocities. At low velocities the heat transfer ratio tends towards unity. Some heat transfer enhancement was seen for the long-fiber runs at low velocities and high concentrations. They stated that the Nylon

fibers did not form a strong plug due to their low network strength and thus the fiber wall interaction was feeble. The trends for the heat transfer and pressure drop ratios were similar although the magnitude of the heat transfer ratio was generally slightly less. At low velocities, heat transfer reduction of up to 40% was observed. The crossover from heat transfer enhancement to reduction appeared to correspond to the point at which a water annulus formed around the fiber plug. This can be seen from the wood pulp fiber data as a local maximum in the pressure drop ratio results. They observed that the wood pulp fiber data showed regions of both heat transfer enhancement and reduction. The heat transfer ratio for Nylon fibers almost always lay below unity over the range of velocities, 2-10 m/s.

The heat transfer reduction for the nylon fibers was much less than those for the pulp when $u > 1$ m/s. They observed that the nylon fibers have a thermal conductivity about two/three times greater than that of wood pulp fibers. The higher conductivity may offset some of the heat transfer reduction as a result of the increased thermal conduction within the fibers themselves. They reported that at low fiber concentration (0.03 %) and high bulk velocities (3-10 m/s) some heat transfer enhancement for suspensions which had the same pressure drop as water. They stated that for Nylon fibers at low aspect ratios $r < 60$ the pressure drop and heat transfer coefficients of the suspensions were similar to those for water. The differences are due to the turbulence damping effect of the fibers. They reported that the frictional pressure drop ratio (suspension/water) and heat transfer coefficient ratio curves (suspension/water) were shifted to higher values with the increase of velocities at increased concentrations. This effect shows similar trends both in nylon and wood pulp fibers. In a conventional flow of fluids, there is a correlation between momentum transfer and heat transfer, and it would be estimated that fiber suspensions would modify the mechanisms and transfer rates as well. It is observed that the various mechanisms causing changes in momentum transfer also

affect heat transfer. The h_C values are altered with the variation of flow velocity, concentration of fiber (population), length, flexibility, coarseness (mass per unit length), surface topography and the amount of fibrillar fines present in the suspensions (Fallman, 2009 and Kazi et al., 2015).

The extensive works on the heat transfer of low concentration pulp slurries (< 0.4) have been done experimentally in both pipe and annular pipes, stated that the measurements of pressure drop and heat transfer coefficient are closely related (Gulsoy, 2013; Kazi et al., 1999 and Duffy, 2006). They conducted a series of experiments on the pulp slurries containing the fibers obtained from different sources (different parts of the same tree) and different processes (chemical treatments, mechanical refining at different levels, thermomechanical treatment, bleaching etc.) with fiber characteristics as: fibre length, fibre flexibility etc. Their observations are stated and discussed in the following paragraphs.

Research studies reported that the effect of entrance length of the closed conduit flow on the heat transfer to pulp suspensions which is defined by the length of the conduit from the entry to the point where the fully developed flow begins (Jasberg, 2007; Kazi et al, 2014a and Hartler, 1995). The results showed that change in entrance length does not have any significant effect on the heat transfer coefficient of the fiber suspensions (Kertas, 2013; Kocurek & Stevens, 1983 and Johansson, 2011).

Fiber suspensions flow at low consistency provides data with little variation whereas at higher consistency heat transfer coefficient data provides some variations but the trend remains similar for both short and long entrance lengths in the test section. At a specific velocity of 0.3 m/s, 0.4% fiber produced 52 % higher hc than water and 44 % higher than fiber suspension at low concentration (0.2 %). However at velocity 0.3 m/s and concentration (0.2 %) h_C values are 5.8 % higher than that of water. At 0.2 m/s water, Pinus radiata high coarseness fiber of 0.2 % and 0.4 % concentrations show 1.765,

2.471 and 3.177 kW/m^{2}K values of h_C (Kazi et al., 2014a). It was investigated that the extent of the heat transfer coefficient was above water at same experimental settings at very low fiber concentrations, but gradually decreased till it approaches below the water at somewhat higher concentrations. It should be noted that the results reported by (Kazi, 2001) are related to turbulent flow only. For the laminar flow, Middies and co-researchers reported that fiber suspensions exhibit a higher heat transfer coefficient than water alone at low flow rates where plug flow exists. The fibers in the thin annular layer around the plug are now modifying the heat transfer rate and consequently the magnitude of the heat transfer coefficient. Thus the region of heat transfer augmentation resembles to the plug flow in hydraulic transportation in a pipe. At elevated velocities the heat transfer coefficient for pulp suspensions is lower than that of water at the same flow. They said that the suspension at higher velocities behaves more like a continuum whereas at low velocities the various factors causing a deviation in ratio are due to the plug-like nature of the fiber suspension. Generally, it was observed that at every point of velocity, there is a highest degree of h, at lowest fiber concentration. At very low concentrations of fibre suspension there is significant enhance in heat transfer coefficient but hc values gradually approaching the water values at an increased concentration of fiber suspension. Whereas, at higher fibre concentrations the magnitude of hc values for suspensions obtained are below the water data. Comparing these results to the different research work, almost related results were achieved by previous researchers (Kazi et al., 2015).

Heat transfer to fiber suspensions decreases with increase of fiber flexibility and decrease of freeness degree. The heat transfer coefficient of 80% and 81% of water has been reported for softwood fiber suspensions with two level of freeness (200 and 500 CSF) at 0.4 m/s velocity respectively. In the same freeness degree, the decrease in heat transfer was more sensible where the suspension was containing the more flexible fibers

(thermomechanical fibers) (Kazi et al., 2015). Increases in flexibility and decrease in freeness are the results of beating process, so it is logic to expect that beating results in a heat transfer coefficient reduction. It has been reported that for the three medium densities fibre board (MDF), significantly a lowering in the hC values were evaluated where a more refining energy is applied in order to make a more flexible tendency of MDF. At a velocity of around 0.4 m/s, a lowering of heat transfer coefficient values for low, medium and high MDF are almost 3.3 %, 19.9 % and 25.1 % of water were recorded. Nevertheless, increasing the velocity, an increase in amount of hc values were observed following the same trend (Kazi et al., 2015).

There is a hypothesis that *hc* can be inter-related with the fiber and paper properties and the heat transfer to fiber suspensions can be utilized as a tool for the characterization of the papermaking pulps (Duffy et al., 2000). Once values of hc are associated to theacceptable qualities for paper production, then this could be used as a pulp quality parameter or indicator. However, this question remains that to what extent the diversity in the properties of fibers used in industries resulted from different pulp sources and pulping processes, could affect the characterizations and correlations.

In the case of fiber length, the general trend is that decrease in fiber length causes a decrease in hc. Fiber length can be presented (based on the shape of the fiber cross section) by the aspect ratio (L/D) or equivalent aspect ratio (L/(2*(W+T)). Equivalent aspect ratio is used for the fibers with rectangular cross section where W and T are the fiber width and fiber wall thickness.

The data reported for fiber stiffness (inverse fiber flexibility) versus heat transfer coefficient stated that the fiber stiffness quality strongly influence in the modification of *hc*. It is reported usually that the increase fibre coarseness a corresponding increase in hc values (Lee & Duffy, 1967b; Kazi et al., 2015 and Moayed, 1999).

Various fibers result in the papers with different properties. Research work done for correlating heat transfer coefficient to paper making quality (sheet density 700 kg/m^3) (Nugroho, 2012 and Page, 1989). The results presented as the paper specifications (e.g., tensile index, tear index, burst index, stretch, scattering coefficient and formation index) against the values of heat transfer coefficient of the fiber suspensions and an almost linear relationship obtained based on the graphs.

Wood fibre forms viscoelastic fibre suspensions which are adhesive in nature causing the formation of adhesive flocs having a unique flow different from other slurries. At higher concentration and low flow rates, the ability of the fibres to entangle and flocculate due to their high aspect ratio results in a structured suspension. The adsorption of fibre at low flow rates on the inner pipe wall cause stains on metals surface, leading to the metal corrosion, when fibre are processes chemically. The formation of metallic corrosion products on inner pipe surface have a low thermal conductivity and interrupt heat transfer mechanism. Therefore, it is necessary to inhibit the already deposited corrosion products by the application corrosion inhibitors. In the present research work, Quinzoline Schiff base compounds were employed as organic corrosion inhibitors for the mitigation of corrosion product formed due to sticky fibre adsorption at metal inner surface.

2.11 Electrochemical nature of corrosion

Most of the electrochemical corrosion processes are in aqueous environmentscontaining aggressive species. The general oxidation-reduction reaction for corrosion process at the metal/solution interface in electrochemical environment is presented by equations (Jones 1996; Sastri 1998 & Roberge 1999).

$$M(s) \longrightarrow M^{n+}(aq) + ne^{-}(s) \qquad (2.14)$$

The corresponding cathodic reaction occurs at the cathodic sites (C) at the metal/solution interface:

$$R\ (aq) + ne^{-}(s) \longrightarrow R^{n-}\ (aq) \qquad (2.15)$$

The species R is an oxidizing agent in solution that can receive electrons from the metal. In the corrosion process, all the electrons produced by the anodic reaction move through the remaining sound metal to the cathodic site and are accepted by the oxidizing agent. The overall reaction of the corrosion process can be given by:

$$M(s) + R\ (aq) \longrightarrow M^{n+}\ (aq) + R^{n-}(aq) \qquad (2.16)$$

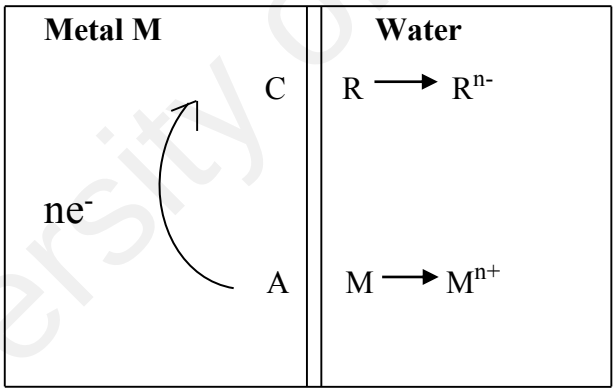

Figure 2.11: Metal dissolution in water containing an oxidizing agent R.

Fig. 2.11 represents a short-circuited galvanic cell at the metal surface. In the presence of excess oxidants, dissolution of metal ions continue leading to a spontaneous reaction and the equilibrium for R(aq) I Rn^{-} (aq) generated are less negative than M(s) and Mn^{+} (aq).

2.11.1 Anodic reaction

The anode is the site at which metal is corroded i.e. at which metal dissolution takes place. Metal is dissolved and transferred to the solution as metal ions. Positively charged atoms of metal detach themselves from the surface and enter into the solution or electrolyte as ions. The electrons flow, as electrical current, to the cathode where they are consumed. This process is known as oxidation (Roberge 1999).

The detached positive ions bear one or more charges. For example in the corrosion of zinc, each Zn atom releases two electrons and the Zn ions will carry two positive charges. The electrons travel through the metal to the cathode area by the following reactions:

$$\text{Metal} \longrightarrow \text{Metal ions} + \text{electrons} \qquad (2.17)$$

$$M \longrightarrow M^{n+} + ne^{-} \qquad (2.18)$$

2.11.2 Cathodic reaction

Electrons reach the cathode by passing through the metal. At a cathode they may discharge, for example, H^+ ions present in acid electrolytes, forming hydrogen gas. This process is known as reduction. In reduction, electrons are consumed. Thus, a cathodic reaction is a reaction that consumes electrons (Roberge, 1999; Baeckmann et al. 1997).

When proton reduction occurs, the concentration of hydrogen ions in electrolyte decreases and thus this increases the alkalinity of the electrolyte in the area of cathode.

2.12 Common methods of corrosion prevention

In most industrial application it is almost impossible to "prevent or stop' corrosion. General, the strategies are carried out in order to mitigate or inhibit corrosion rate to an economically ecological level. Some important corrosion mitigation techniques are as follows (Shreir et al., 1994):

2.12.1 Selection materials and design

Selection of the materials for a particular working environmental parameters including: solution chemical composition, operating temperature, pH, flow velocity etc., considering the physical mechanical and physical, availability, proper method of fabrication as well as the overall cost of component or structure. The general relation between the rate of corrosion, the corrosivity of the environment, and the corrosion resistance of a material is represented by equation (2.19):

$$\text{Rate of corrosive attack} \approx \frac{\text{Corrosivity of the environment}}{\text{Corrosion resistance of metal}} \qquad (2.19)$$

For a given corrosion resistance of the material, as the corrosivity of the environment increases, the rate of corrosion increases. For a given corrosivity of the environment, as the corrosion resistance of the material increases, the rate of corrosion decreases. Often an acceptable rate of corrosion is fixed and the challenge is to match the corrosion resistance of the material and the corrosivity of the environment to be at or below the specified corrosion rate. Often there are several competing materials that can meet the corrosion requirements, and the candidate material provides the most economical solution for the particular service.

Consideration of corrosion resistance is often as important in the selection process as the mechanical properties of the alloy. A common solution to a corrosion problem is to substitute the alloy with another alloy having greater corrosion resistance. It is very important and critical to decide whether or not the application of expensive corrosion-resistant metal or alloy is more economical than a cheaper relatively low corrosion-resistance metal that requires shielding or possible successive replacement. The application of rational design principles can eliminate many corrosion problems and greatly reduce the time and cost associated with corrosion maintenance and repair.

In order to minimize or suppress corrosion, it is necessary avoid geometrical structures that assist corrosive conditions like: (a) The equipment structure facilitates the trapping of dust, dirt and water; (b) The presence of crevices and locations where deposits accumulates on metal surface; (c) To avoid such a design leading to erosion-corrosion or to cavitation destruction in flowing streams systems; (d) Designing of the isolated areas that cannot be re-protected, e.g. by maintenance and painting; (e) Designs in such a way that leads the accessibility to heterogeneity in the metal or in the surrounding environment.

A) Must elude the metal to metal or a non-metallic contact promoting corrosion: such as a bimetallic couple or metal in contact with absorbent or hygroscopic materials containing humidity or moisture conditions as well as to avoid the contact with substances having a tendency off corrosive vapors.
B) Avoid circumstances that leading to stress, fretting or fatigue or fretting corrosion.

2.12.2 Shifting the interfacial potential

Cathodic protection of metal by altering the interfacial potential to adequately negative values either by: sacrificial anode or by impressed current, i.e. by cathodic protection. Metal protection by the surface passivation (formation of a protective film on the metal surface) in order to ensure metals passivate in the corrosive environment under consideration

2.12.3 Protective coating

Coatings for corrosion protection can be divided into two broad groups: metallic and nonmetallic (organic and inorganic). With either type of coating the intent is the same, that is, to isolate the underlying metal from the corrosive media.

2.12.3.1 Metallic coatings

The concept of applying a more noble metal coating on an active metal takes advantage of the greater corrosion resistance of the noble metal. An example of this application is tin-plated steel. Alternatively, a more active metal can be applied, and in this case the coating corrodes preferentially, or sacrificially, to the substrate. An example of this system is galvanized steel, where the sacrificial zinc coating corrodes preferentially and protects the steel.

2.12.3.2 Organic coatings

The primary function of organic coatings in corrosion protection is to isolate the metal from the corrosive environment. In addition to forming a barrier layer to stifle corrosion, the organic coating can contain corrosion inhibitors. Many organic coating formulations exist, as do a variety of application processes to choose for a given product condition.

2.12.3.3 Inorganic coatings

This includes porcelain enamels, chemical-setting silicate cement linings, glass coatings and linings, and other corrosion resistant ceramics. Like organic coatings, inorganic coatings for corrosion applications serve as barrier coatings. Some ceramic coatings, such as carbides and silicides, are used for wear-resistant and heat resistant applications, respectively.

2.12.4 Changing the environment

Following are the possibilities for the corrosion protection to be monitored.

i) For an aqueous corrosion systems, making the availability of lesser aggressive environment by eliminating constituents or modify the conditions that facilitate corrosion process by: decreasing the environmental temperature, reducing the flow velocity, prevent contact of water and moisture, taking away the dissolved O_2 and increasing the pH (in the case of steel).

ii) In the case of atmospheric corrosion, make sure the possibility of suspended solid elimination and dehumidification of air contents.

2.12.5 Addition of inhibitors

Corrosion processes are mitigatied in the form of metallic corrosion reduction rate by the addition of a chemical compounds or additives to the solution incontact with the investigated metal surface (Uhlig 2000). Generally, the corrosion inhibition caused by the formation of a protective film in-situ by reaction with the available corroding electrode surface. As a result, either anodic and/or cathodic corrosion reaction rate is diminished. Normally, only a minute amount of inhibiting materials are needed to be effective (e.g. ~10^{-4}M). Corrosion inhibition is reversible process and optimum concentrations of the inhibiting compound are generally required for maintaining to inhibit the surface film. However, a proper circulation without any obstruction and presence of any stagnant-free areas are also required to maintain inhibitor concentration. According to the definition of corrosion inhibitor, the chemical compounds or additive, when added in small quantity to an aggressive environment, causes an efficient reduction corrosion rate. The inhibition efficiency of an inhibiting compound may be expressed as:

$$\text{Inhibitor efficiency (\%)} = 100 \text{ X } \frac{(CR_{uninhibited} - CR_{inhibited})}{CR_{uninhibited}} \qquad (2.20)$$

Where, $CR_{Uninhibited}$ and $CR_{Inhibited}$ represent the corrosion rates of the uninhibited and inhibited system.

Generally, it was observed that the efficiency of an inhibitor was found to be increased by increasing the inhibitor concentration (for a typical effective inhibitor would give 95% inhibition at a concentration of 0.008 % and 90 % inhibition efficiency at a concentration of 0.004 %). Table 2.1 presents some inhibitors that have been used with

success in typical corrosive environments to protect the metallic elements of industrial systems.

Table 2.1: Some commonly used inhibitors for protecting some corrosive systems

Inhibitors	Metal	System	Concentration
Acids			
Ethylaniline	HCl	Fe	0.50%
Mercaptobenzotriazole (MBT)	..	..	1%
Rosin Amine + Ethylene Oxide	..	..	0.20%
Phenylacridine	H_2SO_4	..	0.50%
Thiourea	Others	..	1%
H_2O			
$NaNO_2$	Fe	..	0.50%
NaH_2PO_4	Fe, Zn, Cu	Boilers	10 ppm
Polyphosphate	..	..	..

A synergistic effect are always exists between different inhibitor the surroundings environment is to be controlled, and mixtures are the common choice in commercial formulations.

There are a variety of chemical compound that exhibits the inhibition properties, but of these, only a very fewer are considered in practice applications. This is due to the desired properties being an inhibitor usually exceeds beyond those which are simply associated to metal protection. Basis for the considerations of the compounds as effective inhibitors are: the availability and cost, their toxic properties, ease of extraction methods and environmental friendly behavior are considered importantly.

Still the susceptibility for synergism exists if the system contains a mixture and the presence of two or more alloys in the system, therefore the selectivity of especial designed mixtures are necessary. As the inhibitors are commonly used for circulatory systems, therefore, the depletion of inhibitors is usually too high for commercially feasibility. Both inorganic and organic compounds are employed as most effective and can be employed as industrial scale inhibitors, but most of them are toxic in nature like: chromate, arsenic and hydrazine etc. therefore, their applications have been limited by some environmental regulations organizations.

2.12.6 Inhibitors classification

Inhibitor consists of chemical capable of reacting with metallic surface, or the surrounding environment in which the surface is exposed to providing adequate level of protection to the exposed surfaces. The working mechanisms of Inhibitors are simple by the virtue of adsorption on the metallic surface and leading to the metallic protection by the formation of protective layer. Inhibitors reduce the rate of corrosion either by: altering the anodic or cathodic polarization tendency by means of Tafel slopes or by suppressing the ionic diffusion to the metallic surface and/or improving the electrical resistance between the metallic surfaces. Inhibitors have been classified the inhibitors on the basis of their differently chemical functionality as:

a) Inorganic inhibitors mostly consist of crystalline salts such as: sodium chromate, phosphate, or molybdates. Metal corrosion reduction rate is only influence by the presence of negatively charged anions of these compounds. For example, then sodium is replaced by zinc ions, the replaced ions improve the corrosion resistance and beneficial to employ as corrosion inhibitor. The resulting compounds after the addition of zinc ions are referred as mixed-charge inhibitors.

b) Organic anionic including: sodium sulfonates, phosphates, or mercaptobenzotriazole (abbreviated as: MBT) are commonly used corrosion inhibitors particularly in cooling water systems and antifreeze mediums.

c) Organic cationic appeared either in liquids or semi-liquid wax type solids. The active constituents of these compounds are generally larger aliphatic or aromatic chain compounds along with positively charged functional group like amines.

One of the most frequently occurred industrial problems are the corrosion attack on different metals and alloys particularly exposed in different acidic media containing aggressive species of varying quantity. The commonly used acids solutions for different process like: acid pickling, scale and surface cleaning, scaling inhibition and etching of metals are hydrochloric acid, sulphuric acid, nitric acid, hydrofluoric acid, citric acid, formic acid, acetic acid, in particularly hydrochloric acid, extensively used in the pickling baths because of its easy economic regeneration from the depleted pickling solution. An enormous amount of money wasted every year due to the metallic corrosion, and an estimated economical loss of 276 USD or an equivalent to 3.1 % GDP of USA (Gerhardus et al., 2002). Research has been proved and predicted that with an appropriate corrosion preventing technology and techniques, it was roughly estimated that about 25 to 30 % SDP loss could be avoided (Gerhardus et al., 2002).

2.13 Corrosion inhibitor

A corrosion inhibitor is a substance which when added in small quantities to a corroding medium brings about an appreciable reduction of the corrosive action. One of the most economical and effective way for the reduction of rate of metallic corrosion is the addition of inhibitors; even a minute amount may affect a net decrease in corrosion rate (Benabdellah, et al., 2006; Raja & Sethuraman, 2008; Wang et al., 2003; EL-Etre, 1998; Ahmed, 2006; Roberge, 2000). A number of factors must be considered for an appropriate selection of a proper inhibitor including; the extraction or processing cost

and amount of the inhibitors being selected, long time persistent hazardous and toxic effects on the surroundings and living species, easily availability and stability in aggressive environment with easier extraction methods. Moreover, the selection of suitable inhibitor depends on the type of acid, its concentration, temperature, flow velocity, the presence of dissolved inorganic or organic substance and type of metallic material exposed to the acid solution.

2.13.1 Organic inhibitors

Literature review reported that a variety of organic compounds could be employed as efficient corrosion inhibitors for acid pickling process (Abdulrahman et al., 2011; Mernari et al., 1998; El-Achouri et al., 2001). The occurrence of heteroatoms such as phosphorus, nitrogen, sulfur, oxygen having a higher electron density ability and the co-existence of double or triple bonds in their structures are responsible for making these organic compounds are effective corrosion inhibitors because of their high adsorption tendency towards d-orbit of metals (El-El-Maksoud & Abd, 2002; El Achouri et al., 2001; Khaled, 2003; Abdallah, 2002). However, the compounds consisting both nitrogen and sulfur in their structure were found to be more resistant to corrosion inhibition as compared to those compounds whose structure only have nitrogen or sulfur (Behpour et al., 2009; Kardas & Solmaz, 2006; Solmaz et al., 2008). Moreover, is it reported that organic compounds comprising sulfur only having the ability of stronger corrosion inhibition in comparison to those containing nitrogen only (Obot et al., 2009). These organic compounds being selected on the basis of above discussed feature perform as corrosion inhibitors by the mode of adsorption and forming protective film at liquid/metal interface. They inhibit the corrosion rate by (a) slowing the anodic and/or cathodic reaction (b) slowing the diffusion of aggressive species to the metal surface and (c) decreasing the electrical resistance of the metal surface.

A general chemical reaction for the adsorption phenomenon of organic inhibitors at themetal/solution interface takes place through the isolation of water molecules by organicinhibitor molecules followed by the following reaction (Solmaz et al., 2011).

$$O.I_{(soln)} + XH_2O_{(ads)} \longrightarrow O.I_{(ads)} + H_2O_{(soln)1} \quad (2.21)$$

Where, O.I (soln) and O.I (ads) denoting the presence of organic inhibitors in aggressive solution and being adsorbed on metal surface, and X showing the number of water molecules displaced by the inhibitor after the addition of inhibitors.

Nowadays, the employment of hazardous and toxic material being a corrosion inhibitors have been limited by the United States environmental protection agency (EPA), department of transportation (DoT) and occupational safety and health administration (OSHA) as a serious environmental threat, therefore, the applications of green corrosion inhibitors becoming more important due to their environmentally friendly aspect and ecological nature as well (Ostovari et al., 2009; Bockris & Swinkels, 1964; Oguzie et al., 2007; Khan et al., 2015).

2.14 Schiff bases as corrosion inhibitors in acid solutions

Schiff base, an organic compound which has the ability to donate lone pair of electrons as well as polar groups and/or π electrons both of these features combined in one molecule and that could be a potential inhibitor in acidic solution. A variety of Schiff base compoundsare known to be applicable as effective corrosion inhibitors for steel, copper and aluminum in acidic medium such as hydrochloric acid, sulphuric acid, acetic acid, formic acid etc. (Emregül and Atakol, 2004; Ashassi-Sorkhabi et al., 2005; Lukovits et al., 2005; El-Rehim et al., 1999; Quraishi et al., 1998).

Schiff base compounds having a general formula R-C=N-R', where, R and R' are aryl, alkyl or cycloalkyl or heterocyclic groups formed by the condensation of an amine and a

carbonyl group. The greatest advantage of many Schiff base compounds is that they can be conveniently and easily synthesized from relatively cheap material. Schiff base compounds with electronegative nitrogen, sulfur and/or oxygen atoms in the molecule, have been reported to be effective inhibitors for the corrosion of steel in acid media due to the presence of the –C=N- group (Behpour et al., 2009; Asan et al., 2006; Behpour et al., 2008; Abdel-Gaber et al., 2009).

2.14.1 Schiff bases corrosion inhibitors in Hydrochloric acid solutions

The corrosion inhibition efficiency of Schiff bases namely N-(2-hydroxyphenyl) salicyaldimine, N,N'-bis-salicyaldehyde-1, 3-diaminopropane, N,N'-bis-(2-hydroxybenzyl) 1,3-diaminopropane on iron substrate in 1M HCl solution by the application of weight loss, potentiodynamic polarization as well as electrochemical impedance spectroscopy (EIS) techniques were evaluated by Emregul &Atakol (2004). These entire Schiff bases act as excellent corrosion inhibitors and among them N,N'-bis-(2-hydroxybenzyl) 1, 3-diaminopropane, which exhibit a maximum inhibition efficiency. Similarly Ashassi-Sorkhabi et al. (2005), reported that the corrosion inhibition efficiency of pyridinimic Schiff bases like benzilidenepyrimidine-2-yl-amine, (4-methyl-benzilidene)–pyrimidine-2-yl-amine, (4-choloro-benzilydene)–pyrimidine-2-yl-amine on mild steel (MS) in 1M HCl solution using gravimetric and electrochemical measurements. The results obtained by employing these compounds as corrosion inhibitor has proved the capability to retard the corrosion in aggressive environment by the virtue of chemical adsorption at liquid-solid interface even by the addition of a small quantity where the adsorption behavior has obeyed the Langmuir isotherm.

In a similar fashion, Quraishi and co-workers (1998) investigated the influence of three macro cyclic compounds on corrosion of MS in HCl using weight loss method, potentiodynamic polarization, AC impedance and hydrogen permeation techniques. All the investigated compounds showed significant efficiencies and reduced permeation of

hydrogen through MS in HCl. Potentiodynamic polarization results reveal that the macrocyclic compounds has acted as mixed inhibitors.

From the view point of molecular parameters, the alteration in the inhibition efficiency of thiosemicarbazide and thiosemicarbazones derivatives can be investigated by quantitative structure activity relationships (QSAR). The results revealed that corrosion inhibition efficiency of derivatives can be viewed in the terms ofenergy of the highest occupied molecular orbital as well as dipole moment, or by the energy difference of E_{HOMO} and E_{LOMO} (Lukovits et al., 2005).

Similarly, it was reported that the quantum chemical calculations based on Density Function Theory (DFT) technique on three polydentate Schiff bases (PSCs), used as efficient corrosion inhibitors for iron in acidic medium in order to establish a mutual relationship between the molecular structure of investigated Schiff bases and inhibition efficiency (Hong et al., 2008). The obtained results revealed that the inhibition efficiency of the investigated PSCs increased with a decrease in the difference of ($E_{LUMO} - E_{HOMO}$) and a simultaneously increase in E_{HOMO} as well; furthermore the particular areas accommodating N atoms provides a basis for a suitable bonding sites for the metal surface as a result of donating electrons to the iron metal.

In another study, it was investigated that the inhibition efficiency of four Schiff bases on mild steel in 1M HCl using gravimetric, electrochemical techniques as well as quantum chemical calculations (Ahmed et al., 2006). The synthesized Schiff bases have been found to be effective inhibitors and having inhibition efficiency greater than 90% at an optimum concentration. Moreover, by correlating the data obtained from quantum chemical calculations and experimentally achieved inhibition efficiency, it is proved that the inhibition efficiency of the investigated Schiff bases were found to be increased by lowering the values of both molecular band gap (ΔE_{MBG}) and electron affinity (EA) as well. Emregul et al (2004), reported the inhibitory effect of the synthesized Schiff

base compounds namely N,N'-bis-(salicylidene)-2-hydroxy-1,3-propanediamine and N,N'-bis-(2-hydroxyacetophenlidene)-2-hydroxy-1,3-propane diimine on MS specimen in 2M HCl solution by using weight loss and polarization techniques. The obtained results showed that the latter Schiff base showed better inhibition property than the former and both follow the Langmuir adsorption isotherm.

The corrosion mitigation studies on MS in 1M HCl medium using the Schiff bases benzylidine-pyridine-2-ylamine, (4-benzylidene)-pyridine-2-yl-amine and (4-chloro-benzidiline)-pyridine-2-yl-amine were investigated and reported by researchers (Ashassi-Sorkhabi et al., 2005). Results obtained using weight loss measurements and electro chemical methods showed that these compounds were excellent inhibitors and increased their efficiency with the increase of inhibitor concentration and varied with the type of functional groups substituted on benzene ring. The polarization curves reveal that compounds are mixed type inhibitors and experimentally obtained adsorption isotherms following the Langmuir equation.

Yurt et al. (2006), synthesized four Schiff bases namely 2-((1E)-2-aza-2-pyrimidine-2-ylvinyl) thiophene, 2-((1Z)-1-aza-2-(2-pyridyl)vinyl) pyrimidine, 2-((1E)-2-aza-2-(1,3-thiazol-2-yl)vinyl) thiophene, 2-((1Z)-1-aza-2(2-thienyl)(vinyl) benzothiazole containing hetero aromatic substituents and reported their inhibition efficiency on carbon steel in 0.1 M HCl, using polarization and EIS studies. The obtained results showed that the investigated Schiff base compounds acts as an anodic inhibitors and variation in inhibition efficiency is mainly a function of type as well as nature of the substituents present in the inhibitor molecule and follow Temkin adsorption isotherm. The corrosion inhibition effect of seven Schiff bases on MS in 1 M HCl were evaluated by using weight loss and electrochemical techniques and reported that polarization studies indicate that theses Schiff bases behave as predominantly cathodic inhibitors (Desai et al., 1986).

A similar study carried out on the corrosion inhibition of aluminum in 1 M HCl by the application of four Schiff bases namely 2-anisalidine-pyridine, 2-anisalidine-pyrimidine, 2-salicylidinepyridine, using weight loss and thermometric methods (Bansiwal et al., 2000). They concluded that these Schiff bases are effective corrosion inhibitors for the protection of aluminum against HCl media and the inhibition efficiency are strongly dependent on the concentration of both inhibitor and acid as well.

Research study carried out the corrosion inhibition testing of Schiff bases derived from benzaldehyde, aliphatic and aromatic primary amines on aluminium alloy 51S in HCl (Desai et al., 1986). Schiff bases showed fairly good inhibition efficiency and conversion of an amine into its Schiff base improved its inhibitive action.

Baeza et al. (2003), reported the inhibition effect of Schiff base like 1,3,4-thiadiazole-2,5-dithiol (namely bismuthiol) on copper in 0.5 M HCl solution using potentiodynamic techniques and revealed that inhibition mechanism was actually due to the adsorption of bismuthiol compound on the active surface sites of copper by blocking it and the chemical adsorption followed Langmuir isotherm.

2.14.2 Schiff bases corrosion inhibitors in sulphuric acid solutions

Hosseini and co-workers (2003) synthesized and studied the action of investigated Schiff bases as effective corrosion inhibition likely N,N'-ortho-phenylene(salicylaldimine-acetyl acetoneimine) and N,N'-ortho-phenylene (salicylaldimine-2-hydroxy-1-napthaldimine) on MS substrate in 0.5 M H_2SO_4 solution using gravimetric, polarization and EIS methodology. The results revealed that the Schiff bases were found to be very effective corrosion inhibitors and a maximum efficiency of 95 % was achieved for both the investigated compounds at an inhibitor concentration of 400 ppm.

In another research study, the inhibition action and effects of two Schiff bases like 2-amino-5-mercapto-1,3,4-thiadiazole (2A5MT) and 2-mercaptothiazoline (2MT) on MS

surface at 1 M H_2SO_4 was examined using polarization and EIS measurements (Doner et al., 2011). Further they revealed that the investigated compounds are good corrosion inhibitors and their inhibition efficiencies attributed to the adsorption of the active sites by simple adsorption and obeying Langmuir adsorption isotherm.

Agrawal et al. (2004), evaluated the performance and inhibitive action of Schiff bases namely *N*,*N*′-dibenzylidene, ethylenediamine *N*,*N*′-di(*p*-methoxybenzylidene), ethylenediamine*N*,*N*′-disalicylidene as effective inhibitor on Zinc surface in 0.5 M and 0.25 M sulphuric acid medium. Research study reported that the investigated inhibitor acts as cathodic inhibitor having protection efficiency more than 99% in both acidic solutions. Moreover, the presence of $–OCH_3$ and –OH functional groups in benzene ring made them very effective corrosion inhibitor.

The inhibition efficiency of two salen Schiff base compounds of bis - (2-hydroxy-3-methoxy)-1, 6-diaminohexane salicyladimine and bis-(2-hydroxy)-1,6-diaminohexane salicyladimine abbreviated as A1 and A2 on the copper specimen in 0.5 M H_2SO_4 using electrochemical polarization and impedance measurements. Obtained results revealed that, the inhibition mechanism was attributed to the formation and growth of initially adsorbed layer at liquid/metal interface protecting the metal against aggressive medium. Both salen Schiff bases act as anodic inhibitors and obeying Langmuir adsorption isotherm (Ravari et al., 2009).

Research conducted for the inhibition efficiency of synthesized sulphanilic acid and sulphanilamide Schiff bases on mild steel 1M H_2SO_4 using both electrochemical and non-electrochemical measurements (Chitra et al., 2014). Polarization results revealed that the investigated Schiff bases perform as mixed type inhibitor and following both Langmuir and Temkin adsorption isotherm. The obtained data also suggests that the addition of halides to the inhibitors turn them more effective by enhancing the corrosion inhibition efficiency.

In a similar fashion, research conducted on synergistic effect of KI on the inhibition efficiency of newly synthesized polynuclear Schiff base, like anthracene-9(10H)-one-3-aminopropanoic acid (A9O3AP), on mild steel substrate in 0.5 M sulphuric acid medium using weight loss and electrochemical methods (Shaju et al., 2012). Results reported that due to the addition of potassium iodide (KI) to the concentration of investigated inhibitors, the inhibition efficiency has been enhanced due to the synergism of KI and inhibitor molecules. Tafel polarization data revealed that A9O3AP acts as a mixed type inhibitor obeying both Langmuir and Freundlich adsorption isotherms, respectively.

The synthesis and corrosion inhibition mechanism of newly dianiline Schiff on the mild steel in 1M sulphuric acid at a temperature of 30°C was examined by various electrochemical monitoring measurements (Citra et al., 2010). Polarization measurements revealed that the synthesized Schiff bases are missed type inhibitor following Langmuir adsorption isotherm. Moreover results revealed that the inhibition efficiency decreases with increase in temperature due to it's desorption in inhibitor molecules at solid surface, leading an increase in activation energy.

The three newly synthesized Schifff base compound *N*,*N*′-ethylen-bis (salicylidenimine), *N*,*N*′-isopropylien-bis (salicylidenimine), and *N*-acetylacetone imine, *N*′-(2-hydroxybenzophenone imine) *ortho*-phenylen abbreviated as S_1, S_2 and S_3 were reported as efficient corrosion inhibitors for MS in 0.5 M H_2SO_4 solution using gravimetric, polarization and EIS measurements (Hosseini et al., 2003). Maximum inhibition efficiencies (97 - 98 %) achieved at a concentration of 300 ppm. At higher concentration, the inhibition efficiency of S2 is higher than the rest of S1 and S3 and followed Langmuir adsorption isotherm.

An inhibition efficiency of 99 % have been reported by the application of synthesized *m*-substituted aniline-*N*-salicylidenes as corrosion inhibitor on zinc in H_2SO_4 solution

using polarization techniques (Talati et al., 2005). The study revealed that the presence of salicylidene portion of the inhibitor containing iminic group play a vital role during inhibition mechanism. The studied compound behaves as a mixed type inhibitor with a predominantly cathodic inhibition and obey Langmuir adsorption isotherm.

2.14.3 Schiff bases corrosion inhibitors in both hydrochloric and sulphuric acid solution

Study of literature review revealed that the influence of pyridinium chloride (PC) and n-hexadecyl pyridinium chloride (HDPC) as efficient corrosion inhibitors on MS in 5N HCl and 5N H_2SO_4 using weight loss, gasometric, polarization, and small amplitude cyclic voltametric techniques (Vasudevan et al., 1998). Polarization studies reported that PC acts as anodic type inhibitor in H_2SO_4 and behave as mixed type inhibitor in HCl solution. It was concluded that HDPC is more inhibitive as compared to PC and the inhibitive behavior of both the investigated compounds performed better in H_2SO_4 solution.

Similarly, the corrosion inhibition efficiency of newly synthesized tetradendate Schiff base, bis –(2-hydroxy-1-naphthaldehyde)1, 6-hexadiamine (namely A1) were evaluated on carbon steel in 1M HCl and 0.5M H_2SO_4 using weight loss and polarization techniques. The results revealed that this inhibitor act as both cathodic and anodic type of inhibitor and at 100 ppm concentration the efficiencies of 97% in HCl and 95% in H_2SO_4 were achieved. This result leads to the conclusion that synthesized Schiff base compound perform better in HCl as compared to corresponding H_2SO_4 solution (Dadgarnezhad et al., 2004).

The effectiveness of three organic triazole compounds namely 5-mercapto-3-butyl-4-salicylidine-1,2,4-triazole (MBST), 5-mercapto-3-butyl-4-benzilidineiminio-1,2,4-triazole (MBBT) and 5-mercapto-3-butyl-4-cinnamylidineimino-1,2,4-triazole (MBCT) as effective corrosion inhibitors on MS in both 1N HCl and 1N H_2SO_4 were evaluated by using weight loss and polarization measurements. The inhibition efficiencies of these

compounds are altering with the variation of the concentration, immersion time as well as the solution temperature. Polarization results suggest that these compounds behave as filming type of inhibitor i.e. forming a protective film at interface. The studies reported that all these compounds were found to be effective corrosion inhibitors and acted as mixed type inhibitor by obeying Temkin adsorption isotherm (Quraishi & Sardar., 2005). Daoud et al. (2015) stated the inhibition efficiency of Schiff base likely, (NE)-N-(thiophen-3-ylmethylidene)-4-({4-[(E)-(thiophen-2-ylmethylidene)amino]phenyl}m-ethyl) aniline (L) as excellent corrosion inhibitor on MS X52 in 1 M HCl and 1 M H_2SO_4 using different corrosion methods, like weight loss, potentiodynamic polarization and electrochemical impedance spectroscopy (EIS) techniques. Polarization studies revealed that the examined compound was a mixed type of inhibitor and the inhibition efficiency increases by increasing the inhibitor concentration. Moreover, the inhibition mechanism is based on the formation of a thick uniform layer at solid liquid interface obeying Langmuir adsorption isotherm.

Fouling comprises of two components: external or outer surface fouling and internal or inner surface fouling. External fouling phenomenon occurs in three distinct mechanisms and fouling can be accomplished to one or more of them: (i) scale formation, as a result of heterogeneous crystallization of mineral salts on solid surface (ii) cake formation, due to the accumulation of suspended solids on surface and (iii) biofouling, from colonization of inherent microorganisms (Heok et al, 2008).

Fouling consists on mainly four categories including colloidal/particulate fouling, organic fouling, inorganic fouling and biofouling, in all the categories, fouling occurs as a result of accumulation and/or deposition of colloidal, organic matter, inorganic salts, and microorganisms from aqueous solution onto solid surface (Tang et al, 2011). Inorganic fouling leads the formation of hard mineral deposits occur on the surface as feed water becomes supersaturated by the presence of inorganic salts (Tang et al, 2011).

Inorganic fouling can also be referred as crystallization or precipitation fouling (Bott, 1995) and the formed adherent inorganic deposits can be referred by the term scale (Cowan, 1976).

2.15 Economic impacts of fouling

The control and/or mitigation of fouling are a persistent and expensive problem penalizing industries, billions of dollars annually (Muller-Stienhagen, 2000). From last two decades of 20th century, efforts have been given for assessment of the cost of fouling for different countries worldwide. In 1979, the fouling cost was evaluated in United Kingdom, and the overall estimated cost of fouling was in the range of 300 – 500 M £ annually (Steinhagen et al., 1993). In a similar fashion for United States, the fouling cost was estimation could be between 8,000 and 10,000 M$ per annum (Garrett-Price et al., 1984). For New Zealand the amount of annual fouling cost had been studies and estimated cost was around 45 M$ (Steinhagen et al, 1993). Whereas cost of fouling on industry level, was studied and estimated amount of 10 M$ annually for a typical petroleum industry whose processing capacity of refining crude oil was 100,000 barrels per day (Van Nostrand et al., 1981). In a recent investigation, the cost of fouling in most industrialized countries increased to 0.25 % to 0.30 % of the gross national product (GNP) (ESDU London, UK, 2000). From the above estimated data, it can be predicted that the cost of fouling are substantial and any considerable reduction in fouling cost may result to both profitability and competitiveness.

Fouling may also lead to increase the pumping cost as a result of additional pressure drop in comparison to the clean surface across the heat exchangers which results in the decrease of fluid velocity throughout the processing units, in order to overcome this situation, a higher pumping energy is required.

The application of additives to mitigate fouling has already been mentioned. Research study reported the effect of industrial effectiveness of antifouling on the preheater of

crude oil distillation unit (Van Nostrand et al, 1981). Fig.2.12, describes the downward fall in heat duty with and without the presence of antifoulants.

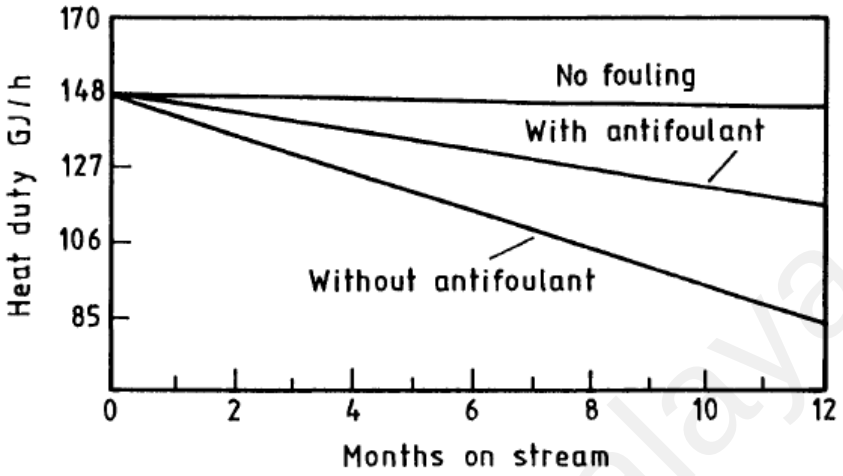

Figure 2.12: Losses in heat duty with and without the presences of antifoulants (Bott., 1995)

2.16 Factors effecting fouling deposits

A number of operating parameters influence on the built-up of fouling deposition which may include the following (Jaroudi et al, 2010).

2.16.1 Flow velocity

Velocity has a considerable effect up to certain level. Literature reported that a considerable decrease in fouling occurred with a high flow velocities (Müller-Steinhagen & Middis, 1989, Cooper et al., 1980 and Walker, 1982). High fluid shearing stress generated as a result of high fluid velocity, leading the removal of deposited fouling. Decrease in fouling at heat transfer surface by increasing the flow velocity of the fluid depending upon the type, compactness and adhesive properties of the foulants. In the case of particulate fouling where the foulant deposits are weaker, the increase in flow velocity may completely terminate the fouling as well. Where as in the case of stronger foulant deposits, altering the velocity beyond the significant level may not reduce the fouling (Walker, 1982).

2.16.2 Bulk temperature

Bulk temperature has to be found a significant factor on fouling and increasing rate of fouling. In the case of inverse salts crystallization, where precipitation occurred in the bulk, the raise in temperature hence alter the crystal formation rate and induced deposition. Bulk temperature also has a strong influence on chemical reaction of fouling.

2.16.3 Heat transfer surface temperature

It may influence a decrease or increase or even no effect at all for fouling (Somerscales and Knudsen, 1981). Increasing surface temperature may increase chemical reaction rate and also the sparingly salts solubility crystallization leading increased fouling. On the other side, fouling reduces due to result of cooling of normal solubility salts. Moreover the strong influence for the salt deposition may also be attributed due to the total surface free energy of material being used.

2.16.4 pH of water

The pH plays an important role regarding the formation and/or precipitation of fouling as well as the nature and the type of fouling materials. However, there is no any straight forward influence of pH on fouling. For calcium carbonate fouling, at below 11 pH and at a low temperature around 7 ^{o}C leads to the formation of calcite, whereas on the other hand, the formation of aragonite takes place at a pH below 10 and 58 ^{o}C (Martin et al., 1998). On the other hand, no significant effect of pH has been observed on the fouling until solution becomes supersaturated (Helalizadeh and Muller, 2000).

2.16.5 Surface energy

In order to define the surface properties, surface temperature is one of the most prominent factors and computes the interruption of the existing bonds once the surface is created. Study of literature reported that due to weaker bonding of deposits at interface results an extra resistance to fouling as well as the tendency of easy cleaning of

surfaces (Oliveira, 1997; Bohnet et al., 1992). However, some researcher invalidates the theory of correlation for both surface energy and deposited fouling as a function of induction time (Foster & Bohnet, 2000). The fouling deposition of gypsum for a number of metals surface evaluated that surface area and metallurgy of heat exchangers are the dominant factor on the fouling rate (Amjad et al., 1988). Moreover, the effect of surface energy on a variety of heat transfer surface and reported that fouling rate in an increasing order of magnitude on various investigated metals: Copper > Aluminum > brass > Stainless Steel (Kazi et al., 2010).

2.16.6 Resident time

It is well known that fouling mechanism is a time dependent process; therefore, resident time has a strong influence on type of heat exchanger selected and rate of fouling.

2.16.7 Non-condensable gases (NC)

These includes gases such as CO_2, it has been reported that even a low concentration of NC gases considerably lowers the performance and overall heat transfer co efficient of desalination units.

2.17 Types of fouling

As fouling is a complex process, involving various physical and chemical phenomenon. Fouling on surfaces can be classified into five different categories (Bott, 1995).

2.17.1 Precipitation fouling

Fluids commonly used in heat exchangers may contain dissolved salts. Inside heat exchanger process conditions are different from the entrance then the presence of these dissolved salts in the fouling fluid becomes supersaturated and the solution becomes crystallize on heat transfer surface. The driving force for precipitation fouling is the concentration difference in the solution and that at the surface. Due to weak adhesive tendency of the deposit on the surface, these deposits mostly affected by fluid flow

velocity and less affected by wall temperature. Moreover, these deposits can "bake on" to hot surfaces and their removal is very difficult as well (Kazi, 2012).

2.17.2 Corrosion fouling

This type of fouling results as a reaction between the heat transfer surface and materials in fluid. This type of fouling is also caused by a chemical reaction but it is different from chemical fouling reaction. In this particular case, the surface reacts with fouling fluids and exhibit corrosion on heat transfer surfaces (Bott, 1995). The presence of theses corrosion products further act as a catalyst affecting other fouling processes.

2.17.3 Biological fouling

This type of fouling results of the sticking of an organic film constituting micro and macro organisms as well as their associated products to the heat transfer surfaces. The growth of microorganisms (algae, bacteria, mold, etc.) in the fluid may also result biological fouling. Such type of fouling mostly encountered in milk factories and cooling water plants.

2.17.4 Chemical reaction fouling

Such type of fouling occur when deposits accumulates as a result of chemical reaction, leading the production of a solid phase at or near the heat transfer surface. Surface temperature plays an important role and also affects the reaction rate. Such type of fouling is mostly tenacious and need a special care for its cleaning from hot surfaces in order to provide a satisfactory operation (Mueller-Steinhagen, 2000).

2.17.5 Particulate fouling (Solidification fouling)

This type of fouling results the accumulation of suspended solid particles in the process fluids onto heat transfer surface. Fine particles settle and deposit at the heat transfer surface whereas heavy particles settle at the bottom of the units by gravity. Example of such type of fouling can be found in dust deposit on air cooled condenser etc. (Kazi, 2012).

2.18 Fouling development stages

Fouling is a complex transient process and its deposition on surfaces involves a sequence of the following stages.

2.18.1 Initiation or delayed period

It is a particular time period that quickly follows the start-up of heat exchanger and may last from a few seconds or minutes to several hours or days. It is a particular time when the depositions are allowed to established on heat transfer surface. This duration is influenced by type of fouling, surface temperature, surface roughness and surface finishing. In the induction time period, formation of the nuclei for the crystallization of deposit formed for biological growth. For example, particulate fouling has no induction time period, whereas the crystallization fouling having an induction time of several weeks. In a similar fashion, several inverse soluble salts, the delay period is found to be inversely proportional with surface temperature (Shah & Sekulic, 2003).

2.18.2 Mass transport

Fouling substances (either dissolved or suspended) in the fluid which are responsible for the deposit formation on surface are transported from the bulk to heat transfer surface across the boundary layer. The driving force for such a transport is the system physical properties and the concentration difference between the species in the bulk and the surface. The rate at which these species can be expressed by the following equation:

$$\frac{dm}{dt} = h_D(C_b - C_w) \qquad (2.22)$$

Where, C_b and $C_w$are the concentrations of the species in the bulk and at wall, respectively, and h_D is the mass transfer coefficient and can be evaluated through Sherwood number and dependent of flow conditions and geometry.

2.18.3 Deposition or attachment

At this stage, the species deposit and finally adhered among itself and to the heat transfer surface. If the transport rate of the species to the wall is greater than the corresponding rate of their integration to crystal lattice, then the deposition is termed to be adhesion controlled. On the other hand, if the integration rate is higher than diffusion rate, then disposition is called to be diffusion controlled (Mwaba, 2003).

2.18.4 Removal

There is always a contest between the deposition and the removal of fouling spices, until a steady deposition growth takes places at the surface. Some parts of the deposit layer may be removed by the action of shear forces at the interface of fluid and deposited layer. The amount of the deposited foulants removed may highly be influenced by the strength of the deposited foulants.

2.18.5 Aging

Once deposition commenced aging starts which undergoes the transformation of crystal either strengthening or weakening the deposited layer with time. The mechanical properties of the deposited layer during aging process may be changed by altering the chemical or crystal structure as well as the changes in chemical composition of layer facilitated by a chemical reaction. On the other hand, corrosion fouling on surface result a weak layer of biofouling due to slow poisoning of these corrosion products for microorganisms (Kazi, 2012).

2.18.6 Change in deposition thickness with time

The following figure comprises the various regions of deposited growth rate with time (Bott, 1995).

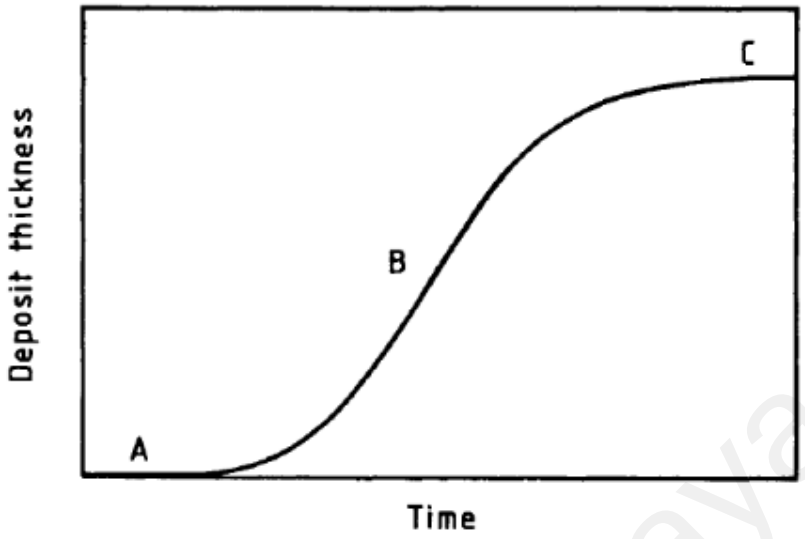

Figure 2.13: Change in deposition thickness with time (Bott, 1995)

Section A: This section represents the induction period of fouling in which fouling initiates with time.

Section B: In this section, a steady deposition growth occurs on the surface, here the rate of disposition removal increased with the corresponding rate of deposition gradually fall down.

Section C: At this particular section, both rates i.e. the rate of removal and the rate of deposition almost seem to be equal and the thickness of the deposited layers become constant.

2.18.7 Composite fouling

Some commonly used salts causes fouling like $CaCO_3$, $CaSO_4$, SiO_2, and $Mg(OH)_2$. In this particular type of fouling, fouling accomplished by the involvement of more than one fouling spices or by the combination of more than one fouling mechanism undergoes simultaneously (Hong & Elimelech, 1997).

Various parameters such as solubility, crystal strength and structure have a strong influence of composite fouling. Synergistic fouling commenced as a result of composite

fouling, therefore, more attention and detailed research required for composite fouling mechanism (Taborek, 1983).

2.19 Common types of water formed deposits

Various types of scale included on Reverse Osmosis (RO) membrane can be classified as alkaline, non-alkaline scale and silica base scale. In order to predict the scale on the basis of solubility data, the examination of a fouled membrane provides the necessary platform for such assessment. The commonly formed scale including calcium carbonates ($CaCO_3$), calcium sulfate ($CaSO_4.XH_2O$), barium sulfate ($BaSO_4$), Strontium sulfate ($SrSO_4$), and scilicet etc. (Darton, 1999 & Karime, 2008).

2.19.1 Calcium Carbonate ($CaCO_3$)

Calcium carbonates one of the most commonly used laboratory and industrial substances, due to the break–up of bicarbonate ions; it is mostly available in alkaline scale form. It includes in one of the most common dispersed minerals, for example lime stone and chalk. The scaling tendency of calcium carbonate to form is commonly predictable as well as controllable. Scaling of calcium carbonate is a significant issue for reverse osmosis plants, boilers and chemical industries (Sheikholeslami, 2003a).

Following are some common types of chemical reaction involving calcium carbonates as a reactant for the production of various chemicals at different parameters.

1. The reaction of calcium carbonate with strong acid like HCl.

$$CaCO_3\ (s) + 2HCl\ (aq) \longrightarrow CaCl_2\ (aq) + CO_2\ (g) + H_2O\ (l)$$

2. Heating of calcium carbonates at 840 ^0C causing the release of carbon dioxide gas.

$$CaCO_3\ (s) \longrightarrow CaO + CO_2$$

3. The formation of calcium bicarbonate by the action of calcium carbonate with carbon dioxide and water.

$$CaCO_3\ (aq) + CO_2 + H_2O \longrightarrow Ca\ (HCO_3)_2$$

Six various forms of calcium carbonate has been reported, out of these forms, three of them are naturally occurring anhydrous crystalline polymorphic forms or anhydrous forms like calcite, aragonite and vaterite, and the remaining three hydrated form including, calcium carbonate monohydrate (MCC), amorphous calcium carbonate (ACC), and calcium carbonate hexahydrate (CCH) respectively (Tzotzirt et al., 2007; Xylaet al., 1992). Calcite crystal structure presents a uniform rhombohedral morphology possessing a sharp but straight edges and having an average particle size of around 10 μm. whereas the clusters of aragonite are in agglomerates form having an outward needle orientation n. Furthermore, the shape of vaterite is usually spherical with a ranging diameter of almost 0.05 – 5 μm.

The survey of literature reveals that, the most important factors responsible for the formation and controlling of the final stable crystallization phase are temperature and pH (Tzotzi, 2007, & Andritsos et al., 1997). The transformation of ACC from calcite to vaterite takes place at a relatively low temperatures (below 30 ^{o}C), whereas on the other hand, transformation from aragonite to vaterite occur at higher temperature (above 40 ^{o}C) (Sawada, 1997; Rodriguez-Blanco et al., 2011).

2.19.2 Calcium sulfate ($CaSO_4$)

One of the most common scales among the non-alkaline scales is calcium sulfate. On the other hand the most dominant problems in water treatment plants is the cleaning of such deposited scales, which is relatively more difficult to the rest of alkaline scale. One of the best practices to avoid the problem of calcium sulfate scaling especially in RO plants is the operation of such systems below its saturation system. Some chemical and physical properties of calcium sulfate are listed the table 2.2.

Table 2.2: Chemical properties of calcium sulfate (Patnaik, 2003)

Appearance	White powder
molar mass	136.14 g/mol (anhydrous)
molar mass	145.15 g/mol (hemihydrate)
molar mass	172.172 g/mol (dihydrate)
Density	2.96 g/cm^3 (anhydrous)
Density	2.3 g/cm^3 (dihydrate)
Soluability in water	0.0021 mol/100 ml (25 ^{o}C, anhyrrous)
Soluability in water	0.24 mol/100 ml (20 ^{o}C, dehydrate)
Soluability product, K_{SP}	2.4 x 10^{-5} (dehydrate)

Like calcium carbonate, calcium sulfate is a well-known popular foulants in heat exchangers equipment and follow the same inverse solubility behavior like carbonates as well. There are three different crystallographic forms in which the precipitation of calcium sulfate occurs: calcium sulfate anhydrite ($CaSO_4$), calcium sulfate hemihydrate ($CaSO_4.\frac{1}{2}H_2O$) commonly known as plaster of paris and calcium sulfate dihydrate ($CaSO_4.2H_2O$) may also known as gypsum (Lee, 2000). Gypsum is one of the most common forms at ambient temperatures. Literature reported that, the two primary morphological forms of gypsum are: needles and platelets, having a monoclinic and prismatic structure (Gilron & Hasson, 1987; Lee, 2000; Lewis et al., 2006; Bosbach et al., 1996; Sheikholeslami, 2000).

It was reported that at room temperature the needle morphology was found in a solution whose concentration was initially above than 0.4 M of $CaSO_4$, while at an initial concentration of less than 0.25 M, produced platelet morphology (Seewoo et al., 1984). On the other hand, it was found that the opposite results regarding the crystal

morphology of $CaSO_4$, at a concentration of 0.3 M favors a needle-like structure, whereas smooth surfaces resulted at high concentration around 0.725 M of $CaSO_4$ (Christoffersen, 1976).

The crystalline morphology of calcium sulfate was found to be strongly dependent on the crystallization mechanism and the ratio of supersaturation. Under the conditions of low supersaturation ratio of < 2.27, the generations of needle like crystals were to be noticed, which were dominated by the surface crystallization morphology and as result of lengthy induction time period as well. In comparison, at a supersaturation ratio of $CaSO_4$ around 10.86, leading the formation of plate- like crystal morphology, by the domination of bulk crystallization (Lewis, 2002).

The solubility tendency of $CaSO_4$ in water as a function of temperature variable is shown in Fig. 2.14. In a temperature range around 40 ^oC, the solubility of calcium sulfate has to be found decreased by raising the operating temperature normally for solid phases only. In the normal processing conditions, the layer close to the heat transfer surface (boundary layer) is considered to be the hottest portion of the processing fluid. Therefore, any expected precipitation may takes place over that particular region (Helalizadeh et al., 2000).

The relative solubility of calcium sulfate may also be strongly influenced by the presence of the concentration of other dissolved ions initially present in that particular system and found to be increased by increasing the relative concentration of other ions or substance found in solution. A detail investigation of deposited calcium sulfate in the form of hemi-hydrate in mixed salt crystallization fouling, other industries and as well as seawater desalination units has been reported (Marshall & Slusher, 1968; Helalizadeha et al., 2005).

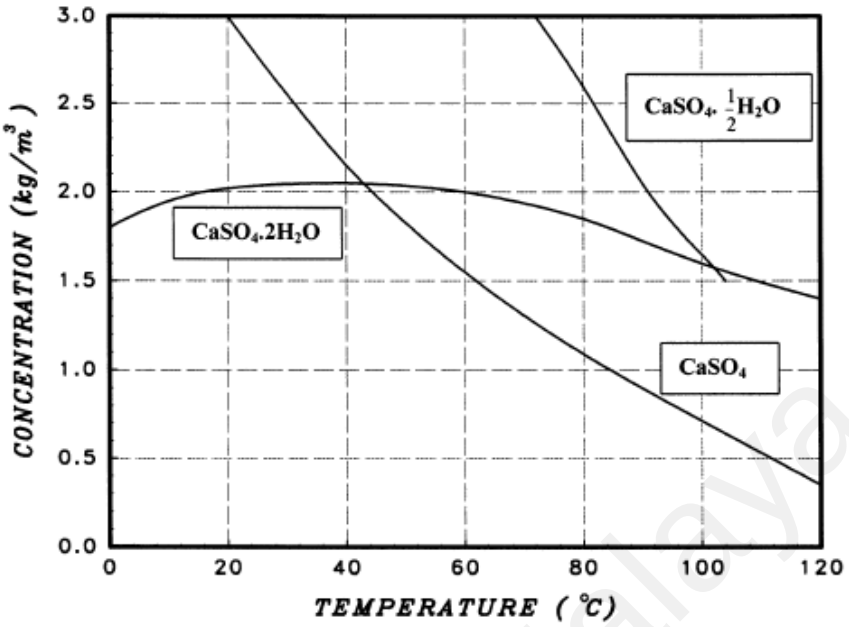

Figure 2.14: Solubility phenomenon of $CaSO_4$ in water as the function of operating temperature

2.20 Basic principles of fouling

Generally the accumulation of undesired foulant or deposit on heat transfer surface causing a net increase in overall heat resistance for heat flow. Fig. 2.15 shows a schematic diagram for the temperature distribution and flow direction over a fouled surface of a heat exchanger for individual fouling layers. Where, T1 and T4 represent the temperature of the hot bulk and cold fluid streams respectively. At turbulent conditions, these temperatures prolong almost to the boundary layer in their respective fluids, resulting a proper mixing and heat is carried out physically instead of conduction in solids or by slowly moving fluid streams. Due to the stagnant conditions of the boundary layer also offer an additional resistance during heat flow.

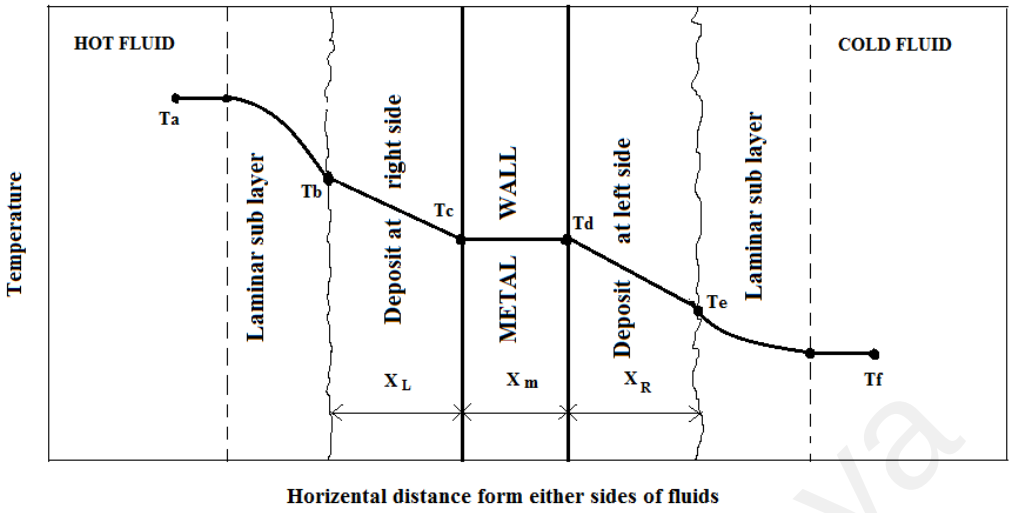

Figure 2.15: Temperature distribution across a fouled surface

In comparison, to the thermal conductivity of foulants, which are relatively very low to that of metals. Therefore, for driving heat through these deposits, a relatively large amount of temperature difference is required; however, the temperature difference through the metal surface is comparatively low. Table 2.3 summarizes the data including the thermal conductivities of some frequently occurring foulants and some common construction materials.

Table 2.3: Thermal conductivity of some metals and foulants (Bott, 1995)

Metals	**Thermal conductivity (W/mK)**	**Foulants**	**Thermal conductivity (W/mK)**
Brass	400	Alumina	0.42
Copper	114	Carbon	1.6
Monel	23	Calcium Sulfate	0.74
Titanium	21	Calcium carbonate	2.19
Mild Steel	27.6	Titanium oxide	8

Generally the resistance to heat flowing across a metallic surface is given by:

$$\frac{x}{\kappa} \qquad (2.23)$$

Where, x denotes thickness of the solid and κ is the thermal conductivity of the corresponding solid.

Considering the Fig. 2.14, resistance occurred during the heat flow through the solids are given below. For the deposit at the either sides of the metallic sides, therefore, the resistances for these foulant deposits are:

For the deposit at the left side is $\frac{x_L}{\kappa_L}$, having a thermal conductivity of κ_L and for the deposit at the right side of metallic surface is $\frac{x_R}{\kappa_R}$, with a thermal conductivity of κ_R, and similarly for metal wall $\frac{x_m}{\kappa_m}$, where κ_m denotes the thermal conductivity of metal.

Heat flux (q) for a steady state conditionis:

$$q = \frac{T_b - T_c}{\frac{x_L}{\kappa_L}} = \frac{T_d - T_e}{\frac{x_m}{\kappa_m}} = \frac{T_e - T_f}{\frac{x_R}{\kappa_R}} \qquad (2.24)$$

Also, $q = h_h (T_a - T_b) = hc (T_e - T_f)$

Where, h_h and h_c represents heat transfer coefficient for hot as well as cold fluids respectively. Re-arranging equation (2.24):

$$q = \frac{T_a - T_b}{(\frac{1}{h_h})} = \frac{T_e - T_f}{(\frac{1}{h_c})} \quad (2.25)$$

Where, the reciprocal of heat transfer coefficients i.e. $1/h_h$ and $1/h_c$ denotes the resistance to heat flow for hot and cold fluids respectively. The total thermal resistance R_T to heat flow is the summation of all individual resistances as shown in equation (2.26) below:

$$R_T = \frac{x_L}{\kappa_L} + \frac{x_R}{\kappa_R} + \frac{x_m}{\kappa_m} + \frac{1}{h_h} + \frac{1}{h_c} \quad (2.26)$$

In order to achieve the heat transfer between hot and cold fluid streams, the overall temperature will be the sum of all individual temperature differences. i.e.

$$T_{total} = (T_a - T_b) + (T_c - T_d) + (T_e - T_f)$$

$$\text{Or } T_{total} = T_a - T_f$$

Therefore, the final relation can be deduced as below:

$$q = \frac{T_a - T_f}{R_T} \quad (2.27)$$

If A is the required heat transfer area, then heat transfer rate can be calculated as well by the following relation:

$$Q = A\ \frac{(T_a - T_f)}{R_T} \tag{2.28}$$

Generally, during the designing of the heat exchangers desired area, the exact values of heat transfer, the temperature of processing fluids, the individual heat transfer coefficients of streams as well as the fouling resistance values from the either sides or streams of a particular heat exchanger must be estimated.

Alternating equation (2.28) for calculating heat flux when the heat transfer surfaces are clean can be represented by equation (2.29):

$$q = U_C\,(T_a - T_f) \tag{2.29}$$

Where, U_C is the overall heat transfer coefficient for clean surfaces. i.e.

$$\frac{1}{U_C} = \frac{x_m}{\kappa_m} + \frac{1}{h_h} + \frac{1}{h_c} \tag{2.30}$$

Including the fouling resistance on both sides of a heat exchanger, equation (2.30) becomes:

$$\frac{1}{U_D} = R_T = \frac{x_L}{\kappa_L} + \frac{x_R}{\kappa_R} + \frac{x_m}{\kappa_m} + \frac{1}{h_h} + \frac{1}{h_c} \tag{2.31}$$

Rearranging equation (2.31), for calculating heat flux over fouled surfaces

$$q = U_D(T_a - T_f) \tag{2.32}$$

Temperature which is the driving force varies along the length of exchanger; therefore it must be necessary to take the mean values of temperature difference using equations (2.31) and (2.32).

If the temperature difference between the hot and cold streams at the either sides of heat exchanger are ΔT_1 and ΔT_2 respectively. Then arithmetic mean of the temperature difference may be taken as below:

$$\Delta T_m = \frac{T_1 - T_2}{2} \tag{2.33}$$

But more precisely by using the application of log mean temperature difference (Hewitt et al., 1994).

$$\Delta T_m = \frac{\Delta T_1 - \Delta T_2}{\ln(\frac{\Delta T_1}{\Delta T_2})} \tag{2.34}$$

Substituting mean temperature difference in equation (2.33) in order to get heat flux:

$$q = U_D \Delta T_m \tag{2.35}$$

Taking total heat transfer area A, than equation (2.35) deduced as:

$$q = U_D \mathrm{A}\, \Delta T_m \tag{2.36}$$

During the designing of heat exchanger, the area is mostly unknown, where re-arrangement of equation (2.36) is done for estimation of heat transfer area.

$$A = \frac{q}{U_D \Delta T_m} \tag{2.37}$$

During the calculation of U_D, the selections of individual fouling resistances have a strong influence on the size as well as the capital cost of the heat exchanger.

In circular tubes of heat exchangers, fouling build-up at the inner and the outer sides, depending upon the flow velocity of the fluid, leading to the formation of an additional insulation layer formed on heat transfer surfaces and lowering the over-all efficiency of heat exchanger.

For a smooth tubular heat exchanger under the condition of deposit, the overall heat transfer coefficient (U_f) can be obtained by the addition of inner and outer thermal resistances as given below:

$$U_f = \frac{1}{\frac{A_o}{A_i h_i} + \frac{A_o R_{fi}}{A_i} + A_o ln\,(d_o/d_i)^{1}/_{2\pi KL} + R_{fo} + {}^{1}/_{h_o}} \tag{2.38}$$

Where, $R_{fi}\ and\ R_{fo}$ are the inner and outer surface resistances of the tubes. Thermal resistance as a result of fouling is generally the difference in resistances of fouled and clean tube walls:

$$R_f = \frac{1}{U_f} - \frac{1}{U_c} \tag{2.39}$$

Where, $U_f\ and\ U_c$ represents the overall heat transfers coefficients for fouled and clean surfaces and generally (U_f) can be evaluated by the application of the rate of heat transfer equation (2.40) :

$$U_f = \frac{Q/t}{A.\Delta T_f} \quad (2.40)$$

Where, Q/t is the rate of heat transfer and ΔT_f is the temperature difference between the heated surface and the bulk temperature of the solution. According to the definition of fouling resistance and heat transfer coefficient, the following equation (2.41) for a constant heat duty can be derived (Kazi, 2012):

$$\frac{A_{fouled}}{A_{clean}} = 1 + U_{clean}R_f \quad (2.41)$$

Deposition of foulant on the rough surface is quite different from that of a clean surface, therefore, leading the alteration of degree of turbulence, particularly near the vicinity of solid surfaces (Bott, 1995).

2.21 General models of fouling

Deposition built up rate on surfaces could be calculated generally by the difference between deposition and removal rates. Therefore,

Accumulation = Inputs – Outputs

Mass deposition rate = mass deposit rate - mass removal rate

Mathematically it can be represented as:

$$\frac{dm}{dt} = \frac{\Upsilon_D}{\Upsilon_R} \quad (2.42)$$

Where, m is the mass deposit at surface, and Υ_D and Υ_R denotes mass flow rates for deposition and removal per unit area respectively.

Due to the increased resistance of the foulant layer may leads either the reduction of inner pipe surface or increasing the fluid velocity as well resulting a net increase in Reynolds number.

For clean conditions, if d_C the diameter of the clean tube having a velocity of u_C and V is the volumetric flow rate, than u_C can be calculated by the following relations (2.43 to 2.45):

$$u_c = V.\frac{4}{\pi d_c^2} \tag{2.43}$$

On the other hand, for fouled conditions, the inner diameter d_f is reduced to $\frac{d_f}{2}$ and the corresponding velocity is given by:

$$u_f = \frac{V4\,.\,V}{\pi d_c^2} \tag{2.44}$$

$$u_f = \frac{16.V}{\pi d_c^2} \tag{2.45}$$

Velocity increased four times and Reynolds number doubled due to the presence of fouled deposits.

The main objectives of fouling models are to comfort the designers and operator of heat exchangers, for making assessment as a consequence of foiling on the efficiency of heat exchangers for particular operating conditions (Bott, 1995).

Curve (A) stands for a straight line relationship with fouling time for strong deposits where the establishment of the fouling layer remains constant after the commencement

of the initiation period. In this case, the rate of removal is constant or negligible or can say that deposition rate is faster than that of removal rate. The falling curve (B) is achieved by a decrease in deposition rate and may due to the tendency of a low mechanical strength of initially formed deposits. On the other hand for asymptotic curve, the rate of deposit removal increases with time period for weak deposits and ultimately becomes equal to the rate of deposition after the initiation time.

.

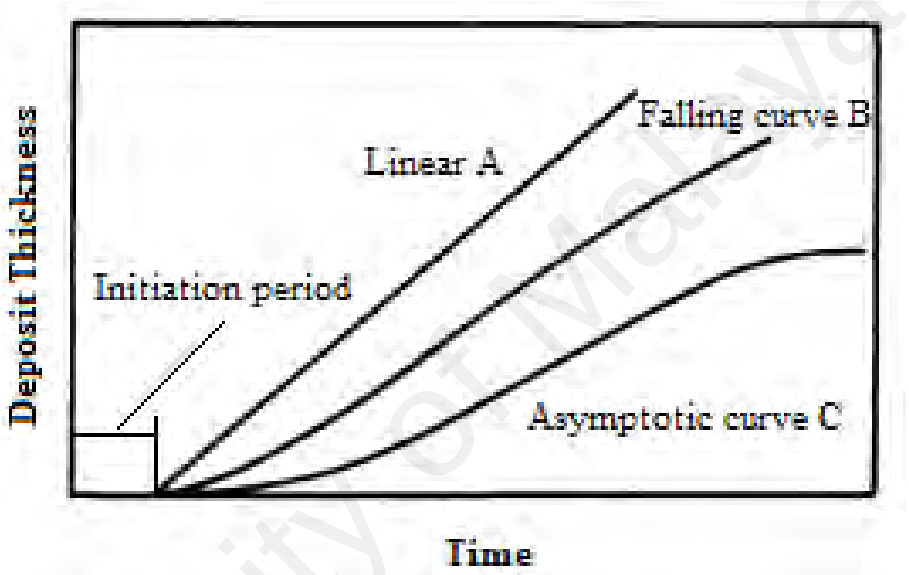

Figure 2.16: Ideal possibilities for fouling rate curves (Bott, 1995)

Several authors reported linear fouling curves for crystallization (Ritter, 1983, Reitzer, 1964; Hasson, 1962). However in the literature review, there is reluctance whether or not the rate of fouling may continue linear for a long time period. It was found that, increase in fluid velocity as a result of reduction in tubes cross-sectional area due to the formation of deposits can increase the removal rate of fouling, resulting the change of linear rate to that of falling rate (Bott & Walker, 1971). Similarly the asymptotic natures of crystallization fouling have been reported by several investigators as well (Middis et al., 1998; Watkinson & Martinez, 1975; Kazi, 2012; Bohnet, 1987). In a similar fashion, the asymptotic trend of calcium phosphate fouling along with particulate fouling has

been reported by Cooper et al. (1980). In some similar studies, investigators reported the asymptotic behaviour as a result of low adhesion of particles to the surrounding wall and may be easily removed as well (Muller & Middis, 1989).

2.22 Crystallization and scale formation

Scale formation on heat exchangers surfaces are mostly arising principally due to the presence of dissolved inorganic salts in the aqueous solutions such as, the utilization of natural water for cooling or desalination processes. The fundamental principle responsible for the deposition of these salts is crystallization mechanism in which a solid structure phase has to be formed from the bulk phase, resulting a tenacious scale and generally difficult to remove from surfaces and ultimately it reduces heat transfer capability. Convenient protective steps to be taken in order to avoid the risk of serious consequences like metal failure in boilers at high temperature as well as brutal rapture occur due to plastic flow circumstances (Betz, 1980).

The process of crystallization arises by the combined action of nucleation as well as growth rates. Both of these processes are guided by the solution supersaturation. Therefore, crystallization established in the system by attaining a desired severity of supersaturation through a series of stages including: fulfillment of supersaturation, creation of nuclei and finally growth or advancement of crystals.

2.22.1 Solubility and supersaturation

In a heat exchangers, there is always a temperature gradient exists from bulk to the solid wall and the flowing stream can be in the form of saturated, unsaturated and supersaturated suspensions of foulants. In a saturated solution, the solid phase is at equilibrium with the liquid phase at a specific temperature. Solubility can be defined as the amount of solute needed to gain solution equilibrium at a particular temperature and when the dissolved solids in a given solution exceeds than saturation equilibrium, then the solution is termed to be supersaturated solution. On the other hand, if a solution

contains a solute in a quantity less than the required saturation is referred as unsaturated. Whereas for, both unsaturated and supersaturated solutions denoting equilibrium states. For a supersaturated solution, equilibrium condition is achieved by dissolving the excess amount of dissolved solids. Supersaturated solutions have the ability of provoking to initiate deposit formation.

For a given solution having a concentration C, the degree of supersaturation S, can be defined by the following relation:

$$S = \frac{C}{C_s} \tag{2.46}$$

Where, C_s representing the equilibrium concentration for a given temperature. In heat exchangers, supersaturation can be generated either by the evaporation of water from the process fluids as in evaporators or by the cooling the dissolved normal salts solubility below its solubility limits or heating the dissolved reverse salts solution at a level above its solubility temperature as well. In such types of exchangers, supersaturation may be achieved close in the vicinity of solid walls even the bulk solution is unsaturated.

It was realized that the generation of supersaturation is necessary, but not enough circumstances for crystallization may occur (Mersmann & Kin, 1988). In some real cases, supersaturated solution exists for a long time period without the presence of assembling crystals. Transformation of solid to liquid phase, needs two essential steps, one is overthrown of existing energy barrier causing stabilityof the system to obtain nucleation and other is successive change of lowering energy state. This state of lowering energy is accomplished through the mechanism of crystal growth.

2.22.2 Nucleation

In nucleation, the creation of tiny stable particles that can “seed” the process ofcrystallization, takes places in the new phase. Following report to demonstrate the

process of nucleation consisting of two main types i.e. primary and secondary nucleation (Nielson & Wilson, 1991).

2.22.2.1 Primary nucleation

This type of nucleation further consists of two categories, homogenous and heterogeneous nucleation. It is also referred as spontaneous crystallization. The definite understanding of this type of nucleation has not yet been accomplished, but it is expected to the formation of critical chunks of molecules having some extent of stability and makes sure the facilitation of newly created crystals and also extends its growth. Unlikely, homogenous nucleation is not directly liable for forming scale in heat exchangers, because of homogenous nucleation is frequently combine with pure solution, in which no involvement of other particle or crystals exists.

2.22.2.2 Secondary nucleation

In heterogeneous nucleation establishment of nucleates is induced artificially. These induced particles could be foreigner particles in the form of contamination in the process fluids or may be the rough surfaces of heat exchangers or the corrosion products lead the formation of nuclei, resulting the formation of crystallization in process equipment.

The primary nucleation is responsible for these two mechanisms. Once the micro crystals developed in the presence of supersaturated solution proceeds further crystallization in that locality leading the creation of macro-crystallization process, commonly called as secondary crystallization. The difference between nucleation and its various forms are presented on Fig. 2.17.

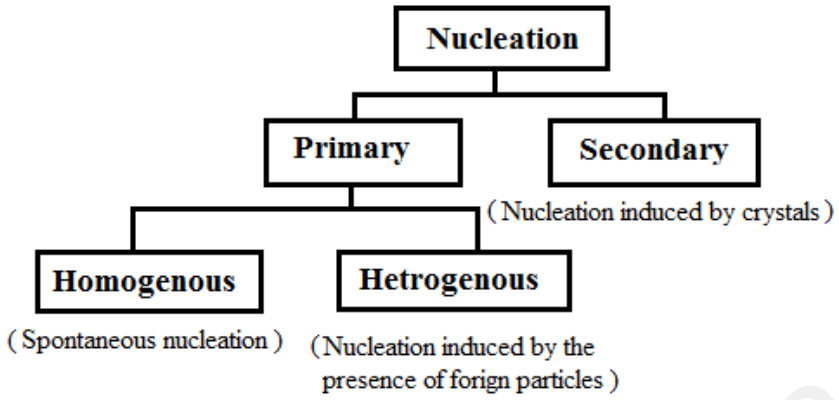

Figure 2.17: Schematic diagram for various types of nucleation (Bott, 1995)

Thermodynamic calculations are generally applied for the establishment of nucleation for a small particle existing in a supersaturated solution. The energy difference between the particle existing in solution and the solution itself is described as overall access free energy. This overall access free energy for spherical shape nuclei can be given by the following relation:

$$\Delta G = 4\,\pi\, r^2\, \sigma + 4/3\,\pi\, r^3 \Delta G_v \qquad (2.47)$$

Where, r is radius, σ is surface tension and ΔG_v is free energy change of transformation per unit volume of the nucleation.The heterogeneous nucleation mechanism in a supersaturated solution for a foreign particle or body is pictured in Fig. 2.18.

Depending on the type of lattice structure as well as surface of solid, the formation of solute can built on solid structure. Three types of energies are in contact at the point of interface including; interfacial energy between crystals and solution denoted by (γ_{CS}), between foreign particles and solution (γ_{FS}) and finally interfacial energy between foreign particles and crystals (γ_{Fc}).

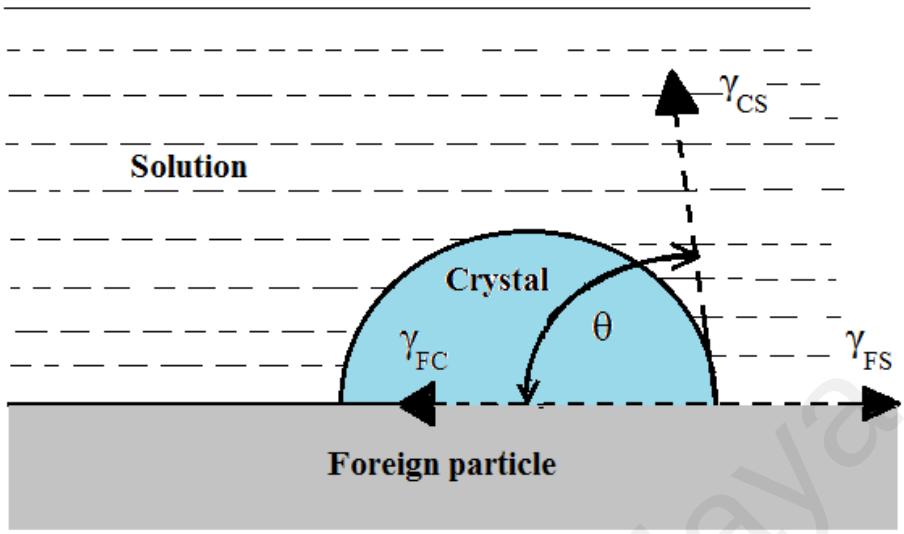

Figure 2.18: Contact angle and interfacial free energies at the boundaries for heterogonous nucleation (Mawaba, 2003; Zaho & Chen, 2013)

Where the values of contact angle θ ranging from 0 – 180^o between the surface of the foreign particle and growing crystal, depending upon the wetting ability between the growing crystal phase and foreign particle by the solution. At a contact angle of 0^o, means a complete wetting of particle, in which both supersaturation and nucleation mechanism recommended for the establishment of heterogeneous nuclei contribute towards zero. On the other hand, a contact angle of 180^o resembles a non-wettability tendency by the liquid as a result, no nucleation is needed.

2.22.2.3 Crystal growth

In this stage, during the passage of time, the tiny particles formed during the nucleation stage grow in size until become a finite visible crystal size. The factors influencing the crystal growth are solution concentration and temperature at liquid-solid interface. In 1972, Mullin reported three different theories regarding the growth of crystal mechanism, including the existence of diffusion layer, theories respecting diffusion and surface energy theory. In heat exchangers interface are almost different from those of the bulk solutions because of the existence of concentration gradient and temperature.

Moreover, also analyzed the crystal growth mechanism and concluded a sequence of steps developing simultaneously for an ionizing solute from saturated solution. He classified the following occurring steps:

1. Ions transformation from bulk solution to liquid-solid interface.
2. Adsorption phenomenon of ions on the neighboring surface or wall.
3. Surface movement of ions to the lattice.
4. Dehydration process of adsorbed ions and lattice
5. Integration tendency of ions into lattice.
6. Counter-diffusion of water molecules through boundary layer to the bulk solution.

For scaling mechanism, all the above steps may be associated into the mechanisms of transportation of ions from bulk solution to crystal growth and ions integration into crystal lattice or structure.

2.23 Fouling mitigation techniques

Strategies for fouling mitigation have long been examined and reported. Gilmour (1965), examined that the deterioration of shell and tube type heat exchangers efficiency as a result of fouling are the consequences of their poor thermal design. Several attempts have been proposed for the complete removal of deposits or minimizing degree of the fluid forming deposits (Kazi et al, 2009 and Muller-Steinhagen et al., 2007). These techniques can be categorized as: (1) Chemical methods (2) Mechanical methods (Cho et al., 2004).

2.23.1 Chemical method

A number of emerging technologies needs crystallization techniques for the proper implementation of the size, structure and morphology of the built-up deposits of inorganic salts. A number of chemical compounds as additives whether organic or inorganic play a vital role during crystallization and fouling mitigation are achieved by

chemical method. Additives are one of the easiest, cheap and most effective approaches commonly used for fouling mitigation.

These additives present at a very low concentration in process solutions, they are entirely divergent, and as well as more effective to impact crystallization consisting of tremendous-valence metal ions, surfactants, anti-foulants and polymers (Puckorius & Zimmie, 1972). Commonly it is a well-known fact that the presence of additives compounds or other foreign molecules in crystallization process can extremely influence nucleation (Pina et al., 1998 & Orme et al., 2001). A variety of chemicals have been developed and investigated as competent additives widely used for fouling mitigation as well as to prevent scaling on industrial scale (Harris & Marshall, 1981; Krisher, 1978). Application and the selection of scale inhibitors are one of the most frequently and effective way to impede undesirable inorganic or mineral salts deposition containing various effective functional groups like sulfonic acid, carboxylic acid, or phosphoric acid (Grohe et al., 2006). These inhibitors are designed in such a way that they possess the ability of producing a number of co-ordinate bonds with the surrounding cations of the available minerals surface, resulting to reduce surface energy sufficiently by the selective adsorption of the designed inhibitors or additives and suppress the growth rate. In 1971 Bott, categorized the additives in the following types including:

2.23.2 Sequestering agents

Containing EDTA, which is commonly used water additive, having ability of making strong complex with the presence of contains like Ca^{++}, Mg^{++}, and Cu^{++} with exchanging Na^{+}, therefore, avoid scaling. The proper utilization of these sequestering agents is uneconomical especially at high level of hardness (Teng et al., 2016).

2.23.3 Threshold agents

These include polyphosphates which are commonly used to minimize scale deposit in boiler feed water and cooling systems and even very minute quantity are adequate for

mitigating scale in supersaturated solutions. Their mechanism of mitigating scale is to prevent the development of nucleation leading to inhibit crystallization (Garrett, 1985).

2.23.4 Crystal modifying agents

These include such as polycarbxylic acid alters the crystal mode and further reduce the creation of large crystal size. In such a mechanism the altered crystals does not have the ability to settle down on hot surfaces, but they continue in the suspended form in the bulk, leading to particulate type of fouling, when their concentration exceed to some certain limits. The use of additives could not completely retard crystallization fouling, further leading the various forms of crystalline deposits contrasting from those formed in the presence of additives, leading a looser strength deposit which can be removed easily by fluid velocity. By a proper control of pH of the bulk solution, crystallization may further be reduced due to the fact that deposit solubility increases with decreasing pH level.

2.23.5 Seeding

Seeding is one of the well-known commercial methods to mitigate fouling, comprises the addition of external seeds to the scaling medium. In this kind of mechanism, crystallization takes place on the already added seeds instead of heat transfer surfaces. For avoiding of calcium sulphate scale, it is necessary to add calcium sulphate seeds to the scaling solution (Gainey & Thorp, 1993; Rautenbach & Habbe, 1991). The seeds added to bulk solution not necessarily to be crystalline nature, but should have exhibits of the identical crystallographic characteristics like atomic similarity and lattice arrangement (Telkes, 1952).

2.23.6 Dispersants

In order to mitigate the particulate fouling, dispersants are one of the particular chemical techniques commonly employed to minimize surface tension of formed fouling deposits.

The working mechanism of such method is to enhance the fragmentation of suspended particles into smaller size particles so that they are unable to settle down, rather remains in suspended form in bulk solution, resulting to avoid the contact of foulants away from heat transfer surface. The presence of some foreign particles like corrosion products, play a role of catalyst resulting corrosion fouling. As a result of corrosion fouling, a highly roughened heat transfer surface produced, which further leads crystallization fouling. Therefore, corrosion inhibitors commonly (polyphosphates and chromates) are added to mitigate corrosion, forming a protective metal oxide layer for preventing the corrosion of metal surface (Bansal et al., 1993).

The fouling mitigation by chemical means have several limitations and drawbacks. By the addition of various fouling and chemical inhibitors containing mostly inorganic and toxic chemical like chlorine, chromium, phosphates, zinc etc. These chemical effluents leaving from chemical plants to the larger water bodies like rivers, lakes, oceans and also having several side effects on human being jeopardizing, and effecting life of other living species (khan et al., 2015). Several organizations like Environmental protection agency (EPA), US Department of Transportation (DoT), and Occupational Safety and Health Administration (OSHA) have been limited the use of toxic chemicals in the form of inhibitors.

Therefore, the application of environmental-friendly compounds or natural products as inhibitors becomes more desired due to their biodegradable in nature and ecological attitude (McLaughlin et al., 1998; Rahim et al., 2008). Recently, researchers have been synthesized some alternate additives which are less toxic and biodegradable in nature (Ross et al., 1997; Darling & Rakshpal, 1998).

2.24 Summery of the presnt work

The present work focued on correlating the hard wood fibre (acacia mangium and acacia mangium hybrid) suspension and flow rates with their heat transfer coefficient *hc* and and pressure drop $\Delta P/m$ in the closed conduit flow. It was observed that the presence of a small quantity (0.2 wt.%) of wood fibers in water flowing through a heated pipe resulted an enhancement in heat transfer coefficient *hc* at a domain of pulp flow velocity from 1 m/s and continues up to the end of the investigated range of velocity. The maximum increase in h_C observed mostly at the maximum velocity of 3.6 m/s. At higher fibre concentration in suspension such as 0.4 wt. % and 0.6 wt.%, the values of h_C were observed decreasing below water values. The effect of fibre refining (fibre beating) has significant effect on *hc*. It is usually found that at low degree of beating i.e 2000 degree, both (Acacia mangium and Acacia mangium hybrid) do not significantly affect *hc* values throughout the velocity range, whereas, by the increase in beating degree (4000 and 8000 degree) it would like to reduce the *hc* values in a regular pattern. On the other hand, the *hc* values obtained at concentration of 0.6 wt. % and 1.2 m/s correlated well with fiber length, flexibility ratio and slenderness ratio. The *hc* values would be decreased by a decrease in fiber length and fiber slenderness ratio or increase in flexibility ratio. However, an approximate linear relationship between *hc* values and fiber/paper properties (from a specific wood fiber species) has shown that the specific fiber and paper properties could be predicted by monitoring heat transfer data. Previous research on pine fibre has shown a similar type of corelations (S.N. Kazi, PhD thesis 2001). This reveals that h_C or pressure loss data obtained from a specific fiber species cannot be used as an indicator for pulp and paper quality from other fiber species.

For fibre friction losses the drag reduction has occurred at fiber concentration of 0.6 wt. % throughout. Lower drag ratio provides higher drag reduction. The flow behavior of wood pulp fibre suspensions in drag reduction region are similar to those reported for

wood fiber suspensions, where maximum drag reduction is followed by increase in drag ratio to near the water line at higher velocities. By increasing the degree of beating for both wood fibres (Acacia mangium and Acacia mangium hybrid) correspondingly increases the drag reduction level, in the present investigation the maximum values are observed at a flow velocity of 1.6 m/s.

In the pulp and paper industries, there occurs corrosion due to use of chemicals. Inaddition, the existence of corrosion products also observed at the fouling sites. So the exploration of noval metals, corrosion and fouling mitigation have taken under consideration in this research work.

Fouling on heat transfer surfaces are mitigated by various means among them natural fibre additions as an eco-friendly additive is a promising one. As the heat transfer values and frictional pressure losses during the flow of fibre suspension were found to be effected by the corrosion fouling, therefore, the employment of Schiff base compounds as corrosion inhibitor were added at different concentration using weight loss and electrochemical methods with FESEM analysis. The inhibition mechanism based by the virtue of formation of compact layer at liquid/solid interface following the Langmuir adsorption isotherm. Moreover, the inhibition efficiency of HL_1 is greater than HL_2 for MS in the case of HCl, whereas on the other hand, HL_3 has greater inhibition efficiency as compared to HL_4, depending on the chemical structure of the investigated inhibitors. All the results of corrosion achieved form electrochemical measurements and weight loss methods are in good agreement, with a minor deviation in numerical values.

Formation of mineral scales on heat exchangers and equipment surfaces is a persistent and an expensive problem in heating and cooling water systems. Gelatin has high or even more mitigation efficiency as compared to other chemical additives where a maximum efficiency of 95% could be achieved even at a low concentration of 0.5 g/L. The fibre modifies the fouling deposition mechanism on heat transfer surfaces but also

suppresses the scale formation rate as well. To generate more data in the specified field, fouling with supersaturated $CaSO_4$ solution was investigated on a stainless-steel surface. It was observed, less fouling desposition on heat transfer surfaces by adding pinr natural wood pulp fibres in the $CaSO_4$ fouling silution. The addition of a little amount of fibre in the suspension provided a significant effect of fouling retardation. In the present study, fouling retardation of $CaSO_4$ solution was performed by adding Gelatin as natural measure

CHAPTER 3: MATERIALS AND METHODOLOGY

3.1 Pipe line flow loop

A detailed overview of the test rig and the measuring equipment are presented in this section. The experimental set-up is shown in Figure 3.1. The main parts of the setup consists of a tank with volume of 100 L, variable speed pump, magnetic flow meter, pressure transducer across the test section, heated pipe test section, chiller for cooling inside the tank, and a recycle piping system.

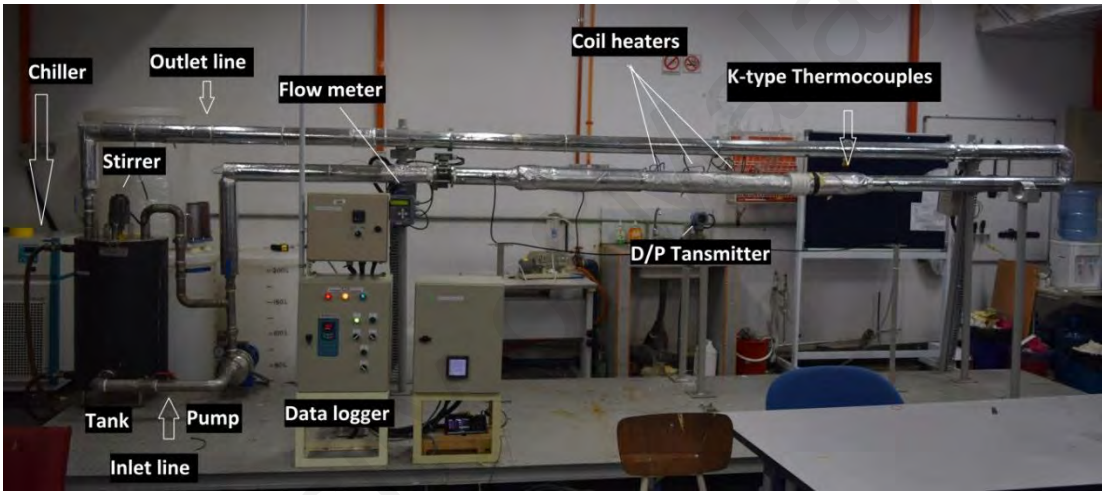

Figure 3.1: Photo of the test rig and the measuring equipment

The pipe has a circular cross-section and is made of stainless steel. The fluid is pumped from a tank by a centrifugal pump. The suspension is then passed through a magnetic Flow transmetter and the test section. The fluid is then returned to the stock tank through the return line. Fluid in the jacketed tank is again cooled to the desired tank temperature by a chiller. All the flow loop piping except the test section is stainless steel pipe. The test section is made from Aluminium. The whole test rig is insulated in order to avoid heat loss to the atmosphere. Inlet and outlet fluid temperatures were measured by type-K thermocouples located in the centre of the flow.

The hermocouples are inserted facing downstream in the elbows before and after the test section to reduce fiber stapling. The test section is installed far away from the flow

meter at discharge section of the loop to avoid disturbance and obtain steady state at the point of measurement. Frictional pressure loss across the test section and on the Al straight piping were measured by pre calibrated pressure transducers. The heat transfer test section was designed and constructed at the University of Malaya. The sectional view of the experimental test section is presented in Figure 3.2.

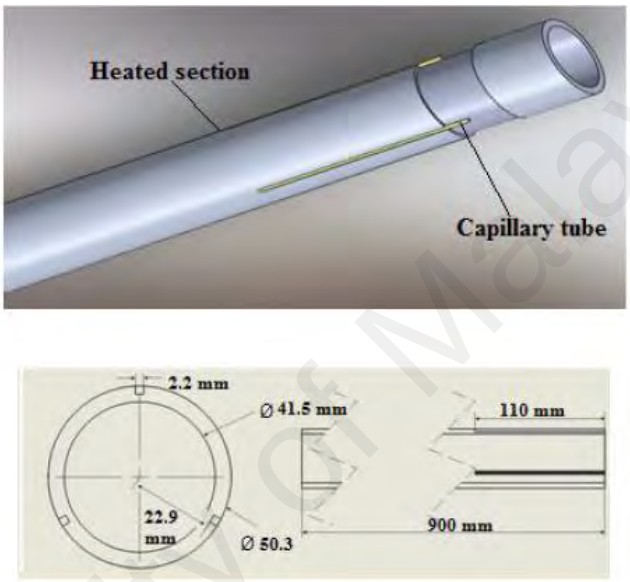

Figure 3.2: Overview of experimental test section

The heat transfer test section is a 900 mm length of 41.5 mm internal diameter Aluminum pipe. At least three grooves were cut sideways the test section that was to be heated beginning from the discharge end of the heated test section and continuing up to 110 mm inside along the section. The functions of these longitudinal grooves have provisions to house the thermocouples. The grooves were cut as deep as possible while ensuring that the inside surface of the pipe was not disturbed. The length between surface of the grooves and the tube inner surface was retained at 2.25 mm. Care should be then to keep the thermocouple in location three stainless steel 1.5 mm diameter thermo-wells were installed. Stainless-steel capillary tube thermo-wells were laid in the grooves downstream from the heated section with one end exiting outside the pipe wall.

Grooves of the test section were filled with high temperature resistance paste to fix the thermo-wells in location. Three Omega type–K thermocouples were inserted up to the end of the capillary tubes to obtain the wall temperature at a point approximately 110 mm from the discharge end of the heated section. One set of pressure tapping, across the test section was connected to differential pressure transducer to obtain friction loss measurements. The test section was heated by ten flat coil heaters each with wattage of 900 W. The heaters were clamped on the outside of surface of the test section. The specifications of the equipment used in test rig are presented in Table 3.1.

Table 3.1: The specifications of the test equipment

Name	**Specification**	**Quantity**
Chiller	HX-45H (JEIO TECH) Cooling capacity: 4.7 KW @ 20ºC Working Temperature Range: 3-40 ºC	1
Stirrer Blade	15x100 mm	1
Stirrer Motor	DC, Max speed 200 rpm, Variation speed	1
Tank	100 Liter, SS	1
Pump	COM500/22/A (LOWARA) Power: 2.71 KW, Speed: 2795 RPM	1
Flow meter	8000 A SERIES (FOXBORO) Magnetic flow meter	1
Data Logger	GRAPHTEC GL220	1
D/P cell transmitter	Model: Model IDP10 (FOXBORO) Sensor temperature limits:-46-121 ºC Calibration range: 0-200 KPa	1

3.2 Data acquisition

Data for the inlet and outlet temperatures and wall temperatures are logged using a data logger (Graphtec, midi logger GL220). The current and voltage were measured by 1000 A true RMS clamp meter (Agilent) to calculate the heater power. All measurements were taken after the heat transfer loop had reached steady-state conditions at the chosen velocity, bulk temperature and heat flux. The velocity was systematically increased; the heat flux was adjusted to achieve the desired amount. The thermocouples were calibrated to measure the surface temperature according to equation (3.1):

$$T_W = T_t - \frac{\dot{q}}{\lambda/_x} \tag{3.1}$$

Where, the heat flux ($\dot{q}$) was the amount of total heat supplied through the phase angle power controller to the heaters divided by the heated area. The actual wall temperature (Tw) was calculated from the temperature measured in the test section (T_t) with a correction to account for the distance of the thermocouple below the heating surface to the inner wall of the pipe in fluid contact. The wall resistance for each thermocouple (λ/x) was determined by calibrating the test rig with water as presented in Appendix B. The local heat transfer coefficient $h_C$was calculated from equation (3.2):

$$h_c = \frac{\dot{q}}{(T_w - T_b)} \tag{3.2}$$

The bulk temperature Tb, position-weighted the average of inlet and outlet temperatures streams (T_i and T_o). The bulk temperature was calculated by the relation in equation 3.3, selected on the basis of assumption that the fluid stream temperature increases linearly through the heated section and stayed constant at the unheated region of the test rig.

This is practical because the rise in temperature between thermocouples located at inlet and outlet was usually less than 1°C.

$$T_b = T_i + \frac{X_1}{X_2}(T_o - T_i) \qquad (3.3)$$

Where, X_1 and X_2 denotes the distance of thermocouples tip along the flow direction and heated length respectively.

3.3 Experimental procedure

3.3.1 Pulp suspension preparation

The experimental study consisted of several sets of runs to meet the defined objectives. Pulp fiber suspensions were prepared from two wood pulp samples: Acacia mangium and Acacia mangum hybrid prepared by the mechanical and chemical process (soda process) and were used a primary pulp source. All samples provided by the Forest research institute Malaysia (FRIM).

3.3.2 Preparation and characterization of fibre samples

3.3.2.1 Preparation of fiber suspension

The present research work was carried out for some several set of runs in order to fulfill the required objectives. Pulp fiber suspensions were prepared from two wood pulp samples: Acacia mangium and Acacia mangium hybrid. For a known concentration the required calculated amount of the sample, based on the moisture content was disintegrated. The specimen was added to 2000 mL tap water (1.2% consistency) at 20 ± 2°C and was disintegrated at 3000 rpm until all fiber bundles were dispersed. The disintegration process was done according to the TAPPI standard where the revolutions were not more than 50,000 (TAPPI, 2002).

After disintegration, the pulp suspension was added to the tank and dispersed by the agitator homogenously. The concentration of the slurry was adjusted to the desired

value. To measure the pulp consistency, the standard provided by TAPPI was followed (TAPPI, 1993). For beating process, Acacia mangium fibers were beaten (before adding to the tank) by the PFI refining mill for three different degrees of beating i.e. 2000, 4000 and 8000 respectively.

3.3.2.2 Fibre sample preparation and measurements

Several shape descriptors are often used for approximating the longest axis of fibre objects. However, due the fibre curled shape, of fibres, none of the mentioned dimension descriptors will provide a good estimation of the fibres dimensions. In addition, one of the simplest method ususally employed for estimating the fibre dimensions is the longest length path of fibre across the fibre's skeleton. Add 5 gm (oven dried) of fibre in 50 ml beaker containing 30 ml of distilled water putting a few drops of red ink (for proper visualization in Leica microscope). After proper stirring a few drops of fibre-samples were dropped on glass slides after proper drying kept it in miscropscope with adjusting it upto 500 pixels. Fibres with complete length and diameter were chosen randomly and an average of 50 fibres length and diameter were selected and get an average length as well as diameter through fibre skeleton. (Fig A.9 and Fig.A.10, Appendix A)

3.3.2.3 Preparation of hand sheets

A flowchart of papermaking process is presented in Figure 3.3. Hand sheets of all the fibers were made according to the TAPPI standard T-205 (TAPPI, 2002). A description of sheet making process has been presented in Appendix A.

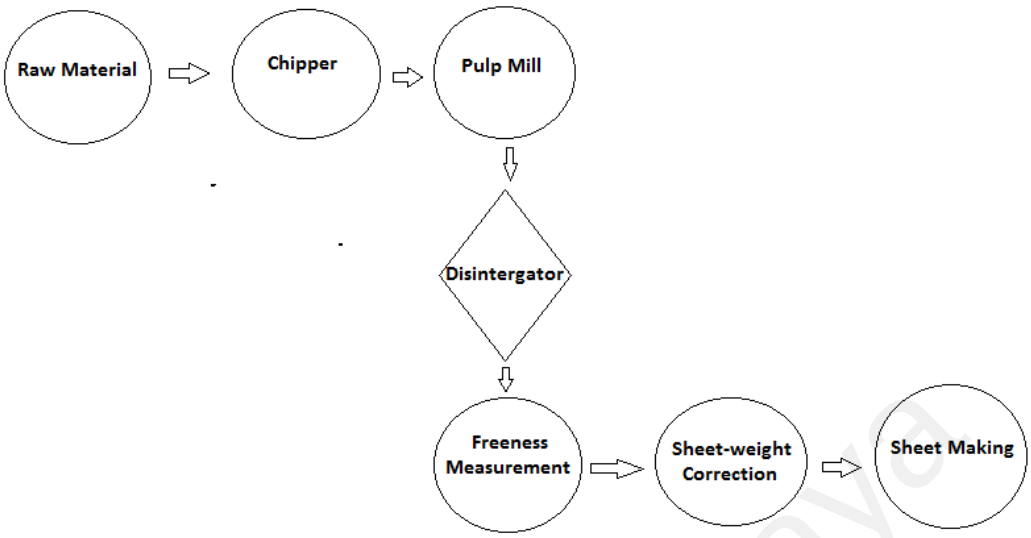

Figure 3.3: Flowchart of sheet making process

3.3.2.4 Characterization of fibers and hand sheets

For the present research study, fiber length (L), fiber width (W) and lumen diameter (d) were measured based on an average of 50 measurements by using a Quantimeter Image Analyzer equipped with a Lecia microscope and Hipad digitizer (from Quantimet 520, Cambridge Instruments). Three derived values: slenderness ratio (L/ W) and flexibility coefficient (100 × d/D) were calculated using the measured data (Mossello, Harun, Resalati, et al., 2010).

The microscopic images (Appendix A, Figures A.1- A.5) of fibers were taken using the scanning electron microscope (SEM). Physical properties of hand sheets were examined using different devices and according to TAPPI procedure (Appendix A, Table A.1). Determine the average mass per unit area of five conditioned sheets by weighing them together on a balance sensitive to 0.001 g. The grammage is ten times the weight of the five sheets. Tensile index, burst index and tear index were measured using tensile tester, burst tester and tear tester respectively. Brightness was determined by opacity-meter. No. of fold, was obtained using MIT folding tester.

3.3.3 Experimental runs for heat transfer study of pulp suspension

The experiments were set on different concentrations. For each concentration the run consisted of a series of measurements of temperature differential as a function of suspension bulk velocity with constant bulk temperature and heat flux. For the experimental set of data, the bulk velocity was ranging from 0.4 to 2.8 m/s for heat transfer data in increments of approximately 0.4 m/s. The heat flux was manually adjusted with the power controller to give a constant power of 3400 Watts. Once this condition was satisfied at steady state, measurements were recorded to determine the heat transfer coefficient. The experimental parameters are listed in Table 3.2.

3.3.4 Experimental runs for pressure loss study of pulp suspension

The procedures conducted for pressure loss study consisted of several set of runs. The effects of temperature and additives on pressure loss were investigated. For pure pulp suspensions the experimental settings were almost same as the heat transfer with the difference in bulk velocity where the range is between 0.4 m/s to 3.6 m/s. In order to study the effect of temperature on pressure loss the experiments were conducted at two bulk temperatures of 23 °C and 30 °C for 0.6 % A. mangium pulp suspension.

Table 3.2: A summary of experimental conditions for heat transfer and pressure loss studies

Parameter	Heat transfer study	Pressure loss study
Bulk Temperature	30 ºC	For water and all samples
Samples	Acacia Mangum Mechanical (AM)	Acacia Mangum Mechanical (AM)
Pulp type	Acacia Mangum Un-bleach (AMUn-B)	Acacia Mangum Un-bleach (AMUn-B)
Power	For bulk temperatute 30 ºC 3400 Watt	For bulk temperatute 30 ºC 3400 Watt

Table 3.2 “continued”

Parameter	Heat transfer study	Pressure loss study
Pulp type	Acacia mangium bleach	Acacia mangium bleach
Pulp concentration	For unbeaten samples: (0.2%, 0.4%, 0.6% wt.) For beaten samples: (0.6wt.%)	For unbeaten samples: (0.2%, 0.4%, 0.6%) For beaten samples: (0.6 wt.%)
Velocity range	0.4-2.8 m/s	0.4-3.6 m/s

3.3.5 Characterization of pulps and hand sheets

The fiber properties e.g., Fiber length, fiber width and lumen were measured using the Fiber analyzer. The microscopic images of fibers were taken using the scanning electron microscope (SEM). Physical properties of hand sheets were examined using different devices and according to Tappi procedure. The microscopic morphology of the prepared sample was observed using a high resolution FEI Quanta 200F field emission scanning electron microscope (FeSEM).

The rheology of all suspension was studied using a *Bohlin CVOR* rheometer with plate and kept the plate (40 mm) at temperature of 23 °C. Before starting the actual measurements, a 15 min pre-shear interval at 300 s was applied on the sample. The intensive pre-shear period was implemented to break down the flocculated Acacia mangium network structure. Then the sample was left to rest for at least 10 min. Oscillation measurements were performed after the pre-shear and rest of the periods. Frequency sweep was measured from 0.02 to 100 Rad/s at 0.5% strain.

3.4 Preparation of electrodes

The working electrodes were commercial mild steel and carbon steel sheets were purchased locally. The specimens were fixed on a polyester base in such a way that only

2.56 cm^2 of their cross-sectional area were uncovered to the corrosive solution of 1 M HCl and 1 M H_2SO_4. The working electrodes surfaces were abraded mechanically with sand papers of different grades starting from: 600, 800, 1000, 1200 and 1500. Initially, the electrodes surfaces were cleaned with double distilled water, CCl_4, followed by ethanol for degreasing, dried and kept in desiccator for the removal of humidity. For each separate run freshly abraded electrode was utilized. The HCl and H_2SO_4 solutions were prepared from analytical grade concentrated hydrochloric acid (37 %), sulphuric acid (98 %) and deionized distilled water. All the tests were done in the presence of aerated and non- stirring conditions in 1 M HCl and 1 M H_2SO_4 acidic solutions with a concentration range of 25, 50, 75 and 100 ppm at room temperature.

3.5 Inhibitors synthesis

Quinazoline Schiff bases were synthesized according to the scheme mentioned below. All the chemicals and solvents required for the synthesis purpose were purchased from Merck Marker Pvt. Ltd (Malaysia).

In a typical practice one equivalent of aminobenzyhydrazide was dissolved in 50 mL methanol, adding two equivalents of substituted aromatic salicyaldehyde in the solution and refluxed the reaction mixture for 2 h.The precipitate formed during the reaction was evaporated and followed by the subsequent filtration and washing with a cold methanol and finally dried. The pureness of the compounds was tested by TLC, CHN analysis, and H and C-NMR. The detailed characterization and synthesis of the quinazoline Schiff base inhibitor was reported according to the previous published report (Fadhil et al., 2014).

The Quinazoline Schiff bases compounds were synthesized and characterized earlier by Fadhil et al. in 2014. These compounds were investigated for anticancer activity against MCF-7 human breast cancer cell line. The selections of these Quinazoline Schiff bases were used for the first time as anti-corrosive additive for iron and steel alloy in different

solutions. Quinazoline Schiff bases have the advantage to the rest of other inorganic and other toxic chemical like chromate, phosphates etc. as they are environmentally friendly and biodegradable in nature, readily availability, renewable sources, and favorable ecological aspects and can be synthesized by simple procedure at low cost. In Addition, due to the presence of C=N-, -OCH_3, -OH, -NO_2 group as well as the occurnace of electronegative heteroatoms like Nitrogen, Oxygen and Sulfur atoms in their molecular structure, Quinazoline Schiff bases are considered to be excellent corrosion inhibitor. So the present investigation has considered mild steel as the substrate for investigation its effect in the presence of H_2SO_4.

The details of the synthesized Schiff base compounds are listed in Table 3.3.

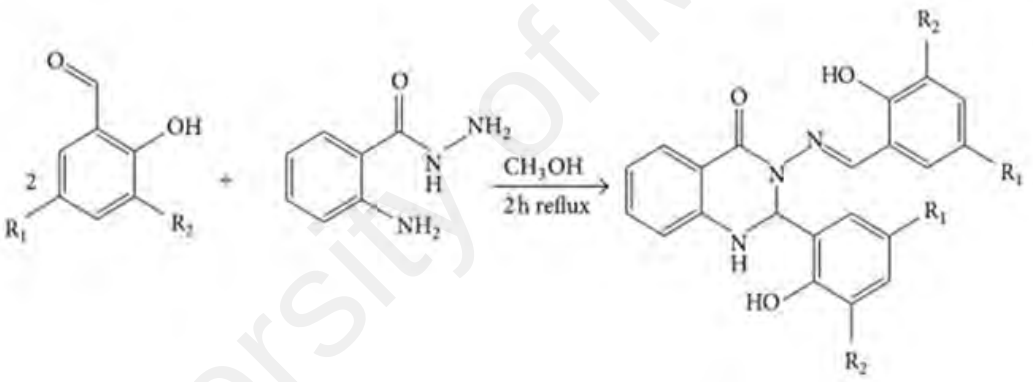

Scheme: A general path way for the synthesis of Schiff base compounds

3.6 Analysis of corrosion products

Specimens of Mild steel and Carbon steel with dimensions of size 0.2 cm × 0.2 cm × 0.1 cm after polishing with series of different grades of emery papers as: 600, 800, 1000, 1200 and 1500, followed by degreasing with trichloroethylene and finally submerged in 1M sulfuric acid and 1M hydrochloric acid solutions with and without inhibitors (HL_1, HL_2 HL_3 and HL_4). After exposure of 24 hours into corrosive solutions, the specimens were separated, washed and finally scraped of the corrosion products.

Table 3.3: The Abbreviation of Quinazoline Schiff Bases as corrosion Inhibitors

Inhibitors	Abbreviations
3-(5-methoxy-2-hydroxybenzylideneamino)-2(5-methoxy-2-hydroxyphenyl)-2,3-dihydroquinazoline-4(1H)-one (MMDQ)	HL_1
3-(5-nitro-2-hydroxybenzylideneamino)-2(5-nitro-2-hydroxyphenyl)-2,3-dihydroquinazoline-4(1H)-one (NNDQ)	HL_2
2-(3,3-Dimethyl-2,3-dihydro-indol-2-ylidene)-3-[(2-hydroxyphenyl) imino] propylidene (DHP)	HL_3
2-(3,3-Dimethyl-2,3-dihydro-indol-2-ylidene)-3-[(2-hydroxyphenyl) imino] propanal (DHAP)	HL_4

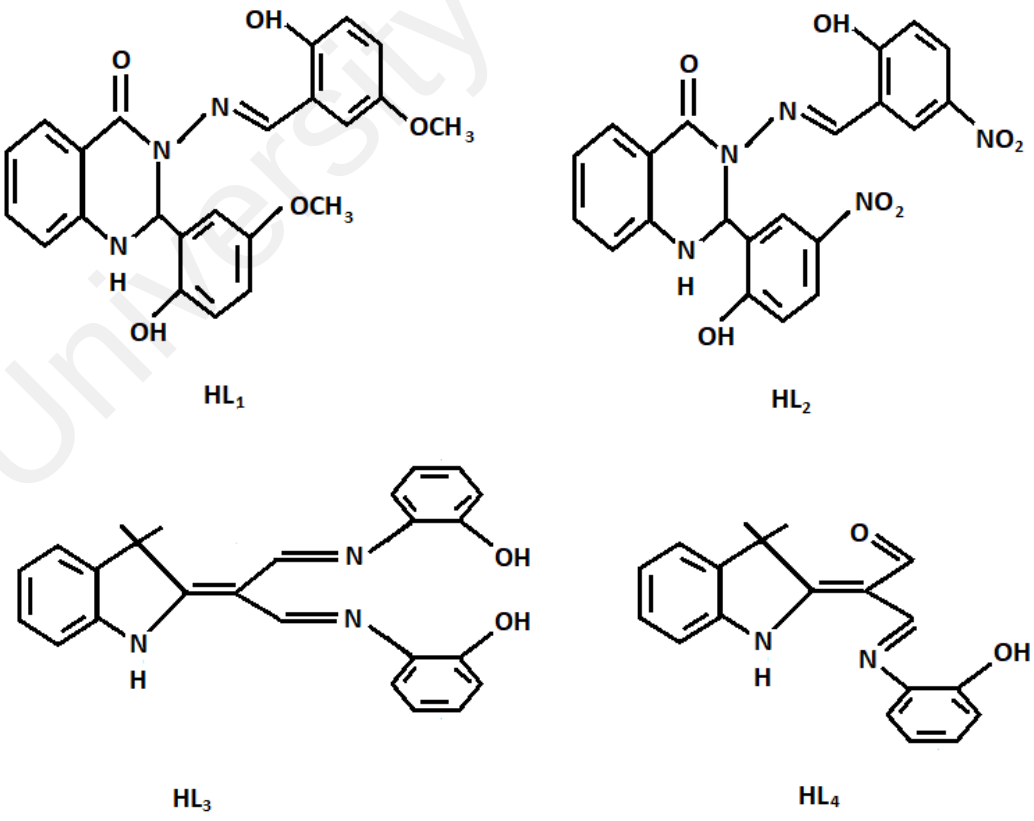

Figure 3.4 The chemical structures of the investigated compounds

3.7 Weight loss measurements

The abraded MS and CS specimens of 2.0 cm x 2.0 cm x 0.1 cm after washing, degreasing with acetone followed by proper drying and placed in a desiccator for several hours. The chemical weight composition of MS (wt. %) were: Fe, 99.604; C, 0.103; Si, 0.03; P, 0.021; Mn, 0.230; Al, 0.012 CS (wt. %) Fe, 99.60; C, 0.103; Si, 0.03; P, 0.021; Mn, 0.230; Al, 0.012.The specimens were weighted initially, using electrical balance and immersed in 1 M acidic solutions with and without the addition of Schiff bases. After an exposed time of 24 h specimens were taken out, again rinsed thoroughly with deionized water, dried and re-weighed. The corrosion rate in mg cm^{-1} h^{-1} was calculated by equation (3.1) (Yadav et al., 2012).

$$C_R = \frac{W_1 - W_2}{A\ X\ t} \qquad (3.1)$$

Where, W_1 and W_2 are the average weights of specimens before and after the exposure respectively and A is the total available surface area of the specimens in cm^2 and t is the immersion time in h.

In a similar fashion, surface coverage (θ) and inhibition efficiency η_{WL}(%) were calculated by the equations (3.2) and (3.3) respectively.

$$\theta = \frac{C_R^0 - C_R}{C_R} \qquad (3.2)$$

$$\eta_{WL}\ \% = \frac{C_R^0 - C_R}{C_R} X\ 100 \qquad (3.3)$$

Where, $\theta$is the surface coverage, η (%) and C^o_R and C_R are the corrosion rates in the absence and presence of the inhibitors, respectively.

3.8 Electrochemical measurements

A conventional three electrodes cell was utilizes in these experiments, with CS (2.56 cm^2) as the working electrode, a platinum wire and saturated calomel electrode (SCE) as the counter electrode and reference electrode respectively.

General purpose electrochemical software (GPES) and Frequency response analysis (FRA) software were used for anodic and cathodic Tafel curves and EIS experimental measurements and open circuit potential (OCP) techniques. These software were installed in a computer interfaced with an (AUTOLAB PGSTAT 30, Netherlands) instrument. The current-potential range were between +0.3 to -0.3 V_{SCE} at a scan rate of 10 mV s^{-1}. The impedance measurements were carried out at OCP values in a frequency range of 100 kHz – 10 mHz with peak to peak amplitude of 5 mV. Prior to all electrochemical measurements (Tafel curves and EIS) the CS specimens were immersed into the test solution containing inhibitors at various concentration for a time period of 1 hr in order to establish a steady state open circuit potential (E_{ocp}). An overview of the test up is shown in figure 3.5.

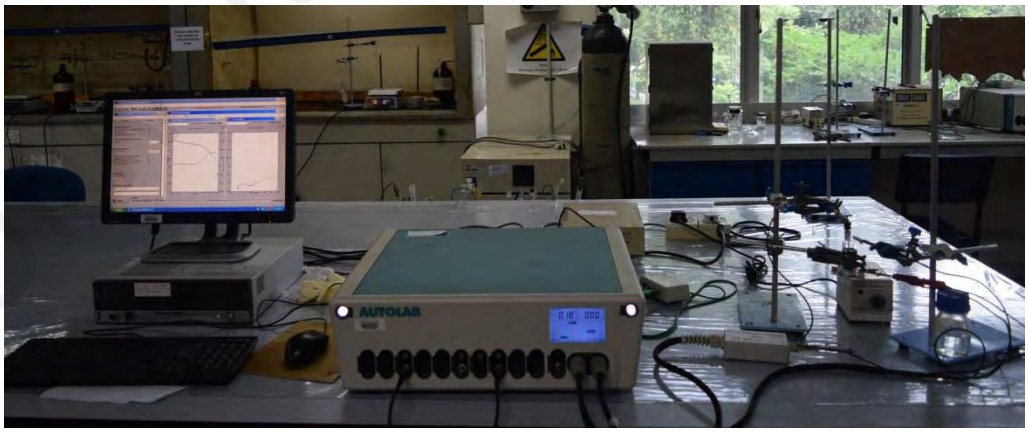

Figure 3.5: A conventional three electrodes (AUTOLAB PGSTAT 30, Netherlands) cell setup

The linear Tafel segments of the anodic and cathodic curves were extrapolated to obtain the corrosion potential (E_{corr}) and corrosion current density (i_{corr}). The $\eta_P(\%)$ at different inhibitors concentrations were calculated from the equation (3.4) [34]:

$$\eta_P\% = 1 - \frac{i_{corr}}{i^o_{corr}} X\ 100 \qquad (3.4)$$

Where, i^0_{corr} and i_{corr} are the corrosion current densities (mA/cm^2) in the presence and absence of the inhibitors, respectively.

The inhibition efficiency η_{RP} (%) calculated by polarization resistance in below relation (3.5) [34]:

$$\eta_{RP}\ \% = \frac{R_P - R^0_P}{R_P} X\ 100 \qquad (3.5)$$

Where, R_P and R^0_P are polarization resistance of the inhibited and uninhibited solutions respectively.

3.9 Field emission scanning electron microscope (FESEM) studies

The specimens for both NS and CS having dimensions of 2 cm x 2 cm x 0.1 cm were submerged in 1M HCl and 1MH_2SO_4 solution for 24 h in the presence and absence of Schiff Base inhibitors at ambient temperature at non-stirring conditions. The FESEM analyses for the investigated Schiff bases were carried out at a concentration of 100 ppm in both 1 M HCl and 1 M H_2SO_4 solutions. The changes occurred during surface morphology of the specimens were investigated by field emission scanning electron microscopy (FESEM), with a JEOL JSM-840A at an accelerating voltage of 10 KeV.

3.10 Techniques used in corrosion study

Electrochemical and surface analysis techniques have been utilized to study the corrosion behavior by varying the temperature and flow speed on Al alloy metal. Among the techniques employed are OCP (Open Circuit Potential), LPR (Linear Polarization Resistance Measurements), AC Impedance measurements and potentiodynamic data (Marcus 2002).

3.10.1 Open Circuit Potential Measurement

When a metal specimen is immersed in a corrosive medium, both reduction and oxidation process occur on its surface. Typically the specimen oxidizes (corrodes) and the medium (solvent) is reduced. The specimen must function as both anode and cathode, and both anodic and cathodic current occur on the specimen surface. Any corrosion processes that occur are usually the result of anodic currents.

When a specimen is in contact with a corrosive liquid and the specimen is not connected to any instrumentation, it assumes a potential (relative to reference electrode) termed the corrosion potential, E_{corr}. A specimen at E_{corr} has both anodic and cathodic current present on its surface. However these currents are exactly equal in magnitude so there is no net current to be measured. The specimen is at quasi-equilibrium with the environment (even though it may be visiblecorroding). The E_{corr} can be defined as the potential at which the rate of oxidation is exactly equal to the rate of reduction, and should be measured with an electrometer. Open circuit measurements can be used as an indicator of the development of active corrosion, and their success depends upon the long term stable performance of the standard reference electrode.

3.10.2 Polarization Resistance Technique

The linear polarization resistance method is capable of measuring the corrosion rate of a system. It is achieved by shifting the corrosion potential typically 10 to 20 mV towards more noble or more active. Both the potential and the current required to achieve this

potential are recorded. The potential is stepped in increments (called over-potentials, typically 1mV) from one extreme to the other and each of these steps is recorded. The plotting of these data yields a polarization curve. When this is done, it is observed that the applied current density is a linear function of the electrode potential.

Figure 3.6, shows a typical diagram of the potential-current linear relationship, the slope of this curve has dimensions of a resistance i.e.

$$[\Delta E / \Delta I] = R_p \qquad (3.6)$$

Where, R_p is the polarization resistance in ohms or ohm-cm^2 in case of ΔI, Rp is inversely proportional to corrosion rate and the corrosion current density is given by Stern-Geary equations. Thus, for charge transfer controlled reaction:

$$I_{corr} = (b_a \times b_c) / [2.303 (b_a + bc) R_p] = B/R_p \qquad (3.7)$$

Where, b_a and b_c are the anodic and cathodic Tafel slopes, respectively, B is the Tafel constant, and Icorr is the corrosion current. By dividing Icorr (Amps) by the surface area (cm^2) of the polarized steel, we obtain the corrosion current density, Icorr.

If the cathodic process is diffusion controlled equation (3.7) reduces to:

$$I_{corr} = b_a / (2.303 R_p) \qquad (3.8)$$

Some of the limitations of the Tafel extrapolation method can be overcome by using the linear polarization measurement technique. Corrosion rate measurement can be made directly and rapidly. Because the extent of polarization of specimens is little, the measurement technique does not damage the specimen significantly, and so the

measurement approach can be used several times on the same specimen. It generally measures corrosion rate accurately.

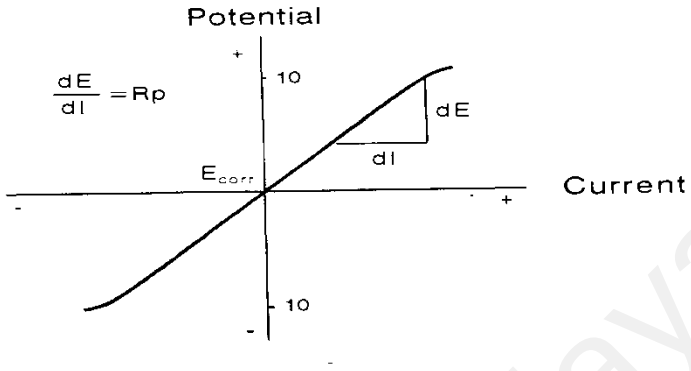

Figure 3.6: E - I linear relationship at ±10 mV over potential from E_{corr}

Any more accurate estimates or measurements of Tafel slopes will reduce considerably the uncertainty of corrosion rates obtained from R_p. However, if relative values of corrosion rates are of greater interest than absolute values (which is often the case), the polarization resistance method becomes more attractive.

In laboratory, the change in Icorr with time or the kinetics of the corrosion be of more interest than the absolute values of Icorr. The same is true industrially. Often a large change of corrosion in a process stream is far more important than the exact value of corrosion rate, especially if the corrosion rate is known within a factor of 2.

3.10.3 Polarization Curves

Polarization curves are commonly used for corrosion rate determination. The corrosion current density can be estimated usually by Tafel extrapolation of the anodic and/or the cathodic lines of the polarization curve. The method is rapid compared to conventional weight loss, and provides a direct measure of corrosion current density (i.e. corrosion rate). Polarization curves are also useful for studying the inhibition mechanisms, and they may also indicate passivity.

However, the method can be time consuming. Since several hundred milli-volts are applied to the specimen. Because of this large polarization of the corroding electrode, it is possible that irreversible changes occur due to the measuring process, so that further tests with the same electrode cannot be expected to provide reliable results. This method is, therefore, of only limited value for corrosion monitoring purposes. The method is based on the kinetics of the electrochemical reactions, which is the rates of both anodic and cathodic reactions follow Tafel behavior, i.e.

$$E = a + b \text{ Log } i \qquad (3.9)$$

Where, E is the electrode potential of the specimen, i is the current density and "a" and "b" are constants. The "b" constant in this equation is often referred to as the Tafel slope and is usually expressed in mV/decade. The corrosion current can be estimated if the electrochemical corrosion processes follow this Tafel behavior.

The exponential behavior of current density with potential means that the anodic contribution to the net current density can generally be ignored if the specimen potential is made significantly more negative than the open circuit potential (corrosion potential) value (i.e. > 50mV), while the cathodic contribution is usually negligible at potentials more positive than the corrosion potential (i.e .> 50 mV). These relationships are shown graphically in the form of polarization curve, Figure 3.7.

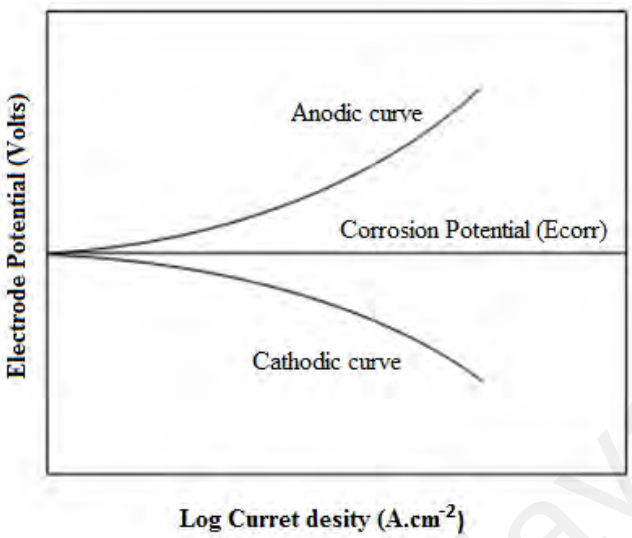

Figure 3.7: Polarization curve diagram (Mark et al. 2008)

Based on these observations, several ways can be used to estimate the corrosion current from the polarization curve (Marcus 2002). The specimen can be polarized to potentials more negative than the corrosion potential, and sufficient data points taken to obtain a reliable Tafel line. Then the current density data can be extrapolated back to the corrosion potential to obtain the corrosion current density as shown in Figure 3.8a. The second method is analogous to the first in that the specimen can be polarized anodically to more positive potentials than the corrosion potential, and the same process is repeated as shown in Figure 3.8b. The third method requires that both cathodic and anodic polarizations be carried out as described above, and the corrosion current density is obtained at the intersection of the anodic and cathodic extrapolated lines as shown in Figure 3.8c. Another source of error in using polarization curve to estimate corrosion rates is the scan rate effect. In order to obtain a true polarization curve, it is necessary to hold the potential constant until a constant current is achieved. In practice it is normal to use a potentiodynamic scan, which gradually increases the potential and records the current continuously.

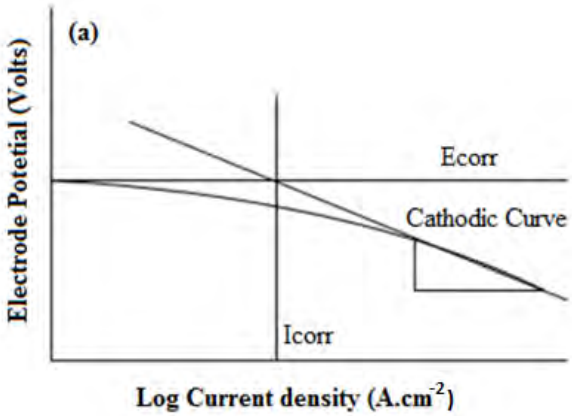

Figure 3.8: Illustration of three Tafel extrapolation methods (a) of estimating corrosion current density (Marcus, 2002)

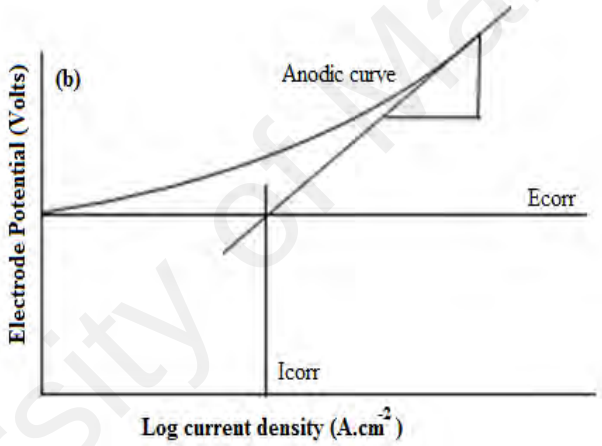

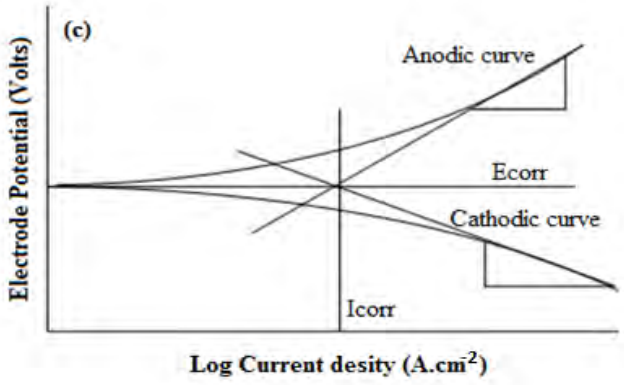

Figure 3.8: Illustration of three Tafel extrapolation methods (b, c) of estimating corrosion current density (Marcus, 2002)

3.10.4 Electrochemical impedance spectroscopy (AC techniques)

Electrochemical impedance spectroscopy (EIS) was employed for investigating the chemical and physical practices at liquid/solid interfaces. Furthermore, it become an increasingly standard for a number of applications in field of corrosion research due to their promising in obtaining mechanistic data and due to their reliability of using the techniques for corrosion monitoring, such as: characterization of batteries, fuel cells, organic coatings, sensors, conducting polymers and for the corrosion analysis (Krause 2003; Perez 2004 & Brett 1993). However, in order to calculate accurate corrosion rates, Tafel constants still have to be determined, if possible simultaneously by any independent method. In principle, an electrochemical process may be modeled by electrical circuit elements, such as resistors, capacitors and inductors. In DC (direct current) theory, Ohm`s law defines resistance (R) in terms of the ratio between voltage (E) and current (I), relationship as shown in the following equation:

$$R = V/ I \qquad (3.10)$$

Where, E (Volt) is the applied potential, I (Ampere) is the current R (Ohm) is the resistance. In this case, the resistance is composed of only one or more actual resistance of the resistors.

When the frequency is not zero, as would occur from imposition of an alternating current, Ohm's law in terms of impedance "Z" is given by:

$$E = IZ \qquad (3.11)$$

Where, the impedance Z, measured at a single-frequency by employing an AC voltage to the electrochemical cell and calculating the phase shift and the amplitude of the resulting current applied at that particular frequency. The frequency being scanned

through the frequency range and the spectra are analyzed by simulation of an electrical equivalent circuit and termed as 'fitting procedure'. The equivalent circuit composed of essentials electrical components such as resistors, capacitors and inductors are the representative of the system. Under these conditions, the resistance is caused by all circuit elements that can impede the flow of current, e.g. resistors, capacitors and inductors. The AC impedance basic circuit elements are shown in table 3.4.

Table 3.4: An AC Impedance basic circuit elements

Elements	**AC Impedance equation**	
Resister	$Z = R$	
Capacitor	$Z = 1/j\omega c$	$\omega = 2\pi f$
Inductor	$Z = j\omega c$	$\omega = 2\pi f$

The excitation signals applied to the cell has the form:

$$E(t) = E_o \sin(\omega t) \qquad (3.12)$$

Where, E(t): potential at time t; Eo: is the maximum potential amplitude of signal; ω: is the radial frequency (in $rad.s^{-1}$) which can be related to frequency f (Hz) as ($\omega = 2\pi f$). The current response I(t) is sinusoidal at the same frequency as the applied sinusoidal potential but shift phase.

$$I(t) = I_o \sin(\omega t + \varphi) \qquad (3.13)$$

Where, I_o is the maximum current amplitude and φ is the phase shift by which the voltage lags the current as shown in Fig 3.6 (a). (Perez 2004; Krause 2003; Brett 1993 & Bard 1980).

The relation for the perturbation potential and the response for current can be corelated in the form of complex function:

$$E_t = E_o \exp(j\omega t) \quad (3.14)$$

$$I_t = I_o \exp(j\omega t - \varphi) \quad (3.15)$$

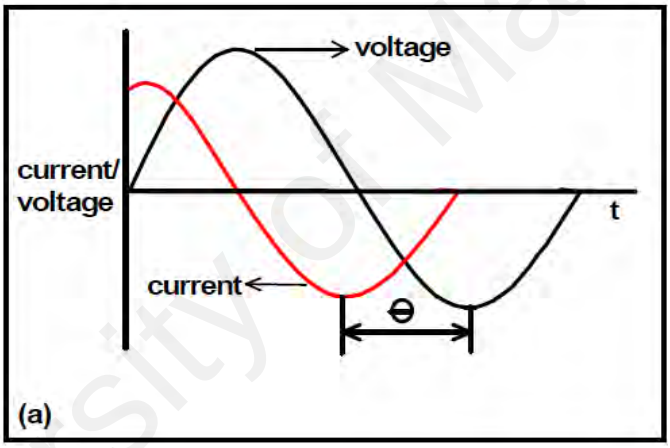

Figure 3.9 (a): Applied sinusoidal voltage and resulting sinusoidal current response

The impedance for the cell may calcualted by the ratio of potential and current:

$$Z(\omega) = E_o / I_o \exp(j\varphi) = |Z| \exp(j\varphi) = |Z|(\cos\varphi + \sin\varphi) = Z_{real} + jZ_{imag} \quad (3.16)$$

The impedance of a single frequency for a complex plane can be symbolized by a vector of length with argument φ (angle between the vector and the real axis of the impedance Z_{real}). Whereas, the imaginary part of impedance denoted by Z_{imag}, and j representing a complex number Fig.3.9 (b).

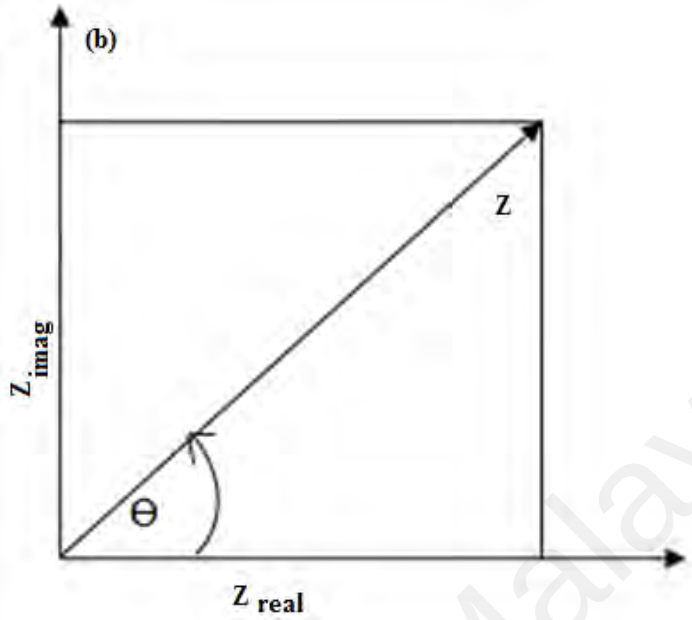

Figure 3.9 (b): Vector representation of real (Z_{real}) and imaginary (Z_{imag}) part of impedance (Z)

The |Z| and φ are associated to Z_{real} and Z_{imag} by the relation:

$$|Z|^2 = (Z_{real})^2 + (Z_{imag})^2 \qquad (3.17)$$

The phase angle is derived using the equation (3.18):

$$\text{Tan } \varphi = Z_{imag} / Z_{real} \qquad (3.18)$$

Often the objective of AC impedance is to model the corrosion process i terms of circuit elements such as those shown in Table 3.2 and from that model to be able to make conclusions about characteristics of the corrosion process.

Any corroding system can be modeled by an equivalent circuit which will best suit the system. Regardless of the system, whether it involves simple corrosion, or diffusion controlled corrosion or adsorption, a corroding system can always be modeled as a

combination of resistor, capacitor, and inductor and Warburg impedance in series and/or parallel arrangements (Brett & Brett, 1993).

The polarization resistance in terms of impedance is defined as:

$$Rp = \lim_{\omega \to 0} \mathrm{Re}(Z_f)\, E \qquad (3.19)$$

Where, Re (Z_f) denotes the real part of the complex faradaic impedance Z_f and Co corresponds to the angular frequency of the AC signals, where $\omega = 2\pi f$. For determination of R_p, a sinusoidal current or potential perturbation of very small amplitude (to ensure that the measurement is performed in the linear portion of the system) is applied as a function of frequency. The impedance behavior of an electrode may be expressed in Nyquist plots of Z_{imag} (imaginary component) as a function of Z_{real} (real component) or in Bode plots of Log $|Z|$ and phase angle, versus log frequency.

3.10.5 Data presentation

Electrical equivalent circuits are used for the analysis of the impedance data, and within the circuit, simple electrical elements such as resistance (R) and capacitance (C) are connected to model the electrochemical process (Krause 2003 & Brett 1993). The resistance indicate the equivalent circuit represents the electrical conductivity of the electrolyte and the capacitance (double-layer capacitance) caused by the charge which is in excess at the electrode-electrolyte interface. The most widely used equivalent circuit for the analysis of the impedance data is the Randles equivalent circuit (Krause 2003, Brett & Brett 1993), shown in Fig 3.10 (a). The Randles equivalent circuit shows the solution or electrolyte resistance (R_s) connected in series to the parallel combination of charge transfer resistance (R_{ct}) and the double-layer capacitance (C_{dl}).

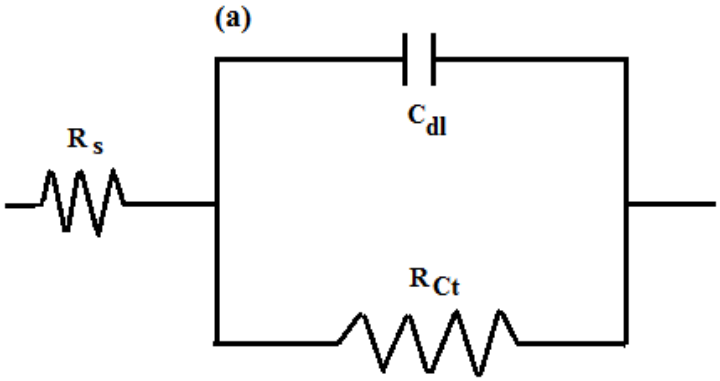

Figure 3.10 (a): Randles circuit for the electrochemical system

Impedance data can be graphically represented in two ways using Nyquist and Bode plot (Krause, 2003). The most widely used impedance data representation is the Nyquist plot or sometimes referred to as complex plane.

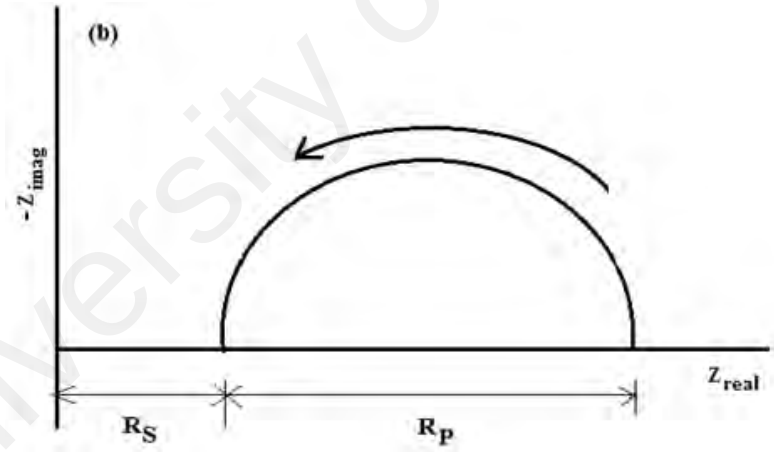

Figure 3.10 (b): Nyquist Plot of simple charge transfer corrosion processes

3.10.5.1 Nyquist plot

The Nyquist plot Figure 3.10 (b) shows a semi-circle with an increasing frequency in a counter clockwise direction. At very high frequency, the imaginary components Z_{imag}, disappears, leaving only the solution resistance, R_s. At low frequency, Z_{imag}, again disappears, leaving a sum of R_s and the polarization resistance, R_p.

The Nyquist plot used in electrochemical analysis has several merits and demerits.

Merits:

a) A very simple representative of the RS system.

b) The shape of impedance plot does not vary by changing the Ohmic resistance.

c) The charge transfer resistance is a simplest presentation as diameter of the semi-circle.

Demerits:

a) An indirect illustration on frequency.

b) The complex impedance equation for this diagram is (Shreir, 1994; Jones 1996 & Brett, 1993).

$$Z = R_s + [R_p / (1+ \omega^2 R_p^2 C^2)] + [j \omega R_p^2 C/ (1+ \omega^2 R_p^2 C^2)] \qquad (3.20)$$

From Figure 3.6 (b) at the apex of the semicircle:

$$\omega_{max} = 1/(C R_p) \qquad (3.21)$$

It is possible, therefore, to obtain all three parameters (R_s, R_p and C) from a complex impedance plot provided a sufficient frequency range is investigated.

3.10.5.2 Bode plot

The Bode plots Fig. 3.11(a) and 3.11(b) give analogous results and provide more information than that of Nyquist plot because the frequency is explicit in Bode plots and implicit in Nyquist plots. Certain characteristics of these Bode plots can be used to obtain circuit elements, R_s, R_p and C.

For example, R_s is the high frequency limiting value of Z, R_p is the difference between the low frequency limit and high frequency limit Figure 3.10 (a). The double layer

capacitance can be evaluated from the peak in phase angle plot Figure 3.10 (b) according to (Fontana, 1987; Rammelt 1992).

$$\omega_{max} = [1/CR_p] [1+ (R_p / R_s)]^{1/2} \qquad (3.23)$$

Where, $\omega_{max} = 2\pi f_{max.}$ Unfortunately, a number of corrosion processes are not as simplest case of one reaction dominating the process as represented by the circuit Figure 3.7(b). Complications can arise from a number of sources. In the frequent case of control by diffusion, the rate of the reaction is influenced by the diffusion of one or more of the reactants or products to or from the surface. The AC impedance response to a corrosion process dominated by diffusion control frequently has a unique characteristic known as Warburg impedance (W). The Nyquist plot and the corresponding equivalent circuit created by this phenomenon are shown schematically in Figure 3.12(a) and 3.12(b). The Warburg impedance is evidenced at low frequency on the Nyquist plot by a straight line superimposed at 450 to both axes.

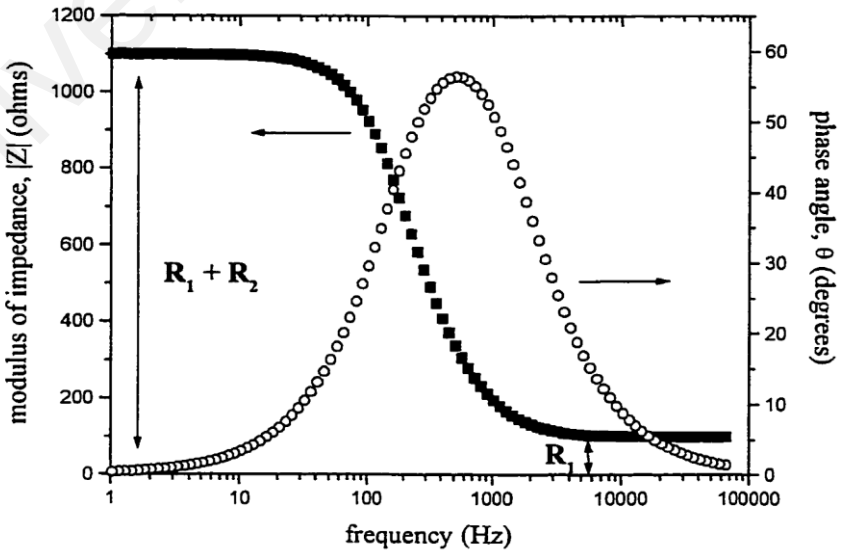

Figure 3.11 (a): Bode type plots of circuit in 3.10 (a)

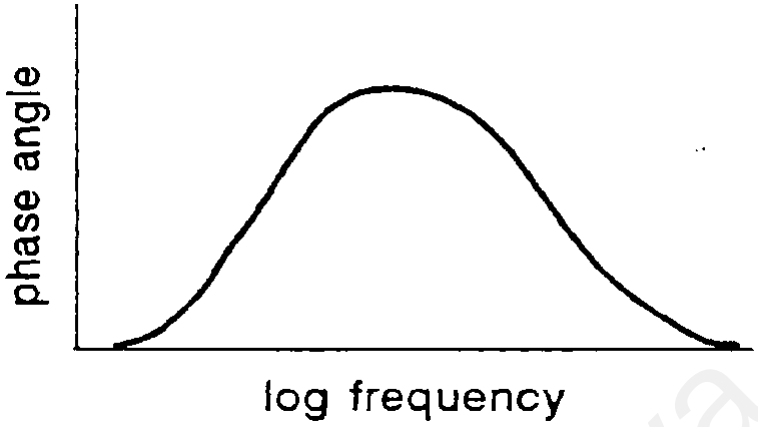

Figure 3.11 (b): Bode type plots of circuit in 3.10 (a)

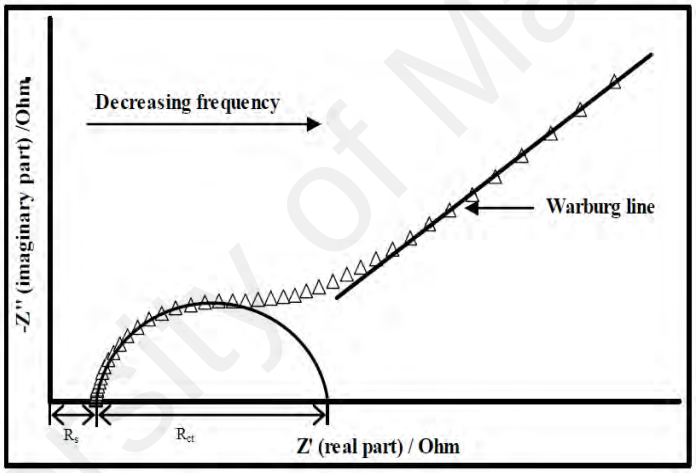

Figure 3.12 (a): Nyquist plot of simple charge transfer process in the presence of diffusion

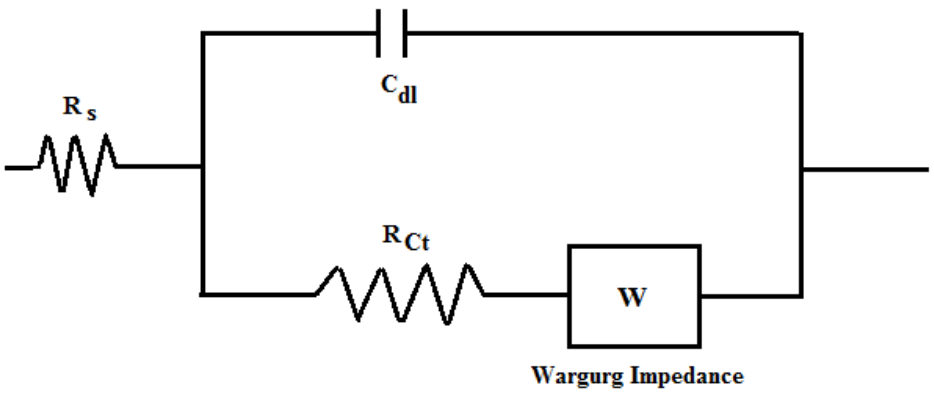

Figure 3.12 (b): Equivalent circuit corresponding to impedance response in figure 3.7 (a)

As indicated in figure 3.12 (a), the extrapolation of the high frequency semicircle to the real axis yields R_T, a quantity that may be inversely proportional to the rate of the charge transfer corrosion process.

The Warburg impedance for a reaction under pure diffusion control is given by (Marcus, 2002):

$$Z_w = [\sigma / \omega^{1/2}] - [j (\sigma / \omega^{1/2})] \qquad (3.24)$$

The Warburg coefficient, σ, can be used to calculate a diffusion coefficient. In most corrosion systems, the impedance diagrams are rather complex, perhaps exhibiting several capacitive and inductive loops. The Nyquist plot will frequently have a low frequency portion that lies below the real axis. This behavior seems to arise from one of a number of sources, for example, some types of adsorption processes. An example of an impedance response in the presence of inductance is shown in Figure 3.13.

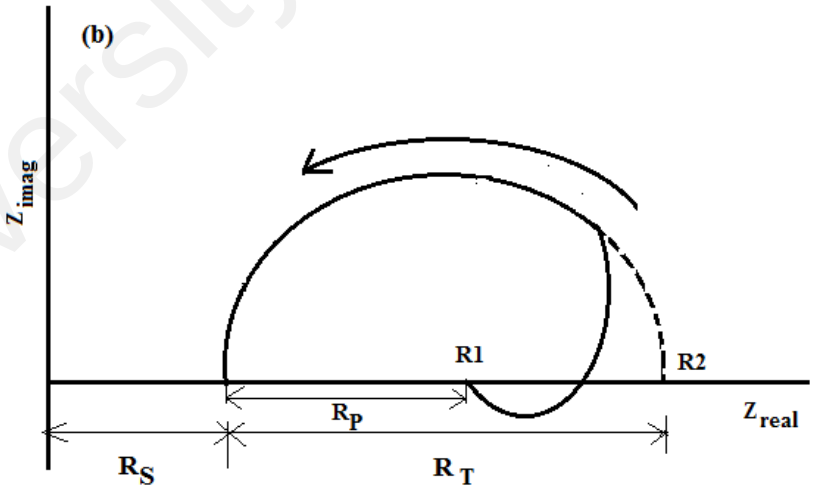

Figure 3.13: Nyquist plot of simple charge transfer corrosion process in the presence of inductance

The polarization resistance R_p is defined as R_1-R_s, while the charge transfer resistance R_T is defined as R_2-R_s. There is a controversy over which value is related to corrosion rate. Usually, R_1-R_s are used for corrosion rate calculation. Under some circumstances R_2-R_s seems to be more appropriate.

3.11 Adsorption isotherm studies

The mutual interaction of active functional groups and/or ingredients of inhibitors with the active sites at solid substrate can be explained by the development of adsorption isotherms. Adsorption mechanism plays a vital role in the inhibition action of metallic corrosion using organic inhibitors. The application of adsorption isotherms are widely practiced in order to evaluate the performance of organic types of inhibitors and more importantly for determining the actual mechanisms of electrochemical reactions. The adsorptive tendency of corrosion inhibitor may be evaluated by the development of isotherms that provides important research information to the nature of inhibitor interaction. Three most widely used types of adsorption isotherms are frequently employed for covering the relevant data relating to these adsorption isotherms, are the Langmuir, Frumkin and Temkin adsorption isotherms, having the following relationship with surface coverage (θ) and inhibitor concentration (C) in the solution (Sastri, 1998):

Langmuir adsorption isotherm:

$$\frac{\theta}{1-\theta} = K_{ads}\, C \qquad (3.25)$$

Temkin adsorption isotherm:

$$e^{f\theta} = K_{ads}\, C \qquad (3.26)$$

Frumkin adsorption isotherm:

$$\frac{\theta}{1-\theta} e^{f\theta} = K_{ads}\, C \qquad (3.27)$$

Where, θ represents degree of surface coverage, C denotes inhibitor concentration in the test solution and K_{ads} is constant called equilibrium constant for adsorption process, exhibiting a mutual interaction between adsorbed and adsorbing inhibitor molecules. The adsorption graphs are usually plotted as log $\frac{\theta}{(1-\theta)}$ against the corresponding values of log (C) for Langmuir adsorption isotherm, where as in the case of Temkim the values of log $\frac{\theta}{C(1-\theta)}$versus log (θ), and for Frumkin the adsorption curves are achieved by plotting (θ) versus log (C). The adsorption graphs having a straight line will be considered as one of the best adsorption isotherms.

The surface coverage value (θ) can be achieved from the gravimetric method with the help of the following relation as well, equation (3.28) (Hosseini et al., 2003):

$$\theta = \frac{\text{Inhibition efficiency in percentage}}{100} \qquad (3.28)$$

3.12 Thermodynamic parameters calculations

The numerical values of the activation energy (Ea) for steel corrosion reaction were obtained from the Arrhenius equation. The values of activation energy were obtained from the slopes, by plotting the values of log (corrosion rate) against the values of 1/T (Vashi & Cahmpaneri, 1997). The equilibrium adsorption constant is correlated to the energy of adsorption, ΔG^{o}_{ads} by the relation given below (Gulsen, 2008):

$$\Delta G^{o}_{ads} = - RT \ln (55.5\ K_{ads}) \qquad (3.29)$$

Where, R represents universal gas constant having values of 8.3142 $JK^{-1}mol^{-1}$, T stands the temperature and expressed in absolute scale and the value signifying 55.5 showing water concentration in the test solution (moles/liter). More negative values of ΔG^{o}_{ads}

representing a spontaneous process, strong interaction between the investigated inhibitors molecules and solid surface, and a more stable layer of adsorbed inhibitor molecules at liquid-solid interface as well. In addition, the value of the ΔG^{o}_{ads} provides important information regarding the nature of adsorption mechanism. A physical adsorption (physisorption) occurs when the corresponding values of ΔG^{o}_{ads} are -20 kJ mol^{-1} or more positive, indicating mutual electrostatic interaction between the charged inhibitor molecules and charged solid metal surface, on the other hand, those around -40 kJ mol^{-1} or more negative are consistent with chemisorption, exhibiting a co-ordinate bond as a result of transfer or sharing of charge from the inhibitor to the solid surface (Donahue & Nobe, 1965).

The adsorption value of - 40 kJ mol^{-1} is usually appropriated as a threshold value between physical and chemical adsorption (Hosseini et al., 2003).Fouling experimental test rig designed for different concentration of sparingly soluble salts in water, different fluid flow velocities of foulant liquid, various temperature range for the foulants disposition and the application of various materials used for industrial application, current fouling test rig has been constructed in GARUDA MEKAR (M) Sdn Bhd Unit G-02-08, Puchong Selangor Darul Ehsan, Malaysia.

3.13 Test material

A number of metals and alloys used as engineering construction of material are selected as a test material in the designed fouling test rig for the fouling behavior of sparingly soluble salts at different process variables. The test metals are circular pipes, purchased from Baolai Steel Group Co., limited, China having the following specifications as given in table 3.5.

Table 3.5: General dimensions of different metals used for experimental fouling test rig

No.	Metals and Alloys	Outer diameter	Inner diameter	Thickness	Length
1	Stainless Steel 316L	12.7 mm	8.48 mm	2.11 mm	900 mm
2	Aluminum	12.7 mm	8.48 mm	2.11 mm	900 mm
3	Copper	12.7 mm	8.48 mm	2.11 mm	900 mm
4	Carbon Steel	12.7 mm	8.48 mm	2.11 mm	900 mm
5	Brass	12.7 mm	8.48 mm	2.11 mm	900 mm

3.13.1 Demineralized water

The demineralized water produced from distiller is almost free of all dissolved mineral salts having a pH level of 7, as a result of application of different processes like distillation, deionization, membrane filtration, electrodialysis or some other technologies, and is neither acidic nor basic in nature. Demineralized is usually done where water is normally used for chemical processes and the minerals contains may interfere with other chemicals present. The amount of dissolved salts in demineralized water is usually low as 1 mg/L, but in some cases it also varying and found almost less than 10 mg/L (Patnaik, 2003). Demineralized water having electrical conductivity is generally less than 2 mS/m and in some cases may even be lower (< 0.1 mS/m).

3.13.2 Stainless steel 316 L

The type of stainless steel used in current investigation is commercially available SS316 L and having a composition of < 0.03 % C. 16-18.5% Cr, 10-14 % Ni, 2-3 % Mo, < 2 % Mn, < 1% Si, < 0.045 % P and < 0.03 % S (Patnaik, 2003). SS316 L has been used extensively for a number of industrial applications including: Food processing equipment particularly in chloride environments, Pharmaceuticals and textile industries,

Heat exchangers, condensers evaporators and tank, Chemical processing equipment, Marine and architectural applications etc.

Table 3.6: Physical and mechanical properties of different metals and alloys

Metal/Alloy	Density (g/cm^3)	Thermal Conductivity at 293 K ($W.m^{-1}.K^{-1}$)	Specific heat ($kJ.Kg^{-1}.K^{-1}$)	Tensile strength Ksi (min)	Hardness (Brinell) MAX
SS 316L	7.85	16.3	0.48	70	217
Aluminum	2.70	273	0.91	40.03	95
Copper	8.96	401	0.37	35	152
Brass 70/30	8.73	109	0.4	9.6	60
Medium Carbon Steel	7.85	36	0.49	45	163

(http://www.pennstainless.com/stainless-grades/300-series-stainless-steel/316l-stainless-steel/)

3.13.3 Major reagents

Table 3.7, representing all the reagents utilized with their quantity and respective grades for this research work. One of the main reagents currently under investigation is the application of calcium sulfate, having an inverse soluble characteristics as well as a major foulant agent of heat transfer surfaces.

Table 3.7: List of major reagents used for fouling on heat exchanger surfaces

No	Chemical required	Quantity	Corresponding grades
1	Sodium sulfate	1.8 Kg	Commercial/Laboratory grade
2	Calcium nitrate tetra hydrate	3 Kg	Commercial/Laboratory grade
3	Gelatin	500 gm	Analytical grade
4	Absolute Ethanol	3 Liter	Analytical grade
5	Phenolphthalein Indicator	50 gm	Laboratory grade

Table 3.7"continued"

No	Chemical required	Quantity	Corresponding grades
6	Poly(acrylic acid)	100 gm	Laboratory grade
7	Ethylene diamine tetraacetic Acid (EDTA)	250 gm	Laboratory grade
8	Erichrome black T indicator	50 gm	Analytical grade
9	Liquid Ammonia	2.5 Liters	Analytical grade

3.14 Organic antifouling additive (Gelatin)

Gelatin products are nearly odorless and tasteless having a transparent, brittle solid and faintly yellow in color. The inhibitor selected for the present research work is analytical grade Gelatine purchased from CHEMOLAB suppliers Malaysia, having a molecular weight of 450 gm. As it is protein substance and derived from collagen, therefore, it is s properly categorized as a derived protein.

It has the ability of forming a strong, flexible film and transparent gels which are easily soluble in hot water, as well as the ability of forming a strong positive binding action as well. Therefore, commonly used in paper production, pharmaceutical and food processing industries. Figures, 3.14 and 3.15 represents the photographic view and the chemical structure of the gelatin. Table 3.8, presents some physical properties as well as the amino acid profile for gelatin.

Figure 3.14: Photograph of the gelatin granules

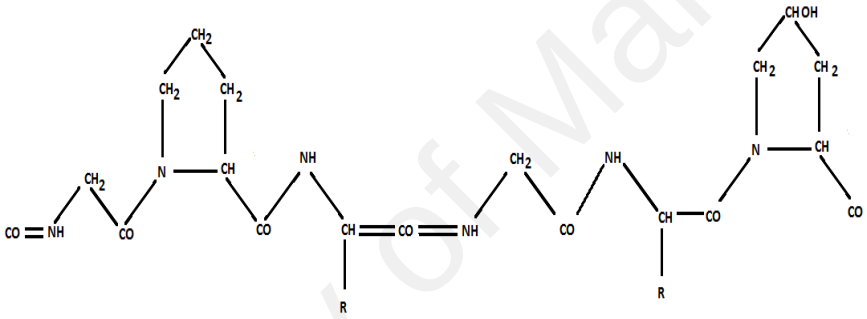

Figure 3.15: The chemical structure of gelatin

Table 3.8: Some physical properties and amino acid composition of gelatin

Color	Yellowish
Odor	Odorless
Viscosity (mp)	44 - 55
pH	4.5- 5.5
Moisture contents	8 - 13%
Relative density	1.3 - 1.4
Amino acid (g/100 g of the sample)	
Glutamic acid	8 - 10.6 %
Aspartic acid	4.8 - 5.4 %
Glycine	30.8 - 33.4 %

3.15 Annular fouling test rig (equipment set-up)

A schematic diagram for the designed annular fouling test rig for the current experimental set-up is shown below in Fig. 3.16.

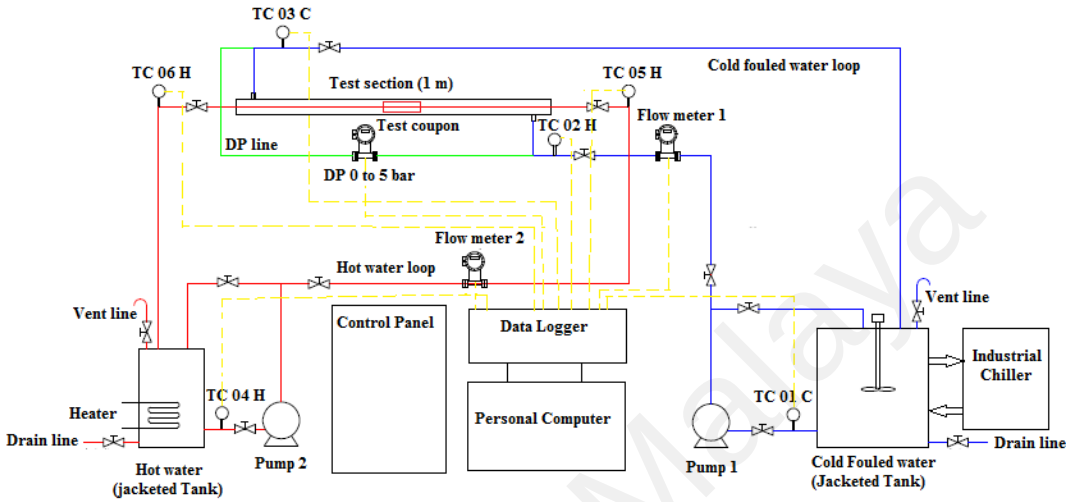

Figure 3.16: Schematic diagram for the designed annular fouling test rig.

3.15.1 Equipment

The experimental set-up consists of two close circuit water loops such as: outer cold fouling water loop, inner hot non-fouling water loop and test sections along with coupons, each loop comprises of centrifugal pumps, steel tanks, on/off valves, stirrers, magnetic flow meters, along with data acquisition system.

3.15.2 Outer fouling cold water loop

Fouling water close loop circuit consists of jacketed SS tank along with a digital stirrer and having volume capacity of 18 liters. The sparingly inorganic fouling salt solution of various concentrations has to be prepared in a given stoichiometric ratio inside the tank with the proper agitation until a clear transparent salt solution is to be produced. An Industrial chiller having a tank capacity of 7 gallons and temperature stability of $\pm$ 2.0 ^{o}F (for heat load of 25 % or greater) along with a temperature range of 5 ^{o}C to 50 ^{o}C and

cooling capacity of 5200 Watt at 0 ^{o}C was connected to the tank with the help of silicon flexible hose for maintaining the tank temperature to the desire set point. All the piping materials for distribution of fouled solution from tank to test section is made of standard PVC material having an inner diameter of ½ inches. The main test section is made up of schedule 40 Perspex materials for the visual observation of the deposits on the metallic test section for a desired time period of 72 hours. There are three K-type thermocouples installed at the tank out let labeled as (TC 01 C), inlet of the test section (TC 02 C) and at the outlet of test section (TC 03 C). The proper supply of fouling solution of various concentration with and without additives at various temperatures were pumped (AKARI MAGNET PUMP, Model: EX 100 RM), with the specifications of maximum capacity 120 L/min, head 8.6 m, and pump speed of 2800 rpm (labeled as pump 1). The pump was installed at the cold fouling water inlet line. The flow rate of the fouling solution can be monitored by the help of a Sensor- Mounted Display Flow Meter ($\pm$ 1.5 % accuracy at m^3/s) having a velocity range of 0.3 – 10 m/s at 0 – 60 ^{0}C, power input of 12-30 VDC installed on inlet line and electrically coupled with PC in order to get online data after every 30 minutes interval.

A pressure transducer (DP Harp Transmitter, Model EJA110E) with a pressure range of 0 – 5 bar at 95 ^{0}C and current input values of 4 – 20 mA DC was installed between the input and output of the test section to attain the pressure difference during the investigation (Before, at the time and once fouling has been commenced). A digital camera (Logitech HD 1080 Pascal) was attached and focused very close to the metallic coupons of the inner test section for the obtaining more insight and clear fouling deposits images and videos.

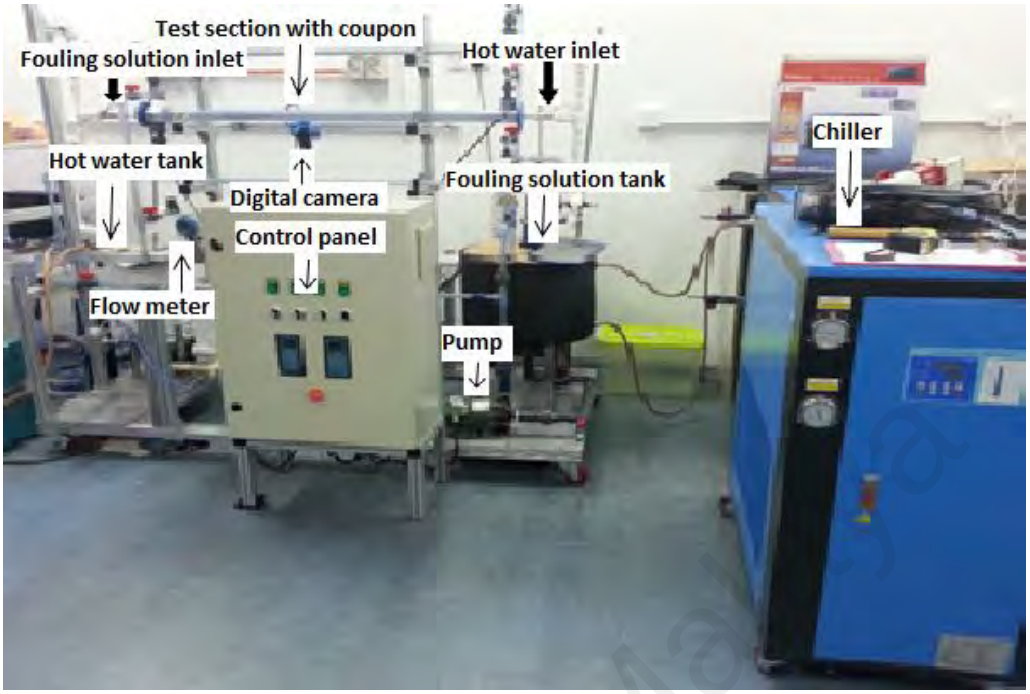

Figure 3.17: Annular fouling experimental test rig

3.15.3 Inner non-fouling hot water loop

The inner hot non-fouling water circulation loop comprises of proper insulated SS water tank installed with a heater having an immersion depth of 5 inches and power of 1000 Watt, with a capacity of 15 liters. The availability of a stand-by thermostat was also made possible to make sure in the case of failure of heater. The water temperature must be maintained for the hot inlet water line so that a net temperature difference hot water and cold fouling water should not exceed 15 ^{0}C. Three K- type thermocouples labeled as (TC 04 H, TC 05 H and TC 06 H) were installed at the outlet of the tank, inlet and the outlet of the hot water line and interlinked to the data logger for digital display.

A (ARAKI MAGNET PUMP, Model: Ex-70R) pump with a maximum capacity of 88 L/min and a speed of 2830 rpm was installed on the inlet line for inner metallic test section. The hot water flow was monitored by the installation of an Electromagnetic flow meter (Model: NFLO-KF700-A-F-A-DNI5-L-2-1-1), power supply of 24 VDC on the hot water inlet line. Hot water flow was controlled by maintaining the sensor

temperature at the pump outlet by regulating hot water heter power and flow rate of hot water. All the parameters like temperature, flow rates and pressure difference were monitored properly by the installed software (Totally Integrated Automation, version 12) along with "Wincc Runtime" software in a mini PC for the online display of the measured parameters.

3.15.4 Test section specification

The designed fouling test rig consists of the inner metallic test sections made of SS 316L, having a length of 900 mm and inner diameter and outer diameters of 8.48 mm 12.7 mm respectively. The test sections were designed with coupons of the same metal and mounted far ahead at the middle of the test section, this precaution should be necessaryin order to get the fouling deposits in a fully developed and stream line flow and to avoid the chances of any eddies formation close to the inlet section of the section. The test section along with coupons were allowed for a time period of 72 hours in a fouling solution so that a considerable thickness of the deposits with and without different concentrations of additives for fouling mitigation. The test coupons and rods after mineral deposits have been separated carefully from the test rig, kept in the desiccator for 24 hours and then subsequently taken away for surface morphology by the Scanning electron microscopy (SEM), and composition of the fouled surface were performed by XRD measurements.

3.16 Preparation of fouling solution

The main objective and focus for the existing set-up is the fouling of calcium sulfate on heat exchanger surfaces, therefore, calcium sulfate solution was prepared by the proper stoichiometric ratio of calcium nitrate and sodium sulfate. For this purpose, the known proportions of calcium nitrate tetra hydrate $Ca(NO_3)_2.4H_2O$ and sodium sulfate Na_2SO_4 were mixed thoroughly in distilled water in order to get aqueous solution of calcium

sulfate for the fouling purpose. Calcium sulfate dihydrate (Gypsum) solution has been prepared by the following chemical reaction equation (3.30):

$$Ca(NO_3)_2.4H_2O + Na_2SO_4 \longrightarrow CaSO_4.2H_2O + 2NaNO_3 + 2H_2O \qquad (3.30)$$

The selection of a proper concentration of calcium sulfate promotes the sufficient disposition on heat transfer surfaces and practically applicable in order to avoid the precipitation of calcium sulfate particles in the bulk solution. Moreover, the installation of agitator in the tank makes a proper suspension of calcium sulfate particles in the bulk solution. In order to keep the desired concentration of the calcium sulfate in bulk solution, the sample of solution were taken thoroughly after every 3 hours from the sample line and analyzed properly by titrating the sample with an EDTA complex, and after calculation, the concentration of the solution remains the same as original by the addition of either the chemical or water as per requirement. In a similar fashion, the suspension concentration was maintained as well.

For the preparation of a certain concentration of solution, salt weight can be calculated by the equation (3.31) (Al-Mutairi, 2007):

$$\text{Weight of } CaSO_4.2H_2O \text{ (gm)} = \frac{\text{M.wt.}CaSO_4+2h_2O}{\text{M.wt.}CaSO_4} \text{ X } \frac{CaSO_4.\text{Conc.(ppm)}}{1000} \qquad (3.31)$$

3.17 Experimental procedure

The main objective of the current research was to investigate the formation of mineral scale fouling on different metallic heat exchanger surfaces by the chemical treatment of the addition of green or environmental friendly additives. The outcome from the current research investigation provide a comprehensive knowledge regarding the formation, development and mitigation of fouling, crystallization, and the influence of various

factors on fouling scale mechanism like different molar concentrations, temperature of the hot surface, flow velocity of fouling solution, the application of various metals and alloys surfaces and finally the application of different concentration of various plants extracts additives or polymers as a green fouling inhibitors for the fouling mitigation.

For the current annular fouling test rig, concentrations of calcium sulfate solution and antifouling additives along with fluid flow rates are listed in table 3.9.

Table 3.9: Experimental set-up conditions for various parameters

No	Various parameters	Parameters range
1	$CaSO_4$ solution concentration	4.0 g/L
2	Additive concentrations	0.5 g/L, 0.25 g/L, 0.125 g/L, 0.06 g/L
3	Outer cold fouling solution temperature	35 ^{0}C
4	Inner hot non-fouling solution temperature	50 ^{0}C
5	Hydraulic area	0.0023 m
6	Outer cold fouling solution flow	6.1 (L/min)
7	Inner hot non-fouling solution flow	10.5 (L/min)
8	Inner hydraulic diameter	0.054 m
9	Inner Diameter of hot Tube (ID)	0.00847 m
10	Outer Diameter of hot Tube (OD)	0.0127 m
11	Run time for one batch	72 hours
12	Cold hydraulic flow	5068.92 Re

For the sequential operation of annular fouling test rig, the fouling solution was heated up to 25 ^{o}C and maintained this particular temperature via industrial chiller. Once the desired temperature has been reached, both the inlet and outlet valves were open so that

the hot water was allowed to flow inside the metallic test pipe sections. The temperature for the hot water inside hot water circulation loop tank was raised and maintained by heater inside the tank for the whole time period of batch and the concentration of the bulk fouling solution was properly checked after every 3 hours by taking samples from fouling solution tank.

After a time period of 72 hours, both the pumps were switched off and all the valves should be closed and draining the fouling solution through drain valve and taking the sample for analyzing the solution concentration by titration method. The pipe test sections and test coupons were released carefully from the annular fouling rig and keeping the coupons in the glass container for the proper natural drying for further analysis. Once the samples were completely dried, the crystal surface morphology of the crystallization fouling on different metallic test coupons were analyzed by Scanning electron microscope (SEM), as well as the material identification analysis was performed by using X-Ray Diffraction (XRD).

3.18 Determination of the concentration of calcium sulphate dihydrate ($CaSO_4.2H_2O$) in the solution

Complexometric titration with EDTA (Ethylene Diamine Tetra Acetic Acid) has been used for the analysis of dissolved $CaSO_4$ in the solutions and suspensions (Skoog & West, 1974). To perform the test for quantitative analysis of dissolved calcium ion in the solution, several reagents and solutions are required for the titration such as EDTA solution, Eriochrome black T solution, Ammonia-ammonium chloride buffer solution pH 10 and magnesium complex of EDTA. The standard procedures for preparation of the reagents are mentioned below.

1. EDTA solution (0.01M): Dissolve 3.722 g of analytical reagent grade of disodium dihydrogen ethylene diamine tetra acetic acid in distilled water and dilute to 1000 ml. Eriochrome black T solution: Dissolve 200mg of the solid in a solution consisting of 15

ml of triethanolamine and 5 ml of absolute ethanol. Solution should be kept under refrigeration when not in use or be freshly prepared every two weeks.

2. Ammonia- ammonium chloride buffer solution, pH 10: Dilute 570ml of aqueous NH_3 (specific gravity 0.90) and 70g of NH_4Cl to approximately 1 liter of dilute solution with distilled water.

3. Magnesium complex of EDTA, 0.1M: To 37.2 g of EDTA ($Na2H2Y.2H_2O$) in 500 ml of distilled water, add an equivalent quantity 24.65g of Magnesium sulphate ($MgSO_4.7H_2O$). Introduce a few drops of Phenolphthalein followed by sufficient sodium hydroxide to turn the solution faintly pink. Dilute the solution to 1 liter. When properly prepared, portions of this solution should assume a dull violet color when treated with pH 10 buffer and a few drops of Eriochrome black T (Erio T) indicator. Furthermore a single drop of 0.01M Na_2H_2Y should cause a color change to blue, while an equal quantity of 0.01M Mg^{2+} should cause a change to red. The composition to the solution should be adjusted by addition of Mg^{2+} or Na_2H_2Y until these criteria are met.

3.19 Quantification of fouling

To quantify fouling, the main technique is to stat the average deposit on the fouling surface in a given time period (mass of deposit in Kg per unit surface area in m^2). Whereas the fouling rate is expressed in the terms of Kg/ m^2.s and is achieved by dividing the deposits on the unit surface of heat exchangers in a desired operating time period. The amount of normalized fouling rate (Kg/m^2.s) additionally calculated from the foulant concentration in the process fluids (Kg/Kg) during the preceding operations and very useful for comparing the fouling rate.

The deposition rate can be calculated by the equation 3.32:

$$\text{Deposition rate} = \frac{\text{Final weight} - \text{initial Weight}}{\text{total pipe surface area} * \text{run time period} * 24 * 60} \qquad (3.32)$$

Whereas:

The total pipe surface area = 2 π r*L

r = radius of the pipe specimen andL = length of the pipe specimen

3.20 Sample characterization

3.20.1 Samples preparation for characterization techniques

After the completion of each batch of test run, the pipes and coupon specimens of different materials were kept or put in glass container during the normal drying and the drying time period for each of the coupons specimen is 7 days. The crystal morphology of the crystallization fouling on heat transfer surface of the various material pipes were analyzed by using SEM, XRD techniques.

3.20.2 Scanning electron microscope (SEM)

A Scanning electron microscope (SEM) is commonly employed for the microstructure surface characterization of the functionally graded test samples and for EDX analysis. The main objective of this particular test was to get a representative image of the surface for the gradient and its different compositions. Before the SEM characterization analysis of the fouled surface the dried coupon samples of various materials at different tests were carefully carried out under the microscopic study. For the surface investigation of the fouled surfaces a Philip XL30 (SEM-EDX) and Phenom EFI CO. (SEM) was employed at a various magnification and different location of the fouled surface samples to investigate deep surface morphology and the elemental compositions of the test samples.

For such a surface morphological analysis of various solid samples SEM is one of the most common and useful tool that produces the image of the sample by scanning it with a focused beam of electrons. Philip XL30 (SEM-EDX) has a useful magnification in excess of 200, 000 times and a resolution of 3.5 nm at an accelerating voltage of 30 KV and Phenom EFI CO. (SEM) had a magnification range of 20,000 – 24, 000 times and

the resolution capacity is around 30 nm as well. The working principle of SEM is based on the bombardment of electron on the surface of the investigated samples and the reflection image is measured. The electrons interact with atoms with the investigated sample, producing various signals that can be detected and that contain information about the sample's surface topography and composition. The electron beam is generally scanned in a raster scan pattern, and the beam's position is combined with the detected signal to produce an image. The emission of free electrons were created by the proper heating of tungsten cathode at desired temperature and then accelerated towards a positive electrode. The electrons at the edge of the anode, having a maximum speed of their velocity and the beam having a width keep remain between 5 - 10 micrometers. A condenser is employed properly for the focusing of electrons beam and passes through the diaphragm for regulating the horizontal distance from the studied samples. The detector for electrons capturing reflectivity strongly depends on the direction and intensity for presenting the image in a clearer or darker point.

3.20.3 X-ray diffraction analysis (XRD)

X-ray crystallography is a most commonly used tool for identification of the atomic as well as molecular structure of crystals. The resultant crystalline atoms produces a beam of incident X-rays and to diffract it into different but specific directions. By measurement the angles and intensities of diffracted beams, resulting a acrystallographer which are three-dimensional pictorial representation of electrons density within the crystal. From the resulting electron density, the mean positions of the atoms in a specific crystal, their chemical bonds, and the other revelent information can be determined. Different materials can form crystals like organic or in-organic salts, metals, minerals, different biological molecules, for their atomic and molecular structure analysis; X-ray crystallography has been employed as essential tool for the improvement of different scientific fields. The fingerprint characterization of the

investigated samples after SEM analysis were then determined employing a Philip X'pert MPD PW 3040 XRD having an X-ray wavelength radiation of 1.54056 Å. The investigated samples were scanned ranging from 10^o – 80^o 2θ angles with a step size of 0.020 and count timing for each step was 1.5. Diffraction patterns were occurred due to the outcome of the scattering of X-radiation by the atoms with a comparable spacing having a magnitude to the wavelength of radiation. By the striking of incidental X-ray beam having a wavelength λ on the two parallel planes of atoms at an angle of θ, and diffracted by the atoms in the plane A and B separated by d spacing. Bragg's Law governed the resulted constructive diffracted rays:

$$n\lambda = 2d\text{Sin}\ \theta \qquad (3.33)$$

CHAPTER: 4 RESEARCH RESULTS AND DISCUSSIONS

4.1 Water run results

Water run experiment was carried out in order to reduce and analyse the water run data for calculating the Nusselt number and for the comparison with the existing correlations as shown in figure 4.1.

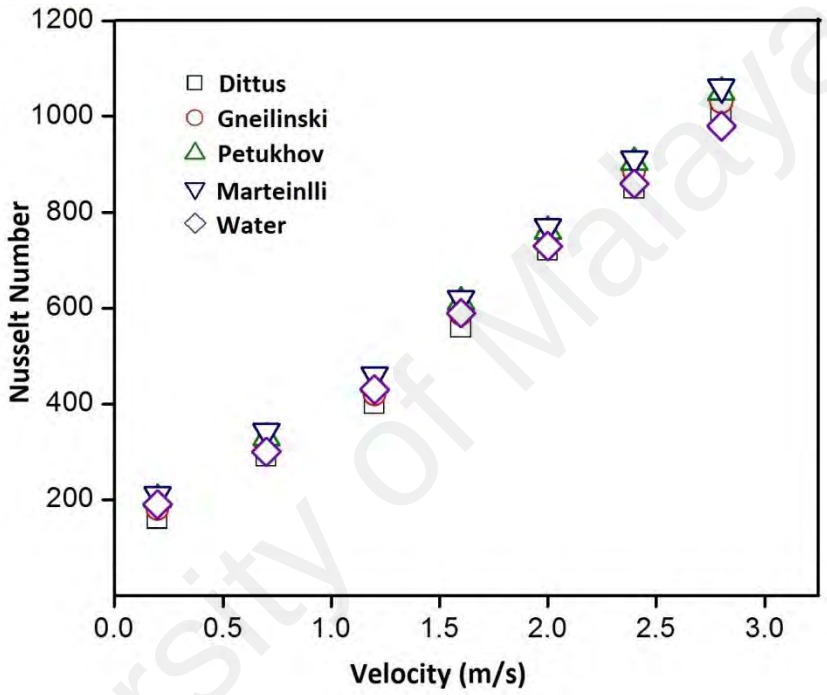

Figure 4.1: Comparison of Nusselt number at increasing velocity obtained from the present data and the standard correlations

Figure 4.1, realized that there is relatively little difference between the current experimental measurement and the existing correlations which confirms a high confidence level on the acquired data.

In figure 4.2, there is a lowest average deviation of experimental results Nu obtained from the Gniellinski equation which is 2.25 %. Whereas, other equations like Dittus, Martinali and Petukhov also show slightly higher deviations from experimental values over the velocity range.

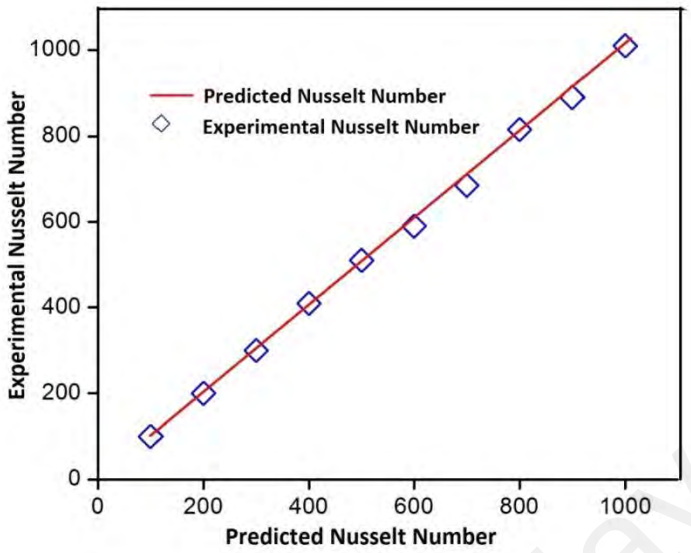

Figure 4.2: Comparative analysis Nusselt numbers at increasing velocities between present data and Gneilinski correlation

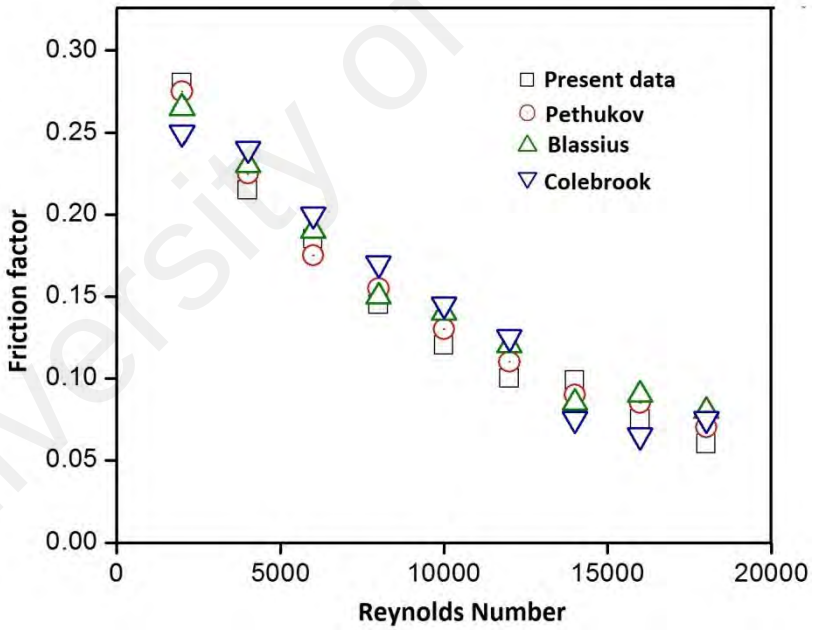

Figure 4.3: A plot of friction factor against Reynolds number for water and its evaluation with the present work correlations

Furthermore, some other uncertainty analysis was conducted based on the method described in Appendix C. it is important to measure the uncertainty analysis to make possible the reliability of both raw as well as derived data. Moreover, for determining

the range where the true and actual values of each acquired and calculated properties is likely to exist (Zubir, 2015).

Uncertainty list for the different parameters governing the present heat transfer and pressure loss experiments is presented in Table 4.1:

Table 4.1: List of uncertainty for various parameters for present heat transfer and pressure loss experiments

Parameters	Uncertainty (%)
Heat flux	2.06
Heat transfer coefficient	2.1
Nusselt Number	2.12
Velocity	0.57
Reynolds Number	1.39
Friction factor	2.38

4.2. Heat transfer to fibre suspensions

4.2.1 Effect of fiber concentration

In order to examine the effect of concentration on heat transfer to fiber suspension a series of experimental tests were conducted using the acasia manngium samples. The heat transfer to acasia mangium were studied at different suspension (0.2 wt.%, 0.4 wt.%, 0.6 wt.%) concentrations and at various flow velocities. Figures 4.4 and 4.5 show heat transfer coefficient as a function of velocity for acasia mangium suspensions with three different concentrations of 0.2, 0.4 and 0.6 wt% at bulk temperature of 30 °C and velocity ranging from 0.4 to 2.8 m/s.

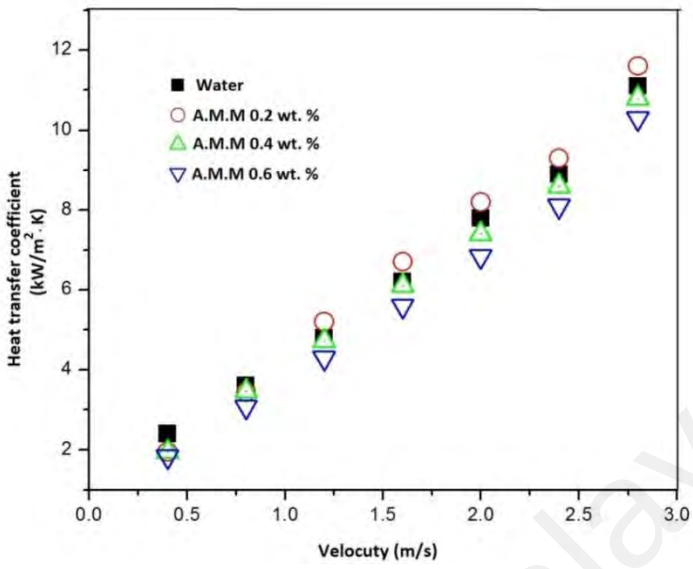

Figure 4.4: Heat transfer coefficient as a function of flow velocity for water and different concentrations of Acacia mangium mechanical (A.M.M) pulp fiber suspensions. The heat transfer data were obtained at bulk temperature of 30 °C

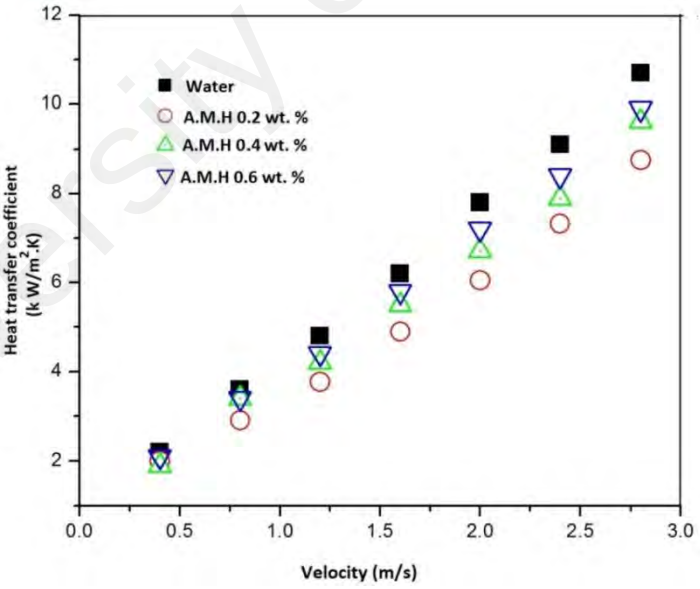

Figure 4.5: Heat transfer coefficient as a function of flow velocity for water and differentconcentration of Acacia mangium hybrid (A.M.H) pulp fiber suspensions. Data for heat transfer were attained at bulk temperature of 30 °C

The obtained trends for both of the two set of data representing the same trends. The velocity range can be divided into three ranges. Low range (velocity < 1 m/s), middle range (1 m/s ≤ velocity ≤ 2 m/s) and high range (velocity < 2 m/s).

In figures (4.4 and 4.5), the obtained results in a comparison with water run and the three concentrations of both samples suggested that flow of fiber suspension at velocities lower than 1 m/s results in a lower heat transfer coefficient than water. Moreover, concentration effects on heat transfer coefficient are more dominated when the velocity increases beyond 2 m/s. However, at the middle and high velocities range the suspensions with the lowest concentration (0.2 wt.%) tends to show the heat transfer coefficient higher than water in the case of acacia mangium only.

In fact, the thermal conductivity of fiber suspension have lower values than water, due to this particular fibre behaviour, the enhancement of $h_C$contributed by fibres by the virtue of modification of turbulent eddies. This kind of behaviour has been found more dominantly for Acacia mangium at a maximum flow velocity of 2.8 m/s. The comparison of the h_C values to that of water in the case of Acacia mangium at pulp suspension concentration of 0.2 wt. % is 26 %.

Unlike the suspension at 0.2 wt.% concentration, two others suspensions (0.4 wt.% and 0.6 wt.%) show lower h_C value compared to that of water. The h_C values obtained from suspensions with 0.4 wt.% concentration are more close to the water throughout the velocity range while the 0.6 wt.% suspensions show lowest heat transfers coefficient values for acacia mangium. However, in the case of acacia mangium hybrid, The h_C values obtained from suspensions with 0.4 wt.% concentration are more close to the water throughout the velocity, whereas the lowest h_C values were found for a pulp concentration of 0.2 wt.%. The values of h_C for both suspensions with 0.4 wt.% and 0.6 wt.% concentration were found to be more closely particularly at a velocity beyond 2 m/s. In order to obtain a clear insight in the variations in h_C values obtained for different

samples at different concentrations, it is necessary to obtain a heat transfer coefficient ratio (defined as the ration of h_C value of pulp sample to that of water).

In such a heat transfer ratio, the heat transfer ratio for water taken as unity for the reference.In figures 4.6 and 4.7 the values of heat transfer ratio of pulp slurries were plotted againstthe different velocity ranges of 0.4 m/s to 2.8 m/s. In these figures, the difference in $h_C$values provides a more clear vision for different source samples at different pulp concentrations.

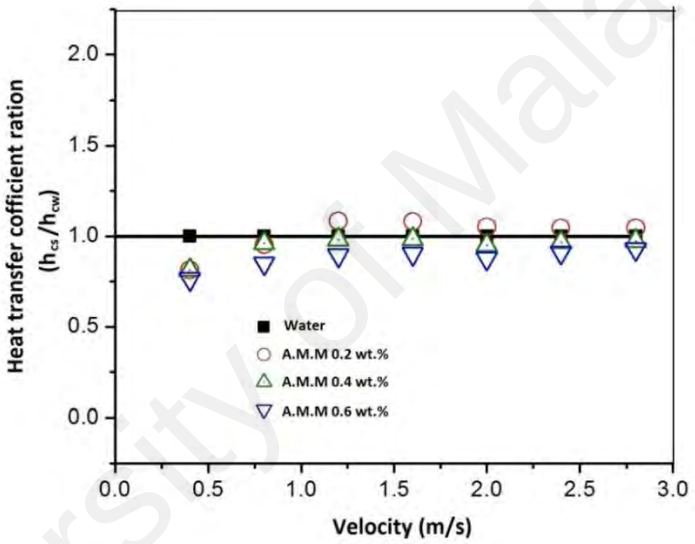

Figure 4.6: Heat transfer coefficient ratio as a function of flow velocity for water and different concentrations of Acacia mangium pulp fiber suspensions. The heat transfer data were obtained at bulk temperature of 30 °C

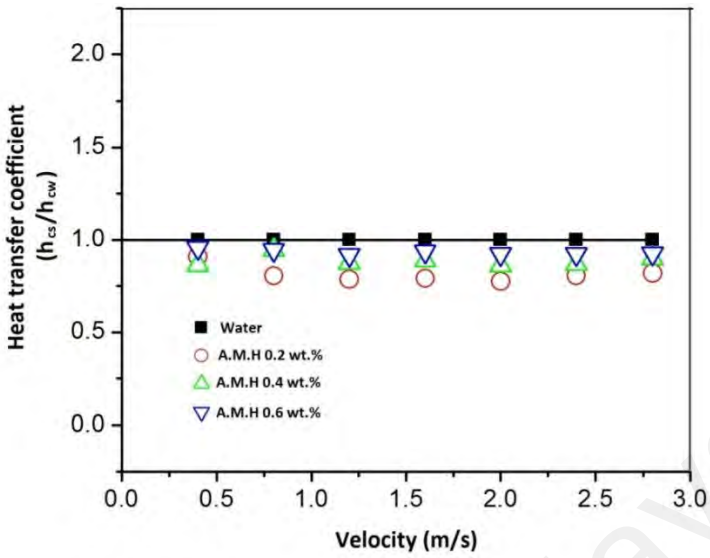

Figure 4.7: Heat transfer coefficient ratio as a function of flow velocity for water and different concentrations of Acacia mangium hybrid pulp fiber suspensions. The heat transfer data were obtained at bulk temperature of 30 °C

In the above figures (4.6 - 4.7), it can be seen that for suspensions with a concentration of 0.2 wt.%, the h_{CS}/h_{CW} values for Acacia mangium is close to water. Whereas, a contrast trends were observed for Acacia mangium hybrid at a concentration of 0.6 wt.% the h_{CS}/h_{CW} were found much closer to water instead for same pulp source at a concentration of 0.2 wt.% and 0.4 wt.% respectively. A maximum heat transfer coefficient was observed at 0.6 wt.% for Acacia mangium whereas for Acacia mangium hybrid it was seen at 0.2 wt.%.

4.2.2 Effect of refining (beating)

Fibre modifications are desirable for the production of special product. By the application of controlled beating, desired properties hopefully achieved. In refining process, where the cutting of fibres takes plays will results with an increase in the formation quality, but with an undesirable results of low strength papers. Pulp refining is a promising approach to improve the pulp quality by changing the fiber characteristics (Gharehkhani et al., 2015).

Figure 4.8 characterizes heat transfer coefficient as a function of velocity for Acacia mangium fibres with a degree of beating like 2000, 4000 and 8000. The degree of beating based on the type of fibre, in the case of hard wood, requirement of gentle beating as well as more amount of energy for developing strength as compared to softwood. Higher degree of beating have an adverse effect on drainage and paper properties as well, therefore, selection of degree of beating strongly based on fibre source, the desired fibre and paper properties.

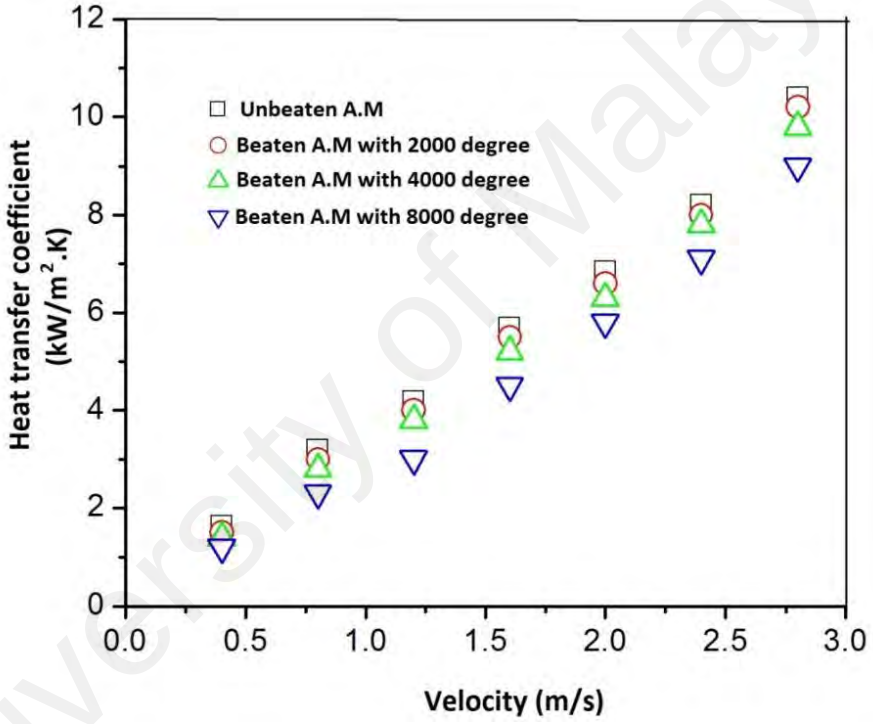

Figure 4.8: Heat transfer coefficient as a function of velocity for three different degree of beating AM at 2000, 4000 and 8000 of fiber suspensions. The experiments were executed at bulk temperature of 30 ^{0}C and fibre concentration of 0.6 wt.%

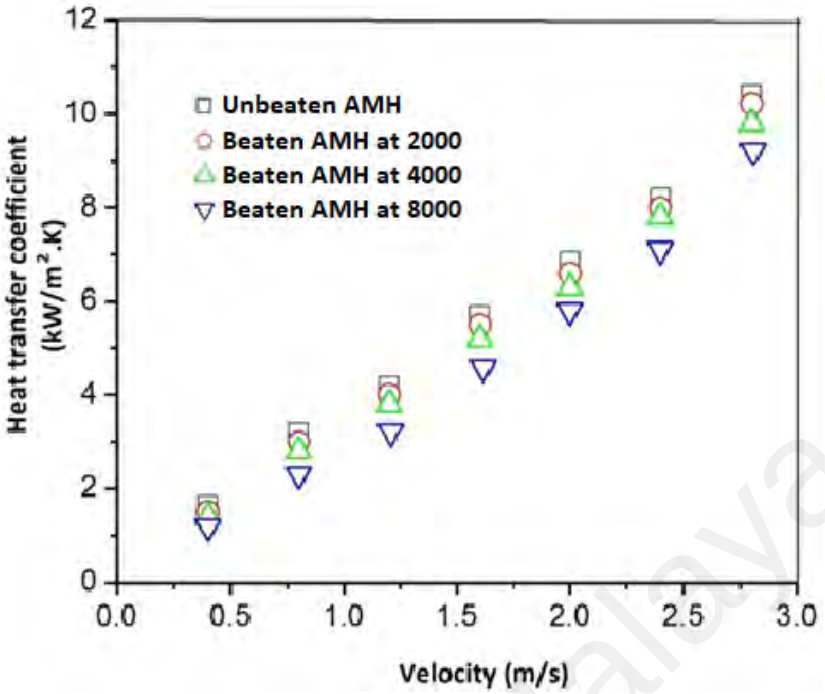

Figure 4.9: Heat transfer coefficient as a function of velocity for three different degree of beating AMH at 2000, 4000 and 8000 of fiber suspensions. The experiments were executed at bulk temperature of 30 ^{0}C and fibre concentration of 0.6 wt.%

In Fig.4.8 and Fig 4.9, it was observed that no significant change occurred for AM and AMH samples after beaten at various degree of beating renaging from 2000, 4000 and 8000. Degree of beating reflects the intensity of pulp fibre beating during PFI mill. Beating is done in order to change wood pulp fibre properties desirable for paper machine runnability and particular product properties. PFI mill is an important tool for changing pulp and handsheet properties and in addition for expecting pulp strength properties. An optimal concentration of pulp suspension of 0.6 wt.% has been considered for beating process in order to compare the beating and bleaching effects of pulp fibre suspension for heat transfer coefficient and pressure drop analysis.

Low degree of beating has no significant effect on the heat transfer coefficient at particularly low velocities. Furthermore, a more increase in the degree of beating leading to a successive decrease in h_C value of suspension. This reduction in h_C values were observed as a result of increase in fiber flexibility and fines production. Such a

systematic decrease in h_C values with corresponding increase in degree of beating was observed in figure 4.10.

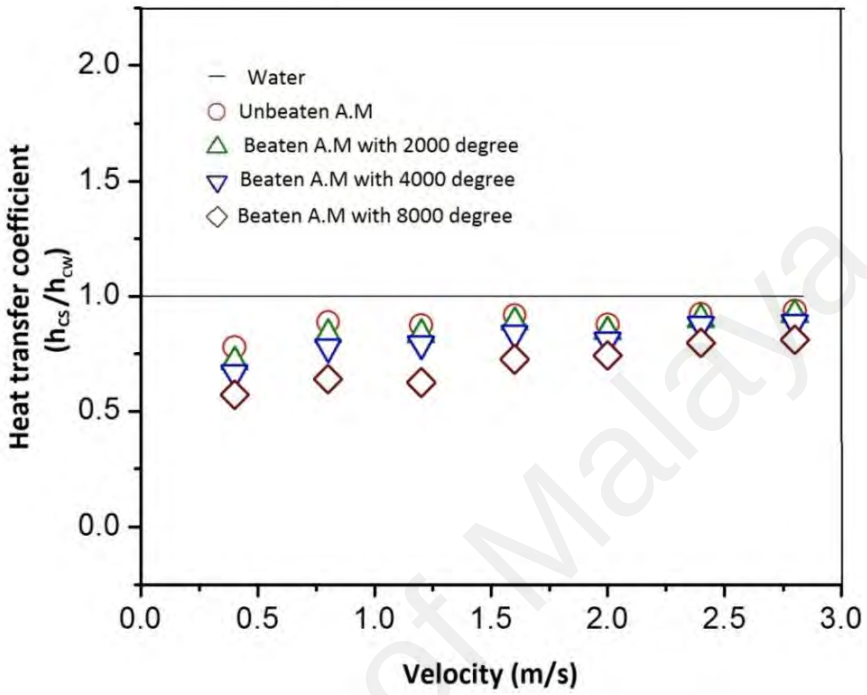

Figure 4.10: Heat transfer coefficient ratio as a function of velocity for unbeaten and beaten (for 2000 and 4000 and 8000) fiber suspensions. The experiments were accomplished at bulk temperature of 30 ^{0}C and fibre concentration of 0.6 wt.%.

The values for the heat transfer coefficient ratio for unbeaten and three different Acacia mangium samples at a beaten degree of 2000, 4000 and 8000 are 0.93, 0.92, 0.88 and 0.81 at velocity of 2.8 m/s. The lowering in values of h_C could be possible due to a number of factors including: lessening in coarseness and fiber length, or an increase in relative fiber number and longitudinal elasticity (as decrease in thickness in cell wall) or a by the combined action of them.

Kazi (2001) reported that the individual fiber suspension behavior during the heat transfer was obviously dominated by fibre flexibility. With the increase of fibre flexibility in suspension the values of h_C, decreases due to the adsorption of more energy from fiber-eddy collision and as a result of more fibre interaction. The data

obtained from beaten suspensions were used to correlate the fiber properties with h_C values in the next section.

4.2.3 Effect of bleaching

In paper and pulp industries, fibres obtained from a natural source like wood were processed in different techniques in order to achieve some specific requirements for the intermediate as well as the final products. In this context, the heat transfer measurement of the considered fibres is a distinctive and accurate method in order to evaluate the intensity of a particular treating event on the fibre. Comparatively, fibres from chemical pulping are more flexible to that of mechanically pulp fibres. Moreover, fibres from chemical pulping will conform in an excellent way as compared to mechanical during the paper formation and offering good strength properties as well (Johansson, 2011).

Fibre become more flexible as a result of bleaching and it was observed that the flexibility of unbleached pulp fibres is 68 percent to that of bleached pulp fibres using Steadman method it is almost 83 percent when measured employing the TamDoo and Kerekes method (Paavilainen, 1993).

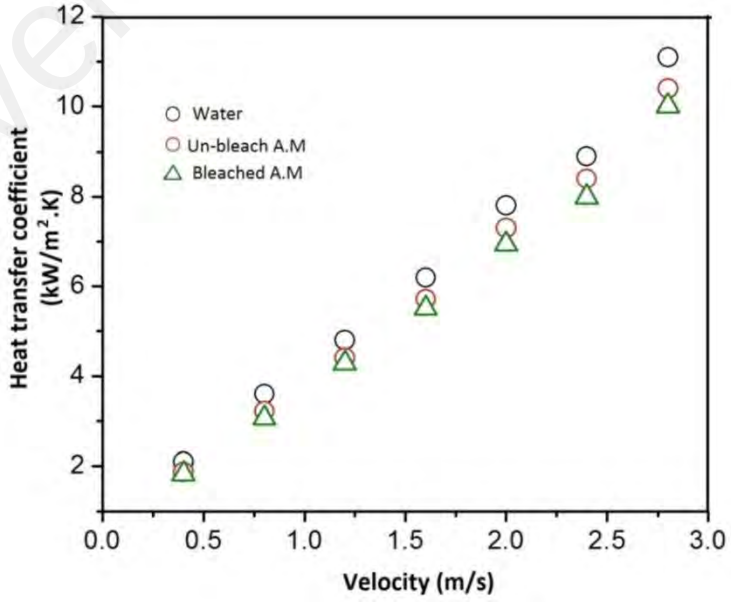

Figure 4.11: Heat transfer coefficient versus velocity for water, unbleached and bleached Kraft pulp fibre suspensions. The experiments were carriedout at bulk temperature of 30 ^{0}C and fibre concentration of 0.6 wt.%

Figure 4.11 represents the influence of heat transfer coefficient on water velocity for unbleached and bleached Kraft Acacia Mangum at fibre concentration 0.6 wt% and at bulk temperature 30 ^{o}C. During the experimental analysis, it was evaluated that at lower flow velocity < 0.5 m/s, the values of hc for both unbleached and bleached are almost same. Whereas, when velocity increased around > 0.5 m/s, a small variance occurred between unbleached and bleached suspensions. In a region where the velocity values are around 2.8 m/s, a down fall of 1.3 precent was observed for bleached pulp below the unbleached fibres suspension as a result of due to higher flexibility of bleached pulps.

4.3 Heat transfer and fibre properties correlation

A very little amount of literature available for the studies to determine how various fibersproperties would modify turbulence in pipe line flow. These studies aimed to find technical and systematic relationship between the fiber/paper properties and heat/momentum transfer data to provide a means of measuring and monitoring fiber characteristics and pulp quality. It had been found in pipe flow that specific fiber characteristics and some fiber and paper properties could be assessed by both heat transfer measurements and friction loss determination (Kazi et al., 2014b). Following those studies there was a need to evaluate heat and momentum transfer measurements or both h and $\Delta P/L$ values for wood fibers over a range of flow conditions.

The most important and well-known fiber properties are length, width, wall thickness and lumen diameter. The measurement and the preparations of the test samples were done by using Leica microscope graticule to regulate eyepiece focusing test specimen. Select the lowest and highest magnification by proper focus the specimen. Slowly turn eyepiece with graticule clockwise until you can clearly see the measurement lines. Take an average of 50 samples for the each of the fiber length as well as fiber luman diameter, after the properly measuring the desired fiber dimensions the test data were tabulated in Table 4.2.

Table 4.2: Fibre properties of A. Mangium for the present experimental investigation

Fibre type	FL (mm)	FD (mm)	FLD (mm)	FWT (µm)	Flexibility ratio	Slender ratio
Acacia Mangium	1.02	0.02	0.014	2.55	73.23	51.29
Beaten A.M at 2K degree	0.95	0.022	0.0177	2.57	74.05	47.5
Beaten A.M at 4K degree	0.84	0.025	0.0211	2.6	75.3	44.6
Beaten A.M at 8K degree	0.69	0.028	0.0241	2.62	76.9	40.8
Acacia mangium hybrid	1.09	0.018	0.013	2.51	73.31	57.4

Due to the longer fiber length and higher flexibility of the samples of AMH as compared to AM. The heat transfer coeffieicnt for AM is higher than that of AMH.longer and flexible fiber have less heat ransfer coefficient as compared to short and less flexible fiber as in the case of AM. The length of Acacia mangium hybrid sample is the longest in length and lowest width of lumen diameter as compared to the Acacia mangium. However, the length of the Acacia mangium samples decreases with increasing the degree of beating. However, beating with fibrillation and fiber shortening causes the reduction in slenderness ratio with alternative increase in flexibility coefficient of pulp fibre. These results are similar to the previous reports (Main et al., 2015; Mossello et al., 2010).

Figure 4.12 to 4.14 presents the effect of various fiber dimensions and fiber properties on the magnitude of heat transfer coefficient for the same fiber concentration and flow velocity (0.6 wt.% & 1.2 m/s). The obtained heat transfer data were achieved at a bulk temperature of 30°C.

Four different samples of Acacia mangium (0 degree, 2000 degree, 4000 degree and 8000 degree of beatings) were considered to study the relationship between fiber properties and the values of heat transfer coefficient. However with different species of pulp samples the result may not be statistically significant (see Appendix D). Some of the fiber properties are interactive as seen by the fact that some other pulp species tested

were not lying on the similar regression line. This is a complex situation as there are essentially distributions in fiber properties somewhat than true mean values.

From a logical standpoint it makes sense to select one species of pulp with different physical properties which can be obtained by different degree of beating. Fiber length is the most common parameter which is used to describe the paper sheet properties (Jahan et al., 2010). Beating the fibers is a way to tailor the fiber length. A long fiber can have more fiber joints and therefore create a stronger network compared to a shorter fiber. It is not always clear, how the long fibers are affecting the paper strength. The longer fibers have the tendency to form more or bigger flocs compared to shorter fibers. The flocculation leads to a more uneven sheet, which may affect the paper properties. This can be avoided by lowering the fiber concentration of the long fiber stock during forming and by improving the dewatering elements on the wire (Johansson, 2011).

Variation of heat transfer coefficient based on different fiber length for Acacia mangium samples are presented in figure 4.12. A clear trend is that a decrease in fiber length causes a decrease in h_C.

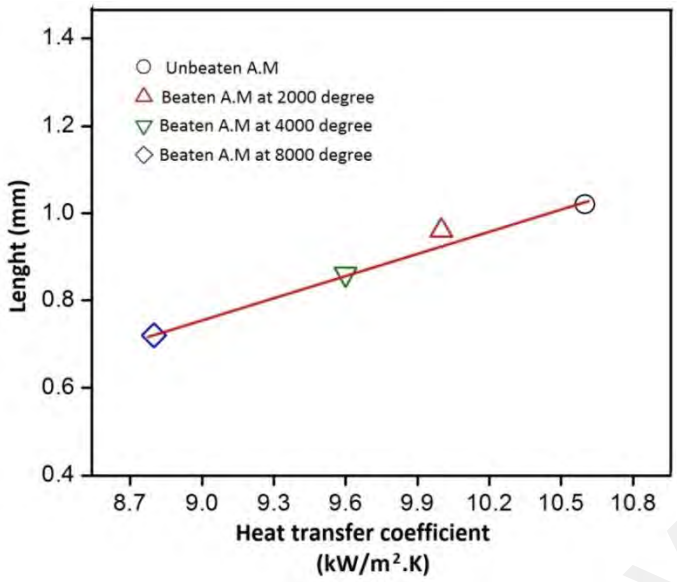

Figure 4.12: Fiber length as a function of heat transfer coefficient for Acacia mangium with no beating, Acacia mangium with 2000, 4000 and 8000 degree of beating respectively

Figure 4.13, represents the fiber length to fiber width (L/W) versus h_C and can be assigned as slender ratio. Figure 4.13 shows the changes in h_C by slender ratio for four different Acacia mangium samples. Data are obtained at concentration of 0.6 wt.%, bulk temperature of 30 °C and at the velocity 1.2 m/s.

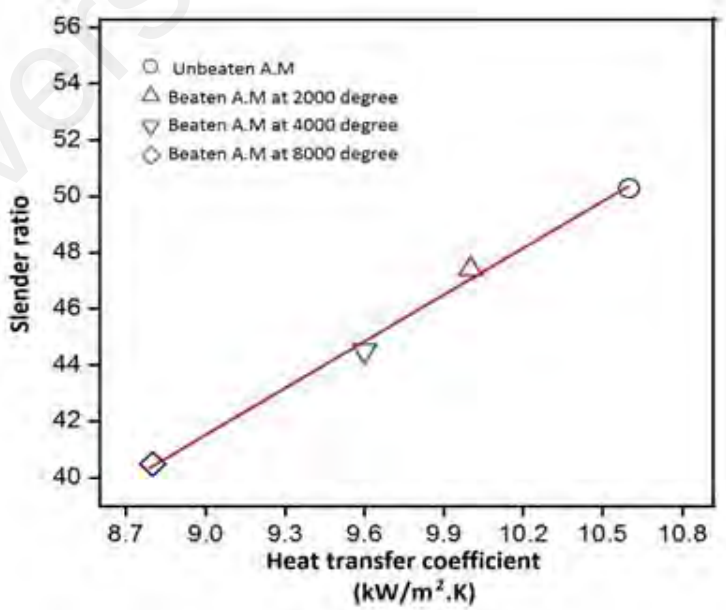

Figure 4.13: Slender ratio (L/W) as a function of heat transfer coefficient for Acacia mangium with no beating and with 2000, 4000 and 8000 degree of beating respectively

In Fig. 4.13, it was observed that the vales of h_C plotted against slender ratio show a similar trend as observed previously in figure 4.12. The samples with larger slender ratio values yield a higher value of heat transfer coefficient h_C.

Figure 4.14, shows a fiber characteristic study and plotted by the flexibility ratio against h_C, where almost same deviation was observed from the linear trend as observed in Fig. 4.12.

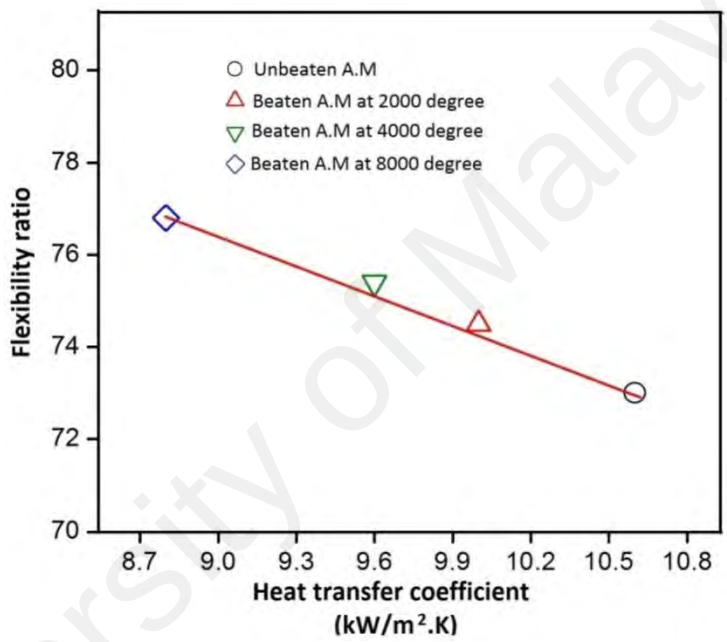

Figure 4.14: Flexibility ratio (Lumen/W) as a function of heat transfer coefficient for Acacia mangium with no beating, Acacia mangium with 2000, 4000 and 8000 degree of beating respectively

Finally, the comparison of various samples of Acacia mangium with no beating and beating effects for fibre length, slender ration and flexibility ratio, it is found that at a beating of 2000, 4000 and 8000 degree, there is a corresponding increase in flexibility ratio of 1.6 %, 2.2 % and 4.5 % respectively. Whereas, on the other hand beating of Acacia mangium at 2000, 4000 and 8000 degree yield a net decrease in h_C value of 2.9 %. 5.1% and 8.7% respectively. It can be concluded that the values of h_C for the same or different samples can be correlated with the flexibility of the investigated fibres.

4.4 Heat transfer and paper properties

Some most important and basic paper properties like tensile index, burst index and tear index are significant parameters during paper making process. Some of these basic paper properties of the samples are presented in Table 4.3.

Table 4.3: Fundamental paper properties of some samples

Fibre type	Tensile Index	Burst Index	Tear Index	Folding endurance	Brightness
A. mangium	1.05	46.1	1.29	1.33	32.5
A. M beaten at 2000 degree	1.31	69.8	1.38	3.5	32.1
A. M beaten at 4000 degree	1.89	89.6	1.45	2	31.7
A. M beaten at 8000 degree	2.21	107.1	1.52	2.5	31.1
A. mangium hybrid	6.52	37.3	1.315	1.3	31.06

The consequences of beating are: a higher flexibility and fiber swelling as a result of fibrillation as well as the existence of more number of fine productions. This promotes an improved inter-fiber bonding in paper formation and causing an increase in the values of burst and tensile strength indices (Main et al., 2015; Nayeri et al., 2013). The tensile index, burst index and stretch-to-break are improved when fines are added, especially when adding secondary fines (Johansson, 2011).

Figure 4.15 indicates the tensile index of Acacia mangium samples versus h_C. The h_C increases with a decrease in tensile index which corresponds to the results obtained for flexibility ratio plotted against h_C. Previously similar result was reported for the

correlation of paper properties along with heat transfer coefficient h_C. (Kazi, 2001; Kazi et al., 2015).

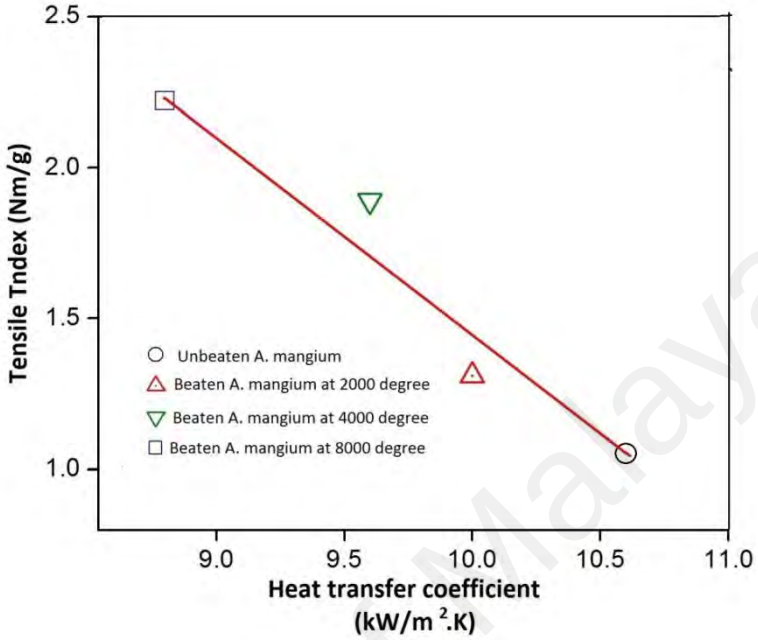

Figure 4.15: Tensile index as a function of heat transfer coefficient for Acacia mangium with no beating, and with 2000, 4000 and 8000 degrees of beating

Bursting strength measures the paper resistance to being burst when hydraulic pressure was applied to the paper (Kertas, 2013). Figure 4.16, shows the heat transfer coefficient values of the fiber suspensions as a function of paper sheet burst index for the unbeaten and beaten Acacia mangium samples. The bulk temperature of the fiber suspensions was maintained at 30 °C. The relationship between burst strength of paper sheets and their heat transfer coefficient presenting that a longer samples of A. mangium (without beaten) delivers the highest hc value and produces lowest burst index strength papers, followed by A. mangium sample when degree of beating at 2000, 4000 and 8000 respectively.

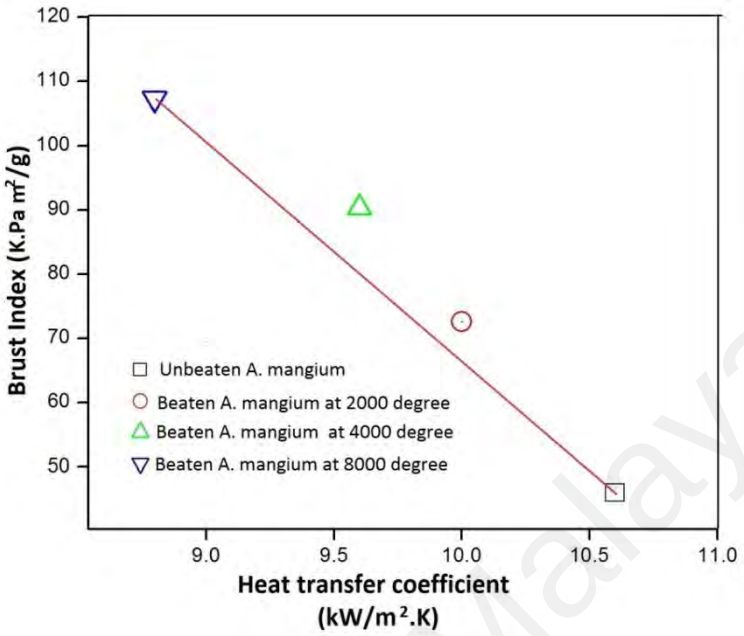

Figure 4.16: Burst index as a function of heat transfer coefficient for Acacia mangium with no beating, and with 2000, 4000 and 8000 degrees of beating

Figure 4.17 represents the relationship between tear index and h_C for Acacia mangium samples. The effect of beating decreases tear index of pulp samples. This phenomenon can be explained as fibres tightly bonded and more fibers are ruptured in the preliminary cutting however, rupturing of fiber rupture requires less energy as compared to pulling out of fibers from web of fibres, therefore, pulp tear strength become reduced (Mossello et al., 2010). Tear index followed a different trend from that of tensile and burst index. Samples obtained with less tear index and having a lesser h_C.

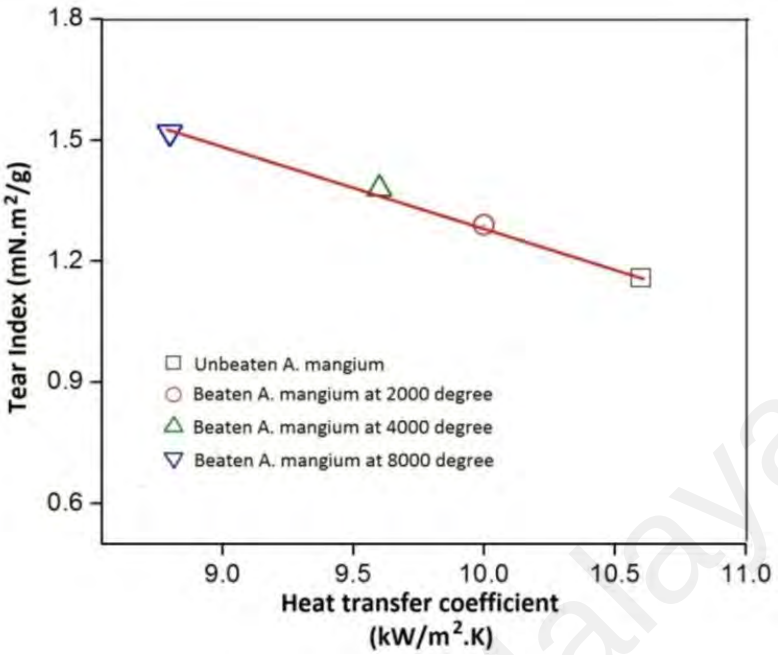

Figure 4.17: Tear index as a function of heat transfer coefficient for A. mangium with nobeating, and with 2000, 4000 and 8000 degrees of beating

Folding endurance tests have been used to estimate the ability of paper to withstand repeated bending, folding, and creasing (TAPPI, 2006). The paper was folded backwards and fronts repeatedly between two rollers that rolling at 120 double folds per minute (Hassan et al., 2014). Increase in folding endurance would reduce the heat transfer coefficient h_C as shown in figure 4.18.

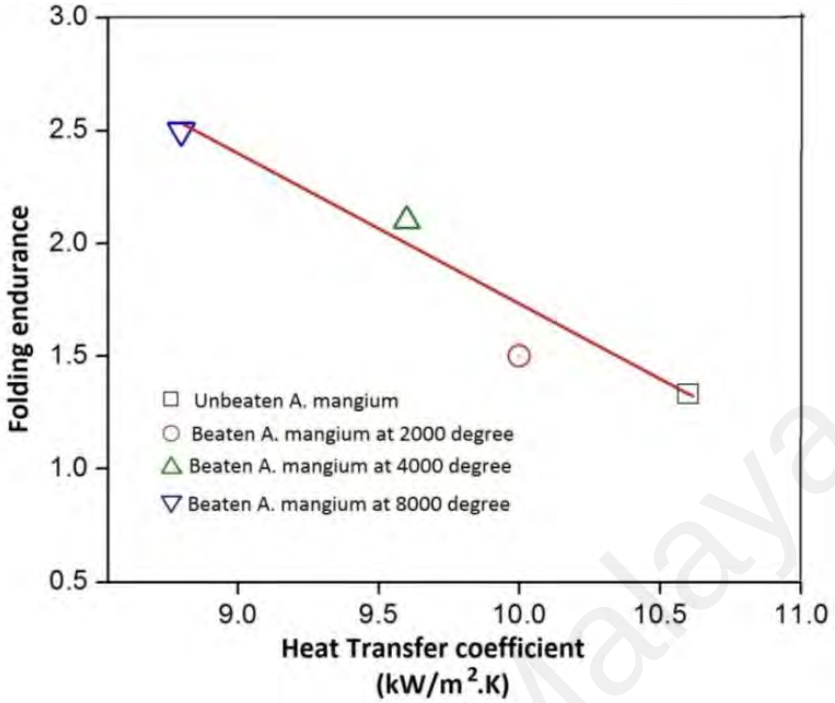

Figure 4.18: Folding endurance as a function of heat transfer coefficient for Acacia mangium with no beating, and with 2000, 4000 and 8000 degrees of beating

All the strength properties except tear index will increase during beating. This happens as the tear strength depends on the individual strength of the fibers and the other properties rely on the fiber joints. Moreover, the increase of fiber joints will lead to a decrease of the light scattering coefficient. The bulk, opacity and porosity are other properties decreased by the effect of beating as well (Johansson, 2011).

Beating degree has slight effect on fiber brightness. Brightness of Acacia mangium papers formed by different degrees of beating was studied and compared with $h_C$values obtained by their suspension flow in order to correlate these results. The heat transfer coefficient to fiber suspensions as a function of brightness (%) for the Acacia mangium were plotted in figure 4.19. It is detected that unbeaten A. mangium shows the highest brightness values parallel to heat transfer coefficient 10.7 kW/m2.K. In contact, an Acacia mangium sample with 8000 degree of beating indicates the lowest brightness of the papers and the lowest $h_C$values of the suspensions.

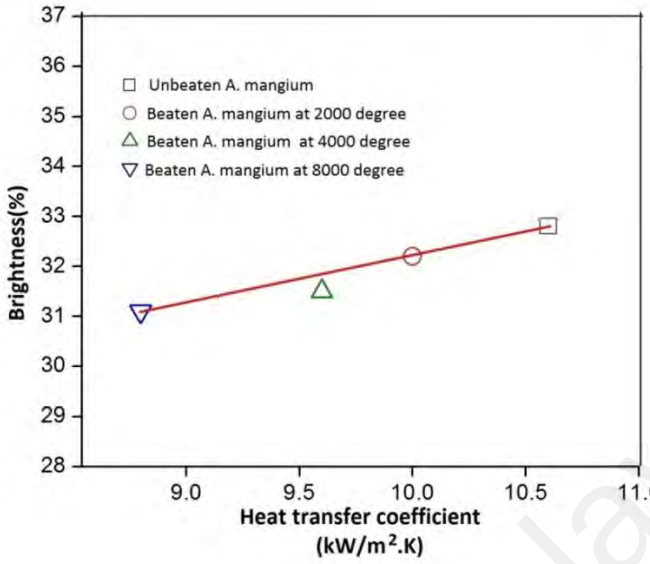

Figure 4.19: Brightness (%) as a function of heat transfer coefficient for A. mangium with no beating, and with 2000, 4000 and 8000 degrees of beating

4.5 Pressure drop of fiber suspension

4.5.1 Effect of fiber concentration

Figures 4.20 and 4.21 represents both the pressure and friction factor plotted against the values of water, whereas the Reynolds number for water and different concentrations of Acacia mangium suspension at bulk temperature of 30 °C.

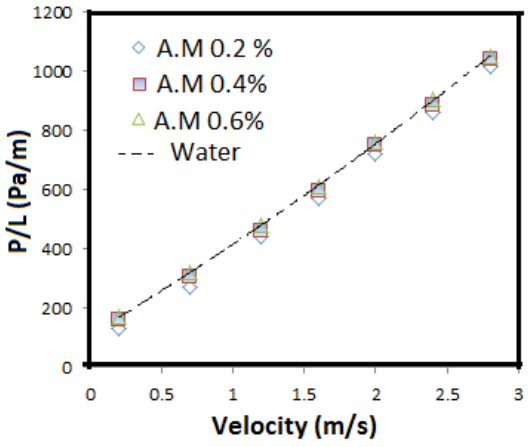

Figure 4.20: Pressure drop versus velocity for water and Acacia mangium suspensions with different fibre concentrations

The trends for the present research data obtained for water and pulp suspension are similar to the typical trend investigated by (Duffy et al., 1972). At lowest velocity the data for Acacia mangium samples suspensions are higher to that of water. Whereas, on the other hand, by increasing the velocity, there is a drop down of the pressure loss data to below water data and further increase in velocity slightly increases the pressure drop near to the water data. In order to study the drag reduction behavior of the pulp suspension the pressure drop data are presented as the drag ratio data.

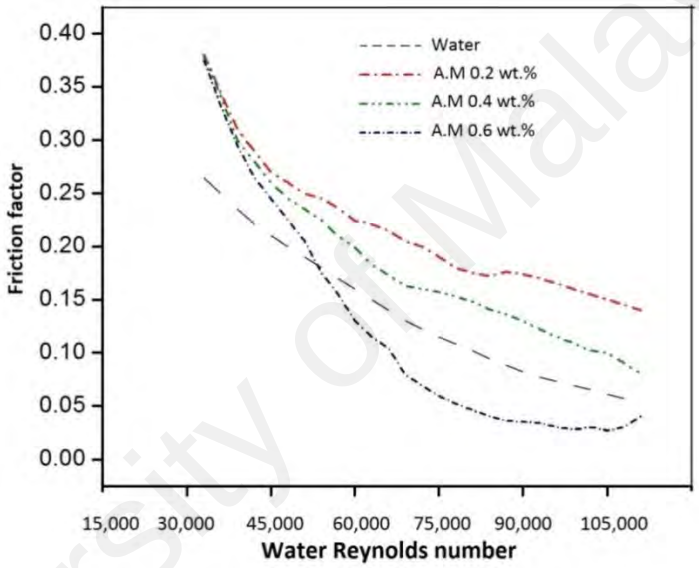

Figure 4.21: A plot of friction factor against water Reynolds number for water and Acacia mangium suspension with different fibre concentrations

Figures 4.22 and 4.23 represents frictional pressure drop as drag ratio versus water velocity for Acacia mangium and Acacia mangium hybrid samples at different concentrations at bulk temperature of 30 °C. It should be mentioned that the pressure drop data obtained from the pulp suspensions are reliable (Appendix D).

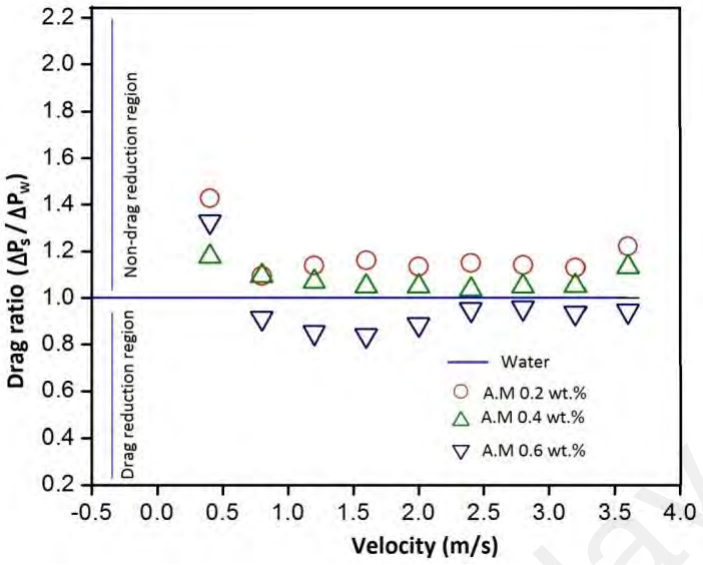

Figure 4.22: Drag ratio for Acacia mangium pulp suspensions of different fibre concentrations as a function of velocity

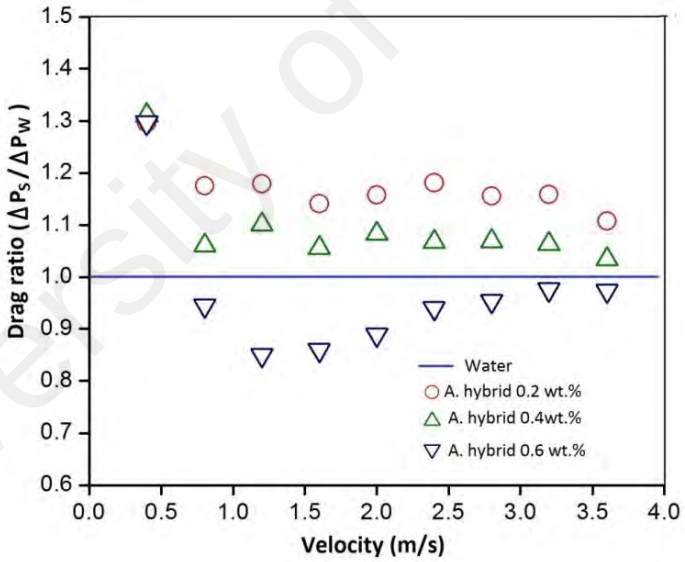

Figure 4.23: Drag ratio for Acacia hybrid pulp suspensions of different concentrations as afunction of velocity

Water data were set as a unity. At lowest velocity value (0.4 m/s) the data are higher than water means no drag reduction. It is logic as usually floc formation occurs in such low velocity, so the drag ratio of fiber suspension is higher than water. From 0.8 m/s up to the 3.6 m/s the data are more close to the water data. By considering the water data as a border for drag reduction and non-drag reduction regions, it can be stated that there is

a strong dependency between the concentration and obtaining the drag reduction. For suspensions at concentration of 0.2 and 0.4 wt.% the drag ratio data are higher than the water line in the low and middle velocity range while at the 0.6 wt.% sample has lower drag ratio than 1 in the whole range except at 0.4 m/s. In general, the presence of very low amounts of fibers in slurries enhances the pressure drop. A critical concentration can be defined where the data are still higher than unity in the most velocities and further increase in fiber concentration results in reduction in pressure drop and drag ratio values moved to lower than water. In the non-reduction region, the drag ratio data obtained from the suspensions of 0.4 wt.% concentration are more close to the water data compared to the suspensions of 0.2 wt.% concentration.

Increasing the concentration up to 0.6 wt.% the data are moved below water line where there is a drag reduction region. The magnitude of the drag ratio decreases and then increases at velocity range of 0.4 to 2 m/s where a maximum drag reduction occurs in this region. In the high range of velocity the drag ratio data increase close to water line. Figure 4.24 shows the drag ratio versus velocity for water, Acacia mangium and Acacia mangium hybrid samples of concentration 0.6 wt.%.

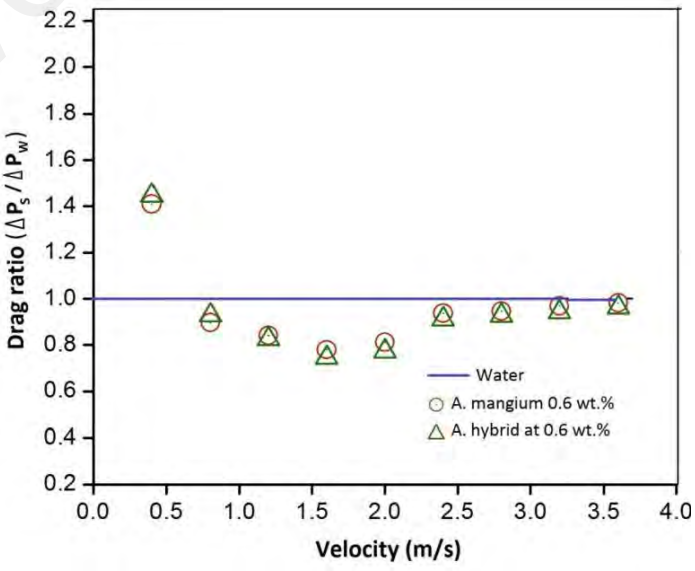

Figure 4.24: Drag ratio as a function of velocity for different pulp suspensions of fibre concentration 0.6 wt.%

The results show that Acacia hybrid would produce slightly higher amount of drag reduction as compared to Acacia mangium. The momentum transfer behavior of all samples is almost same where a maximum drag reduction followed by increment in drag ratio. As it can be seen the maximum drag reduction occurred in the middle range of velocity. The values of drag ratio data for Acacia mangium are almost higher than that for Acacia mangium hybrid sample. It means Acacia mangium suspension poses more drag reduction. The maximum drag reduction for Acacia mangium and Acacia mangium hybrid are 7.9 % and 10.6 % respectively.

4.5.2 Effect of pulp beating

Figure 4.25 presents the data of pressure drop as a function of velocity for unbeaten and beaten Acacia mangium fibers suspensions at concentration of 0.6 wt.%, velocity range of 0.4 to 3.6 m/s and bulk temperature 30 °C. The results show that the pressure drop values of sample with low degree of beating are close to the unity as compared to values without beating. In other words, the suspensions with 2000 degree of beating behave more or less same behavior as unbeaten fiber suspension. Around 0.8 m/s is the onset of plug disruption and with further increase in velocity noticeable reduction of $\Delta P/L$ occurred.

Increase in beating degree reduces the pressure drop of the suspension. The reduction in $\Delta P/L$ with the flow of beaten Acacia mangium with 8000 degree is due to beating effect on fiber surface roughens by formation of fibrils which affects fiber-fiber and fiber-liquid interactions. Moreover, an increase in the degree of beating result a net increase in fine production and fiber flexibility and fines formation. The consequences of fiber shortening, fiber straightening and a net increase in the specific surface area of fibrils cause a lower value of $\Delta P/L$ as compared to a lower degree of beating (2000 and 4000 degree). The findings are in agreement with previous study done by (Kazi et al., 2014b).

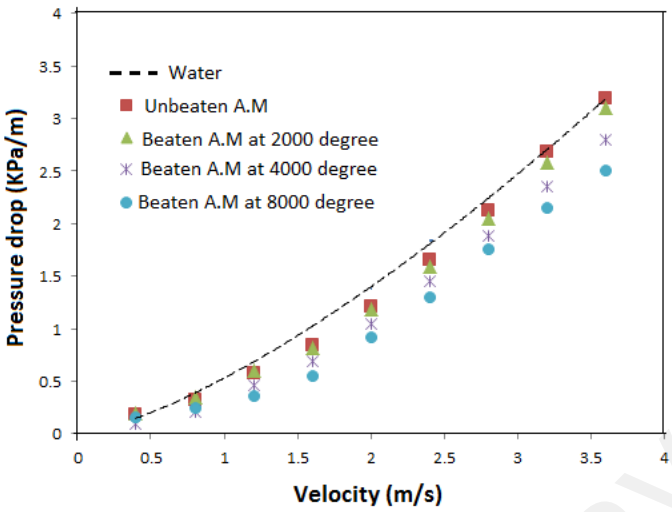

Figure 4.25: Pressure drop versus velocity for water, Unbeaten Acacia mangium and beaten Acacia mangium samples with two different beating degrees

Figures 4.26 presents the data of drag ratio as a function of velocity for unbeaten and beaten Acacia mangium fibers suspension at concentration of 0.6 wt.%, velocity range of 0.4 to 3.6 m/s and bulk temperature of 30 °C. However in case of drag ratio, there is insignificant difference between the unbeaten and beaten Acacia mangium with 2000 degree, further beating to 4000 and 8000 degree results in lower drag ratio where the maximum drag reduction of 36 % occurred at 1.6 m/s velocity.

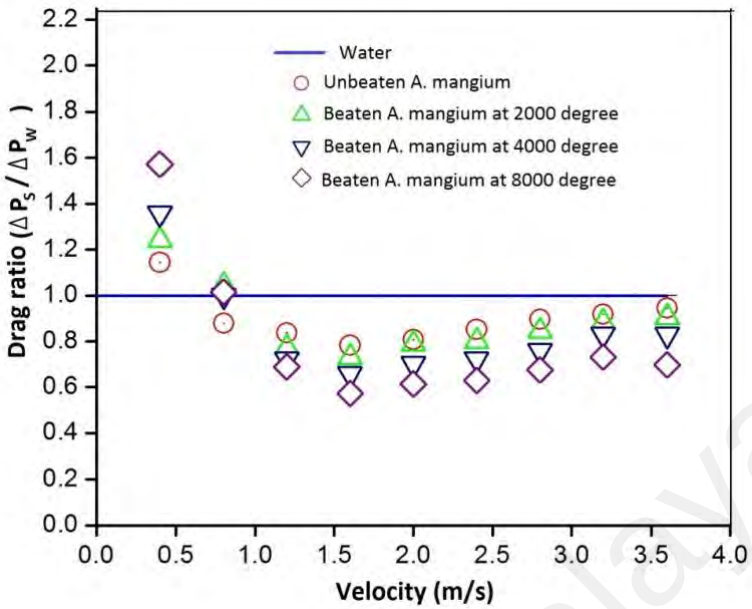

Figure 4.26: Drag ratio versus velocity for water, unbeaten and beaten A. mangium samples with three different beating degrees

Detailed study of drag ratio data reveals that beating degree of 8000 slightly delayed the drag reduction phenomena. It can be claimed that beaten sample can produce lower drag ratio than unbeaten samples.

4.6 Pressure drop and fiber properties

Like heat transfer study, there is a hypothesis regarding the relationship between pressure drop and fiber properties. Figure 4.27 shows variation of pressure drop data versus fiber length. Different properties of fibers were obtained using the different degrees of beating. A decrease in fiber length due to beating would reduce the pressure drop values. However, beating has some negative effets like pulp freeness and drainage. Increasing in degree of beating reduces the pressure drop of the suspension. The reduction in P/L with a flow of beaten AM and AMH with 4000 degree is due to beating effect on the fibre surface roughness by the formation of fibrils which affets fibre-fibre and fibre-liquid interaction. Further beating increases fibre flexibility and fne contents and ΔP/L is lowered. However, beating effect of AMH is a bit different from AM. In the case of AMH ΔP/L is a bit lower than the corresponding AM. As far as, the fibre length

of AM is lower than the AMH as shown in table 4.3. The findings are in aggrement with previous study done by (Kazi et al, 2014b). Beaten and unbeaten AM and AMH SEM images have been provided in appendix A.

Comparing the sample Acacia mangium with no beating effects, a decrease of 7.3 % in fiber length results a decrease of 18.2 % pressure drop. Same trend is presented in Figure 4.29 for variations of pressure drop versus slender ratio.

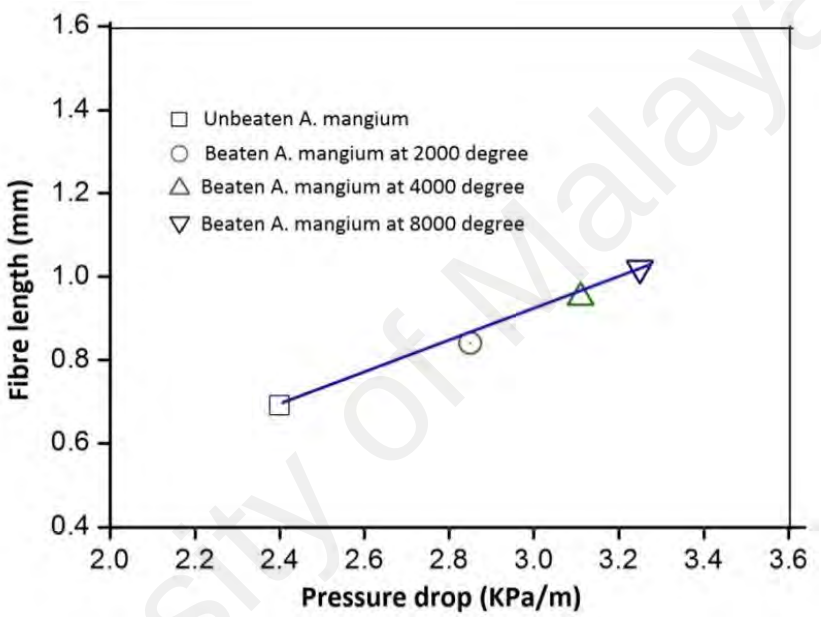

Fig 4.27: Fiber length as a function of pressure drop for Acacia mangium with no beating and with 2000, 4000 and 8000 degrees of beating

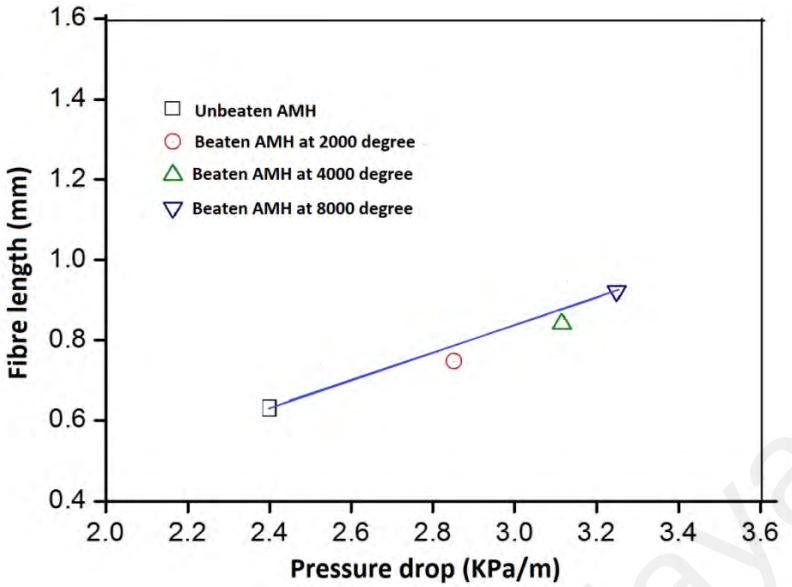

Fig 4.28: Fiber length as a function of pressure drop for Acacia mangium hybrid (AMH) with no beating and with 2000, 4000 and 8000 degrees of beating

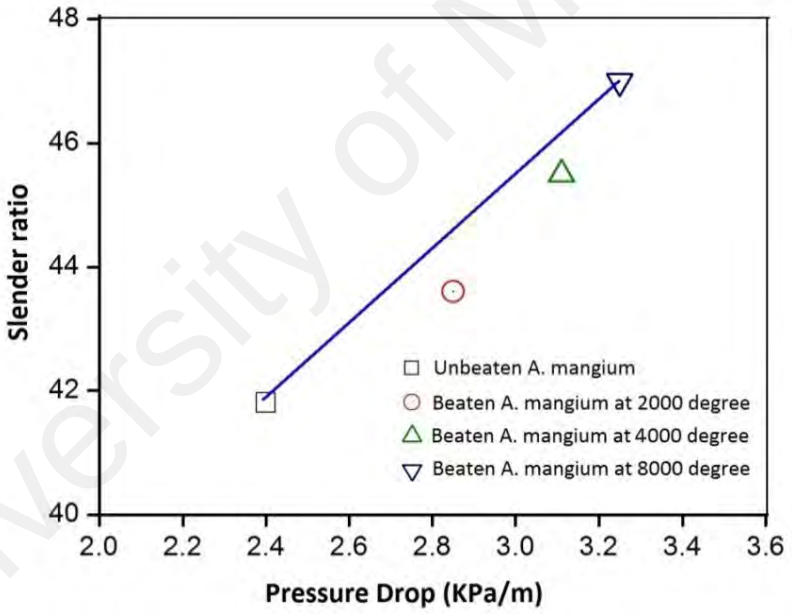

Fig 4.29: Slender ratio as a function of pressure drop for Acacia mangium with no beating and with 2000, 4000 and 8000 degrees of beating

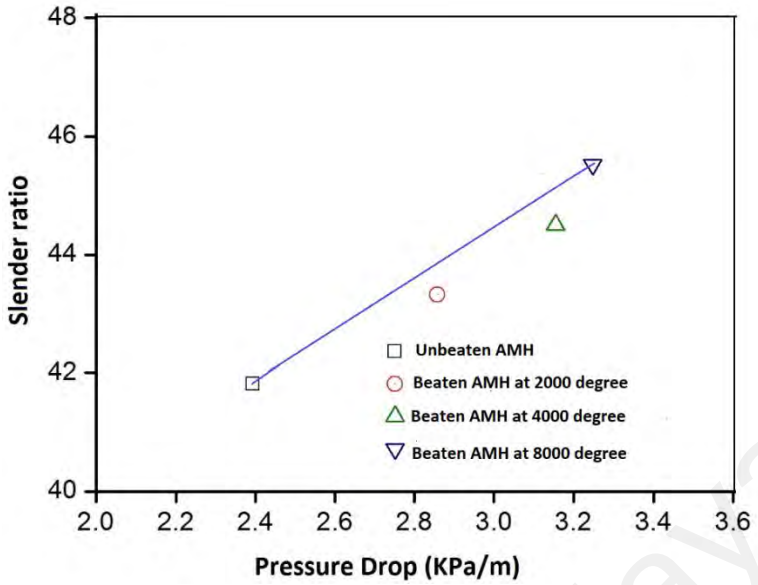

Fig 4.30: Slender ratio as a function of pressure drop for Acacia mangium hybrid (AMH) with no beating and with 2000, 4000 and 8000 degrees of beating

Figure 4.31 and Fig.4.32 shows the changes of pressure drop versus flexibility ratio for AM and AMH samples. A decrement in linear trend of pressure drop can be seen with increment of flexibility ratio.

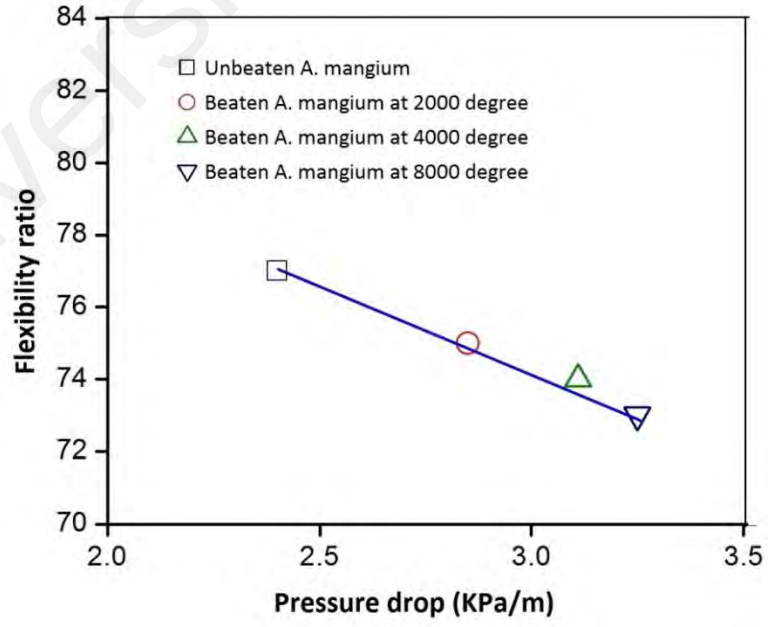

Fig 4.31: Flexibility ratio as a function of pressure drop for Acacia mangium with no beating and with 2000, 4000 and 8000 degrees of beating

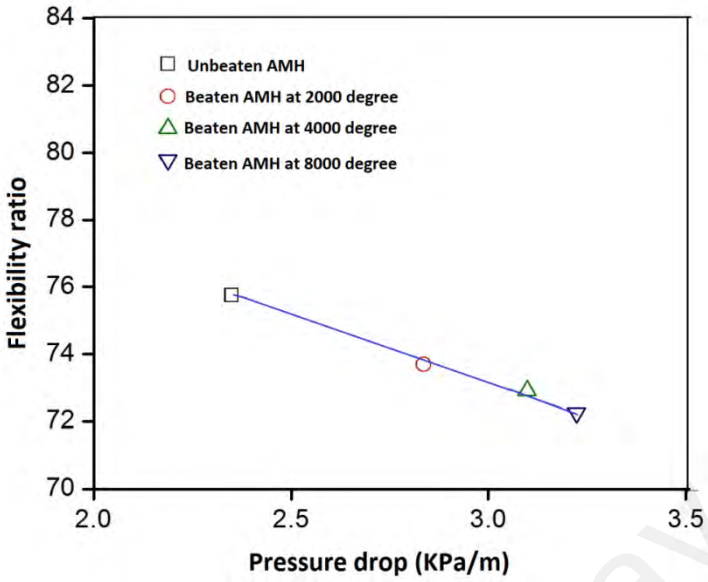

Fig 4.32: Flexibility ratio as a function of pressure drop for Acacia mangium hybrid (AMH) with no beating and with 2000, 4000 and 8000 degrees of beating

In conclusion, the trends of variations in pressure drop data with fiber properties are similar to those variations were recorded heat transfer coefficient data with fiber properties. However the variations of pressure drop data are correlated with fiber properties more linearly.

4.7 Pressure drop and paper properties

Frictional pressure drop measurement of fiber suspensions were used to correlate ΔP/L data with the properties of paper sheets made from the same type of fibers. Paper properties were obtained from laboratory-made hand sheets prepared from the same pulp fibers. Some of the data are presented in graphical form in figures 4.33 to 4.37.

In figure 4.33, approximate linear relationship is found for paper tensile index versus pressure drop at the velocity of 1.2 m/s and temperature of 30 °C. The hand sheets used for tests were at the same grammage. The decrement order of tensile index remains according to the degree of beating, such as unbeaten, beaten with 2000, 4000 and 800 degrees respectively.

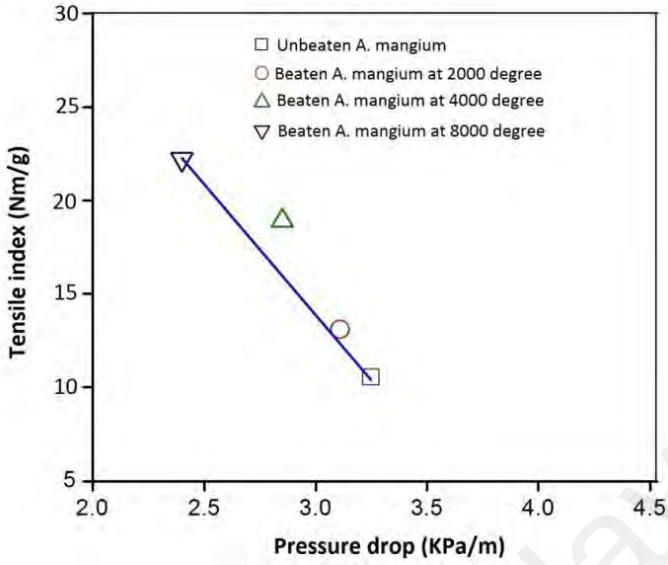

Figure 4.33: Tensile index as a function of pressure drop for Acacia mangium fibre suspensions of unbeaten and beating with 2000, 4000 and 8000 degrees

In figure 4.34, the trend for burst index versus pressure drop remains the same. Burst index increases with the decreases of pressure drop of fiber suspensions.

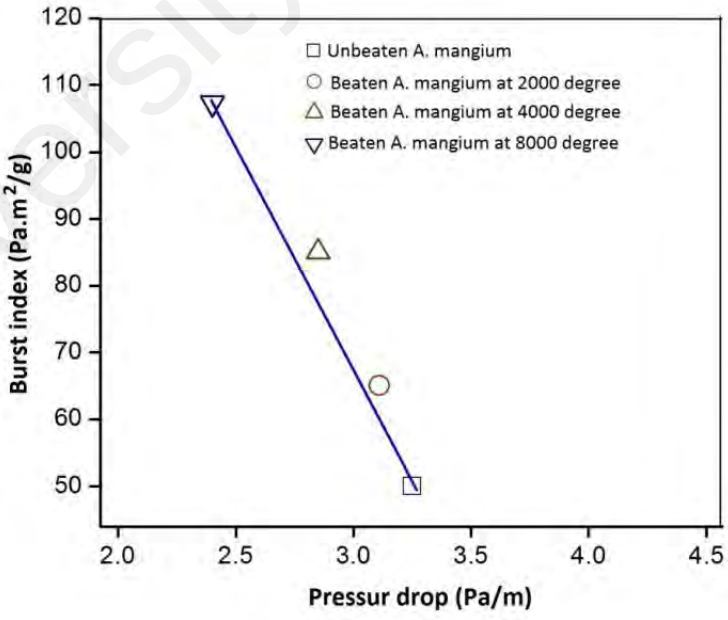

Figure 4.34: Burst index as a function of pressure drop for Acacia mangium with no beating, and with beating of 2000, 4000 and 8000 degrees

Figure 4.35, depicts increase of tear index with the enhancement of frictional pressure drop. The fibre tear strength opposed the tensile strength of fibre, whereas the tearing index value decreased with increase of beating degree.

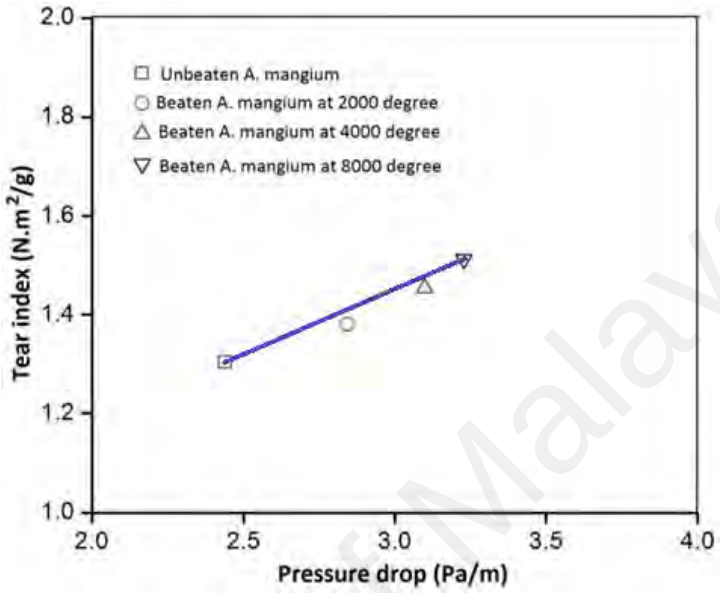

Figure 4.35: Tear index as a function of pressure drop for Acacia mangium with no beating, and with beating of 2000, 4000 and 8000 degrees

The tear index test is most profound test method for analyzing the fibre physical properties (Main et al., 2015). The effect of beating cause some physical changes in fiber dimension like: shortening of fibers and therefore attributing to the decrease the fibre tear strength. It is noticeable that sometimes decrease in tear index resulted from beating process is not significant. Main et al. (2015) reported only 0.4% decrement of tear index for coconut coir fibers at beating degree of 2000 to 8000 revolutions respectively.

Figure 4.36, represents paper folding endurance as a function of pressure drop of suspensions of the unbeaten and beaten fibers as well. Although folding endurance increases with decrease of pressure drop, the relationship is not as good as tensile, burst and tear indices.

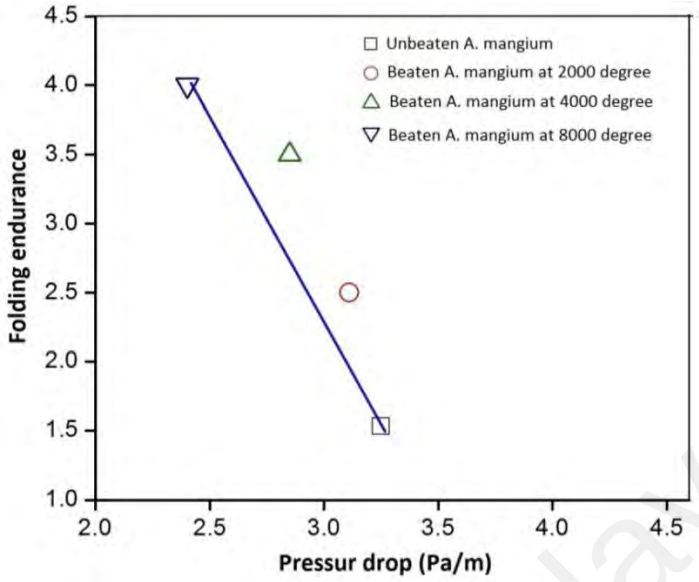

Figure 4.36: Folding endurance as a function of pressure drop for Acacia mangium with no beating, and with beating at 2000, 4000 and 8000 degrees

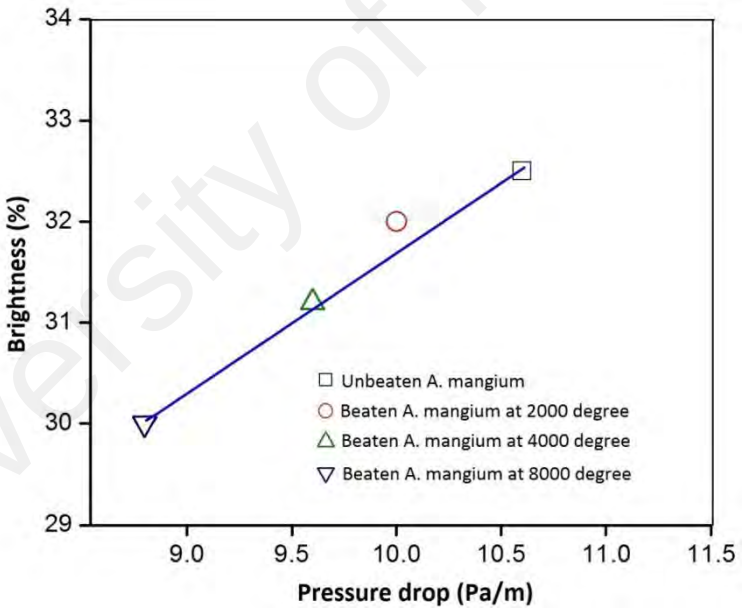

Figure 4.37: Brightness as a function of pressure drop for Acacia mangium with no beating, and with beating at 2000, 4000 and 8000 degrees

Figure 4.37, shows that paper brightness correlate well with frictional pressure drop for fiber suspensions of beaten and unbeaten Acacia mangium pulps. It is obvious in the figure 4.37 that the brightness increases with increase in pressure drop. Brightness is achieved by multiple times of bleaching. Due to bleaching fibre flexibility increases

resulting to decrease in suspension pressure drop. Similar results are obtained in case of tear index of produced papers.

In the pulp and paprer industries, the presence of corrosion products were revealed, due to the applications of various chemical used as well as chemically treated fibre like bleaching of fibre. Moreover the occurance of corrosion was aslo evident at the fouling sites as well. Therefore, the account for corrosion mitigation techniques has been taken under consideration in the present research work.

4.8 Stirring time and multiple runs

One of the concerns associated with experimental work was to define a proper procedure to run the pulp samples.

To find out the data whether data obtained from the experiments have been affected by soaking/stirring time or multiple runs, a supplemtry experiment was conducted with AM sampels (0.2wt.%) concentration and data were taken in the velocity range 0.4 - 3.6 m/s at 30 ^{o}C (Figure 4.38). At the end of the first run the samples were kept inside the tank under stirring. After 30 hours stirring, the second experiment was conducted at the same procedure. Results show a significat difference between pressure loss data taken from the first and second run.

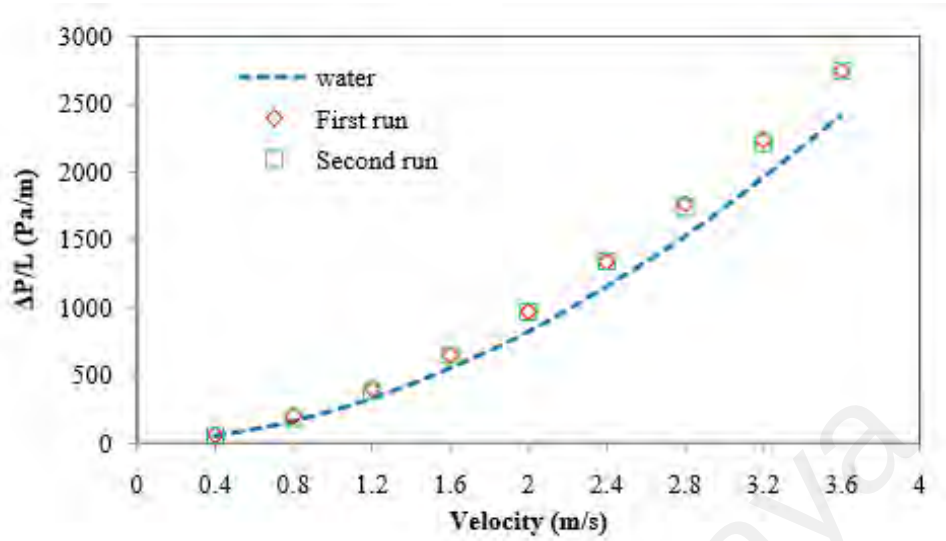

Figure 4.38: Friction head losses as a function of velocity for two runs of AM samples at a concnetrations of 0.2wt.% and bulk temperature of 30 ºC.

4.9 Weight loss and electrochemical methods of corrosion inhibition

The obtained results from weight loss method and the electrochemical techniques were carried out in order to evaluate the corrosion inhibition efficiencies of the investigated Schiff bases like HL_1, HL_2 HL_3 and HL_4 at different concentrations on MS, and CS in both 1M HCl and 1 M H_2SO_4 solution at non-stirring as well as at ambient temperature conditions are presented in this section.

4.9.1 Weight loss measurements for investigated Schiff bases

The weight loss measurements for the MS and CS coupons immersed in blank, as well as different concentrations solution of Schiff bases of 25 ppm, 50 ppm, 75 ppm and 100 ppm prepared in 1M HCl and 1 M H_2SO_4 solution, after a time period of 24 hours exposure are summarized in table 3.1. The obtained results conclude that the addition of Schiff bases decreases corrosion rate, whereas increasing the inhibition efficiencies and surface coverage as well. The FeSEM analysis for MS and CS strongly suggests that coupons surface were severely damaged in the absence of inhibitors resulting metal

dissolution in acidic medium, whereas coupons were least damaged in the presence of inhibitor solutions. In addition, the corrosion rates were suppressed in the presence of inhibitor due to the development of compact and dense protective film as a result of inhibitor adsorption on the active sites of metal surfaces. At a concentration of 100 ppm the Schiff bases HL_S exhibits a maximum inhibition efficiency (88 % to 94 %), representing the efficient inhibitors for both MS and CS in HCl solution. The weight loss (A) and corrosion inhibition efficiency (η_{WL}) through weight loss measurement for a time interval of 24 hours for MS, and CS coupons immersed in 1 M HCl and 1 M H_2SO_4 with and without inhibitor solutions for HLs were plotted against immersion time shown in the table 4.4.

Table 4.4: Corrosion inhibition effects of LHs attained from the weight loss method of MS and CS after 24 h immersion in 1 M HCl and 1 M H_2SO_4 solution in the absence and the presence of the Schiff bases at ambient temperature

Concentration	**Corrosion current**	**Surface coverage**	**Inhibition Efficiency**
(ppm)	**A ($mg.cm^{-2}.h^{-1}$)**	**(θ)**	**η_{WL} (%)**
HL_1 (MS in 1 M HCl)			
Blank	0.00560	-	-
25	0.00250	0.55	55
50	0.00118	0.78	78
75	0.00063	0.88	88
100	0.00031	0.94	94
HL_2 (MS in 1 M HCl)			
Blank	0.0056	-	-
25	0.0036	0.37	37
50	0.0025	0.65	65

'Table 4.4, continued'

Concentration	Corrosion current	Surface coverage	Inhibition Efficiency
(ppm)	**A ($mg.cm^{-2}.h^{-1}$)**	**(θ)**	**η_{WL} (%)**
HL_2 (MS in 1 M HCl)			
75	0.0017	0.80	80
100	0.0011	0.89	89
HL_3 (CS in 1M H2SO4)			
Blank	0.0098	-	-
25	0.0066	0.48	48
50	0.006	0.63	63
75	0.0054	0.81	81
100	0.005	0.9	90
HL_4 (CS in 1M H_2SO_4)			
Blank	0.0098	-	-
25	0.0068	0.44	44
50	0.0062	0.58	58
75	0.0056	0.75	75
100	0.0052	0.88	88

It is found, that minimum weight loss was found for the immersed coupons in the solution containing inhibitor with the highest concentrations. Similarly, all trends were found to be decreased in the weight loss with a corresponding increase in investigated Schiff base inhibitor concentration. The weight loss for the coupons in acid solutions was the highest for HL_1 and lowest for HL_4. Table 4.4 concluded that among all the

investigated Schiff bases weight loss were found to be decreased in the order of HL_4 <HL_2 <HL_3 <HL_1.

4.9.2 Corrosion rate and percentage corrosion inhibition efficiency

In this study the corrosion rate were demonstrated in $mg.cm^{-2}.h^{-1}$ for both MS and CS specimens in 1M HCl and 1 M H_2SO_4 with and without the presence of different inhibitor concentrations. The data were derived from the weight loss method performed at ambient temperature. The corrosion rates for Schiff bases HL_1, HL_2, HL_3 and HL_4 immersed for a period of 24 hours are recorded in table 4.4.

From table 4.1 it is found that corrosion rates were decreased with the increase in inhibitor concentration. Minimum corrosion rates were to be observed for the maximum concentrations of inhibitor solutions. In addition, for HL_1 the corrosion rate has obtained least among the rest of the investigated Schiff bases.

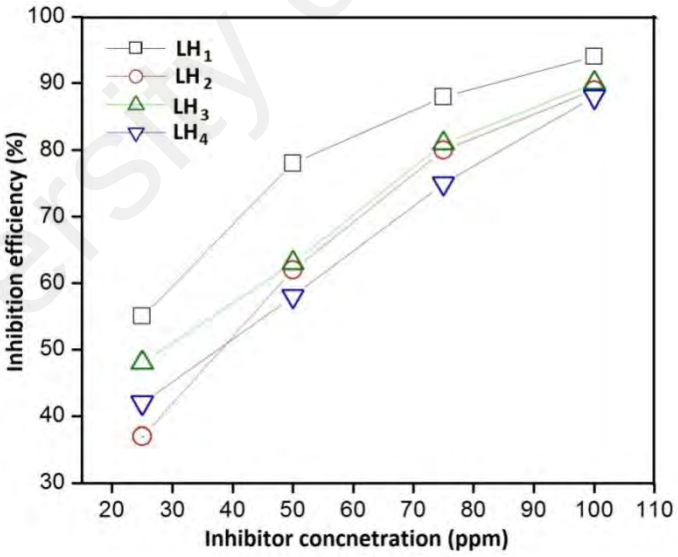

Figure 4.39: Plot of percentage inhibition efficiency against the concentration of Schiff bases HL_1, HL_2, HL_3 and HL_4

In Fig 4.39, HL_4 the inhibition efficiency was found to be 44 % for a relatively lower concentration of 0.0001 M equivalent to 25 ppm and a maximum efficiency of 88% (almost double than that at 25 ppm) was achieved at a very low concentration of 0.0004

M corresponding to 100 ppm. Where as in the case of HL_1, the value of inhibition efficiency around 78 % was achieved even at a low concentration of 0.0001 M corresponding to 25 ppm, whereas the incremental rise in efficiency become more slowly by the increase in inhibitor concentration, finally a maximum inhibition efficiency 94 % was recorded with a concentration of 0.0004 M equivalent to 100 ppm. Similarly, for HL_2 and HL_3, the inhibition efficiency rapidly enhanced up to 90 % and 89 % at a maximum concentration of 0.004 M (100 ppm). It was noticeable that the inhibition efficiency was not enhanced furthermore beyond 100 ppm (0.0004 M) due to precipitation of the inhibitor particles in acidic solution, this information conclude that 0.0004 M are found to be optimum inhibitor concentration for all investigated Schiff bases in acidic medium.

Figure 4.40, characterizes an arrangement of SEM micrographs of the abraded MS and CS immersed for 24 hours in 1 M HCl and 1 M H_2SO_4 solutions without inhibitors at ambient temperature conditions. It was observed that in uninhibited HCl and H_2SO_4 solutions the metal surfaces were extensivley damaged and roughned by aggressive solutions as well as the presence of porous corrosion product layers. Whereas in Fig 4.41, the FESEM images in the presence of inhibitor solution at optimum concentration at ambient temperature suggests that the presence of inhibitor in acidic medium reduce the damaged metal surface, results a diminished corrosion rate as a result of establishment of compact, dense and uniform shielding film of the HLs shielding the surfaces from the aggressive solution attack. Inaddition, in the presence of inhibitor solution, the immersed sepcimens are in a better condition with smooth surface appreance incomaprision to thoses without inhibitors. This indicates a better improvement in the reduction of corrosion rate along with a protective film formation on substrate surface, resulting corrosion inhibition.

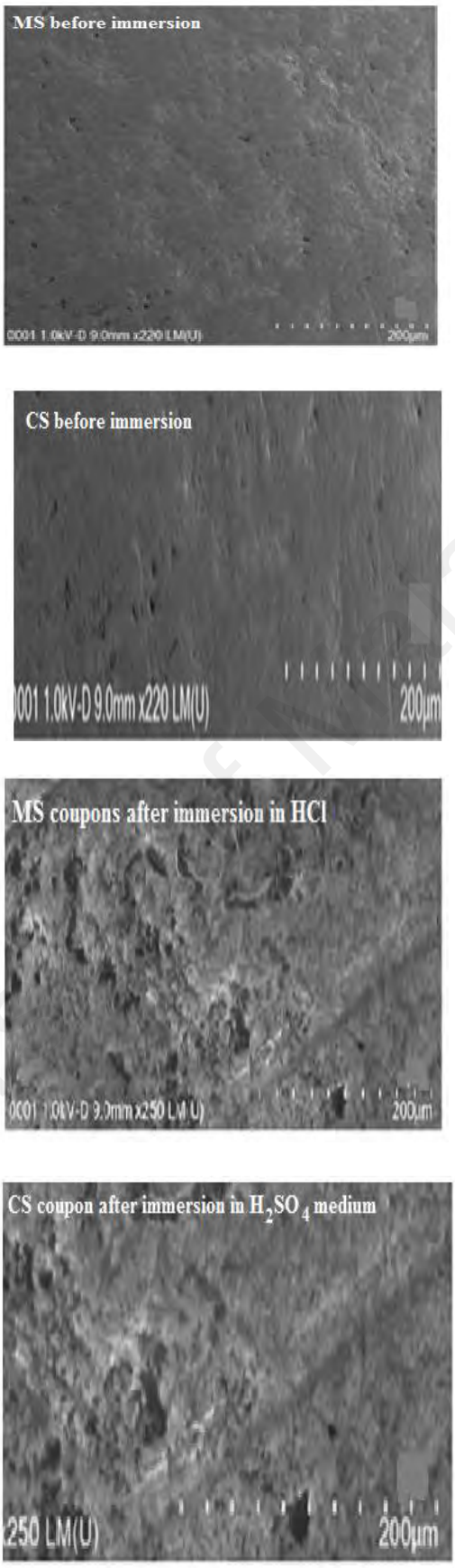

Figure 4.40: SEM micrographs of mild and carbon steel abraded surfaces before and after immersion in HCl and H_2SO_4 solution for 24 hours without the inhibitors at ambient temperature

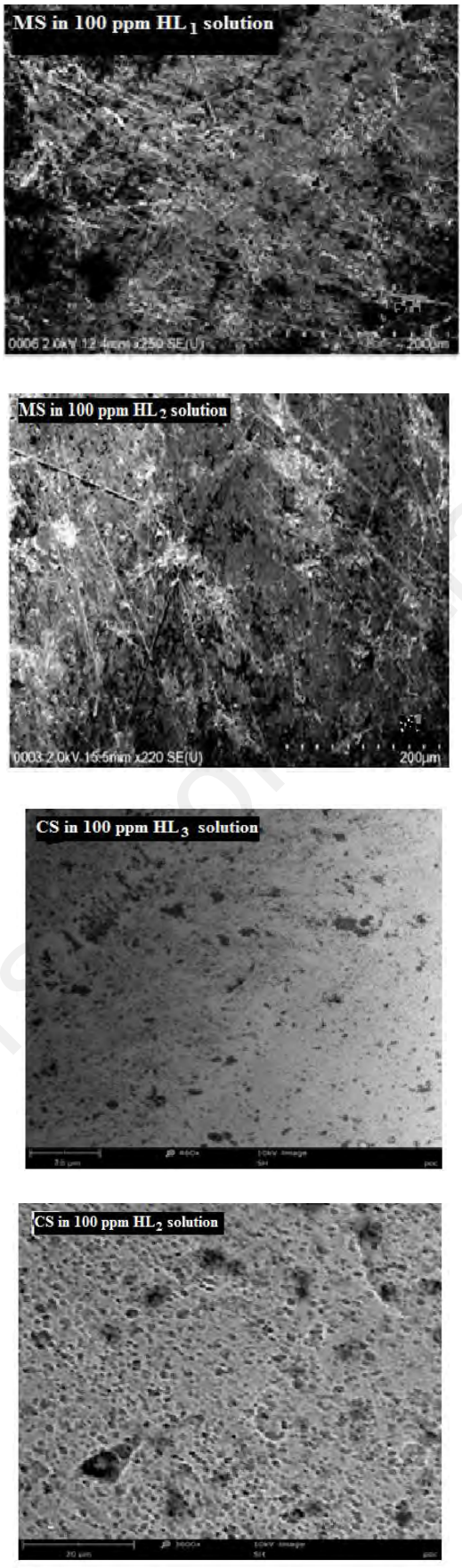

Figure 4.41: SEM images of mild and carbon steel surfaces with the optimum concentration of HLs after immersion in 1 M HCl and 1 M H_2SO_4 for 24 hours at ambient temperature

4.10 Open circuit potential measurement (OCP)

The OCP for both MS and CS were measured carefully at different concentrations of Schiff bases (HLs) with and without the addition of Schiff Base corrosion inhibitors. Fig. 4.42 represents the variation of OCP for MC in 1 M HCl and CS in 1 M H_2SO_4 solutions with and without the addition of Schiff base inhibitors. Furthermore, the additions of Schiff bases to acidic solutions, a more negative shift of OCP were observed for HL_1 and HL_2, whereas in contrast there is positive shift of OCP values were observed for HL_3 and HL_4 at all concentrations. This result revealed that all Schiff bases inhibitors (HL_S) have the potential to inhibit the corrosion of MS and CS in 1 M acidic solutions. Maximum shifts in OCP for investigated inhibitors HL_1, HL_2, HL_3 and HL_4 were 78.2 mV, 59.2 mV, 19 mV and 16 mV observed at 100 ppm concentration.

These OCP results suggest that all the investigated Schiff Bases (HL_S) can retard both the oxidation of oxide-free ion and liberation of hydrogen ions on the surface (de Souza & Spinelli, 2009). A negative shift for OCP was seen by the addition inhibitor, leading to the inhibition effect of LH_1 and LH_2 on the corrosion of mild steel. The shift of OCP values in a more positive direction with increasing concentration of Schiff base inhibitors, suggests the solidity of the surface layer for inhibitors (Hermas & Morad, 2008).

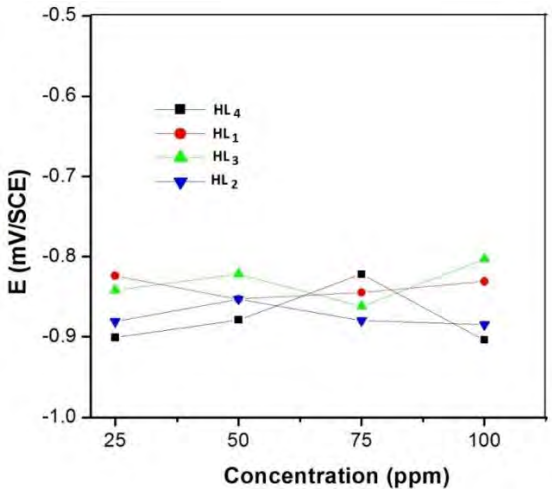

Figure 4.42: OCP change for different concentrations of Schiff bases added in 1 M HCl and 1M H_2SO_4 solutions

4.11 Potentiodynamic polarization measurements

Potentiodynamic polarization curves were recorded to investigate the corrosion inhibition effects on the electrochemical behavior of MS and CS in both 1.0 M HCl and 1.0 M H_2SO_4 in the absence and presence of the HLs Schiff bases at different concentrations. The associated electrochemical parameters such as corrosion potential (E_{corr}), corrosion current density (i_{corr}), anodic and cathodic Tafel slopes (b_a & b_c) were obtained from the intersection of anodic and cathodic Tafel lines, corrosion inhibition efficiencies η_P $(\%)$ were claculated and presented in table 4.5:

Table 4.5: The polarization parameters and the corrosponding corrosion inhibition efficiencies for both MS and CS in 1 M HCl and 1 M H_2SO_4 solution in absence and presence of various concentrations of LHs at ambient temperature

Inhibitors	Concentration (ppm)	- E_{corr} (mV vs. SCE)	ba (mV/dec)	bc (mV/dec)	Icorr ($mAcm^{-2}$)	η_P (%)
	Blank	0.894	161.5	192.6	543.05	-
HL_1	25	0.901	134.3	142.2	74.1	86
	50	0.954	121.1	114.1	67	87.6
	75	0.982	118	112.3	51.06	90.6
	100	0.101	68.2	61.5	37.13	93.1
	Blank	0.894	161.5	192.6	543.05	-
HL_2	25	0.886	221	159.4	102.11	81.2
	50	0.913	196.3	139.1	70.03	87.1
	75	0.932	167.1	121.1	56.14	89.6
	100	0.953	121.3	91.4	47.01	92.3
	Blank	0.987	126.5	121.3	9.5	-

'Table 4.5, continued'

Inhibitors	Concentration (ppm)	- E_{corr} (mV vs. SCE)	ba (mV/dec)	bc (mV/dec)	Icorr ($mAcm^{-2}$)	η_P (%)
HL_3	25	0.842	92.2	113.5	4.8	49.4
	50	0.825	76.3	98.3	3.6	62.1
	75	0.812	63.3	86.1	1.9	80
	100	0.800	54.2	71.2	0.7	92.6
	Blank	0.987	126.5	121.3	9.5	-
HL_4	25	0.904	109.4	114.7	5.2	45.2
	50	0.831	92.2	91.2	4.0	57.8
	75	0.833	84.1	79.2	2.1	77.8
	100	0.825	71.2	65.4	1	89.4

Table 4.5 reveals that, in the presence of Schiff base inhibitors (HLs) the Icorr values become lower. The corrosion current values obtained for MS and CS in the presence of HL_S are lower than the corresponding values without the presence of inhibitors i.e. blank solution. These results show that the presence of investigated inhibitors (HL_S) lowers the values of the corrosion current. The lowest values of Icorr were observed in the case of HL_3 at a concentration of 0.0004 M (100 ppm). It is evident that, the inhibition efficiency increases with rise in inhibitor concentrations for both MS and CS test coupons in the presence of acidic solutions. Maximum efficiency for MS in HCl and CS in H_2SO_4 were found 93% and 92% respectively at a very low concentration of 0.0004 M corresponding to 100 ppm. This shows that all the investigated Schiff bases (HL_S) are effective corrosion inhibitors for both MS and CS in different acidic solutions. The values of inhibition efficiency were found to be holding constant after reaching the maximum inhibition efficiency at 0.0004 M (100 ppm). A similar trend was also

observed for weight loss method. Table 4.2 reveals that there are significant changes in the values of E_{corr} for both inhibited and uninhibited acidic solutions.

From Fig. (4.43 - 4.46), it can be seen that by the addition of Schiff bases (HL_S) to the aggressive solution, the magnitude of corrosion current densities for both the anodic and cathodic curves are decreased and shifted to a lower direction for all investigated inbibitors as compared to the blank solution. This phenomenon indicated that the inhibitor may suppress anodic metal dissolution and cathodic hydrogen evolution reactions with the increase of the inhibitor concentration. This result suggests that the inhibitor molecules were adsorbed on active sites of the solid surface (Salmoz et al., 2011). Generally in acid mediums, there are the passage of metal ions from the metal surface into the aggressive solution in the case of anodic corrosion, whereas for cathodic reaction, the discharge of hydrogen ions yielding a hydrogen gas (Solmaz et al., 2008).

From table 4.5, it is found that the corrosion current densities decreases with the increase in inhibitor concentration, while the inhibition efficienies increases as expected. Furthermore, it is found that,the values *ba* is nearly same with the presence of inhibiitors (HL_1 and HL_2), however the values of *bc* were found to be less or more fluctuatiing in the presence and the absence of inhibitors, in the case of HL_1 and HL_2 for MS in the HCl solution. Whereas, on the other hand, a constrast found for inhibitors HL_3 and HL_4, where *ba* valuesare more or less same in the presence and the absence of inhibitors, and *bc* is nearly same in the presence of inhibitors for CS in H_2SO_4 solution. These results indicating that the addition of investigated Schiff bases did not modify the mechanism of the corrosion process.

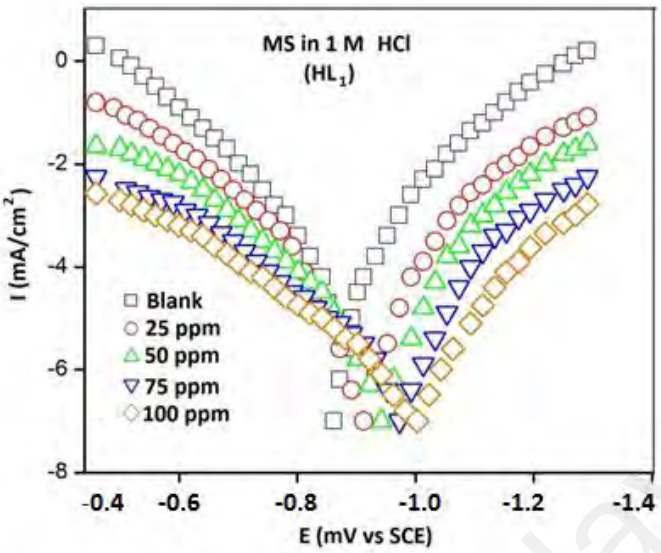

Figure 4.43: Polarization curves for MS in 1 M HCl at different concentration of HL_1

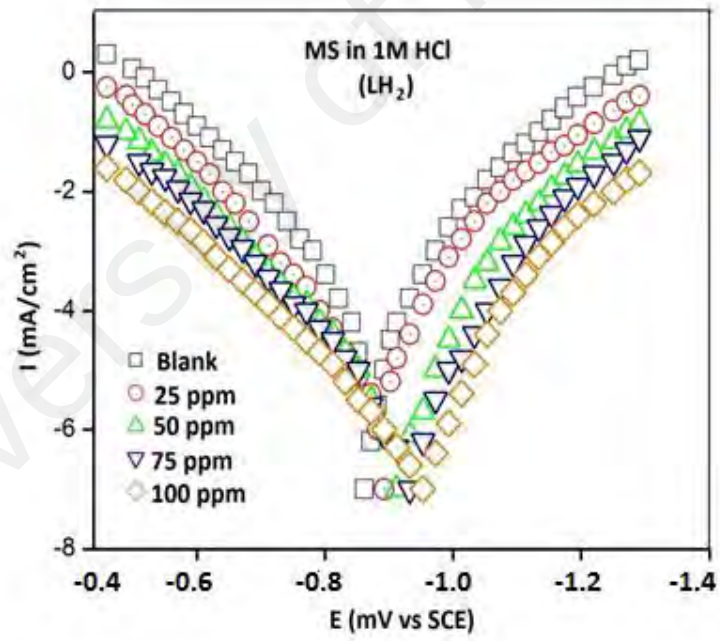

Figure 4.44: Polarization curves for MS in 1 M HCl at different concentration of HL_2

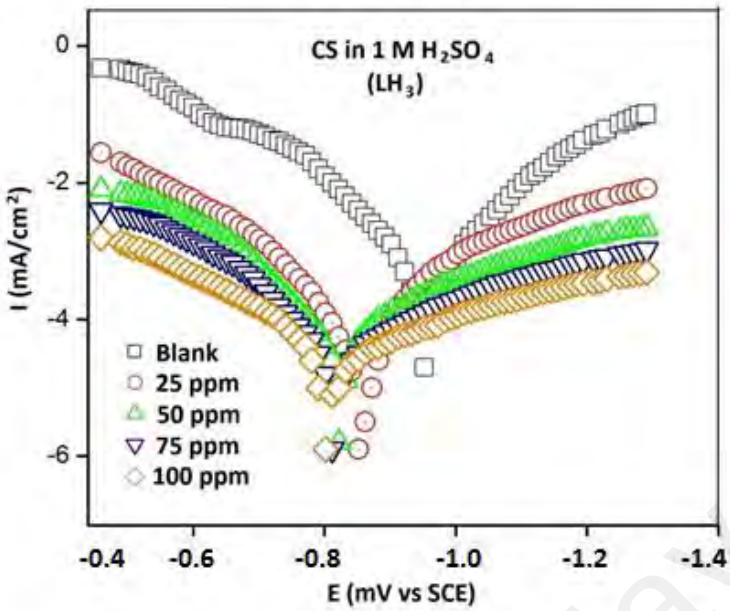

Figure 4.45: Polarization curves for CS in 1 M H_2SO_4 at different concentration of HL_3

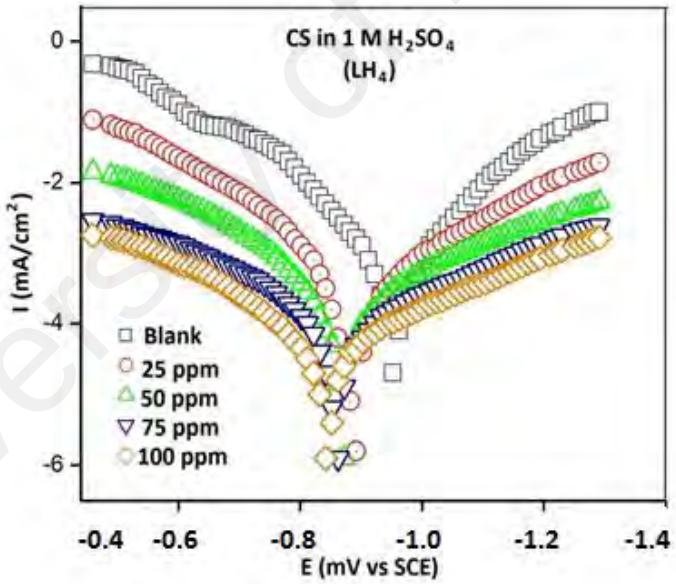

Figure 4.46: Polarization curves for CS in 1 M H_2SO_4 at different concentration of HL_4

The data in table 4.5 reveals that in the presence of inhibitors, the values of E_{corr} for LH_1 and LH_2 in the case of MS shifted towards cathodic region of 67- 78 mV and for CS that shifted towards the anodic region of 63 - 76 mV range respectively. This result can be attributed to the inhibitor which reduces corrosion rate by anodic mode. This

pheonomenon leads the equilibirum in a passive direction, resulting the formation of thin passive oxide layer over the anodic sites, therefore, increasing anodic potential and suppressing oxidation process. If the displaced values of corrosion potential is higher than 85 mV to the crossesponding values in the blank solution, then the inhibitor can be classified as anodic or cathodic type (Noor, 2009).

In the present work, the maximum displacement observed for CS in HCl solution were 79.3 mV and 59.1 mV for HL_1 and HL_2 respectively, on other hand, a displacement of 18.7 mV and 16.3 mV were observed as well for HL_3 and HL_4 as well, which strongly suggests that the LH_S may be classifed as mixed type inhibitor in both solutions, but with a predominantly cathodic effects in HCl (HL_1 and HL_2) and anodic effects in H_2SO_4 solution (HL_3 and HL_4).

Table 4.6: Polarization parameters for MS and CS in acidic solutions at 100 ppm for HL_1, HL_2, HL_3 and HL_4

Inhibitors	Concentration (ppm)	Substrate	Solution	- E_{corr} (mV vs. SCE)	Icorr ($mAcm^{-2}$)	η_P (%)
Blank	-	MS	HCl	0.894	543.05	-
HL_1	100 ppm	MS	HCl	0.101	37.13	93
HL_2	100 ppm	MS	HCl	0.953	47.01	91.3
Blank	-	CS	H_2SO_4	0.987	9.5	-
HL_3	100 ppm	CS	H_2SO_4	0.801	1.9	90.6
HL_4	100 ppm	CS	H_2SO_4	0.825	1	89.4

Fig. 4.47 and 4.48 represents the obtained polarization curves for the investigated Schiff bases, in the case of MS in 1 M HCl for HL_1 and HL_2, whereas on the other hand for CS in 1 M H_2SO_4 for HL_3 and HL_4 at the optimum inhibitor concentration of 100 ppm. Table 4.3 reveals that the values of inhibition efficiencies for all the Schiff bases (HLs) at the optimum concentration of 0.0004 M (100 ppm) are found that $HL_1 > HL_2$ for MS in HCl, whereas for CS in H_2SO_4 it was observed that $HL_3 > HL_4$ respectively.

The reason of highest inhibition efficiency in the case of HL_1 is the presence of hydroxyl group (-OH) and methoxy group ($-OCH_3$) having a strong electro donating group in their structure, however, occurance of nitro group ($-NO_2$) exhibit a lower inhibition efficiency in the case LH_2, leading to a strong deactivating group responsible for weak bind with metal surface.

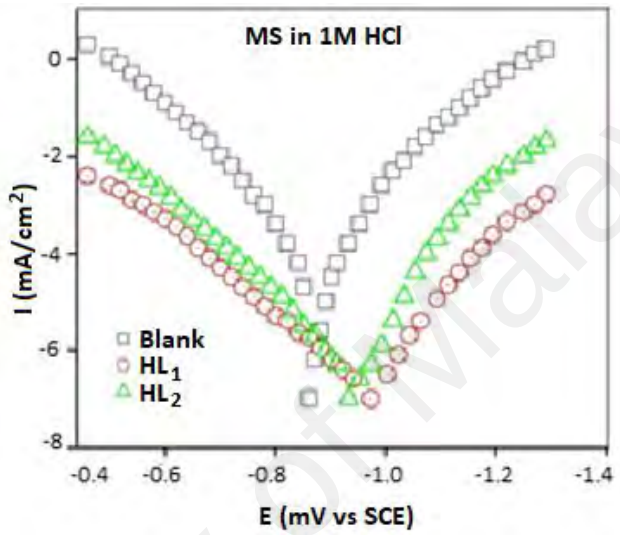

Figure 4.47: Polarization curves for MS in 1 M HCl at 100 ppm concentration for HL_1 and HL_2

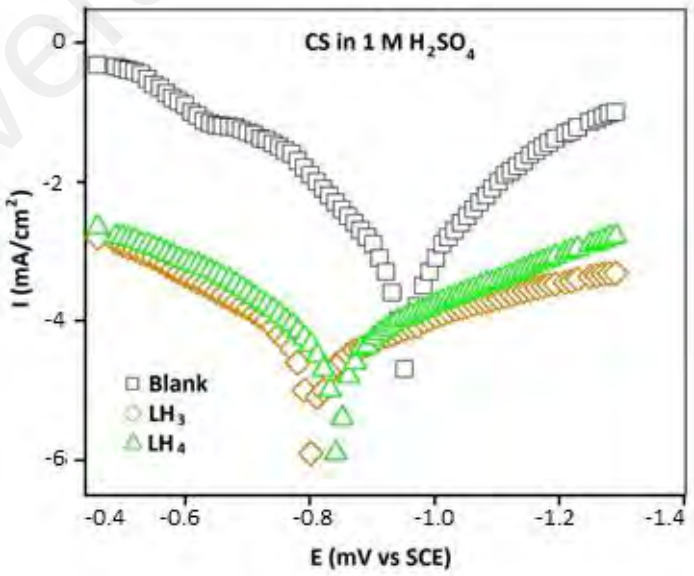

Figure 4.48: Polarization curves for MS in 1 M HCl at 100 ppm concentration for HL_3 and HL_4

4.12 Electrochemical Impedance Spectroscopy measurements

Fig. (4.49 - 4.52) displays the Nyquist plots presentation of mild steel and carbon steel in the absence and presence of additives in acidic solutions with different concentrations of the Schiff base compounds (HLs). It can be seen clearly from all figures, that the Nyquist plots show a single capacitive semicircle shape at higher frequencies in the presence and absence of inhibitors for only one time constant. This indicates that corrosion of both MS and CS in HCl and H_2SO_4 soultions are mainly controlled by charge transfer process (Rahim et al., 2008 & Ju et al, 2008). The deviation of the depressed Nyquist plots from ideal semicircle are genereally atttributed to the frequency dispersion of interfacial impedance which results as inhomogenities of the surface, impurities, adsorption of inhibitors as well as surface roughness and the formation of porous layers (Popova et al., 2003; Aljourani et al., 2009). It is usually found that the diameter of the semicricle as well as ploarization resistance (R_P) were increased with the increase in investigated Schiff bases inhibitos (HLs) concentration.

It is also evident that a maximum corrosion inhibition efficiency of 92% was found for inhibitor HL_1 for an optimum concnetration of 100 ppm (0.0004 M), by further increasing the inhibitor concnetration beyond the threshold values, no more further increase was occured and reamin almost the same as observed in the case of weight loss and Tafel polarization measurements. The values of polarization resistance (Rp), constant phase element (CPE) and inhibitor efficiency for various concnetration of inhibitor are tabulated in table 4.4.

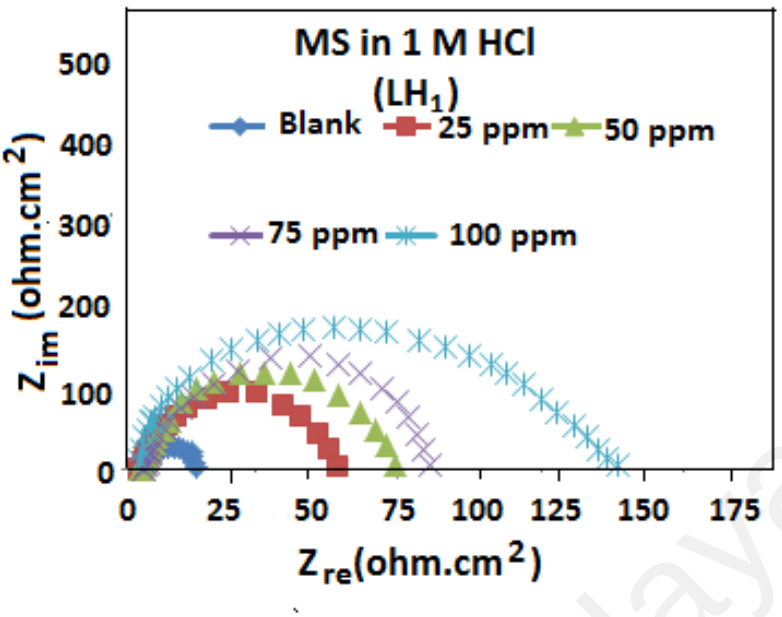

Figure 4.49: Nyquist plots of MS in 1 M HCl with various concnetrations of HL_1

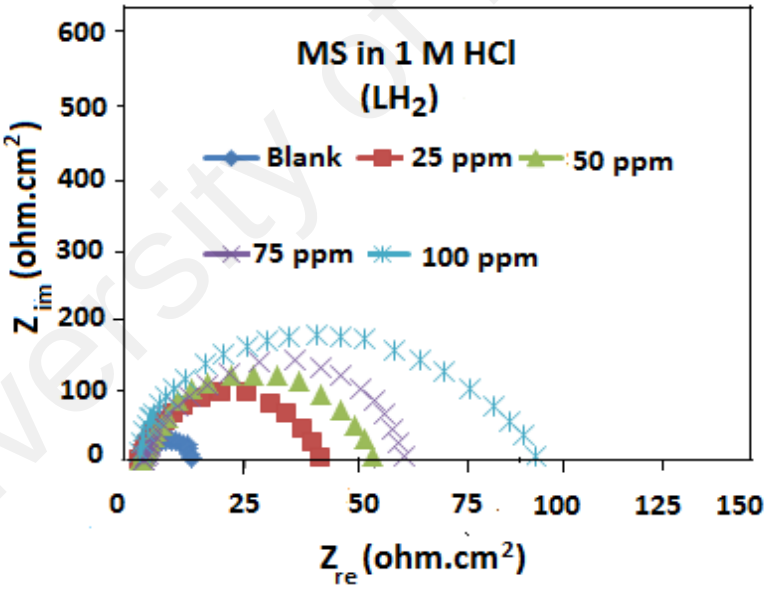

Figure 4.50: Nyquist plots of MS in 1 M HCl with various concnetrations of HL_2

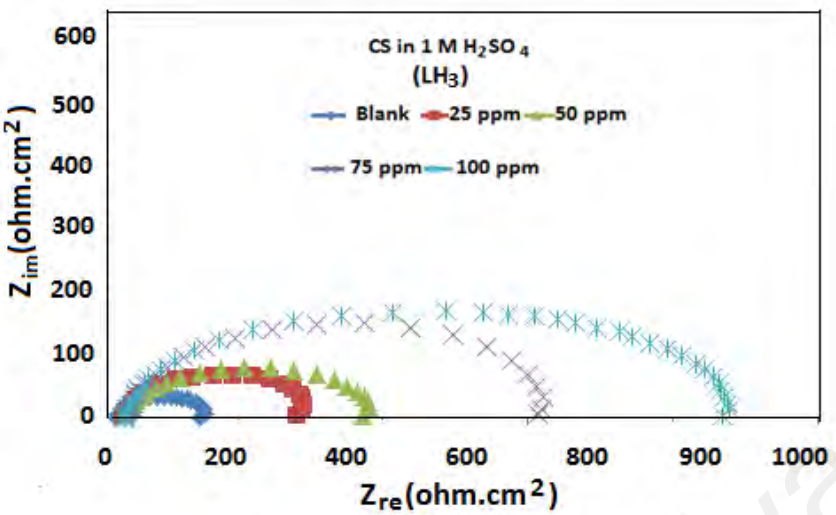

Figure 4.51: Nyquist plots of CS in 1 M H_2SO_4 with various concnetrations of HL_3

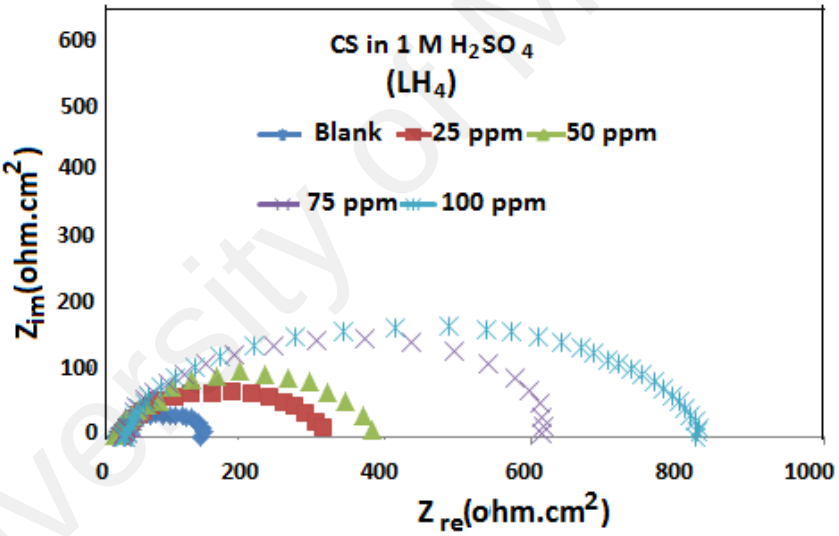

Figure 4.52: Nyquist plots of CS in 1 M H_2SO_4 with various concnetrations of HL_4

In Fig. (4.49 – 4.52) it can be observed that the diameter of the semi circle increases more with the addition of investigated Schiff bases to the aggressive solutions. The consequences are a net increase in polarization resitance (R_P) and alternative decrease in capacitance, which further increases the resistance to the flow of electroncs and providing more corrosion inhibition resistance. It can be inferred that the Schiff base inhibits corrosion of MS and CS in both 1 M of HCl and H_2SO_4 at all the

concentrations. It was reported that the inhibition efficiencies were increased as a result of adsorption of the inhibitor molecules on the metal surfaces.

Table 4.7: The EIS parameters for MS and CS in 1 M HCl and 1 M H_2SO_4 in uninhibited and inhibited solutions at different concentrations of HLs at ambient temperature

Inhibitors	**Concentration (ppm)**	**CPE(10^{-4}) (F)**	**n**	**R_P (Ω)**	**η_{EIS} (%)**
HL_1	Blank	7.89	0.87	11.63	-
	25	6.29	0.82	55.14	78
	50	5.81	0.66	58.97	80
	75	5.35	0.79	75.04	84
	100	4.73	0.69	153.68	92
HL_2	Blank	7.89	0.87	11.63	-
	25	5.8	0.68	31.94	67
	50	3.31	0.66	50.08	76
	75	3.11	0.65	61.17	80
	100	2.95	0.64	122.22	90
HL_3	Blank	2.07	0.87	107.28	-
	25	1.95	0.93	205.12	47
	50	1.34	1.02	310.76	65
	75	1.11	1.03	492.26	78
	100	0.89	1.06	955.05	89
HL_4	Blank	2.01	0.87	107.28	-
	25	1.55	0.93	198.42	46
	50	0.85	1.01	249.97	57
	75	0.81	1.02	424.88	75
	100	0.73	1.03	893.22	88

In table 4.7, EIS result shows that the Rp values increase and CPE values decrease with increasing of the Schiff base concentrations. The increase in Rp values can be attributed to the increase in adsorption of Schiff base consituents over the metal surfaces leading to the formation of a protective layer at metal/solution interface; which further inhibits the exchange of electrons between the metal surface and corrosive solution. On the other hand, the decrease in CPE with an increase in the inhibitor concentrations can result from a decrease in the local dielectric constant and/or an increase in the thickness of the double layer which results an increase in the inhibition efficiency. The change in CPE values was attributed to the gradual replacement of water molecules originally absorbed on the metal surface by the adsorption of inhibitor molecules on solid surface, therefore, it inhibits the degree of metal dissolution (Aljourani et al., 2009).

Fig. 4.53 shows the electrical equivalent circuit diagram to model liquid/solid interface which consists of a constant phase element (CPE), polarization resistance (Rp), solution resistacne (Rs), and n represents the phase shift which may be attributed to the surface inhomogenities (Oguzie et al., 2007 and Solmaz et al., 2011). CPE was used instead of double layer capacitance for getting a more appropriate fit to the experimental results (Quraishi& Sardar, 2001). In general, the CPE is required for the distribution of the relexation time, as a result of surface inhomogenities and (n) represents the degree of surface inhomogenity (Noor, 2009). The fitted parameters obtained were tabulated in table 4.4.

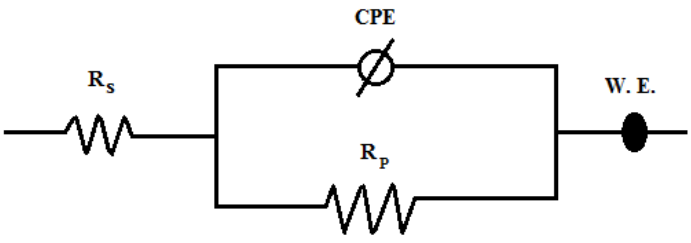

Figure 4.53: Equivalent circuit diagram to fit the EIS data for MS and Cs in both 1.0 M HCl and 1.0 M H_2SO_4

The analysis of the inhibition efficiency through EIS spectrum for all the four investigated Schiff bases (HLs) at different solution concentrations were tabulated earlier. The Nyquist plot for all the investigated inhibitors HL_1, HL_2, HL_3 and HL_4 at an optimum concentration of 100 ppm (0.0004 M) are given in Fig. 4.54 and 4.55.

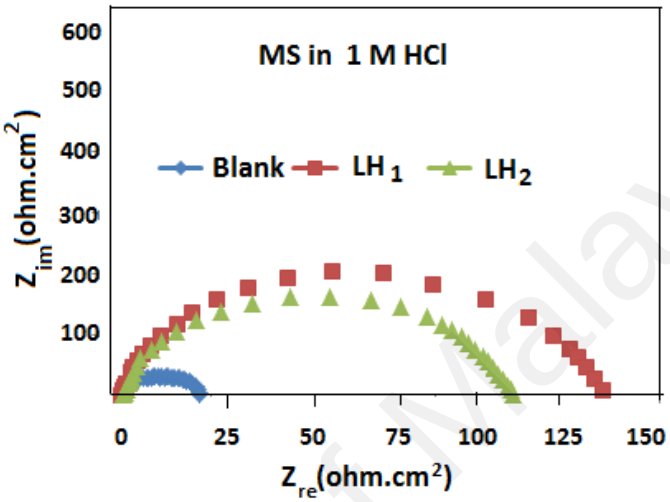

Figure 4.54: Nyquist plots of MS in 1 M HCl at 100 ppm concentration for HL_1 and HL_2

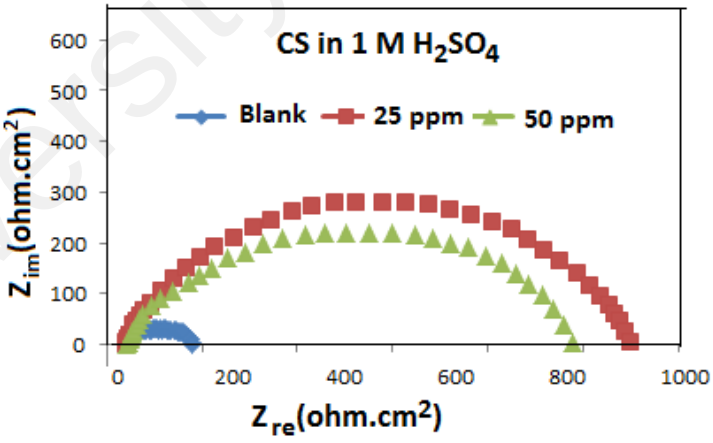

Figure 4.55: Nyquist plots of CS in 1 M H_2SO_4 at 100 ppm concentration for HL_3 and HL_4

The obtained impedance parameters for all the investigated inhibitors HL_1, HL_2, HL_3 and HL_4 at an optimum concentration of 100 ppm are labeled in table 4.8. For all these investigated inhibitors, the Nyquist plots were found to be compressed semicircle

having a single capacitive loop. The semicircle diameter and polarization resistance (R_P) were observed varying with their respective inhibition efficiency as well.

Table 4.8: Impedance parameters for MS and CS corrosion in acidic solutions with 100 ppm (0.0004 M) of HL_1, HL_2, HL_3 and HL_4 at ambient temperature

Inhibitors	Concentration (ppm)	Substrate	Solution	CPE (10^{-4}) (F)	n	R_P (Ω)	η_{RP} (%)
Blank	-	MS	HCl	7.89	0.87	11.63	-
HL_1	100 ppm	MS	HCl	4.73	0.69	153.68	92
HL_2	100 ppm	MS	HCl	2.95	0.64	122.22	90
Blank	-	CS	H_2SO_4	2.007	0.88	107.28	-
HL_3	100 ppm	CS	H_2SO_4	0.895	0.94	955.05	89
HL_4	100 ppm	CS	H_2SO_4	0.735	0.93	893.22	88

4.13 Adsorption isotherm analysis

Corrosion inhibition mechanism can be easily and deeply understood on the basis of nature of adsorption tendency of the organic compounds as corrosion inhibitor on the surface. The extend of surface coverage (θ) was derived from the results obtained from weight loss method for MS and CS in HCl and H_2SO_4 acidic solutions in the presence as well as the absence of evaluated Schiff bases at ambient temperature using equation (3.2) in chapter 3. The obtained values for surface coverage are presented in table 4.9. The achieved results were fitted to various adsorption isotherms as Langmuir, Temkin and Frumkin. The analysis of various adsorption isotherms like Temkin and Frumkin does not yield a satisfactory fitting role to the experimental data. However, in the case of Langmuir isotherm it was found to be the best fit for the adsorption of the investigated inhibitors (HLs). Langmuir adsorption isotherms plots for investigated

Schiff bases like HL_1, HL_2, HL_3 and HL_4 are shown graphically in figure 4.56 to 4.59 and respectively.

Table 4.9: Numerical values of surface coverage (θ) for investigated Schiff bases HL_1, HL_2, HL_3 and HL_4 calculated from weight loss measurements

Concentration (ppm)	Degree of surface coverage (θ)			
	HL_1	**HL_2**	**HL_3**	**HL_4**
25	0.55	0.37	0.48	0.44
50	0.78	0.65	0.63	0.58
75	0.88	0.8	0.81	0.75
100	0.94	0.89	0.9	0.88

The values of free f adsorption energy (ΔG_{ads}) for the corrosion of MS and CS in 1M HCl and H_2SO_4 in the presence of the considered Schiff bases were calculated using eq. (3.29) and presented in table 4.10.

Table 4.10: The free adsorption energy (ΔG_{ads}) for the corrosion of MS and CS in 1M HCl and H_2SO_4

Inhibitors	Concentration (ppm)	ΔG_{ads}	R^2
HL_1	100	-45.6	0.9985
HL_2	100	-34.03	0.9862
HL_3	100	-44.6	0.9947
HL_4	100	-33.32	0.9901

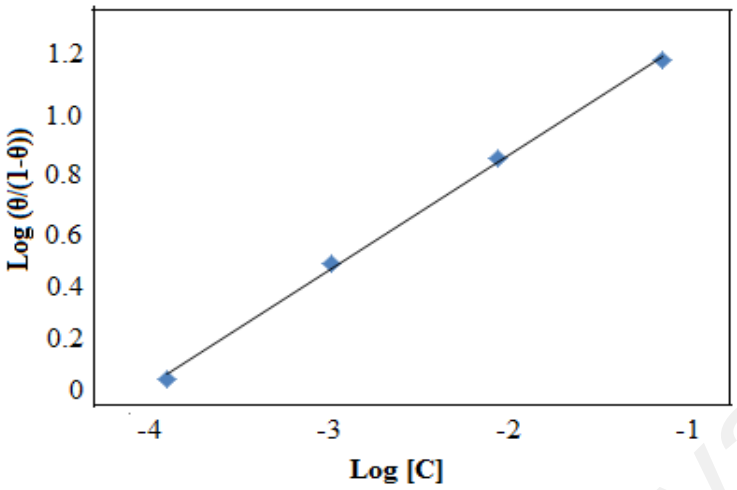

Figure 4.51: Langmuir adsorption isotherm for HL_1 on MS in 1 M HCl

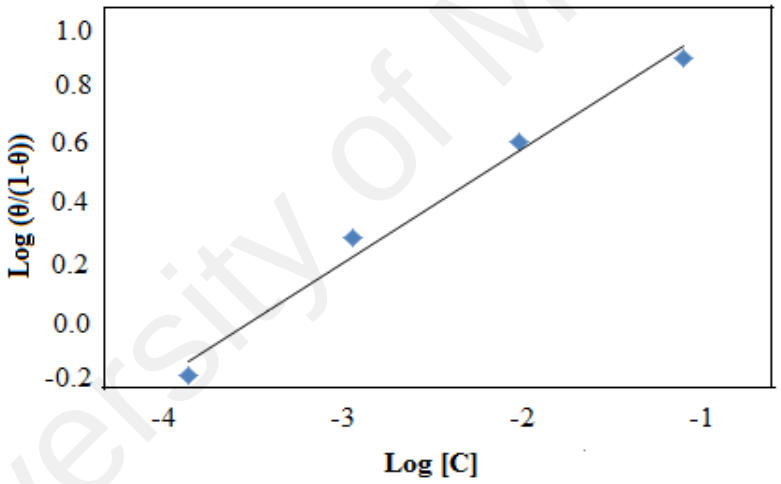

Figure 4.52: Langmuir adsorption isotherm for HL_2 on MS in 1 M HCl

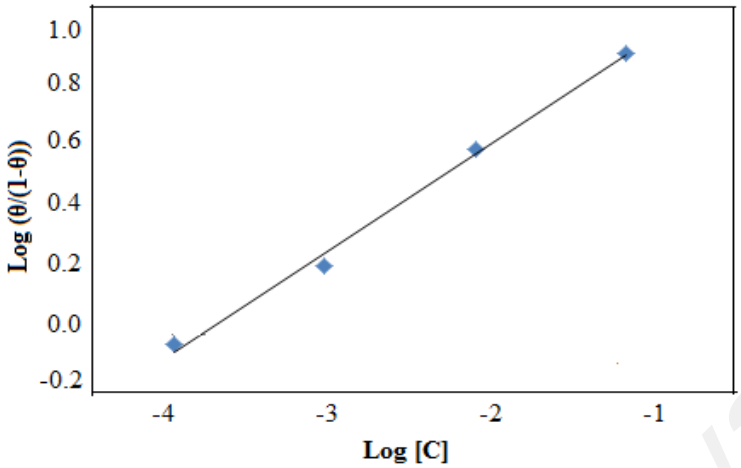

Figure 4.53: Langmuir adsorption isotherm for HL_3 on CS in 1 M H_2SO_4

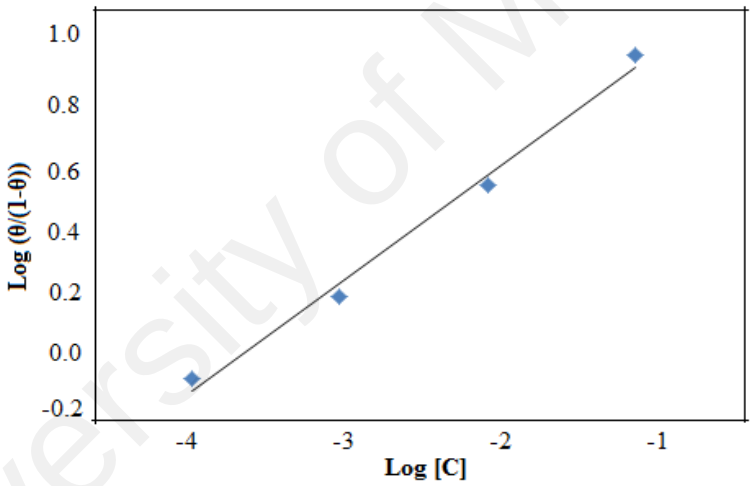

Figure 4.54: Langmuir adsorption isotherm for HL_4 on CS in 1 M H_2SO_4

It has been found that the adsorption of the Schiff bases in all the cases was found to obey Langmuir adsorption isotherm. However, there are some deviations observed from ideal Langmuir adsorption isotherm. This deviation from the ideal may be hypothesized that there are no interaction between the adsorbed molecules and the surface, but this assumption in the case of organic molecules do not appear to be true, because there are the adsorption of polar atoms on the anodic and cathodic active sites of metal surfaces.

But the behaviour of adsorbed species may be due to the mutual interaction of attraction or repulsion (Bansiwal et al., 2000).

The thermodynamic parameters provide useful information regarding the type of adsorption involved. From table 4.7, the obtained value of ΔG_{ads} for the investigated Schiff bases HL_1, HL_2, HL_3 and HL_4 for the corrosion of MS and CS in 1 M HCl and 1 M H_2SO_4 are – 45.6, - 34.03, - 44.6 and - 33.32 $kJmol^{-1}$ respectively. It is generally accepted that the values of ΔG_{ads} around -20 $kJmol^{-1}$ or less are consistent with a physical adsorption process (an electrostatic interaction between the charged inhibitor and the charged metal surface), while those around -40 $kJmol^{-1}$ or higher is associated with a chemical adsorption process (involves the transfer or sharing of electrons between the inhibitor molecules and the metal surface, resulting in a coordinated covalent bond) (Abdallah, 2002). These results reveal that the adsorption process of the investigated inhibitors on MS and CS surfaces are chemisorption for HL_1 and HL_3, whereas for HL_2 and HL_4 comprise a composite combination of both physisorption and chemisorption indicating a strong adsorption due to the charges sharing between SBs molecules and the surrounding CS surface. The low negative value of the free energy of adsorption indicates a spontaneous adsorption process and strong interaction between the Schiff base molecules and MS and CS surfaces (Bayol et al, 2008 & Elachouri et al., 1996).

The percentage inhibition efficiencies resulted from weight loss, polarization and EIS measurements were compared and summarized in table 4.8. The percentage inhibition efficiencies were found following almost the similar trends of enhancement in inhibition efficiency with raising inhibitor concentration and observed the tendency of becoming closer to each other.

Table 4.11: Percentage inhibition efficiency achieved for MS and CS in 1 M HCl and 1 M H_2SO_4 by weight loss, polarization and EIS techniques

Inhibitors	Concentration (ppm)	η_{WL} (%)	η_P (%)	η_{RP} (%)
HL_1	25	55	86	78
	50	78	88	80
	75	88	90	84
	100	94	93	92
HL_2	25	37	81	67
	50	65	87	76
	75	80	89	80
	100	89	91	90
HL_3	25	48	49	47
	50	63	62	65
	75	81	80	78
	100	90	92	89
HL_4	25	44	45	46
	50	58	57	57
	75	75	77	75
	100	88	89	88

The inhibition efficiencies of the Schiff bases towards MS and CS in both HCl and H_2SO_4 are due to the presence of the azomethine group (–C=N-), the existence of electron cloud in aromatic ring and due to the presence of atoms like sulphur, nitrogen and oxygen in the molecules.In addition, the adsorptions of Schiff bases are strongly dependent on the donation of lone pair electrons of oxygen atom present in carboxyl

group and sulphur atom in C=S group as well as nitrogen atoms to the MS and CS surfaces. Moreover, the degree of the percentage inhibition is mainly attributed to the electron density as well as the molecular size of active groups and atoms (Fouda et al. 1995).

The synthesized Schiff bases (HLs) are found to be efficient and excellent corrosion inhibitors for MS and CS in both HCl and H_2SO_4 mediums. Among all the investigated Schiff bases HL1 was the best one due to its maximum inhibition efficiency. The higher efficiency of synthesized Schiff bases are mainly due to the occurrence of azomethine group as well as atoms like oxygen or sulphur and nitrogen atoms in the synthesized Schiff bases.

The application of organic compounds for corrosion and fouling mitigation in process industries play a vital role for metal selection as well we enhancing the efficiency of heat transfer equipements including heat exchangers, chillers etc. There are different ways in order to prolong the service life and the protection of heat trenasfer equipements. As for as the application of Gelatin as anti-fouling addtives are the most promising way for the fouling mitigation. In this section, the data recorded during the present research work has been discussed and analyzed in detail. This data cover the effects of operating parameters like time period, concentration of fouling solution and fouling mitigation additives, operating temperature, different metals and scale formation of calcium sulphate. On the top of this, effect of organic antifouling additive like Gelatin gel on fouling mitigation is being incorporated.

For the present work, the fouling resistance R_f, was determined as a function of the bulk velocity, bulk to surface temperature difference ΔT and concentration of $CaSO_4.2H_2O$ solution to study the fouling behaviour of aqueous $CaSO_4$ solution. $R_f$was also determined as a function of additive concentration to study the fouling mitigation and obtain effective optimum concentrations of additives for efficient fouling mitigation.

4.14 Fouling study of calcium sulphate

The effect of duration time, various temperature, different materials and concentrations on fouling deposition of calcium sulphate test solution has incorporated in this section.

4.14.1 Effect of different materials

As discussed earlier, fouling is a time dependent process; hence various experimental runs were carried out at different intervals of time parameters as stated in table 4.12.

Table 4.12: Input parameters in investigation of different materials

Input Temperature	50 °C
Materials	SS 316L, Al, Cu, Brass
$CaSO_4.2H_2O$ solution concentration	4.0 g/L
pH	8.0

At the end of each run, the weights of the deposit were obtained simultaneously. The obtained data from these runs have been plotted in Fig. 4.60. From Fig. 4.60, it is clear that, the thermal conductivity of the materials play a vital role in inflecting the deposition rate. Materials having higher thermal conductivity lead the higher rate of deposition weight.

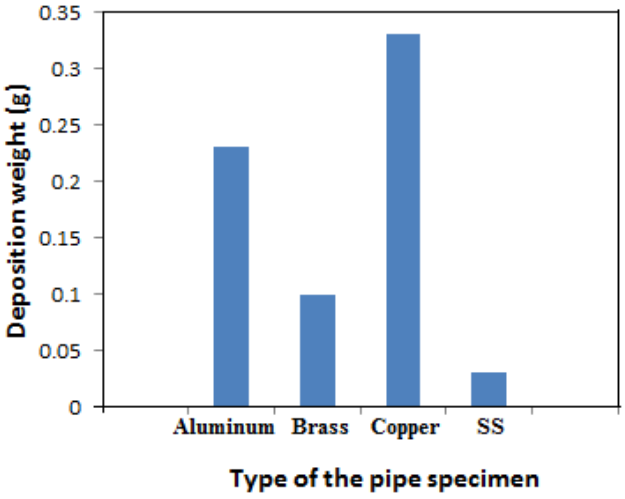

Figure 4.60: Deposition weight versus type of different materials as a function of their thermal conductivity

4.14.2 Effect of time duration

It is well known phenomenon that fouling is a time dependent process, therefore, in this experiment; various runs were carried out at different time intervals, whereas other parameters were kept constant as shown in table 4.13.

Table 4.13: Input parameters on the effect of time duration

Input temperature	50 ^{o}C
Materials	SS 316 L
$CaSO_4$. $2H_2O$ solution concentration	4.0 g/L
pH	8.0
Duration time	300 hours

At the end of each experimental run, the weight of calcium sulphate deposit was obtained. The obtained data were plotted in fig. 4.61. The obtained data reveals that the weight of the deposit gradually increases with the increase of time duration until it reaches to a steady state condition at the time period of 300 hours.

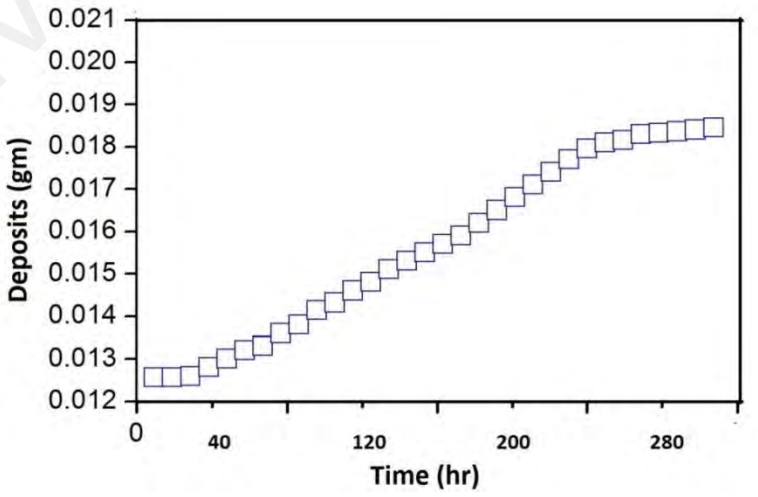

Figure 4.61: Deposition as a function of time for concentrations 4.0 g/l of $CaSO_4$. Experiments were performed at velocity 0.3 m/s, bulk temperature 35 ^{o}C and surface to bulk temperature difference 15 ^{o}C

The obtained fouling curve follow the same asymptotic behaviour as previously mentioned in the literature review (Fig. 2.15) and generally known as asymptotic curve. The fouling resistance R_f, was calculated from the weight of the fouling deposition using the following equation 4.1 (kern and Seaton 1959a):

$$R_f = \frac{ln\left({D_f}/{D_o}\right)}{2\pi L k_f} \qquad (4.1)$$

and

$$W = \left[\frac{\pi}{4}\left({D_f}^2 - {D_o}^2\right) * L\right] * \rho_f \qquad (4.2)$$

Where,

D_f= Average diameter of the fouled tube (to be calculated), m

D_o = External metallic tube diameter, m

L = length of the tube

K_f = Thermal conductivity of the fouling deposited salt, W/m.^{0}C

ρ_f = Density of the fouling deposit, Kg/m^3

W= weight of the fouling deposit measured during experimental run, gm.

The trend of asymptotic fouling behaviour reached to a maximum and became steady state values only when the deposition rate of fouling was equal to the removal rate (Bott, 1995).

The expression described the asymptotic fouling can be measured using the following equation 4.3 (Kern and Seaton, 1959a):

$$R_f = R^*_f \left[1 - exp\left(-\frac{t}{t_o}\right)\right] \quad (4.3)$$

Where,

R^*_f = Asymptotic fouling resistance

t = Duration time of deposit

t_o = time constant

The experiments were carried out with calcium sulphate concentrations of 4.0g/L. The concentration was chosen to ensure a measurable fouling deposit occurred within a reasonable time [69]. The present experimental results are presented in Figure 4.62 where experimental parameters were maintained at ΔT 15 ºC, bulk temperature 35 ºC and flow velocity of 0.3 m/s. A considerably lower fouling resistance is observed at the low concentration below 4.0 g/L, due to the fact that the driving force for deposition is proportional to the square of the difference between the bulk and the saturation concentrations (Middis, 1994). At higher concentrations, 4.0 g/L, fouling resistance increases significantly. Thus in general, fouling resistances increases with the increase of reagents concentration in the solution. Similar observations were reported by other researchers (Krause, 1993; Augustin, 1992). After a certain interval of time (4.3 x 10^3 minutes of exposure), the maximum values of R_f at concentrations of 4.0 g/L was observed around 0.8 x 10^{-3} m^2.K/kW.

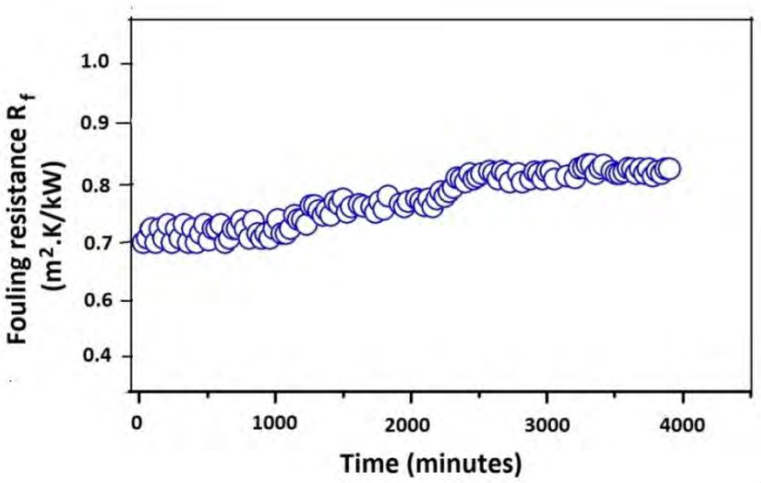

Figure 4.62: Fouling resistance as a function of time for concentrations 4.0 g/l of $CaSO_4$. Experiments were performed at velocity 0.3 m/s, bulk temperature 35 ^oC and surface to bulk temperature difference 15 ^oC

Figure 4.62, represents the corresponding heat transfer coefficient h_C at the same experimental observations as in Fig. 4.61. Heat transfer coefficient changes with the change in deposition on the fouling surface. Similar responses on h_C in opposite way are observed corresponding to certain change in R_f. Thus in either way, both h_C and R_f could be used to represent fouling behaviour.

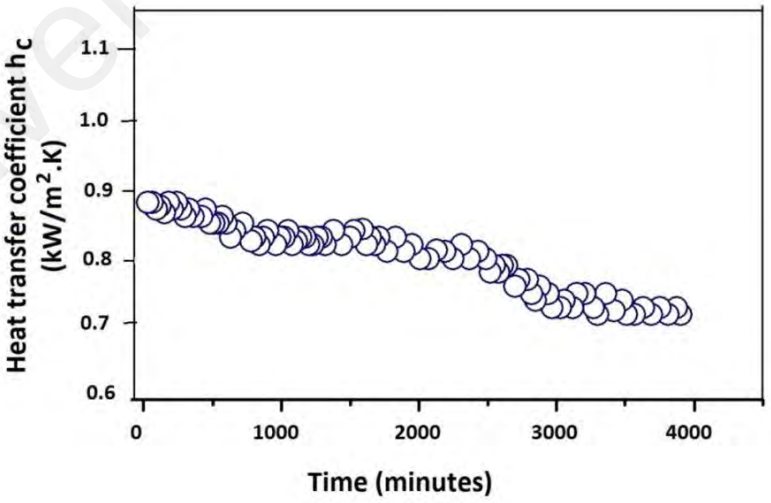

Figure 4.62: Heat transfer coefficient and fouling resistance as a function of time for different concentrations of $CaSO_4$. Experiments were performed at velocity 0.3 m/s, bulk temperature 35 ^oC and ΔT 15^oC

4.15 SEM and XRD analysis of the deposited samples

Scanning electron microscope (SEM) and X-ray diffraction (XRD) analyses were carried out at the end of each experimental test runs for all the deposited samples both in the absence and presence of additives at different concentrations. The results obtained for without additive and in the presence of additive at different concentration in calcium sulphate dihydrate solution are shown in Fig. 4.63.

Figure 4.63 reveals that, a regular needle-like shape crystal with a smooth and compact surface has been found for the calcium sulphate dihydrate crystal deposits in the absence of additives. Whereas, the presence of additive with different concentrations the shape of the deposit were observed to be irregular shape with a rough and loose surface as shown in Fig. 4.64 to 4.67.

On the basis of "dynamic theory of crystal growth", the absorbance of tiny foreign materials or scale inhibitors, leading an abnormal growth of crystals according to the arrangement of crystal lattice structure. Therefore, increasing a twist or internal stress of the larger deposit of crystals, leading to the fracture in the deposited crystals thus resulting the objective of scale inhibition. Similar results were found by some other researchers as well (Kazi et al, 2012; Krause, 1993).

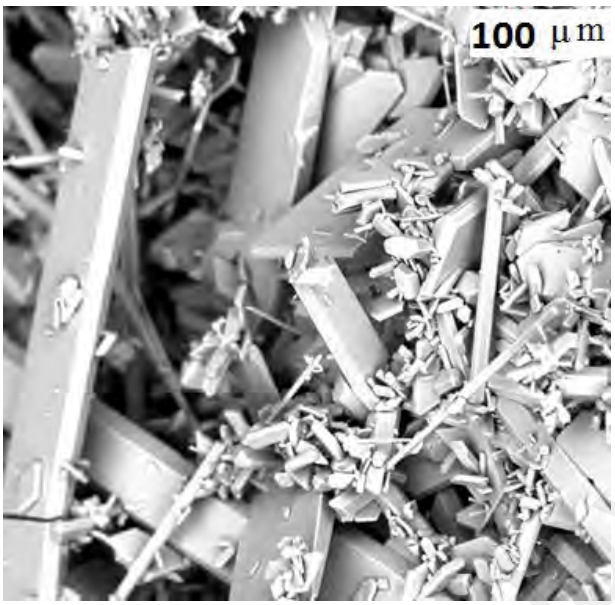

Figure 4.63: SEM image of deposited crystal samples on heat transfer surface without additive. The experiment was performed at ΔT 15ºC, bulk temperature 35 ºC, $CaSO_4$ concentration 4.0 g/L and solution flow velocity 0.3 m/s

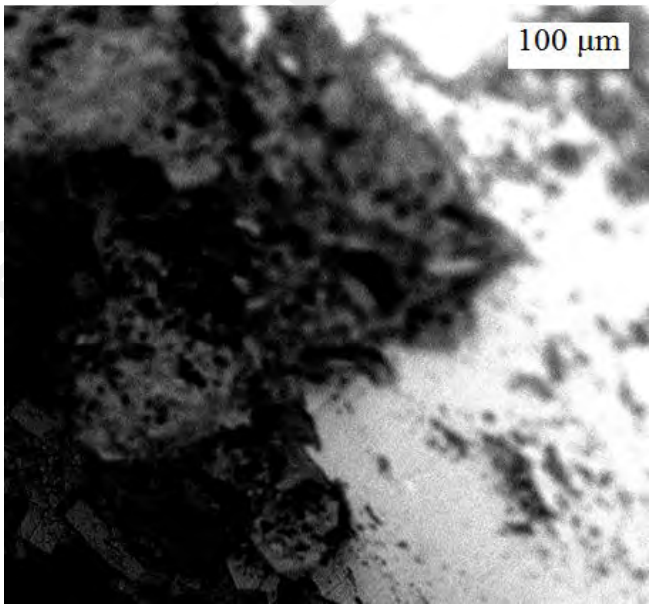

Figure 4.64: SEM image of deposited crystal samples on heat transfer surface with the presence of additive (0.06 g/L). The experiment was performed at ΔT 15ºC, bulk temperature 35 ºC, $CaSO_4$ concentration 4.0 g/L and solution flow velocity 0.3 m/s

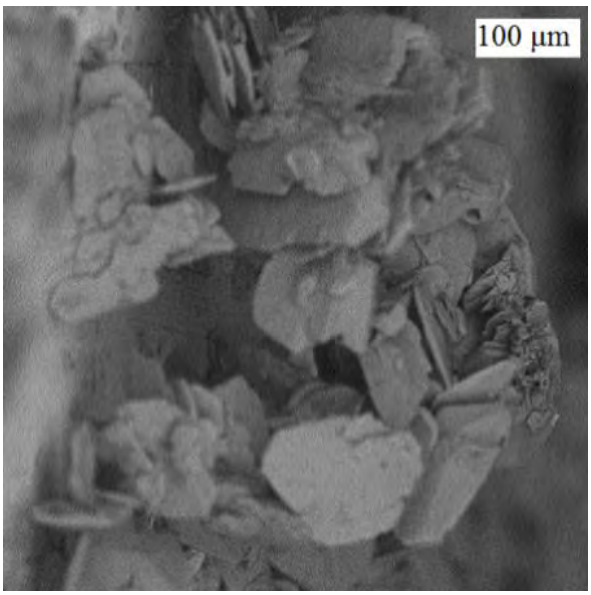

Figure 4.65: SEM image of deposited crystal samples on heat transfer surface with the presence of additive (0.125 g/L). The experiment was performed at ΔT 15ºC, bulk temperature 35 ºC, $CaSO_4$ concentration 4.0 g/L and solution flowvelocity 0.3 m/s

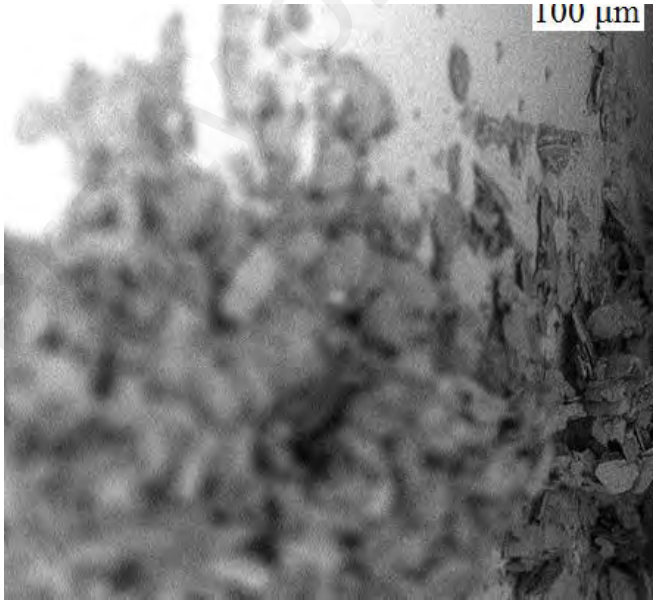

Figure 4.66: SEM image of deposited crystal samples on heat transfer surface with the presence of additive (0.25 g/L). The experiment was performed at ΔT 15ºC, bulk temperature 35 ºC, $CaSO_4$ concentration 4.0 g/L and solution flow velocity 0.3 m/s

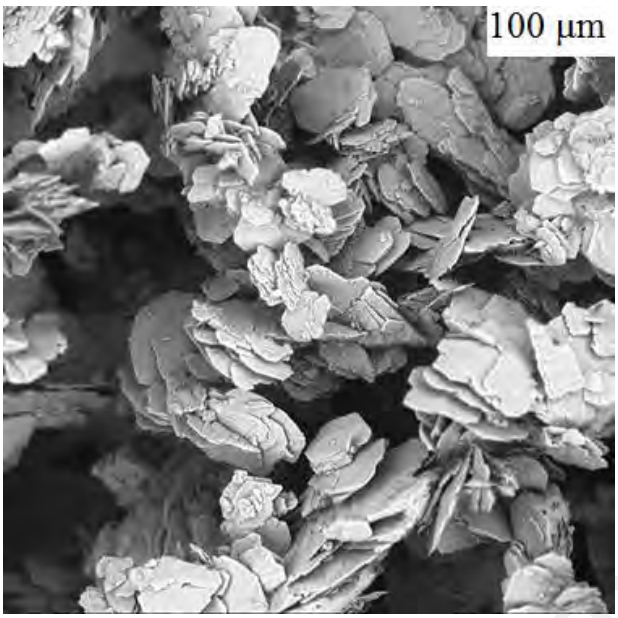

Figure 4.67: SEM image of deposited crystal samples on heat transfer surface with the presence of additive (0.5 g/L). The experiment was performed at ΔT 15ºC, bulk temperature 35 ºC, $CaSO_4$ concentration 4.0 g/L and solution flow velocity 0.3 m/s

Figures 4.68 and 4.69 represents XRD of the fouling surface with no additive and with the presence of fouling additive (Gelatin 0.5 g/L) for $CaSO_4$ deposit run at 0.3 m/s at the same experimental conditions, ΔT 15ºC, bulk temperature 35 ºC and $CaSO_4$ concentration of 4.0 g/L.

It is obvious from the figures that crystals in the blank solution are clearly different from the solution containing Gelatin inhibitor. In Fig. 4.68, it is evident that the diffraction peaks of 11.66º, 20.78º, 23.45º and 29.11º for calcium sulfate dihydrate crystal are very strong, which are the distinctive peaks of calcium sulfate dihydrate crystals. On other hand in Fig. 4.69, the addition of Gelatin inhibitor, diffraction peaks of calcium sulfate dihydrate does not change, however, the relative peak intensities have been changed significantly. The change in diffraction peaks demonstrate that, after the addition of Gelatin inhibitor, a changes in the form and structure of calcium sulfate dihydrate crystal has been occurred, leading to reduction in the degree of crystallinity as well as damaging the crystal structure of calcium sulfate dihydrate. Moreover, this damage leading to loosen in structure of calcium sulfate dihydrate and avoids the dense layer of

fouling on surface, therefore, successively preventing the rate of deposition. The results show that the deposit consists mostly of calcium and sulphur. All the peaks match those of pure gypsum. The absence of a sodium peak indicates that there is no soluble by-product ($NaNO_3$) present in the sample. It confirms that calcium sulphate was present as dihydrate $CaSO_4.2H_2O$ only.

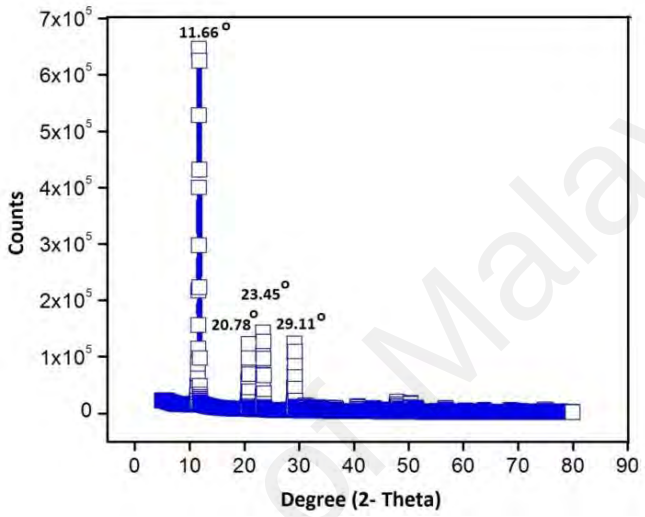

Figure 4.68: X-Ray diffraction pattern (XRD) of deposited samples of $CaSO_4$ without Gelatin additive. The experiments were performed at ΔT 15ºC, bulk temperature 35 ºC and $CaSO_4$ concentration of 4.0 g/L

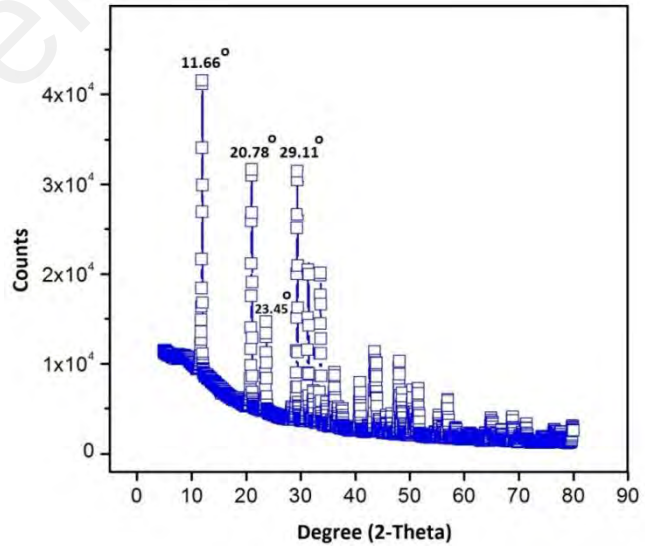

Figure 4.69: X-Ray diffraction pattern (XRD) of deposited samples of $CaSO_4$ with Gelatin additive concentration of 0.5 g/L. The experiments were performed at ΔT 15ºC, bulk temperature 35 ºC and $CaSO_4$ concentration of 4.0 g/L

4.16 Concentration effect of $CaSO_4$ in solution

Some experiments were performed to study the solution concentration level effect on calcium sulphate deposition rate and finally a concentration of 4.0 g/L was selected and considered. The other parameters were kept constant during the experimental runs as described in table 4.14.

Table 4.14: Input parameters on the effect of additive concentration

Parameters	**Range**
Hot water Inlet temperature	50 ^oC
Cold solution Inlet temperature	35 ^oC
Materials	SS 316L
$CaSO_4$ Concentration	4.0 g/L
pH	8
Duration time	72 hours
Hot water flow	6.2 Lit/m
cold solution flow	11.5 Lit/m

Figure 4.70 represents the general photographic view of fouling deposition on the SS 316 pipe heat transfer surface at $CaSO_4$ concentration of 4.0 g/L. From Figures 4.70 (a) and 4.70 (b), it is observed that a relatively higher deposition on surface could be obtained at higher solution concentrations. The objective of the clean surface provides a reference to the fouled deposited surfaces for a better visual comparison as shown in figure 4.66 (a,b).

Figure 4.70: Clean heat transfer surface of SS 316 L before and after the deposition of $CaSO_4$

In metastable saturated solution the immersion of SS 316 L heat exchanger surface, the amount of gypsum formed at the surface was measured by withdrawing the solution sample after a period of 6 hours by the EDTA titration method for analyzing Ca^{2+} ions. The deposited amount at the investigated surface is plotted as a function of time and illustrated in figure 4.70. From the Fig. 4.71 it show that the amount of gypsum deposition on heat transfer surface increases with time, leading a considerable decrease in the values of h_C. This reveals the loss in thermal effectiveness of the investigated heat exchanger.

In Fig. 4.71, it is clear that the trend for deposition slope significantly decreasing when the additive concentration has been increased. By adding 0.06, 0.125, 0.25 and 0.5 g/L of additive separately to the fouling saturated calcium sulphate solution, the fouling deposition were reduced by 60 %, 75 %, 81 % and 90 % after time interval of 72 hours.

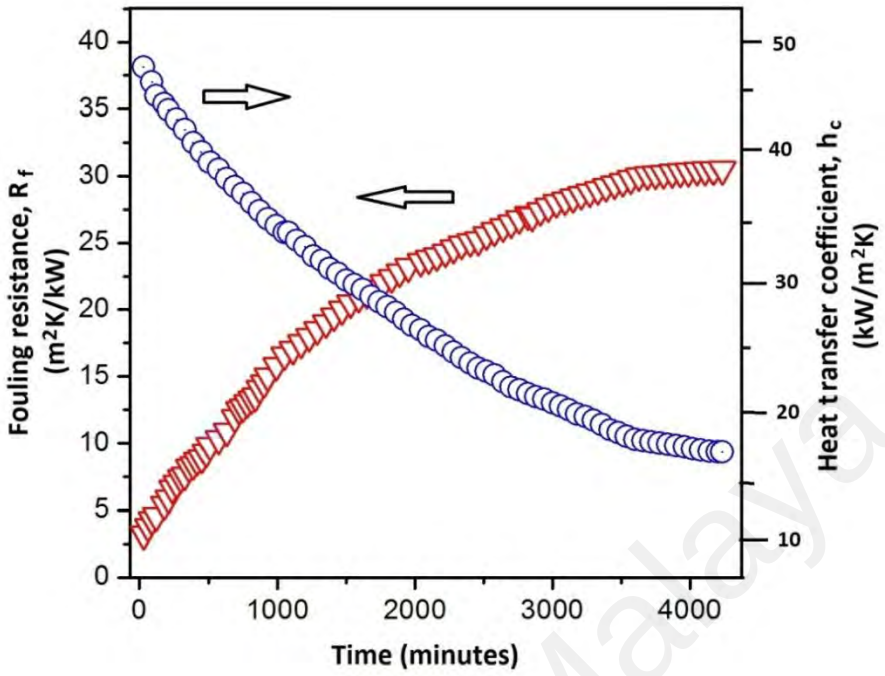

Figure 4.71: Heat transfer coefficient and fouling resistance as a function of time at velocity of 0.3 m/s. Experiments were performed at bulk temperature 35 ^oC, ΔT 15 ^oC and $CaSO_4$ concentration 4.0 g/L

4.16.1 Effect of Gelatine concentration on fouling resistance

Effect of green antifouling additives like Gelatine a plant extract has been studied and discussed in this section**.** The proper utilization of antifouling agents particularly reduces the scale formation of calcium sulphate on heat transfer surfaces. A number of additives have been used as effective fouling mitigation agents in $CaSO_4.2H_2O$ solutions for the purpose of mitigating heat transfer fouling on different heat transfer surfaces (Zahid, 1989; Kazi, 2012).

In this section, four different Gelatin concentrations have been employed to study the fouling resistance and heat transfer coefficient in order to compare and analyze the optimum additive concentration for fouling mitigation. All parameters were kept constant except the different concentrations of additive as mentioned in table 4.15.

Table 4.15: Input parameters on the effect of additive concentration

Gelatin concentration	0.06 g/L, 0.125 g/L, 0. 25 g/L, 0.5 g/L
Hot water Inlet temperature	50 ^{o}C
Cold solution Inlet temperature	35 ^{o}C
Materials	SS 316L
$CaSO_4$ Concentration	4.0 g/L
pH	8
Duration time	72 hours
Hot water flow	6.2 Lit/m
Cold solution flow	11.5 Lit/min

Figure 4.72, represents the fouling resistance R_f as a function of deposition time for SS 316 L surface at different Gelatin concentrations in the fouling solution. It is observed that, the values of fouling resistances R_f a bit below the datum level (zero level) at the initial stage while the corresponding increases in Gelatin concentrations were found to be decreased at additive concentration level of above 0.125 g/L.

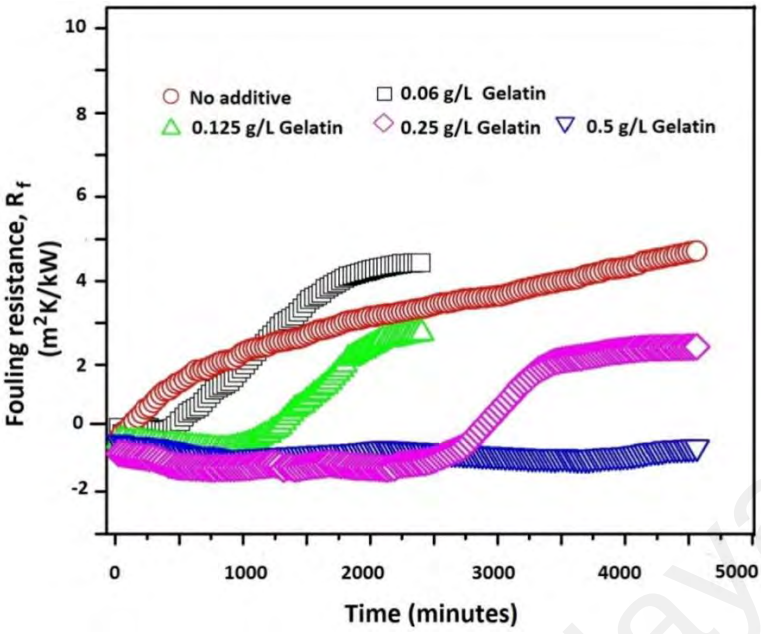

Figure 4.72: Fouling resistance as a function of time for Gelatine at different concentrations. Experiments were performed at bulk temperature 35 ^oC, ΔT 15 ^oC, $CaSO_4$ concentration 4.0 g/L and at velocity of 0.3 m/s.

A plot of fouling resistance as a function of time is presented in fig. 4.69 for different concentrations of Gelatine additive in the fouling solution. It can be observed that the induction time is always greater with additive present than for the solution alone. Induction time generally increases with increasing additive concentration. At the end of the induction period the initial rates of change in R_f are different and depends on the additive concentrations. However, the slopes of the curves are approximately the same from the end of the induction periods before the asymptotic levels are reached.

In fouling solution containing calcium sulphate dihydrate and Gelatin scaling inhibitor the Gelatin molecules are absorbed at the points where crystal grow, therefore, inhibiting crystal growth rate and maintaining the solution in temporary steady state condition. However, in the induction period, definite amounts of growth of the crystal faces are formed in the absence of inhibitor containing solution.

With inhibitor in solution the inhibitor molecules initially absorbs on the active sites, and surrounding the inhibitors crystal grows in such a critical situation, crystal growth continuously but at a poor rate. In such a situation, the crystal structure was distorted

and further addition of the inhibitors, the morphology of the initially formed crystals modifies with a distorted lattice.

Fig. 4.73 to 4.75 show surface morphology of calcium sulphate dihydrate deposits on heat transfer surface SS 316 L without and with different Gelatin concentrations.

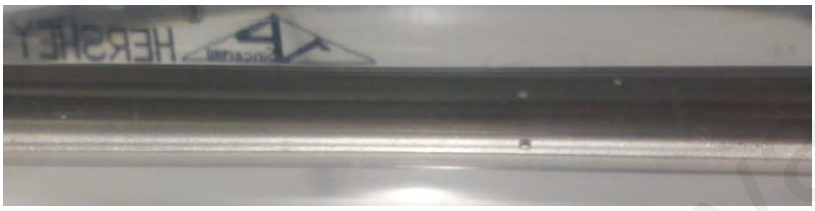

Figure 4.73: Heat transfer surface before commencement of CaSO4 fouling. The experiment was performed at ΔT 15ºC, bulk temperature 35 ºC, $CaSO_4$ concentration 4.0 g/L and solution flow velocity 0.3 m/s

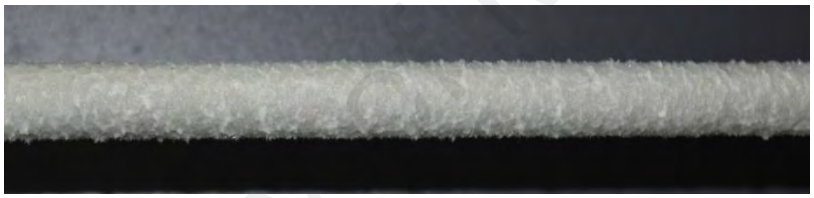

Figure 4.74: Fouling deposition of $CaSO_4$ on heat transfer surface. The experiment was performed at ΔT 15ºC, bulk temperature 35 ºC, $CaSO_4$ concentration 4.0 g/L and solution flow velocity 0.3 m/s

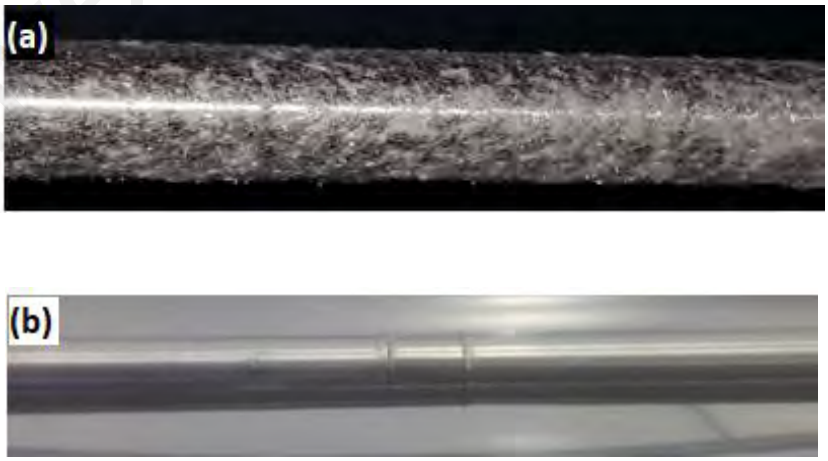

Figure 4.75: Fouling deposition of CaSO4 on heat transfer surface with 0.06 g/L and 0.5 g/L Gelatin. The experiment was performed at ΔT 15ºC, bulk temperature 35 ºC, $CaSO_4$ concentration 4.0 g/L and solution flow velocity 0.3 m/s

4.17 Effect of Gelatine concentration on fouling resistance

A series of different concentrations of Gelatin additive was prepared ranging from 0.03 g/L 0.06 g/L, 0.12 g/L, 0.25 g/L and 0.5 g/L under the same experimental conditions. Fig. 4.76 shows the view of metal surface under the same experimental conditions without any additives in fouling solution before the commencement of fouling. Fig 4.74, demonstrates the capability of Gelatin under the identical conditions, it is evident that by increasing Gelatin concentration the inhibition rate for calcium sulfate dihydrate prominently increased. Increasing the Gelatin concentration from 0.03 to 0.4 g/L, the corresponding calcium sulfate dihydrate inhibition rate increases rapidly, at 0.03 g/L the scale inhibition rate is 50%, but it increases suddenly up to 87 % at a concentration of 0.4 g/L.

Beyond this concentration level, the slope of the curve increases as well, but at a slow rate from a concentration of 0.4 g/L to 0.6 g/L, where the inhibition efficiency approaches to 87.5 % at 0.4 g/L and 90.2% at 0.6 g/L. The 0.5 g/L was selected as the optimum mass concentration for Gelatin in order to inhibit calcium sulfate dihydrate scale.

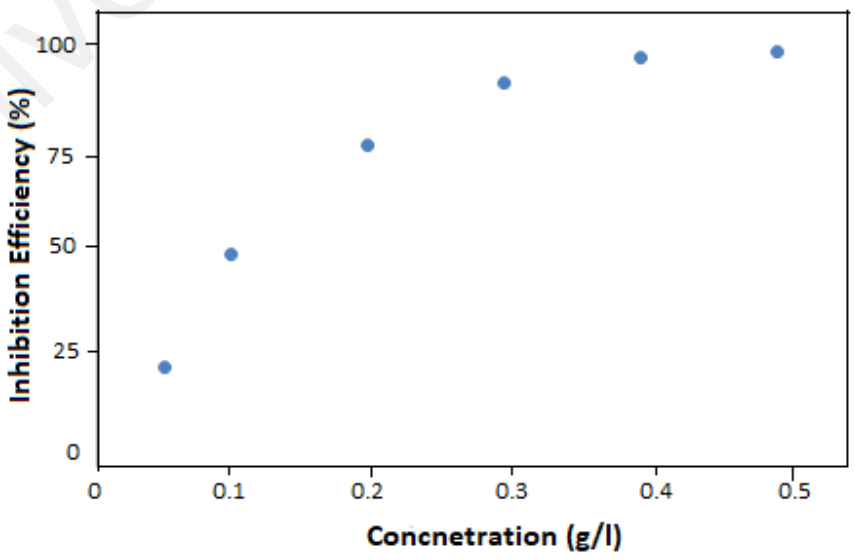

Figure 4.76: The influence of Gelatin on the calcium sulphate dihydrate scaling inhibition efficiency

CHAPTER 5: CONCLUSIONS

The achievements of the present work were to investigate the heat and momentum transfer of wood fiber (Acacia mangium and Acacia mangium hybrid) suspensions in closed conduit flow. Followings are the conclusions which could be drawn from the investigation.

1. Fiber concentration and velocity have great influences on both the heat transfer coefficient h_C and pressure drop $\Delta P/m$ of fiber suspensions flow in pipe.

2. Presence of a small quantity (0.2 wt.%) of wood fibers in water flowing through a heated pipe resulted enhancement in heat transfer. These enhancements in the values of *hc* at a domain of pulp the flow velocity from 1 m/s and continues up to the end of the investigated range of velocity. The maximum increase in h_C observed mostly at the maximum velocity and in the present case it is 3.6 m/s. At higher fibre concentration in suspension such as 0.4 wt. % and 0.6 wt.%, the values of $h_c$were observed decreasing below water values.

3. It is usually found that at low degree of beating i.e 2000 degree, both (Acacia mangium and Acacia mangium hybrid) do not significantly affect *hc* values throughout the velocity range, whereas, by the increase in beating degree (4000 and 8000 degree) it would like to reduce the *hc* values in a regular pattern.

4. The *hc* values obtained from the same species of fibers at the concentrations of 0.6 wt. % and 1.2 m/s correlated well with fiber length, flexibility ratio and slenderness ratio. The results have shown that the *hc* values would be decreased by a decrease in fiber length and fiber slenderness ratio or increase in flexibility ratio which confirm the findings obtained in the previous conclusion.

5. An approximate linear relationship between *hc* values and fiber/paper properties (from a specific wood fiber species) has shown that the specific fiber and paper properties could be predicted by monitoring heat transfer data.

6. Efforts for correlating the h_C values with fiber and paper properties obtained from different species of fibers were not successful. This reveals that $h_C$or pressure loss data obtained from a specific fiber species cannot be used as an indicator for pulp and paper quality from other fiber species.

7. Pressure drop versus velocity curves for wood fibers are similar in nature comparing to those reported previously by various researchers for different sources of wood fibers.

8. In the current research study the drag reduction has occurred at fiber concentration of 0.6 wt. % throughout. Lower drag ratio provides higher drag reduction. The flow behavior of wood suspensions in drag reduction region are similar to those reported for wood fiber suspensions, where maximum drag reduction is followed by increase in drag ratio to near the water line at higher velocities.

9. Increase in the degree of beating for both wood fibres (Acacia mangium and Acacia mangium hybrid) correspondingly increases the drag reduction level, in the present investigation the maximum values are observed at a flow velocity of 1.6 m/s.

10. Pressure loss data from the Acacia mangium samples correlated well with fiber and paper properties. Similar to the heat transfer data, the pressure loss data could be used to correlate fiber and paper properties with the suspension properties.

11. The corrosion inhibition efficiencies of the LHs Schiff base on heat transfer surface have been experimentally studied using potentiodynamic polarization, impedance and FESEM analysis. It has been found that HLs are efficient corrosion inhibitors by the virtue of formation of compact layer at liquid/solid interface following the Langmuir adsorption isotherm. Moreover, the inhibition efficiency of HL_1 has fighest values depending on the chemical structure of the investigated inhibitors as well as acidic nature of the aggressive medium.

12. The polarization curves show that all HLs inhibitors are mixed-type inhibitors, the type of inhibitors is based on the fact of the shift in potential towards the more active or

more novel sides of corrosion potential. In both cases it result the suppression of corrosion currents by either means of retarding the metal dissolution or retarding the hydrogen evolution reactions.

13. The EIS outcomes confirm that a decrease in double layer capacitance and the alternate increase in charge transfer resistance (polarization resistance), when the concentration of the investigated inhibitors were increased. Nyquist plots are the best expression for the EIS analysis, the diameter of the semicircle has increased by the addition of inhibitors, which results a net increase in corrosion resistance but ultimately increases the inhibition efficiencies at higher concentration due to the formation of dense thick layer at the solid/solution interface.

14. The increase in R_P values can be attributed to the increase in adsorption of Schiff base consituents over the metal surface leading to the formation of a protective layer at metal/solution interface; which further inhibits the exchange of electrons between the metal surface and corrosive soultion. Results achieved from electrochemical measurements and weight loss methods are in good agreement, with a minor deviation in numerical values.

15. The negative values of ΔG_{ads} indicate a spontaneous adsorption process and strong interaction between the Schiff bases molecules and substrate. The higher values of ΔG_{ads} suggest the exixtance of chemical adsorption process indicating a strong adsorption due to the charges sharing between HLs molecules and the surrounding substrate surface.

16. The presence of Schiff base inhibitors hinders the dissolution of the steel due to the formation of a dense and uniform protective film by the adsorption of inhibitor molecules to the surface, which decreases the corrosion rate of steel in fibre suspension solutions.

17. The addition of Gelatin has high or even more mitigation efficiency as compared to other chemical additives where a maximum efficiency of 95% could be achieved even at a low concentration of 0.5 g/L.

18. The buildup trends of heat transfer fouling is parabolic in nature and approaches to asymptotic curve which is the indication of crystallization, particulate fouling or a combination of both of them.

19. The addition of green additive Gelatine not only modifies the fouling deposition mechanism on heat transfer surfaces but also suppresses the scale formation rate as well.

20. Increasing the additive concentration to the fouling liquid prolong the induction time by the virtue of retarding scale formation and fouling deposits on heat transfer surfaces.

REFERENCES

Abdallah, M. (2002). Rhodanine azosulpha drugs as corrosion inhibitors for corrosion of 304 stainless steel in hydrochloric acid solution. *Corrosion Science, 44*(4), 717-728.

Abdel-Gaber, A., Masoud, M., Khalil, E., & Shehata, E. (2009). Electrochemical study on the effect of Schiff base and its cobalt complex on the acid corrosion of steel. *Corrosion Science, 51*(12), 3021-3024.

Abdulrahman, A., Ismail, M., & Hussain, M. S. (2011). Corrosion inhibitors for steel reinforcement in concrete: A review. *Scientific Research and Essays, 6*(20), 4152-4162.

Abiola, O., Oforka, N., Ebenso, E., & Nwinuka, N. (2007). Eco-friendly corrosion inhibitors: the inhibitive action of Delonix Regia extract for the corrosion of aluminium in acidic media. *Anti-corrosion methods and materials, 54*(4), 219-224.

Abiola, O. K. (2006). Adsorption of 3-(4-amino-2-methyl-5-pyrimidyl methyl)-4-methyl thiazolium chloride on mild steel. *Corrosion Science, 48*(10), 3078-3090.

Agrawal YK., T. J., Shah MD., Desai MN., Shah NK. (2004). Schiff bases of ethylenediamine as corrosion inhibitors of zinc in sulphuric acid.*Corrosion Science, 46*(3), 633-651.

Ahmad, Z. (2006). *Principles of corrosion engineering and corrosion control*: Butterworth-Heinemann.

Aljourani, J., Raeissi, K., &Golozar, M. (2009).Benzimidazole and its derivatives as corrosion inhibitors for mild steel in 1M HCl solution.*Corrosion Science, 51*(8), 1836-1843

Al-Juhni, A. A., & Newby, B.-m. Z. (2006). Incorporation of benzoic acid and sodium benzoate into silicone coatings and subsequent leaching of the compound from the incorporated coatings. *Progress in Organic Coatings, 56*(2), 135-145.

Amin, N., Abdel-Aziz, M., & El-Ashtoukhy, E. Z. (2014). Effect of pulp fiber suspensions on the rate of mass transfer controlled corrosion in pipelines under turbulent flow conditions. *Chemical Engineering Research and Design, 92*(11), 2333-2338.

Asan, A., Soylu, S., Kıyak, T., Yıldırım, F., Öztaş, S., Ancın, N., & Kabasakaloğlu, M. (2006). Investigation on some Schiff bases as corrosion inhibitors for mild steel. *Corrosion Science, 48*(12), 3933-3944.

Ashassi-Sorkhabi, H., Shaabani, B., & Seifzadeh, D. (2005). Effect of some pyrimidinic Shciff bases on the corrosion of mild steel in hydrochloric acid solution. *Electrochimica Acta, 50*(16), 3446-3452.

Avci, G. (2008). Corrosion inhibition of indole-3-acetic acid on mild steel in 0.5 M HCl. *Colloids and Surfaces A: Physicochemical and Engineering Aspects, 317*(1-3).

Baeza, H., Guzman, M., Ortega, P., & Vera, L. (2003).Corrosion inhibition of copper in 0.5 M hydrochloric acid by 1, 3, 4-thiadiazole-2, 5-dithiol.*Journal of the Chilean chemical society, 48*(3), 23-26.

Bansiwal, A., Anthony, P., &Mathur, S. (2000). Inhibitive effect of some Schiff bases on corrosion of aluminium in hydrochloric acid solutions. *British Corrosion Journal, 35*(4), 301-303.

Batchelor, W., Kure, K.-A., &Quellet, D. (1999).Refining and the development of fibre properties.*Nordic Pulp and Paper Research Journal, 14*(4), 285-291.

Behpour, M., Ghoreishi, S., Gandomi-Niasar, A., Soltani, N., & Salavati-Niasari, M. (2009). The inhibition of mild steel corrosion in hydrochloric acid media by two Schiff base compounds. *Journal of materials science, 44*(10), 2444-2453.

Behpour, M., Ghoreishi, S., Soltani, N., & Salavati-Niasari, M. (2009). The inhibitive effect of some bis-N, S-bidentate Schiff bases on corrosion behaviour of 304 stainless steel in hydrochloric acid solution. *Corrosion Science, 51*(5), 1073-1082.

Beg, M., & Pickering, K. (2008). Mechanical performance of Kraft fibre reinforced polypropylene composites: Influence of fibre length, fibre beating and hygrothermal ageing. *Composites Part A: Applied Science and Manufacturing, 39*(11), 1748-1755.

Behpour, M., Ghoreishi, S., Soltani, N., Salavati-Niasari, M., Hamadanian, M., & Gandomi, A. (2008). Electrochemical and theoretical investigation on the corrosion inhibition of mild steel by thiosalicylaldehyde derivatives in hydrochloric acid solution. *Corrosion Science, 50*(8), 2172-2181.

Benabdellah, M., Benkaddour, M., Hammouti, B., Bendahhou, M., & Aouniti, A. (2006). Inhibition of steel corrosion in 2M H 3 PO 4 by artemisia oil. *Applied surface science, 252*(18), 6212-6217.

Bhardwaj, N. K., Duong, T. D., & Nguyen, K. L. (2004a). Pulp charge determination by different methods: effect of beating/refining. *Colloids and Surfaces A: Physicochemical and Engineering Aspects, 236*(1), 39-44.

Bhardwaj, N. K., Kumar, S., &Bajpai, P. K. (2004b). Effects of processing on zeta potential and cationic demand of kraft pulps.*Colloids and Surfaces A: Physicochemical and Engineering Aspects, 246*(1), 121-125.

Bhardwaj, N. K., Hoang, V., & Nguyen, K. L. (2007a).A comparative study of the effect of refining on physical and electrokinetic properties of various cellulosic fibres.*Bioresource technology, 98*(8), 1647-1654.

Bobkowicz, A., &Gauvin, W. (1965).The turbulent flow characteristics of model fibre suspensions.*The Canadian Journal of Chemical Engineering, 43*(2), 87-91.

Bockris, J. M., & Swinkels, D. (1964). Adsorption of n-decylamine on solid metal electrodes. *Journal of The Electrochemical Society, 111*(6), 736-743.

Bockris, J. O. M., & Reddy, A. K. (2001). *Modern Electrochemistry 2B: Electrodics in Chemistry, Engineering, Biology and Environmental Science* (Vol. 2): Springer Science & Business Media.

Bousfield, D. W. (2008). Rheological issues in the paper industry. Rheology Reviews, 6, 47-70.

Chitra S., P. K., Sivakami C., Salvaraj A. (2014). Sulpha Schiff bases as corosion inhibitor for mild steel in 1 M sulphuric acid. *chemical engineering Research bulletin, 14*, 1-6. (http://www.banglajol,info/index.php/CERB).

Chen, Y., Wan, J., Zhang, X., Ma, Y., & Wang, Y. (2012). Effect of beating on recycled properties of unbleached eucalyptus cellulose fiber.*Carbohydrate Polymers, 87*(1), 730-736.

Chitra1 S., P. K., Selvaraj A. (2010). Dianiline Schiff Bases as Inhibitors of Mild Steel Corrosion in Acid Media.*International Journal of ELECTROCHEMICAL SCIENCE, 5*, 1675-1697.

Clark, J. (1969). FIBRILLATION FREE WATER AND FIBER BONDING.*Tappi, 52*(2), 335-340.

Corrosion Basics an introduction. (1984). *National Association of Corrosion Engineers, (NACE), Texas (1984)*, 1127-1133.

Corrosion, H. U. (1971). Corrosion Control. *An Introduction to Corrosion Science and Engineering*.

Dadgarnezhad, A., Sheikhshoaie, I., & Baghaei, F. (2004). Corrosion inhibitory effects of a new synthetic symmetrical Schiff-base on carbon steel in acid media. *Anti-corrosion methods and materials, 51*(4), 266-271.

Daily, J. W., & Bugliarello, G. (1958).*The effects of fibers on velocity distribution, turbulence and flow resistance of dilute suspensions*: Hydrodynamics Laboratory, Department of Civil and Sanitary Engineering, Massachusetts Institute of Technology.

Dalpke, B., & Kerekes, R. (2005).The influence of fibre properties on the apparent yield stress of flocculated pulp suspensions.*Journal of pulp and paper science, 31*(1), 39-43.

Daoud D., D. T., Issaadi S., Chafaa S. (2014).Adsorption and corrosion inhibition of new synthesized thiophene Schiff base on mild steel X52 in HCl and H 2 SO 4 solutions.*Corrosion Science, 79*, 50-58.

Deasi M.N., D. M. B., Shah C.B.,Deasi S.M. (1986). Schiff bases as corrosion inhibitors for mild steel in hydrocholoric acid solutions. *Corrosion Science, 26*(10), 827-837.

Derakhshandeh, B. (2011). *Rheology of low to medium consistency pulp fibre suspensions.*University of British Columbia.

Doner A., S. R., Ozcan M., Kardas G. (2011). Experimental and theoretical studies of thiazoles as corrosion inhibitors for mild steel in sulphuric acid solution.*Corrosion Science, 53*(9),

Duffy, G. G. (1972). *A study of the flow properties of New Zealand wood pulp suspensions.*ResearchSpace@ Auckland.

Duffy, G., & Titchener, A. (1975).Disruptive shear stress of pulp networks.*Svenskpapperstidning*. 2902-2913.

Duffy, G. G., Titchener, A., Lee, P., & Moller, K. (1976).Mechanisms of flow of pulp suspensions in pipes.*APPITA Aust Pulp Pap Ind Tech Assoc*.

Duffy, G. G. (2006). Measurements, mechanisms and models: Some important insights into the mechanisms of flow of fibre suspensions. *ANNUAL TRANSACTIONS-NORDIC RHEOLOGY SOCIETY, 14*, 19.

Dutt, D., & Tyagi, C. (2011). Comparison of various eucalyptus species for their morphological, chemical, pulp and paper making characteristics. *Indian Journal of Chemical Technology, 18*(2), 145-151.

Ebenso, E., Alemu, H., Umoren, S., & Obot, I. (2008). Inhibition of mild steel corrosion in sulphuric acid using alizarin yellow GG dye and synergistic iodide additive. *Int. J. Electrochem. Sci, 3*, 1325-1339.

El-Etre, A. (1998). Natural honey as corrosion inhibitor for metals and alloys. I. Copper in neutral aqueous solution. *Corrosion Science, 40*(11), 1845-1850.

El-Maksoud, S. A. (2002). Studies on the effect of pyranocoumarin derivatives on the corrosion of iron in 0.5 M HCl. *Corrosion Science, 44*(4), 803-813.

El-Rehim, S. A., Ibrahim, M. A., & Khaled, K. (1999). 4-Aminoantipyrine as an inhibitor of mild steel corrosion in HCl solution. *Journal of Applied Electrochemistry, 29*(5), 593-599.

El Achouri, M., Kertit, S., Gouttaya, H., Nciri, B., Bensouda, Y., Perez, L., . . . Elkacemi, K. (2001). Corrosion inhibition of iron in 1 M HCl by some gemini surfactants in the series of alkanediyl-α, ω-bis-(dimethyl tetradecyl ammonium bromide). *Progress in Organic Coatings, 43*(4), 267-273.

Emregül, K. C., Akay, A. A., & Atakol, O. (2005). The corrosion inhibition of steel with Schiff base compounds in 2M HCl. *Materials Chemistry and Physics, 93*(2), 325-329.

Emregül, K. C., & Atakol, O. (2004). Corrosion inhibition of iron in 1M HCl solution with Schiff base compounds and derivatives. *Materials Chemistry and Physics, 83*(2), 373-379.

Ertas, A., & Jones, J. C. (1996). *The engineering design process*: Wiley New York.

Fällman, M. C. (2009). Turbulence measurements in fiber suspension flows: experimental methods and results.

Faraj, F.L., Zahedifard, M., Paydar, M., Looi, C.Y., N. Abdul Majid, Ali, H. M., Abdulla, M.A. (2014). Synthesis, Characterization, and Anticancer Activity of New Quinazoline Derivatives against Mcf-7 Cells. *The Scientific World Journal*, Vol 2014, Article ID 212096, 15 pages.

Fontana, M. G., & Greene, N. D. (1987). Corrosion Engineer: McGraw-Hill, Inc., Singapore.

Gärd, J. (2002). *The influence of fibre curl on the shrinkage and strength properties of paper.* M. Sc. thesis, Luleå University of technology.

Gao, B., Zhang, X., & Sheng, Y. (2008). Studies on preparing and corrosion inhibition behaviour of quaternized polyethyleneimine for low carbon steel in sulfuric acid. *Materials Chemistry and Physics, 108*(2), 375-381.

Gao, Y., Huang, F., Rajbhandari, V., Li, K., & Zhou, Y. (2009). Effect of separate refining and co-refining of bctmp/kp on paper properties.*Pulp and Paper Canada, 110*(6), 28-33.

Gulsoy, S. K., & Tufek, S. (2013). Effect of chip mixing ratio of Pinuspinaster and Populustremula on kraft pulp and paper properties.*Industrial & Engineering Chemistry Research, 52*(6), 2304-2308.

Haavisto, S., Liukkonen, J., Jäsberg, A., Koponen, A., Lille, M., &Salmela, J. (2011). Laboratory-Scale Pipe Rheometry: A Study of a Microfibrillated Cellulose Suspension. *ProcPapercon, 2011*, 704-717.

Hartler, N. (1995). Aspects on curled and microcompressed fibers.*Nordic Pulp and Paper Research Journal, 10*, 4-4.

Herrington, T. M., & Petzold, J. C. (1992).An investigation into the nature of charge on the surface of papermaking woodpulps 1.Charge/pH isotherms.*Colloids and surfaces, 64*(2), 97-108.

Heymer, J. O. (2009). *Measurement of heterogeneity in low consistency pulp refining by comminution modeling.*University of British Columbia.

Hosseini M., M. S. F. L., Ghorbani G., Arshadi R. M. (2003). Asymmetrical Schiff bases as inhibitors of mild steel corrosion in sulphuric acid media. *Materials Chemistry and Physics, 78*(3), 800-808.

Hong Ju., Z.-P. K., Yan Li. (2008). Aminic nitrogen-bearing polydentate Schiff base compounds as corrosion inhibitors for iron in acidic media: A quantum chemical calculation. *Corrosion Science, 50*(3).

Hubbe, M. A., & Heitmann, J. A. (2007). Review of factors affecting the release of water from cellulosic fibers during paper manufacture. *BioResources, 2*(3), 500-533.

Ishtiaque Ahmad, RajendraPersad., M.A.Quraishi (2010). Thermodynamic, electrochemical and quantum chemical investigation of some Schiff bases as corrosion inhibitors for mild steel in hydrochloric acid solutions.*Corrosion Science, 52*(3).

Jäsberg, A. (2007). *Flow behaviour of fibre suspensions in straight pipes: new experimental techniques and multiphase modeling*: University of Jyväskylä.

Johansson, A. (2011). Correlations between fibre properties and paper properties.

Kardas, G., & Solmaz, R. (2006). Electrochemical investigation of barbiturates as green corrosion inhibitors for mild steel protection. *Corrosion Reviews, 24*(3-4), 151-172.

Kazi, M. S. N., Duffy, G. G., & Chen, X. D. (1999). Heat transfer in the drag reducing regime of wood pulp fibre suspensions. *Chemical Engineering Journal, 73*(3), 247-253.

Kazi, M. S. N. (2001). *Heat Transfer to Fibre Suspensions: Studies in Fibre Characterisation and Fouling Mitigation*.

Kazi, S., Duffy, G., & Chen, X. (2014a).Study of the effect of entrance length on heat transfer to fibre suspensions in annular flow heat exchangers.*International Journal of Heat and Mass Transfer, 78*, 548-556.

Kazi, S., Duffy, G., & Chen, X. (2014b). Validation of heat transfer and friction loss data for fibre suspensions in a circular and a coaxial pipe heat exchanger. *International Journal of Thermal Sciences, 79*, 146-160.

Kazi, S., Duffy, G., & Chen, X. (2015).Heat transfer coefficient of flowing wood pulp fibre suspensions to monitor fibre and paper quality.*Applied Thermal Engineering, 78*, 172-184.

Kertas, M. (2013). Effect of soda-anthraquinone pulping conditions and beating revolution on the mechanical properties of paper made from gigantochloascortechinii (semantan bamboo). *Malaysian Journal of Analytical Sciences, 17*(1), 75-84.

Kertit, S., & Hammouti, B. (1996). Corrosion inhibition of iron in 1M HCl by 1-phenyl-5-mercapto-1, 2, 3, 4-tetrazole. *Applied surface science, 93*(1), 59-66.

Khaled, K. (2003). The inhibition of benzimidazole derivatives on corrosion of iron in 1 M HCl solutions. *Electrochimica Acta, 48*(17), 2493-2503.

Koch, G. H., Brongers, M. P., Thompson, N. G., Virmani, Y. P., & Payer, J. H. (2002). *Corrosion cost and preventive strategies in the United States*.

Kočar, D., Pedersoli, J. L., Strlič, M., Kolar, J., Rychlý, J., &Matisová-Rychlá, L. (2004).Chemiluminescence from paper: II. The effect of sample crystallinity, morphology and size.*Polymer degradation and stability, 86*(2), 269-274.

Kocurek, M. J., & Stevens, C. (1983). Pulp and paper manufacture . Vol. 1: properties of fibrous raw materials and their preparation for pulping. *Pulp and paper manufacture (third edition). Vol. 1: properties of fibrous raw materials and their preparation for pulping.*

Kongdee, A., Bechtold, T., Burtscher, E., &Scheinecker, M. (2004). The influence of wet/dry treatment on pore structure-the correlation of pore parameters, water retention and moisture regain values. *Carbohydrate Polymers, 57*(1), 39-44.

Krause, S. (2003). Impedance methods. *Encyclopedia of electrochemistry*.

Le, D. K. (2001).*Studies on the use of natural hybrids between Acacia mangium and Acacia auriculiformis in Vietnam*: Agricultural Publishing House.

Lee, P. F., & Duffy, G. G. (1976a). Relationships between velocity profiles and drag reduction in turbulent fiber suspension flow. *AIChE Journal, 22*(4), 750-753.

Lee, P., & Duffy, G. (1976b). Analysis of the drag reducing regime of pulp suspension flow.*Technical Association of Pulp & Pap Ind, Jour of, 59*(8).

Leitner, J., Seyfriedsberger, G., &Kandelbauer, A. (2013). Modifications in the bulk and the surface of unbleached lignocellulosic fibers induced by a heat treatment without water removal: effects on fibre relaxation of PFI-beaten kraft fibers. *European Journal of Wood and Wood Products, 71*(6), 725-738.

Loijas, M. (2010).Factors Affecting the Axial Force in Low-Consistency Refining. *Tampere University pf Applied Science, Paper Technology, Tampere, Finland:Valkeakoski Service Center*.

Luettgen, C. O., Lindsay, J. D., & Stratton, R. A. (1991). Turbulent dispersion in pulp flow: preliminary results and implications for the mechanisms of fiber-turbulence interactions.

Lukovits, I., Shaban, A., & Kálmán, E. (2005). Thiosemicarbazides and thiosemicarbazones: non-linear quantitative structure–efficiency model of corrosion inhibition. *Electrochimica Acta, 50*(20), 4128-4133.

Lumiainen, J. (2000). Refining of chemical pulp.*Papermaking part, 1*, 86-122.

M. Donahue Francis, K. N. (1965). Theory of Organic Corrosion Inhibitors: Adsorption and Linear Free Energy Relationships. *Journal of Electrochemical Society, 112*(9), 886-891.

MacKenzie, J., Martinez, D. M., & Olson, J. A. (2014).A quantitative analysis of turbulent drag reduction in a hydrocyclone.*The Canadian Journal of Chemical Engineering, 92*(8), 1432-1443.

Main, N. M., Talib, R. A., Ibrahim, R., Rahman, R. A., & Mohamed, A. Z. (2015). Linerboard Made from Soda-Anthraquinone (Soda-AQ) Treated Coconut Coir Fiber and Effect of Pulp Beating. *BioResources, 10*(4), 6975-6992.

Martinez, D., Kiiskinen, H., Ahlman, A.-K., & Kerekes, R. (2003).On the mobility of flowing papermaking suspensions and its relationship to formation.*Journal of pulp and paper science, 29*(10), 341-347.

Mernari, B., El Attari, H., Traisnel, M., Bentiss, F., & Lagrenee, M. (1998). Inhibiting effects of 3, 5-bis (n-pyridyl)-4-amino-1, 2, 4-triazoles on the corrosion for mild steel in 1 M HCl medium. *Corrosion Science, 40*(2), 391-399.

Moayed, A. R. (1999). *Characterization of fibre suspension flows at papermaking consistencies.*PhD thesis, Department of Chemical Engineering and Applied Chemistry, University of Toronto, 1999, Toronto, Canada.

Mohlin, U., Miller, J., Mohlin, U., & Miller, J. (1995).*Industrial refining-effects of refining conditions on fibre properties.* Paper presented at the Proc. 3rd international refining conference.

Mohlin, U.-B.(1975). Cellulose fibre bonding. 5. Conformability of pulp fibres. *Svenskpapperstidning*.

Moller, K., & Duffy, G. (1978).An equation for predicting transition-regime pipe friction loss [Pulp suspensions flowing].*Tappi [Technical Association of the Pulp and Paper Industry](USA)*.

Mossello, A. A., Harun, J., Shamsi, S. R. F., Resalati, H., Tahir, P. M., Ibrahim, R., &Mohmamed, A. Z. (2010). A review of literatures related to kenaf as a alternative for pulpwoods. *Agricultural Journal, 5*(3), 131-138.

Mou, H., Iamazaki, E., Zhan, H., Orblin, E., &Fardim, P. (2013).Advanced studies on the topochemistry of softwood fibres in low-consistency refining as analyzed by FE-SEM, XPS, and ToF-SIMS.*BioResources, 8*(2), 2325-2336.

Noor, E. A. (2009). Evaluation of inhibitive action of some quaternary N-heterocyclic compounds on the corrosion of Al–Cu alloy in hydrochloric acid. *Materials Chemistry and Physics, 114*(2), 533-541.

Nugroho, D. D. P. (2012). L*ow consistency refining of mixtures of softwood & hardwood bleached kraft pulp: effects of refining power.*Asian Institute of Technology.

Obot, I., Obi-Egbedi, N., & Umoren, S. (2009). Adsorption characteristics and corrosion inhibitive properties of clotrimazole for aluminium corrosion in hydrochloric acid. *Int. J. Electrochem. Sci, 4*(6), 863-877.

Oguzie, E. (2005). Inhibition of acid corrosion of mild steel by Telfaria occidentalis extract. *Pigment & resin technology, 34*(6), 321-326.

Oguzie, E., Li, Y., & Wang, F. (2007). Corrosion inhibition and adsorption behavior of methionine on mild steel in sulfuric acid and synergistic effect of iodide ion. *Journal of Colloid and Interface Science, 310*(1), 90-98.

Oguzie, E., Onuchukwu, A., Okafor, P., & Ebenso, E. (2006). Corrosion inhibition and adsorption behaviour of Ocimum basilicum extract on aluminium. *Pigment & resin technology, 35*(2), 63-70.

Oksanen, T., Pere, J., Buchert, J., &Viikari, L. (1997). The effect of Trichodermareesei cellulases and hemicellulases on the paper technical properties of never-dried bleached kraft pulp. *Cellulose, 4*(4), 329-339.

Orubite, K., & Oforka, N. (2004). Inhibition of the corrosion of mild steel in hydrochloric acid solutions by the extracts of leaves of Nypa fruticans Wurmb. *materials letters, 58*(11), 1768-1772.

Olson, J. A., Drozdiak, J., Martinez, M., Garner, R., Robertson, A. G., & Kerekes, R. (2003).Characterizing fibre shortening in low-consistency refining using a comminution model.*Powder technology, 129*(1), 122-129.

Ostovari, A., Hoseinieh, S., Peikari, M., Shadizadeh, S., & Hashemi, S. (2009). Corrosion inhibition of mild steel in 1M HCl solution by henna extract: A comparative study of the inhibition by henna and its constituents (Lawsone, Gallic acid, α-d-Glucose and Tannic acid). *Corrosion Science, 51*(9), 1935-1949.

Paavilainen, L. (1993). Conformability, flexibility and collapsibility of sulphate pulp fibres. *Paperijapuu, 75*(9-10), 689-702.

Page, D. (1989).*The beating of chemical pulps–the action and the effects.* Paper presented at the Transactions of 9th Fundamental Research Symposium, Fundamentals of papermaking. MEP, London.

Paradis, M. A., Genco, J. M., Bousfield, D. W., Hassler, J. C., &Wildfong, V. (2002). Determination of drainage resistance coefficients under known shear rate.*Tappi J, 1*(8), 12-18.

Perkasa,I . R. (2009). Implementasi Akuntansi Pada Organisasi Keagamaan (Studi Kasus Pada Gereja Kristen Indonesia PondokTjandra Indah Sidoarjo). *Skripsi, FE Universitas Pembangunan Nasional Veteran JawaTimur*.

Penniman, J. G. (1992). Comparison of pulp pad streaming potential measurement and mobility measurement. *Tappi journal, 75*(8), 111-115.

Pinso, C., & Nasi, R. (1992).The potential use of Acacia mangium× Acacia auriculiformis hybrid in Sabah.*Breeding technologies for tropical acacias. Australian Centre for International Agricultural Research, Canberra, Australia*, 17-21.

Polan, M. (1993).Effect s of refining on the flocculation of chemical pulp suspensions.*Institut e of Papermaking, Darmstadt, Germany and Pulp and Paper Centre, The University of British Columbia*.

Protopopoff, E., Marcus, P., & Marcus, P. (2002). Corrosion mechanisms in theory and practice (pp. 53): Marcel Dekker New York.

Quraishi, M., Rawat, J., & Ajmal, M. (1998). Macrocyclic compounds as corrosion inhibitors. *Corrosion, 54*(12), 996-1002.

Quraishi MA., S. R. (2004). Effect of some nitrogen and sulphur based synthetic inhibitors on corrosion inhibition of mild steel in acid solutions. *Indian journal of chemical technology, 11*, 103-107.

R. T. Vashi, V. A. C. (1997). Toluidines as corrosion inhibitors for zinc in sulphamic acid.*Indian Jouran of Chemical Technology, 4*(4), 180-184.

Rahim, A. A., Rocca, E., Steinmetz, J., & Kassim, M. J. (2008). Inhibitive action of mangrove tannins and phosphoric acid on pre-rusted steel via electrochemical methods. *Corrosion Science, 50*(6), 1546-1550.

Raja, P. B., & Sethuraman, M. G. (2008). Natural products as corrosion inhibitor for metals in corrosive media—a review. *materials letters, 62*(1), 113-116.

Rammelt, U., & Reinhard, G. (1992). Application of electrochemical impedance spectroscopy (EIS) for characterizing the corrosion-protective performance of organic coatings on metals. *Progress in Organic Coatings, 21*(2), 205-226.

Ravari F.B., D. A., Shekhshoaei I. (2009). Investigation on Two Salen Type Schiff base Compounds as Corrosion Inhibition of Copper in 0.5 M H2SO4. *G.U. Journal of Science, 22*(3), 175-182.

Roberge, P. (1999). Handbook of corrosion engineering.

Roberge, P. R. (2000). Handbook of Corrosion Engineering Mcgraw-Hill. *New York, NY*.

Rosli, W., Mazlan, I., & Law, K. (2011).Effect of lignin on Acacia mangium kraft pulp refining behaviour.*Cellulose Chemistry and Technology, 45*(9-10), 643-648.

Rosliza, R., Nik, W. W., Izman, S., & Prawoto, Y. (2010). Anti-corrosive properties of natural honey on Al–Mg–Si alloy in seawater. *Current Applied Physics, 10*(3), 923-929.

Rosliza, R., Senin, H., & Nik, W. W. (2008). Electrochemical properties and corrosion inhibition of AA6061 in tropical seawater. *Colloids and Surfaces A: Physicochemical and Engineering Aspects, 312*(2), 185-189.

Ruskin, F., Ayensu, E. S., Bene, J. G., & Morton, J. F. (1983).*Firewood Crops: Shrub and Tree Species for Energy Production*: National Academy Press.

Sastri, V. S. (1998). *Corrosion inhibitors: principles and applications*: Wiley New York.

Sein, C. C., & Mitlöhner, R. (2011).*Acacia hybrid: Ecology and silviculture in Vietnam*: CIFOR.

Sha, J., Nikbakht, A., Wang, C., Zhang, H., & Olson, J. (2015).The Effect of Consistency and Freeness on the Yield Stress of Chemical Pulp Fibre Suspensions.*BioResources, 10*(3), 4287-4299.

Shaju K.S., T. K. J., Raphael VP.,Aby Paul. (2012). Synergistic Effect of KI on Corrosion Inhibition ofMild Steel by Polynuclear Schiff Base in Sulphuric Acid.*International Scholarly Research Network ISRN Corrosion*.doi: doi:10.5402/2012/425878.

Shreir, L., Jarman, R., & Burstein, G. (1994). Corrosion (Metal/Environment Reactions), Vol. 1. *Butterworth-Heinemann, Oxford, England, 4*, 44.

Singh, A., Ahamad, I., Singh, V., & Quraishi, M. A. (2011). Inhibition effect of environmentally benign Karanj (Pongamia pinnata) seed extract on corrosion of mild steel in hydrochloric acid solution. *Journal of Solid State Electrochemistry, 15*(6), 1087-1097.

Smook, G. A. (1992). *Handbook for pulp & paper technologists*: Tappi.

Solmaz, R., Altunbaş, E., & Kardaş, G. (2011). Adsorption and corrosion inhibition effect of 2-((5-mercapto-1, 3, 4-thiadiazol-2-ylimino) methyl) phenol Schiff base on mild steel. *Materials Chemistry and Physics, 125*(3), 796-801.

Solmaz, R., Kardaş, G., Culha, M., Yazıcı, B., & Erbil, M. (2008). Investigation of adsorption and inhibitive effect of 2-mercaptothiazoline on corrosion of mild steel in hydrochloric acid media. *Electrochimica Acta, 53*(20), 5941-5952.

Talati J.D., D. M. N., Shah N.K. (2005). meta-Substituted aniline-N-salicylidenes as corrosion inhibitors of zinc in sulphuric acid. *Materials Chemistry and Physics, 93*(1).

Tschirner, U. W., Barsness, J., & Keeler, T. (2007).Recycling of chemical pulp from wheat straw and corn stover.*BioResources, 2*(4), 536-543.

Uhlig, H. H., & Revie, R. W. (1971). Corrosion and Corrosion Control John Wiley & Sons. *Inc., New York*.

Vaezi, M., Katta, A. K., & Kumar, A. (2014).Investigation into the mechanisms of pipeline transport of slurries of wheat straw and corn stover to supply a bio-refinery.*Biosystems Engineering, 118*, 52-67.

Valek, L., & Martinez, S. (2007). Copper corrosion inhibition by Azadirachta indica leaves extract in 0.5 M sulphuric acid. *materials letters, 61*(1), 148-151.

Vaseleski, R. C., &Metzner, A. (1974). Drag reduction in the turbulent flow of fiber suspensions. *AIChE Journal, 20*(2), 301-306.

Vasudevan, T., Muralidharan, B., Muralidharan, S., & Venkatakrishna Iyer, S. (1998). Inhibition of corrosion of mild steel in acidic solutions by quarternary salts of pyridinium bases. *Anti-corrosion methods and materials, 45*(2), 120-126.

Ventura, C., Blanco, A., Negro, C., Ferreira, P., Garcia, F., &Rasteiro, M. (2007).Modeling pulp fiber suspension rheology.

von Baeckmann, W., Schwenk, W., & Prinz, W. (1997). *Handbook of cathodic corrosion protection*: Gulf Professional Publishing.

Wahyudi, I., Okuyama, T., Hadi, Y. S., & Yamamoto, H. (1999). Growth stresses and strains in Acacia mangium. *Forest products journal, 49*(2), 77.

Wang, L., Pu, J.-X., & Luo, H.-C. (2003). Corrosion inhibition of zinc in phosphoric acid solution by 2-mercaptobenzimidazole. *Corrosion Science, 45*(4), 677-683.

Wan, J., Yang, J., Ma, Y., & Wang, Y. (2011).Effects of the pulp preparation and papermaking processes on the properties of OCC fibers.*BioResources, 6*(2), 1615-1630.

Yağan, A., Pekmez, N. Ö., & Yıldız, A. (2006). Corrosion inhibition by poly (N-ethylaniline) coatings of mild steel in aqueous acidic solutions. *Progress in Organic Coatings, 57*(4), 314-318.

Yahya, R., Sugiyama, J., Silsia, D., &Gril, J. (2010).Some anatomical features of an Acacia hybrid, A. mangium and A. auriculiformis grown in Indonesia with regard to pulp yield and paper strength.*Journal of Tropical Forest Science*, 343-351.

Yuan, L., Wan, J., Ma, Y., Wang, Y., Huang, M., & Chen, Y. (2012). The content of different hydrogen bond models and crystal structure of eucalyptus fibers during beating.*BioResources, 8*(1), 717-734.

Yurt, A., Ulutas, S., & Dal, H. (2006).Electrochemical and theoretical investigation on the corrosion of aluminium in acidic solution containing some Schiff bases.*Applied Surface Science, 253*(2), 919-925.

Zeng, X., Retulainen, E., Heinemann, S., & Fu, S. (2012). Fibre deformations induced by different mechanical treatments and their effect on zero-span strength. *Nordic Pulp and Paper Research Journal, 27*(2), 335.

Zubir, M. N. B. M. (2015). Facile and highly scalable approach to enhance the stability of colloidal system for thermal application.University of Malaya.

LIST OF PUBLICATIONS AND PAPERS PRESENTED

PUBLISHED PAPERS

- Ghulamullah khan*, Kazi Md. Salim Newaz, Wan Jefrey Basirun, Hapipah Binti Mohd Ali, Fadhil Lafta Faraj, Ghulam Mustafa Khan. Application of natural product extracts as green corrosion inhibitors for metals and alloys in acid pickling processes- a review. *International journal of electrochemical science,*10 (2015), 6120 – 6134 **(ISI JOURNAL Q3)**.
- Ghulamullah khan*, Kazi Md. Salim Newaz, Wan Jefrey Basirun, Pervaiz Ahmed, Ladan Magaji, Syed Muzamil ahmed, Muhammad Abdur Rehman Ghulam Mustafa Khan, Badarudin Bin Mohamad Badry . Electrochemical investigation on the corrosion inhibition of mild steel by Quinazoline Schiff Base compounds in hydrocholoric acid solution. Journal of Colloid and Interface Science 502 (2017) 134-145 **(ISI JOURNAL Q1)**.